IONIC CONDUCTION IN POLY(VINYLIDENE FLUORIDE) AND POLY(VINYLIDENE FLUORIDE-CO-HEXAFLUOROPROPYLENE) BASED GEL POLYMER ELECTROLYTES CONTAINING LiX (X = ClO$_4^-$, CF$_3$SO$_3^-$ AND AsF$_6^-$) SALTS

THESIS SUBMITTED TO

TEZPUR UNIVERSITY

IN FULFILLMENT OF THE REQUIREMENTS
FOR THE DEGREE OF

DOCTOR OF PHILOSOPHY
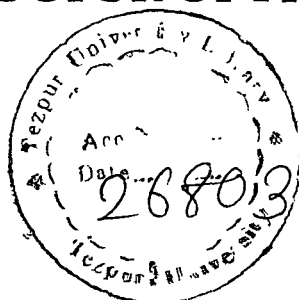
DIGANTA SAIKIA

DEPARTMENT OF PHYSICS
SCHOOL OF SCIENCE AND TECHNOLOGY
TEZPUR UNIVERSITY
NAPAAM, TEZPUR
ASSAM – 784028
INDIA

DECEMBER, 2004

Dedicated to
my
Beloved Parents

Late Nakul Saikia
&
Mrs Banti Saikia

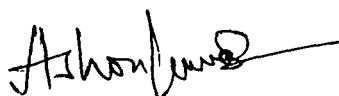# Department of Physics:: Tezpur University

Dr. Ashok Kumar
Reader & Head

P.O.: Napaam, Tezpur
Sonitpur -784 028
Assam, India

CERTIFICATE

This is to certify that the thesis entitled **"Ionic Conduction in Poly(vinylidene fluoride) and Poly(vinylidene fluoride-co-hexafluoropropylene) Based Gel Polymer Electrolytes Containing LiX (X = ClO_4^-, $CF_3SO_3^-$ and AsF_6^-) Salts"** being submitted by **Diganta Saikia** to Tezpur University, Tezpur, Assam in fulfillment of the requirements for the award of the degree of Doctor of Philosophy, is a record of original bonafide research work carried out by him. He has worked under my supervision and has fulfilled the requirements for the submission of this thesis. The results contained in the thesis have not been submitted in part or full to any other university or institute for award of any degree or diploma.

Date: 17·12·2004

(Dr. A. Kumar)

DECLARATION

I hereby declare that the thesis entitled "Ionic Conduction in Poly(vinylidene fluoride) and Poly(vinylidene fluoride-co-hexafluoropropylene) Based Gel Polymer Electrolytes Containing LiX (X = ClO_4^-, $CF_3SO_3^-$ and AsF_6^-) Salts" being submitted to the Department of Physics, Tezpur University, Tezpur, Assam in fulfillment of the requirements for the award of the degree of Doctor of Philosophy, has previously not formed the basis for the award of any degree, diploma, associateship, fellowship or any other similar title or recognition.

Dated: 17.12.2004

Diganta Saikia

(Diganta Saikia)

Department of Physics,
Tezpur University,
Tezpur-784 028 (Assam)

ACKNOWLEDGEMENTS

Diganta Saikia

Preface

Scientific and industrial applications of polymer electrolytes have continuously grown since the first report of ionic conduction in polymers in 1973. There have been phenomenal advances in the available range of materials and characterization techniques for understanding the properties and ion conduction processes in polymer electrolytes. In the present work emphasis has been placed on gel and composite gel polymer electrolytes because of their higher ionic conductivity and possible improvement on these polymer electrolytes to attain ionic conductivity values comparable to that of liquid electrolytes (10^{-2} S/cm).

In the present thesis, Chapter I deals with the review of literature, different types of polymer electrolytes, brief description of ion transport models and swift heavy ion irradiation. In the end statement of the problem and objectives of the present work have been spelt out.

Chapter II focuses on the theoretical aspects of complex impedance spectroscopy and ion transport kinetics in composite and gel polymer electrolytes.

Chapter III describes the experimental details of synthesis of gel and composite gel polymer electrolytes by solution casting method. Characterization techniques and the instruments such as ionic conductivity measurement set up, DSC, FTIR, XRD and SEM employed to characterize the polymer electrolytes in the present work have been briefly explained. Ion beam irradiation facility of 15 UD Pelletron stationed at Nuclear Science Centre, New Delhi has also been described.

In Chapter IV complex impedance spectroscopy, XRD, SEM, DSC and FTIR results of the PVDF-(PC+DEC)-LiClO$_4$ and P(VDF-HFP)-(PC+DEC)-LiClO$_4$ gel polymer electrolyte systems have been analyzed to gain an insight into the different characteristic properties such as ionic conductivity, crystallinity, surface morphology, thermal stability and interactions among different constituents of the polymer electrolytes.

Chapter V emphasizes on three composite gel polymer electrolyte systems viz. P(VDF-HFP)-PMMA-PC-LiClO$_4$-TiO$_2$, P(VDF-HFP)-PMMA-(PC+DEC)-LiCF$_3$SO$_3$-fumed SiO$_2$ and P(VDF-HFP)-(PC+DEC)-LiAsF$_6$-fumed SiO$_2$. Properties such as ionic conductivity, crystallinity,

v

surface morphology, stability and interaction among different groups in the polymer electrolytes have been analyzed to throw new light on the ionic conduction mechanism in composite gel polymer electrolytes.

Chapter VI highlights the Li^{3+} and C^{5+} ion beam swift heavy ion irradiation effects on ionic conduction in $P(VDF-HFP)-(PC+DEC)-LiClO_4$ and $P(VDF-HFP)-(PC+DEC)-LiCF_3SO_3$ gel polymer electrolyte systems. Ion beam induced modification of polymer electrolytes is a new research area and effort has been made to understand the conduction mechanism in view of ion-polymer interaction.

The main conclusions drawn in the present work with a brief mention of future research prospects in this area have been presented in the last Chapter VII.

Diganta Saikia

CONTENTS

Results and Discussion

LIST OF FIGURES

LIST OF TABLES

CHAPTER I

INTRODUCTION

1.1 Historical Developments

Ionic conduction in solids has been known since 1830's when Faraday observed the ionic conduction in nonmetallic solids Ag_2S and PbF_2 [1]. Later Kohlrausch [2] initiated a systematic study of ionic conduction in solids. Tubandt and his group [3] established the Faraday's laws of electrolysis for solid ion conductors. Theoretical models to explain the transport of electricity through ionic solids by the flow of ions were developed by Frenkel [4], Wagner [5] and Schottky [6]. The first detailed study of the structural basis for high ionic conductivity in a crystalline solid was carried out by Ketelaar [7] in Ag_2HgI_4. Reuter and Hardel [8] synthesized a new material Ag_3SI, which showed exceptionally high ionic conductivity (10^{-2} S/cm) above 235 °C. Bradley and Greene [9] and Owens and Argue [10] independently discovered a new family of superionic conductors MAg_4I_5 (M = K, Rb, NH_4, etc.). These materials exhibit conductivities of $\approx$ 0.3 S/cm at room temperature. Yao and Kummer [11] reported an unusually high ionic conductivity in the $Na_2O-Al_2O_3$ (Na-β-alumina) system. Liang [12] discovered that the dispersion of fine insulating Al_2O_3 particles in LiI enhances the Li^+ ion conductivity of LiI by about two orders of magnitude at room temperature from 10^{-7} to 10^{-5} S/cm. All highly conducting solid electrolytes owe their conductivities to disorder regions in their structures.

Depending on structure, solid ion conductors can be classified as crystalline, amorphous (glassy), composite and polymeric ionic conductors. In crystalline ionic conductor, the carrier concentration may be defined as the density of defects with reference to

the perfect lattice and each carrier is identically situated having the same mobility [13]. Alkali halides, Na-β-aluminas, Nasicon, stabilized ZrO$_2$, etc. are some examples of crystalline ionic conductors. In amorphous ionic conductors large amount of free volume assumes all the ions to be potentially conducting but in a broad distribution of states [14]. Lack of grain boundaries, isotropic and generally higher conductivities are the distinct advantages of amorphous (glassy) ionic conductor over their crystalline counterparts [15]. Alkali germanates and lithium niobate glasses are examples of amorphous ionic conductors. In composite ionic conductors, ionic conductivity is believed to occur in the thin interfacial regions surrounding the dispersed particles [16]. Several phenomenologies have been invoked to explain the enhancement in the conductivity of composite electrolytes. Jow and Wagner [17] and Shahi and Wagner [18] proposed that the dispersion of the insulating particles in the host matrix produces a space charge layer at the matrix/particle interface and thus facilitates the ionic motion. LiI (Al$_2$O$_3$) is one of the examples of composite ion conductor.

The most promising class of ionic conductors of today's world is the polymeric ionic conductors. Ionically conducting phases, free from low molecular weight solvents, based on the dissolution of salts in suitable ion-coordinating polymers are key components in new types of batteries for portable electronic devices and electric cars. Batteries for such applications require polymer electrolytes with improved properties, e.g. a high ionic conductivity, high cation transport number and improved chemical, thermal and electrochemical stability. Main reason for using polymeric electrolytes over other solid electrolytes lies in their flexibility and conformability to the electrodes. First measurements of ionic conductivity in polymer-salt complexes were carried out in 1973 by P. V. Wright [19] in collaboration with David Fenton and crystallographer John Parker. Armand, Chabagno and Duclot [20] investigated a wide range of PEO-alkali salts complexes and introduced the

Vogel-Tammann-Fulcher relation for LiSCN and CsSCN complexes. Armand's proposal that they can be used as 'polymeric solid electrolytes' in secondary lithium batteries apparently initiated a burst of research activities amongst electrochemists worldwide. At Sheffield, in the late 1970's, Lee [21] and Payne [22] embarked upon an investigation of morphology of polymer complexes and its relation with conductivity. They reported that fully saturated crystalline region of PEO complexes gave poor conductivity and amorphous region gave higher conductivity. At about the same time, Killis, Le Nest and Cheradame [23] at St. Martin d'hères had independently reached similar conclusions regarding the amorphous PEO by preparing urethane based PEO networks.

With confirmation of the predominance of amorphous phase mobility by Berthier and coworkers [24], the 1980's saw the development of a number of strategies to suppress crystallinity in polyethoxy systems. The branched or comb polyphosphazenes of Shriver, Allcock and coworkers at Pennsylvania [25] and Ward's group at Leeds [26] and the methoxy copolymers developed by Booth's group at Manchester [27] were among the more successful of these. At the same time there were significant theoretical and mechanistic developments including the dynamic percolation model proposed by Ratner and coworkers [28] at Northwestern. Angell at Arizona State University [29] and Torrell at Chalmers [30] discussed the relation between the conductivity and matrix relaxation times. The correlation between conductivity, glass transition temperature and the mechanical relaxation (the WLF equation) was investigated by Cheradame and coworkers [31] and Watanabe [32].

One of the most important steps in the understanding of polymer electrolyte is that the ionic conductivity is a property of amorphous elastomeric phases [24]. High molecular weight amorphous polymers above their glass transition temperatures may exhibit mechanical properties similar in most ways to those of a true solid, which is a result of chain

entanglement and crosslinking of various types. At microscopic level, however, local relaxation processes may still provide liquid like degrees of freedom somewhat similar to that in an ordinary molecular liquid.

Since the discovery that a number of polymer-salt complexes exhibit considerable ionic conductivity, much research effort has been directed to find the optimal combination of host polymer and dopant salt for fast ionic transport. Conductivity of solvent free polymer electrolytes are increased by two different ways: (i) suppression of crystallization of polymer chains to enhance polymer chain mobility and (ii) increase in the carrier concentration. The suppression of crystallization of polymer chains to improve polymer chain mobility can be realized by cross-linking, co-polymerization, comb formation (side chains and dendritic polymers), polymer alloy (including inter penetrating network) and inorganic filler blend. In the combination of cross-linking and co-polymerization, Cheradame et al. [33] achieved an ionic conductivity of about 5×10^{-5} Scm^{-1} at 25 °C by cross-linking block co-polymers of EO and PO, and in the comb formation, Hall et al. [34] obtained a ionic conductivity value of 2×10^{-4} Scm^{-1} at 25 °C by adding PEO side chains to polysyloxane chains. Watanabe et al. [35] extended this method by synthesizing a dendritic polymer by attaching PEO chains to glycidyl ether side chains.

The increase in the carrier concentration can be realized by use of highly dissociated salts and increase in salt concentration. For the polymer electrolytes wherein anions are not fixed in the polymer, polymer-salt systems with salts having a small lattice energy, large anions and plasticity to the polymer have been studied. Vallee et al. [36] obtained ionic conductivity value of 4×10^{-5} Scm^{-1} at 25 °C with a lithium trifluorosulfonyl imide-PEO system, drastically improving the ionic conductivity from 1×10^{-7} Scm^{-1} at 25 °C with a NaI-PEO system. For the polymer electrolytes with anions fixed in the polymer (single ion

conductor), Kobayashi et al. [37] got conductivity value of 1×10^{-7} Scm^{-1} at 25 °C with a carboxylate system, Benrabah et al. [38] obtained conductivity value of 6×10^{-7} Scm^{-1} at 25 °C with a sulfonate system and Fujinami et al. [39] achieved conductivity value of 2×10^{-5} Scm^{-1} at 25 °C with a siloxy aluminate system. Angell et al. [40] described a new type of ionic conductors 'polymer-in-salt' materials in which lithium salts are mixed with small quantities of the polymers polypropylene oxide and polyethylene oxide and they found ionic conductivity of the order of 10^{-3} S/cm. Watanabe et al. [41] obtained the same order of conductivity 1×10^{-3} Scm^{-1} at ambient temperature for polypyridinium, pyridinium and aluminium chloride system.

Considerable efforts have been devoted to the development and improvement of the electrolyte's ionic conductivity for electrochemical device applications [42]. For that purpose a new system has received much attention wherein a polymer matrix is swollen in a plasticizer to get plasticized or gel polymer electrolyte. Main concepts behind the development of gel polymer electrolyte are: (i) the gel polymer electrolyte by physical cross-linking and (ii) the gel polymer electrolyte by chemical cross-linking. For the physical cross-linking gel polymer electrolyte, Feuillade et al. [43] began research with PAN system and later Tsuchida et al. [44] obtained conductivity value of 1×10^{-3} Scm^{-1} at 25 °C with a PVDF system. Iijima et al. [45] achieved conductivity value of 1×10^{-3} Scm^{-1} at 25 °C with a PMMA system. For chemical cross-linking gelled polymer electrolyte, Feuillade et al. [43] began research with a P(VDF-HFP) cross-linking system and Morita et al. [46] obtained conductivity value of 1×10^{-3} Scm^{-1} at 25 °C with a PEO system. Introduction of nanoscale inorganic fillers such as TiO_2, Al_2O_3 and SiO_2 to the polymer electrolytes have proved effective to enhance the mechanical and electrochemical properties of the electrolyte by

forming particle networks into the polymer bulk, inhibiting crystallization, reorganization of polymer chains and interacting with lithium ionic species [47-49].

1.2 Classification of Polymer Electrolytes

1.2.1 Polymer-Salt Complexes

The original solvent free polymer electrolytes introduced over three decades ago consisted of polymers such as poly(ethylene oxide) PEO and poly(propylene oxide) PPO or their blend complexed with suitable salts (LiClO₄, LiCF₃SO₃, etc.) [50-53].

$$[PEO, -(CH_2CH_2O)_n- , T_m \sim 65 \text{ °C, about 85\% crystallinity}]$$

$$PEO_n + LiCF_3SO_3 \quad PEO_n * LiCF_3SO_3$$

Salts dissolve in only those polymers for which exothermic ion-polymer interactions compensate for lattice energy of the salt so as to reduce the free energy of the system [54]. Glass-transition temperature of the polymer normally increases by 50–100 K after dissolution of salt [55,56]. The polymer hardens, stiffens and increases in conductivity by a factor of up to 10^5. Reasonable conductivity can be achieved at 100 °C ($\sim 10^{-5}$ Scm^{-1}) in the polymer-salt complex. At ambient temperature PEO is a poor conductor due to high crystallinity ($<10^{-8}$ Scm^{-1}). Poor ionic transport properties of PEO type solid polymer electrolytes used in lithium batteries at ambient temperatures cause concentration polarization and limit the performance of such batteries.

1.2.2 Plasticized Polymer Electrolytes

In this type of electrolytes small amount of low-molar mass polar liquids are added to first type of electrolytes [57-60]. Plasticized polymer electrolytes represent a compromise between polymer and liquid electrolytes. Liquid plasticizers, however, typically lead to

worsening of the mechanical properties of the electrolyte and increasing reactivity towards the metal electrodes. Plasticizers can increase ionic conductivity by a factor 100.

1.2.3 "Polymer-in-Salt" or "Rubbery" Electrolytes

"Polymer-in salt" or "rubbery" electrolytes were discovered by Angell and co-workers [40,41,61,62]. In these electrolytes high molar-mass polymers are dissolved in low-temperature molten salt mixtures forming a rubbery material. Polypropylene oxide, polyethylene oxide [40], polypyridinium [41], polyacrylonitrile [61] etc. are used as host polymers with lithium and aluminium salts [LiN(CF$_3$SO$_2$)$_2$), LiCF$_3$SO$_3$, AlCl$_3$ etc.]. These polymer materials have glass transitions low enough to remain rubbery at room temperature. Although in this type of electrolytes good ambient lithium-ion conductivities ($\sim 10^{-3}$ S/cm) and high electrochemical stability have been realized, the salt tends to crystallize at lower temperatures, preventing their practical use.

1.2.4 Composite Polymer Electrolytes

In this type of electrolytes nano to micron size inorganic (ceramic) particles are introduced into a polymer electrolyte [63-67]. In addition to improvements in the ionic conductivity, the mechanical strength and interfacial stability are also enhanced in the composites. Common second phase dispersed particles used are Li$_3$N, Al$_2$O$_3$, SiO$_2$, TiO$_2$, zeolites etc. Though the conductivities of composite electrolytes are dramatically improved from those without the nanoparticles, ambient temperature conductivities still remain relatively low for real practical applications. Enhancement of conductivity in this type of electrolyte is attributed to reduction of crystallinity and polymer-ceramic grain boundaries

with high defect concentration that may allow better ion transport (smaller particles give better conductivities at same T_g and crystallinity).

1.2.5 Gel Polymer Electrolytes

The latest development in the field of aprotic electrolytes is presented by the gel polymer electrolytes. These electrolytes are prepared by immobilizing a nonaqueous electrolyte solution within an inactive structural polymer matrix or by increasing the viscosity of a liquid electrolyte by adding a soluble polymer [68]. They are basically salt-solvent-polymer hybrid systems in which first a salt solution is prepared and then it is immobilized with the help of a suitable polymer matrix. Since the electrolyte molecules can preferentially solvate ions, coordinating polymers like PEO are no longer necessary and may be replaced by more robust polymers like poly(vinylidene fluoride) PVDF [69-72], poly(acrylonitrile) PAN [73-76], poly(methyl methacrylate) PMMA [77-80] and poly(vinylidenefluoride-hexafluoropropylene) P(VDF-HFP) [81-84] copolymer. In gel polymer electrolytes the salt generally provides free/mobile ions which take part in the conduction process and the solvent
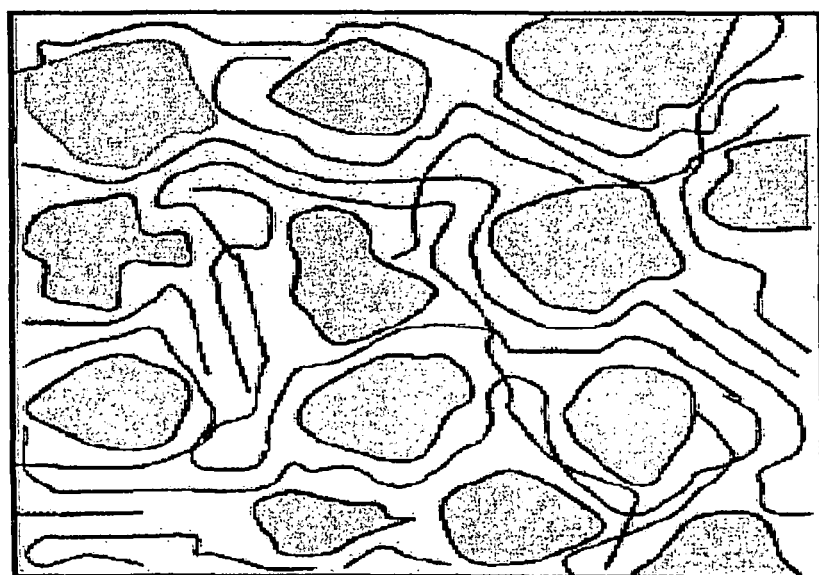
Figure 1.1: Sketch of gel polymer electrolyte with micropores containing "free" solvent within a swollen polymer matrix.

helps in solvating the salt and also acts as a conducting medium whereas the polymer provides mechanical stability by increasing the viscosity of the electrolyte [85]. Gel polymer electrolytes are receiving much attention due to some of their unique properties like high value of conductivity at room temperature (10^{-2}–10^{-4} S/cm), ease of preparation, wide composition range and hence wider control of properties, good adhesive properties suitable for lamination, good thermal/electrochemical stability etc., but also suffer from the same disadvantages as the plasticized electrolytes – viz. release of volatiles and increased reactivity towards the metal electrodes. Common solvents used for gel polymer electrolytes are ethylene carbonate (EC) and propylene carbonate (PC). Figure 1.1 shows the schematic diagram of gel polymer electrolyte with micropores.

1.3 Ion Transport in Polymer: Mechanisms and Models

Polymers are covalently bonded chain structures formed by repetition of similar units, in which the chains are of sufficient length to confer on the material some additional properties not possessed by the individual units. In the molten state or in solution, these polymer chains are randomly coiled and, even when apparently solid, at least part of the material is amorphous, i.e., the randomness persists. Within the solid polymer it is possible for the chains to align themselves in a systematic way by chain folding or by the formation of single or multiple helices, for at least part of their length. These regions possess long range order and are therefore crystalline. Crystallization is initiated at many locations within a polymer and the crystalline domains that develop are not coherently oriented with respect to each other, i.e., some portions of each long chain molecules cannot be aligned within an individual crystalline region and these portions remains amorphous.

9

Intrachain hopping

Interchain hopping

(a)

Intrachain hopping via ion cluster

Intercluster hopping

(b)
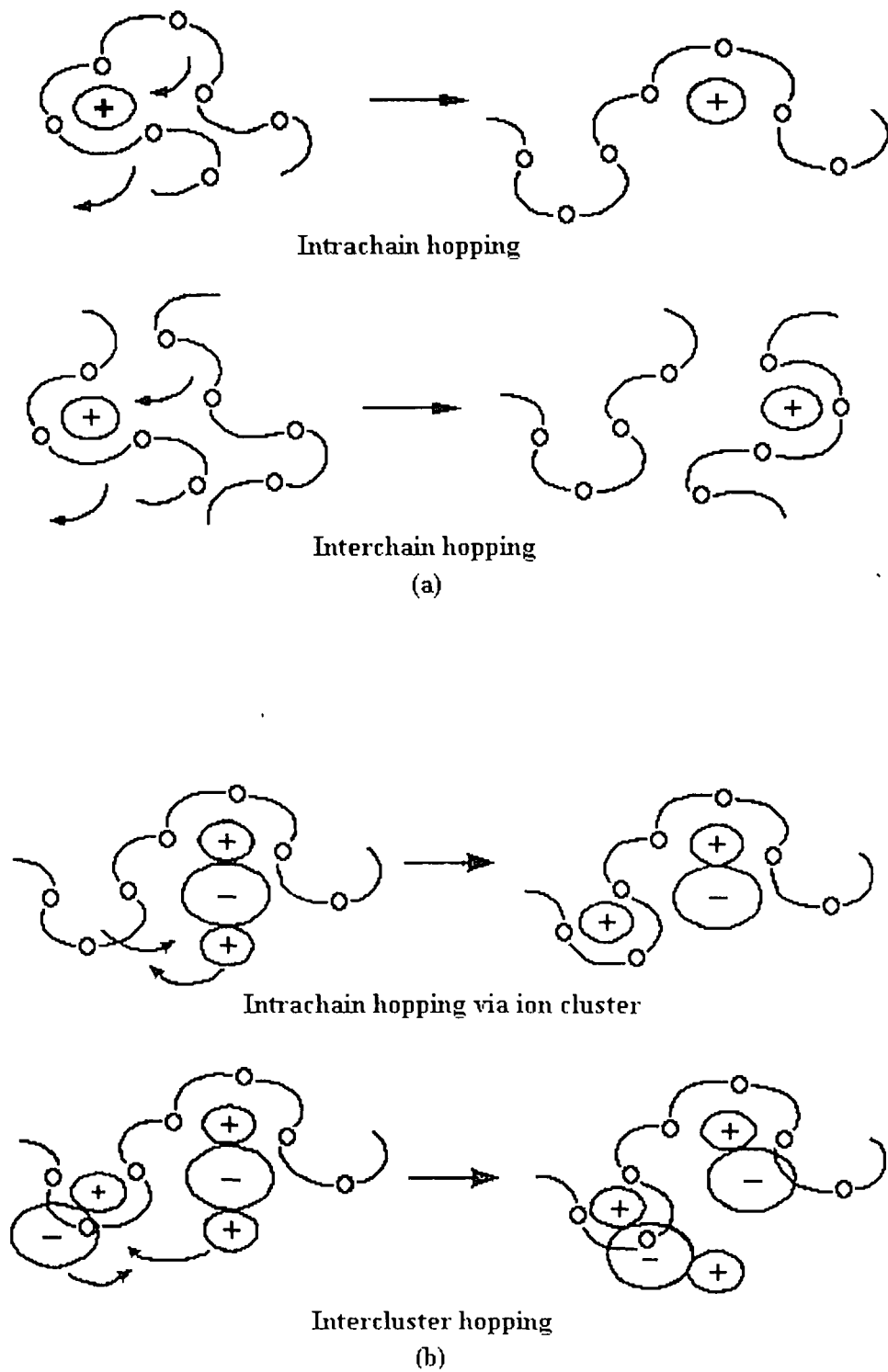
Figure 1.2: Cation motion in a polymer electrolyte

For solvent free polymer electrolytes, such as heteropolymers PEO, salts dissolve because the lone pair electrons on the polymer chain oxygen atoms coordinate with the cations. The cation transport process in polymer electrolytes can be envisaged as a 'roll-on' mechanism in which a cation is initially coordinated to several oxygen (or other) atoms [86]. The linkages to one or more of the polymer segments that lie behind the direction of motion of the cation break and new linkages are formed in the forward direction. The cation motion is clearly facilitated by the flexing of the polymer chain segments which allow old links to be broken and new attachments to be made. For high molecular weight polymer hosts chain diffusion is small and makes little contribution to mechanisms for ion transport. Low barriers to bond rotation allow segmental motion of the polymer chain, thus providing a mechanism for ion transport as conductivity is determined largely by the local mobility (segmental motion) of the polymer segments. Figure 1.2 shows the schematic representation of cation hopping of polymer electrolyte in different ways.

For polymer gel electrolytes, polymer is an important constituent along with salt and solvent. The salt provides ions for conduction and the solvent helps in the dissolution of the salt and also provides the medium for ion conduction. The conductivity of gel polymer electrolytes can be explained by 'Breathing polymeric chain model' proposed by Chandra et al. [87]. According to this model polymer gel electrolytes generally consists of free ions, ion aggregates and polymer chain dispersed in the gel matrix. The breathing of the polymer by folding/unfolding up of its chains results in density/pressure fluctuations at the microscopic level which assist the motion of ions alongwith the dissociation of ion aggregates which results in an increase in conductivity. The polymer chains act on ion pairs to effect dissociation and the dissociated ions in the solvent are further solvated by the polymer chains which results in a change in carrier concentration (n) and mobility (μ) [88].

11

1.3.1 Arrhenius Model

Polymer gel electrolyte is a semi-solid hybrid system wherein ionic conduction essentially occurs through the liquid organic phase trapped in constantly flexing polymeric molecular chains above the glass transition temperature of the polymer. Therefore, for polymer gel electrolyte systems the Arrhenius equation for conductivity

$$\sigma = \sigma_0 \, \exp\left(-E_a / kT\right) \tag{1.1}$$

where σ_0 is the pre-exponential factor, E_A is the activation energy and k is the Boltzmann's constant, often provides a good representation of the conductivity-temperature relationship. Linear graph of log σ vs 1/T is often called an Arrhenius plot, as for an Arrhenius process the logarithm of the relevant performance parameter depends linearly on the reciprocal of temperature. The slope of the curve gives the activation energy for the process. In fact, diffusion is the relevant activated transport process rather than conductivity and the appropriate performance parameter is the diffusion coefficient. The Nernst-Einstein equation provides the link between diffusion and conductivity, but it reveals that D is proportional to (σT) rather than σ, and it would be more appropriate to plot log (σT) instead of log σ. For polymer gel electrolytes the temperature range covered is often quite short and the variation in 1/T is substantially greater than the change in log T so that latter can be considered as approximately constant and log (σT) can be replaced by log σ [89].

1.3.2 Vogel-Tamman-Fulcher (VTF) Model

For the solid electrolytes which involve ion hopping between fixed sites, graphs of log(σ) versus 1/T are straight lines, but for the polymer electrolytes the log(σ) versus 1/T plots are often curved. Such behavior would be expected for materials such as polymer

electrolytes in which conduction occurs in the amorphous region and the conduction process

is better described by the Vogel-Tammann-Fulcher (VTF) equation [90-92]

$$\sigma = AT^{-\frac{1}{2}} \exp\left(- E'_a/k(T - T_0)\right)$$

$$\text{or, } \sigma = \sigma_0 \exp\left(- B/k(T - T_0)\right) \tag{1.2}$$

where B is a constant, whose dimensions are that of energy, but which is not simply

interpreted as an activation term. In configurational entropy terms, T_0 is the temperature at

which the probability of configurational transition tends to zero, and it is generally regarded

as having a value between 20 to 50 K below glass-transition temperature (T_g). The value of

conductivity becoming vanishingly small as T_0 approaches T.

If the conductivity versus temperature dependence curve is linear in larger temperature

range then it is said to Arrhenius. VTF (curved) behavior can be modeled as Arrhenius

(linear) behavior by dividing the entire temperature range into smaller temperature regions.

The interconnection between Arrhenius and VTF behavior of σ (T) are widely reported and

discussed in literature [93]. This behavior is rationalized by arguing that since VTF

dependence is governed by the energy interval $k(T-T_0)$ and the Arrhenius dependence by the

energy kT (where k is Boltzmann constant), for T » T_0 [94] i.e. when T_0 is quite smaller than

T, the curvature of conductivity versus Temperature plot becomes small and VTF equation

approaches Arrhenius equation.
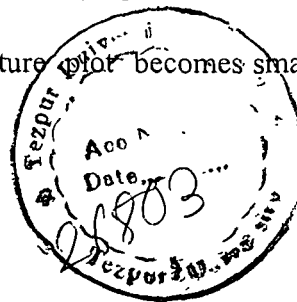
1.3.3 William-Landel-Ferry (WLF) Model

In an amorphous polymer above its glass transition temperature, a single empirical

function can describe the temperature dependence of all mechanical and electrical relaxation

13

processes. The temperature dependence at a number of relaxation and transport processes can be described by WLF equation (Williams-Landel-Ferry) [95]

$$\log\left[\frac{\eta(T)}{\eta(T_s)}\right] = \log a_T = -\frac{C_1(T-T_s)}{C_2 + T - T_s} \tag{1.3}$$

where a_T is the mechanical shift factor (expresses the fluidity or inverse relaxation time or relaxation rate), η is the viscosity, T_s is reference temperature (usually $T_s = T_g + 50$ K) and C_1 and C_2 are constants.

1.3.4 Dynamic Bond Percolation (DBP) Model

Kohlrausch summation and Nernst-Einstein relations do not fit well in polymer ionics and the deviations become more significant as the salt concentration increases. In the former case ions move by a local liquid like process rather than by hopping from site to site in an ordered polymer host. To describe conduction mechanism in polymers adequately, it is important to model it microscopically. Dynamic bond percolation (DBP) theory [96] is a microscopic model for diffusion in dynamically disordered systems. The model assumes that mobile ions move from site to site within the polymer host and the sites lie on a regular lattice.

Assuming simple first-order hopping chemical kinetics for the ion motion, the probability of finding an ion at site j can be written as

$$\frac{dP_i}{dT} = \sum_j (P_j W_{ji} - P_i W_{ij}) \tag{1.4}$$

where W_{ji} is hopping rate from site j to site i.

The difference between dynamic disordered hopping and ordinary hopping is that the hopping rates W_{ij} are themselves time dependent, and evolve on the time scale of relaxation of the

polymer host. The model of equation (1.4) becomes specific to a percolation situation when it is assumed that the W_{ij}'s have only two values: each W_{ij} can be either 0 (probability of 1-f) or a constant value, w (probability f). The assignment of any given bond between cells i and j as available (value w) or unavailable (value 0) itself evolve in time. The simplest assumption is that the value of the bonds as available or unavailable is reassigned randomly after a renewal time, τ_{ren}. This model is then characterized by the two time scales τ_{ren} and the hopping time, 1/w. The renewal time is determined by the local microviscosity of the solvent. The rate of renewal is the inverse local relaxation time that determines bond breakage near the mobile ion.

1.3.5 Free Volume Model

Cohen and Turnbull [97] first proposed the "free volume theory" of transport phenomena in glass forming materials. They derived the equation for diffusion coefficient, D, in a liquid

$$D = ga^{*}u \, \exp\left[-\frac{\gamma V^{*}}{V_f} \right] \qquad (1.5)$$

where g is a geometrical factor, a* is approximately equal to the molecular diameter, u is the average speed of the molecules, γ is a numerical factor introduced to correct for overlap of free volume and V* is the critical volume just large enough to permit another molecule to jump in after the displacement. Cohen and Turnbull defined the free volume as [97]

$$V_f = \overline{V} - V_0 \qquad (1.6)$$

where $\overline{V}$ is the average volume per molecule in the liquid and V_0 is the van der Waals volume of the molecule.

Using the Nernst – Einstein equation

$$\sigma = \frac{q^2 nD}{kT} \tag{1.7}$$

it follows that

$$\sigma = \frac{q^2 nga^*u}{kT} \exp(-\gamma V^*/V_f) \tag{1.8}$$

In these equations, n and q are the concentration and charge of the charge carriers respectively, k is the Boltzmann's constant.

Free volume theory in this form has been applied to polymer electrolytes by several workers [98,99]. This theory predicts that at a constant free volume, the conductivity should decrease weakly with increasing temperature because kinetic theory requires that u vary as $T^{1/2}$. Since the remaining terms in equation (1.8) are approximately temperature independent, equation (1.8) can be rewritten as

$$\sigma = \frac{C}{T^{1/2}} \exp\left(-\gamma V^*/V_f\right) \tag{1.9}$$

where C includes the charge carrier concentration. But the experimental data show that the electrical conductivity at constant specific volume increases strongly with temperature. The conclusion that equation (1.9) is not supported by the data is based on the assumption that the free volume is proportional to the macroscopic volume.

Cohen and Turnbull made the assumption that

$$V_f = V_0 \left(\exp\left[\int_{T_0}^{T} \alpha dT \right] - 1 \right) \tag{1.10}$$

where α is the thermal expansion coefficient [67]. A slightly different approximation often made is that the thermal expansion of the free volume is the difference in thermal expansion coefficients of the bulk material above and below T_g [99]. However, when the microscopic volume is held constant, the ionic conductivity increases strongly with temperature.

16

Consequently, if free volume varies as the macroscopic volume, as follows from the definition given in equation (1.6), free volume theory is not capable of representing the constant volume electrical conductivity for a typical polymer electrolyte. The disagreement between theory and experiment is not surprising since the theory was originally developed for simple van der Waals liquids and metallic liquids [97]. Inability of free volume theory to account for the phenomena governed by segmental motions has been widely pointed out in the literature [100, 101].

One of the first attempts to modify the free volume theory to account for the temperature variation of physical phenomena was made by Macedo and Litovitz [102]. They employed the reaction rate theory of Eyring [103] to arrive at the following equation for the shear viscosity

$$\eta = \left(\frac{RT}{E_v}\right)^{\frac{1}{2}} \frac{(2mkT)^{\frac{1}{2}}}{V^{\frac{2}{3}}} \exp\left[\frac{\gamma V^*}{V_f} + \frac{E_v}{kT}\right] \qquad (1.11)$$

where r is the gas constant, E_v is the height of the potential barrier between equilibrium positions, V is a quantity roughly equal to the volume of a molecule and m is the molecular mass. Next, the Stokes-Einstein equation

$$\eta = \frac{kT}{6\pi Dd} \qquad (1.12)$$

where d is the molecular radius, is used. It is known that the Stokes-Einstein equation breaks down for fragile glasses near T_g [104]. The Nernst-Einstein equation [equation (1.7)] is used to obtain the following equation for the conductivity

$$\sigma = \frac{q^2 n V^{\frac{2}{3}}}{6\pi d(2mkT)^{\frac{1}{2}}} \left(\frac{E_v}{kT}\right)^{\frac{1}{2}} \exp\left[-\frac{\gamma V^*}{V_f} - \frac{E_v}{kT}\right] \qquad (1.13)$$

At constant volume, equation (1.8) can be rewritten as

$$\sigma = \frac{B}{T} \exp\left[-\frac{E_v}{kT}\right] \exp\left[-\frac{\gamma V^*}{V_f}\right] \qquad (1.14)$$

Because of the temperature dependence in the first exponential term, this equation can account for a strong increase of the conductivity at constant volume and was used by Macedo and Litovitz to successfully reproduce the pressure and temperature dependence of the shear viscosity of several liquids [102]. These include several materials exhibiting VTF or WLF behavior. Equation (1.14) can account for VTF or WLF behavior because both types of behavior are represented by the free volume factor.

1.4 Swift Heavy Ion Irradiation of Polymer Electrolytes

Ion beams have become an integral part of numerous surface processing schemes and in the modification of surface layers of solids [105]. Recently there has been a growth of interest in high energy ion irradiation of polymers and other insulating materials [106-111]. Ions couple energy to the target atoms in a solid predominantly through electronic excitation and ionizations and through direct collisional displacement of the target atoms. In case of high energy ion irradiation of polymers, the electronic energy loss of the incident swift heavy ion is released into (i) radiative decay (ii) production of new reactive species (radicals, gases) and defects (unsaturation, scissions, crosslinks) and heat. The decrease in crystallinity has also been reported after ion irradiation [112].

An important parameter characterizing ion-to-target energy transfer is the energy loss dE/dx (eV/Å), defined as the energy deposition per unit length along ion track. The value of (dE/dx) changes with ion energy. When an energetic particle penetrates into a polymer medium, it loses energy by two main processes, viz. by interacting with target nuclei

(screened) and by interacting with target electrons. The former process is called *nuclear energy loss or nuclear stopping* and the later *electronic energy loss or electronic stopping.*

Nuclear Energy Loss

Nuclear energy loss S_n arises from collisions between the energetic particle and target nuclei, which cause atomic displacements and phonons [113]. Displacement occurs when the colliding particle imparts energy greater than certain displacement threshold energy, E_d, to a target atom. E_d is the energy that a recoil requires to overcome the binding forces and to move more than one atomic spacing away from its original site. Since the nuclear collision occurs between two atoms with electrons around protons and neutrons, the interaction of an ion with a target nucleus is treated as the scattering of two screened particles. At low energies (~1 keV/nucleon) the incident ion primarily undergoes nuclear energy loss (S_n) [114]. Nuclear energy loss is derived with consideration of the momentum transfer from ion to target atom and inter atomic potential between two atoms. Thus S_n varies with ion velocity as well as the charges of two colliding atoms. Nuclear energy loss becomes important when an ion slows down to approximately the Bohr velocity (orbital electron velocity, 2.2×10^6 m/s). Therefore the maximum nuclear energy loss occurs near the end of the ion track for high energy ions.

Electronic Energy Loss

Electronic energy loss S_e arises from electromagnetic interaction between the positively charged ion and the target electrons. One mechanism is called glancing collision (inelastic scattering, distant resonant collisions with small momentum transfer) and the other is called knock-on collision (elastic scattering, close collisions with large momentum

transfer). Both glancing and knock-on collisions transfer energy in two ways: electronic excitation and ionization. All excited electrons eventually lose energy as they thermalize. Glancing collision are quite frequent but each collision involves a small energy loss (<100 eV). On the other hand, knock on collision are very infrequent but each collision imparts a large energy to a target electrons (>100 eV). Theoretical and experimental evidence suggested that approximately one half of the electronic energy loss is due to glancing collisions and the other half to knock-on collisions [113]. At high energies (100 keV/nucleon) the incident ion primarily undergoes electronic energy loss [114] $(dE/dx)_e$, and if the films are sufficiently thin compared to the stopping range of the ion, the electronic energy loss is reasonably uniform throughout the film thickness.

On their way through matter, energetic ions lose energy and induce a continuous trail of excited and ionized target atoms. Due to their highly charged state, associated with a high energy transfer, heavy ions are especially suited to create cylindrical zones of irreversible chemical and structural changes. These zones have a diameter of only a few nanometers and are known as latent tracks. Formation of tracks in polymers can be explained on the assumption that particles lose energy during its passage through matter in two ways: (i) along the trajectory, the energy yield being large, all chemical bonds are broken and (ii) in the neighborhood of the trajectory, only the bonds between monomer units are broken. Thus the breaking of chemical bonds plays a more vital role in the formation of tracks than the displacement of ions by mutual repulsion.

1.5 Statement of the Problem

Tremendous progress has been made in the past three decades to develop high conducting solid polymer electrolytes, however, the ionic transport process in polymer

electrolytes is still a subject in the research domain as there is no satisfactory understanding of the structure, dynamics and ion conduction mechanism at the molecular level. For composite polymer electrolytes, it has been recognized that changes in polymer microstructure occur at the interface between matrix electrolyte and the dispersed filler. An attempt has been made to gain an insight into the ion conduction mechanism (ion-polymer, ion-ion and polymer-filler interfacial interactions) in the polymer electrolytes and develop new polymer gel electrolyte systems with: (i) high ionic conductivity (ii) thermal, chemical and electrochemical stability (iii) mechanically strong and flexible (iv) ability to form good interfacial contacts with electrodes (v) ease of processing and (vi) high affinity with organic liquid electrolytes.

To achieve the aforesaid objectives, in the present work the following polymer gel electrolyte systems have been investigated:

(i) $PVDF-(PC+DEC)-LiClO_4$

(ii) $P(VDF-HFP)-(PC+DEC)-LiClO_4$

(iii) $P(VDF-HFP)-PMMA-PC-LiClO_4-TiO_2$

(iv) $P(VDF-HFP)-PMMA-(PC+DEC)-LiCF_3SO_3$- fumed SiO_2

(v) $P(VDF-HFP)-(PC+DEC)-LiAsF_6$-fumed SiO_2

Ionic conductivity of the polymer electrolytes was measured by complex impedance spectroscopy. Wagner polarization technique was employed to measure the total ionic transport number of the polymer electrolytes. The degree of crystallinity/amorphicity, which is an important parameter to know since ionic conduction in polymer electrolytes essentially occurs through the amorphous region, was determined by X-ray diffraction analysis. FTIR analysis was carried out to investigate the different bond interactions among polymer-ion-filler so as to throw new light on the dynamics of ion conduction processes in the polymer electrolytes. Differential scanning calorimetry (DSC) was performed to observe the thermal

21

stability of polymer electrolytes. Scanning electron microscopy studies were carried out to investigate the microstructure and surface morphology of the polymer electrolytes. A systematic and comparative study was conducted between gel and composite gel polymer electrolytes to gain an insight into the conduction behavior with the addition of filler by correlating the conductivity, XRD, FTIR and SEM results. Lithium salts ($LiClO_4$, $LiCF_3SO_3$, and $LiAsF_6$) with low dissociation energies and large anions were chosen for high degree of dissociation and lower mobility of anions in the transport process respectively.

Swift heavy ion (SHI) irradiation is a novel technique for modification of properties of materials through energy deposition by nuclear and electronic energy loss processes. Intensive research efforts are going on in the field of polymer electrolytes, however swift heavy ion irradiation effects on ionic conduction in polymer electrolytes have not been reported. In an attempt to enhance the Li^+ ion diffusivity, P(VDF-HFP)-(PC+DEC)-$LiClO_4$ and P(VDF-HFP)-(PC+DEC)-$LiCF_3SO_3$ gel polymer electrolyte systems were irradiated with 48 MeV Li^{3+} and 70 MeV C^{5+} ion beams of several different fluences. The results show that below certain fluence (ions/cm²) swift heavy ion irradiation reduced the crystallinity of polymer electrolyte films resulting in higher ionic conductivity. At lower fluences chain scission processes appear to dominate leading to decrease in the degree of crystallinity and faster ion transport through the polymer matrix assisted by large amplitude segmental motion of the polymer backbone. On the other hand at higher fluences cross-linking processes appear to dominate due to collective excitations of electrons (plasmons) in the adjacent polymer chains, which increase the degree of crystallinity of the polymer resulting in the decrease in ionic conductivity. FTIR and XRD analyses have been carried out to investigate the interactions as well as crystallinity effect on ionic conduction in irradiated gel polymer electrolytes. Swift heavy ion (SHI) irradiation which can be used to change the degree of

crystallinity/amorphicity depending upon its fluence, is expected to provide a better insight

into the ionic conduction processes in polymer electrolytes. In the present work, perhaps for

the first time, a sincere effort has been made to study the effect of SHI on the ionic

conduction in polymer electrolytes.

CHAPTER II

THEORETICAL ASPECTS

2.1 Complex Impedance Analysis

The complex impedance spectroscopy is a technique to separate the contributions from various processes such as electrode reactions at the electrode/electrolyte interface, and the migration of charge carrying species through the electrolyte and across the polymer-electrolyte interfaces. With the development of both electrode and electrolyte materials for solid state electrochemical devices such as batteries, sensors, fuel cells and electrochromic devices, the impedance spectroscopy has become an inevitable characterization tool [115-118].

The measurement of ionic conductivity or ion transport of a polymer electrolyte sample cannot be measured without connecting the electrolyte to electrodes on both its faces, so that the overall properties are those of the electrode-electrolyte system with its interfaces. The d. c. methods cannot be used because passage of d. c. current leads to build up of a concentration gradient referred to as concentration polarization [119]. Therefore a. c. methods are used to measure the conductivity. In a. c. technique, the resistance, R, is replaced by the impedance, Z, which is the sum of resistance and reactance. The reactance has two components, a capacitive term and an inductive term. For ionic conductors the inductive term is negligible and therefore omitted. The technique involves applying a sinusoidal signal of low amplitude across a polymer electrolyte cell. The output signal is used to determine the impedance modulus and phase shift corresponding to the equivalent circuit which represents the cell assembly, i.e., electrode/electrolyte/electrode. The complex impedance Z at an applied

frequency ω can be written as

$$Z = R - \frac{j}{\omega C} = R + \frac{1}{j\omega C} = Z' - jZ'' \qquad (2.1)$$

where C is capacitance, $j = \sqrt{-1}$, Z' is the real and Z" is the imaginary part of the complex impedance. The magnitude of the complex impedance is $Z = \sqrt{(Z'^2 + Z''^2)}$ and the phase angle is $\theta = \tan^{-1}(Z'/Z'')$.

For a resistance (R) and a capacitance (C) in parallel, the complex impedance Z is given by

$$Z = \frac{R\left(\dfrac{1}{j\omega C}\right)}{\left(R + \dfrac{1}{j\omega C}\right)} \qquad (2.2)$$

or,
$$Z = \frac{R}{1 + \omega^2 C^2 R^2} + j\frac{-R^2 \omega C}{1 + \omega^2 C^2 R^2} \qquad (2.3)$$

Thus, the real and imaginary parts of Z are

$$Z' = \frac{R}{1 + \omega^2 C^2 R^2} \qquad (2.4)$$

and

$$Z'' = \frac{-R^2 \omega C}{1 + \omega^2 C^2 R^2} \qquad (2.5)$$

Elimination of ω from equations (2.4) and (2.5) yields

$$\left(Z' - \frac{R}{2}\right)^2 + Z''^2 = \frac{R^2}{4} \qquad (2.6)$$

which is the equation of a circle of radius R/2, with its centre at (R/2,0).

25
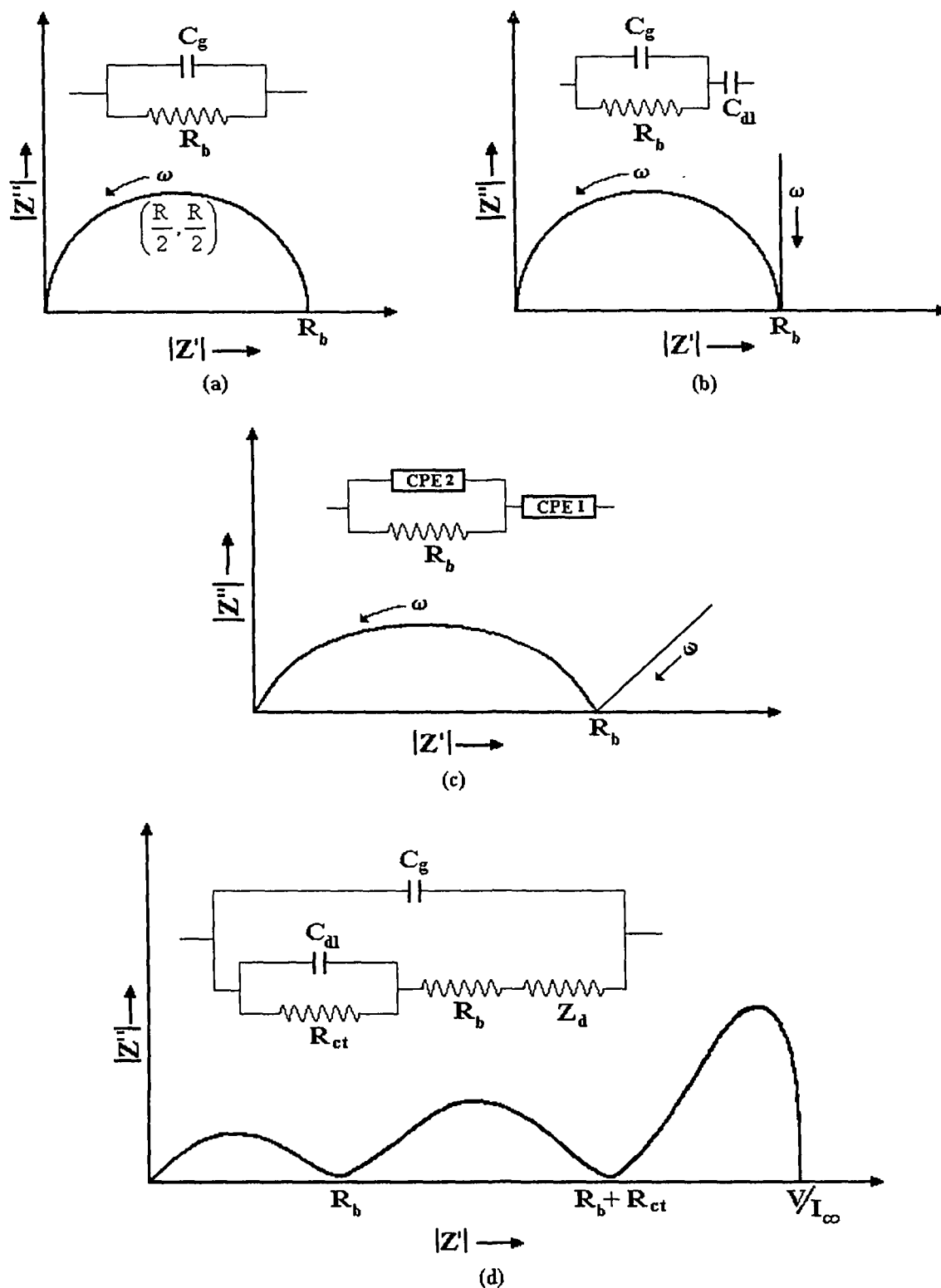
Figure 2.1: Various impedance behaviors observed in polymer electrolytes

26

Figure 2.1 shows the various impedance behaviors observed in the polymer electrolytes. A cell system consisting of an electrolyte and two non-blocking electrodes made up of the same material as the mobile species, has an equivalent circuit (Figure 2.1(a)) which is a parallel combination of a capacitor C_g, representing the geometrical capacitance of the cell, and a resistance R_b representing the bulk resistance of the electrolyte. The bulk resistance can be obtained from the intersection of the semicircle and the real axis of the complex spectra. However, it is often difficult to use non-blocking electrodes. Moreover, the use of blocking electrodes has the advantage of making it possible to determine the electronic contribution to the electrical conductivity using dc polarization measurements. The equivalent circuit for an elementary cell with blocking electrodes is shown in figure 2.1(b). The geometrical capacitance C_g and the bulk resistance R_b have been supplemented by a double layer capacitance at the electrode/electrolyte interface. In this case also the bulk resistance is obtained from the intersection of the semicircle with the real axis. However a 90° line in addition to the semicircle is obtained for perfectly smooth surfaces. The slope of the line decreases with the increasing roughness [120].

In polymer electrolyte flattening of the semi circle and tilting of the spike is observed as shown in figure 2.1(c), which is different from ideal shape as in figure 2.1(b). This behavior can be modeled with a constant phase angle element (CPE) to account for semi-circle flattening and spike tilting. It may be thought as a leaky capacitor, the physical origin of which for polymer electrolytes is perhaps related to the presence of crystalline non-conducting regions interconnected with conducting amorphous material within the spherulites. The impedance of constant phase element is given by

$$Z_{CPE} = k(j\omega)^{-p} \quad \text{where } 0 \leq p \leq 1 \tag{2.7}$$

When p = 0, Z is frequency independent and k is just the resistance R and when p = 1,

$Z = k/j\omega = -j/\omega(k^{-1})$, the constant k^{-1} now corresponding to the capacitance C. When p is

between 0 and 1, the CPE acts in a way intermediate between a resistor and a capacitor. The

use of series CPE terms tilts the spike and parallel CPE terms depress the semi-circle, as

shown in figure 2.1(c).

The value obtained at the intersection of the flattened semicircle and the tilted spike is

the bulk resistance, R_b, of the electrolyte. This is related to the conductivity (σ) by

$$\sigma = \frac{GL}{A} = \frac{L}{R_b A} \tag{2.8}$$

where G is conductance, L is thickness and A is the cross-sectional area of the sample.

The impedance plot with a non-blocking electrode and its equivalent circuit elements

are shown in figure 2.1(d). In addition to the first and second semicircles due to the electrolyte

behavior and charge transfer at the electrode/electrolyte interface respectively, there is a low

frequency region which starts as an inclined spike which falls towards the real axis as the

frequency approaches zero. This is due to the diffusional impedance (Z_d). The first and second

intercepts of the spectrum give the value of R_b and R_{ct} respectively. The value of third

intercept is calculated from d. c. measurement and found to be V/I_∞

2.2 Kinetics of Ion Transport in Polymer Electrolytes

The conductivity σ of a material can be expressed by the relation

$$\sigma = \sum_i \mu_i n_i q_i \tag{2.9}$$

where μ_i, n_i, q_i are the mobility, carrier concentration and charge of the i type of species

respectively. The polymer electrolytes contain no significant conjugation within the polymer

backbone, and the salts on which they are based have negligible electronic conductivities, hence electrons and holes do not contribute to the summation in equation (2.9). Both cation and anion contribute to the conductivity [121]. This represents a complication in the simple interpretation of the temperature dependence of conductivity.

Experimentally one observes fairly straightforward behavior of the temperature dependence of conductivity in homogeneous electrolytes. The straight or curved plots observed when the conductivity is plotted against temperature inverse can be fit in the Arrhenius or VTF [90-92] forms respectively

$$\sigma T = \sigma_0 \exp^{-E_A/kT} \qquad (2.10)$$

$$\sigma = \sigma_0 \exp^{-B/k(T-T_0)} \qquad (2.11)$$

In the Arrhenius form, E_A is the usual activation energy, whereas in the VTF form, B is a constant with dimension of energy, but it is not simply interpreted as an activation term; k is Boltzmann's constant and T_0 is a reference temperature usually associated with the ideal glass transition temperature at which free volume disappears, or the temperature at which the configurational entropy becomes zero. T_0 is usually lies 20 – 50 K below T_g.

The early investigations of the groups in Grenoble generally showed curved plots, corresponding to VTF behavior [20,23,122,123]. Cheradame and co-workers [23,33,122,123] discussed these plots in terms of chain segment mobility of the polymer host material. They used the relation of polymer chain viscosity to glass transition temperature that is summarized in the Williams-Landel-Ferry [95] relation

$$\log\frac{\eta(T)}{\eta(T_s)} = \log a_T = \frac{-C_1(T-T_s)}{C_2 + (T-T_s)} \qquad (2.12)$$

where T_s is an arbitrary reference temperature, usually $T_s = T_g + 50$ K, a_T is called the

mechanical shift factor and C_1 and C_2 are universal constants. Often the WLF equation is coupled with the empirical observation known as Walden's rule [124]

$$D\eta = Const/r_i \qquad (2.13)$$

Stokes-Einstein relation can be written as

$$D = kT/6\pi\eta r_i \qquad (2.14)$$

where D is the diffusion coefficient and r_i is the radius of the ion.

Again one can write the Nernst-Einstein relation as

$$\sigma = DNq^2/kT \qquad (2.15)$$

where N is the number of carriers and q is the charge. Putting the value of D of equation (2.14) in equation (2.15)

$$\sigma = \left(\frac{kT}{6\pi\eta r_i}\right)\left(\frac{Nq^2}{kT}\right)$$

$$\sigma = \frac{Nq^2}{6\pi\eta r_i}$$

$$\eta = \frac{Nq^2}{6\pi\sigma r_i} \qquad (2.16)$$

Using equation (2.16) in equation (2.12), one obtains the temperature dependence of conductivity in the WLF form [95]

$$\log\frac{Nq^2/6\pi\sigma(T)r_i}{Nq^2/6\pi\sigma(T_s)r_i} = \frac{-C_1(T-T_s)}{C_2+(T-T_s)}$$

$$or,\ \log\frac{\sigma(T_s)}{\sigma(T)} = \frac{-C_1(T-T_s)}{C_2+(T-T_s)}$$

$$or,\ \log\frac{\sigma(T)}{\sigma(T_s)} = \frac{C_1(T-T_s)}{C_2+(T-T_s)} \qquad (2.17)$$

On the basis of this, Cheradame's group has argued that WLF behavior is the rule in polymer electrolytes and the fluidity of the polymer chain segments largely determines the conductivity.

Writing the VTF equation in the form

$$\log \frac{\sigma(T)}{\sigma(T_s)} = -\frac{B}{k}\left[\frac{1}{T-T_0} - \frac{1}{T_s - T_0}\right]$$

(2.18)

Comparing equations (2.17) and (2.18)

$$\frac{C_1(T-T_s)}{C_2+(T-T_s)} = -\frac{B}{k}\left[\frac{1}{T-T_0} - \frac{1}{T_s - T_0}\right]$$

$$\text{or, } C_1 = \frac{B}{k(T_s - T_0)}\left[\frac{C_2+(T-T_s)}{T-T_0}\right]$$

(2.19)

Identifying $C_2 = T_s - T_0$

(2.20)

$$C_1 = \frac{B}{k(T_s - T_0)}$$

(2.21)

$$\text{or, } B = kC_1C_2$$

In an attempt to understand how the conductivity mechanism works, quasi-thermodynamic theories [97,125-129], originally developed to deal with molten salts and neat polymers, have in fact been applied with some success to consideration of transport properties in polymer electrolytes. These theories are based on considerations involving the critical role of the glass transition temperature T_g and of the so called equilibrium glass transition temperature T_0. Above T_g, the polymeric material becomes macroscopically rubbery rather than glassy [125-129]. The concept of equilibrium glass transition temperature T_0 is based on the kinetic feature of T_g, depending on the rate of cooling, one can observe different glass transition temperatures and T_0 is idealized as the temperature at which free volume vanishes

or at which the excess configurational entropy of the material vanishes. The theoretical

scheme which treats T_0 in terms of volume is called free volume theory [97,125].

The free volume model is the simplest way to understand the polymer segment

mobility. It states that as temperature increases, the expansivity of the material produces local

empty space i.e. free volume into which ionic carriers, solvated molecules, or polymer

segments themselves can move. The overall mobility of the material is determined by the

amount of volume present in the material. One can obtain, for the diffusivity D, the form

$$D = BRT \exp\left(- V^*/V_f\right) \qquad (2.22)$$

where B and V^* are constant, R is gas constant and V_f is the free volume.

When the volume is expanded in terms of the volume at the glass transition

temperature plus a linear term, the free volume theory yields the form [33,122,130]

$$D = D_0 T \exp\left(- \frac{a}{T - (T_g - C_2')}\right) \qquad (2.23)$$

where the constant a and C_2' are both inversely proportional to the free volume thermal

expansion factor.

Rewriting equation (2.23) as

$$D = D_0 T \exp\left(\frac{-a}{C_2 + T - (T_g - C')}\right) \qquad (2.24)$$

where $C_2 \equiv C_2' - C'$. If $C' = 0$, the free volume argument yields the WLF relation of equation

(2.12).

Druger, Nitzan and Ratner [96,130-134] have developed a dynamic percolation model

for description of ion transport in polymer electrolytes. Percolation theory is extremely useful

in understanding transport processes in disordered media and has been recently used in the

interpretation of the free volume behavior of several disordered materials like, polymers,

molten salts etc. This is a microscopic model that characterizes the ionic motion in terms of jumps between neighboring positions.

The rate of jumping (i.e. of ion motion) between any two sites (i.e. between two different positions in the material) is then represented in terms of simple first order chemical kinetics, using the master equation

$$\frac{dP_i}{dT} = \sum_j (P_j W_{ji} - P_i W_{ij}) \qquad (2.25)$$

where P$_j$ is the probability on site j and W$_{ji}$,the rate of ion motion from site j to site i.

The dynamic percolation model takes into account the dependence of ionic motion rates on the fluidity, or rate of segmental motion, of the polymer host. A characteristic rate of renewal, $\lambda = \tau_{ren}^{-1}$, is defined which characterizes the rate at which a motion pathway from one site to another becomes available for the ion to move. In static percolation theory applied, for example, to electron hopping in amorphous metals, the rates W$_{ij}$ of equation (2.25) are taken to be

W$_{ji}$ = 0 (probability 1 − f)

W$_{ji}$ = w (probability f) $\qquad (2.26)$

with w being some average rate and f be the fraction of available bonds. For polymer electrolytes above T$_g$, the segmental motion changes the local coordination environment of the ion with a characteristic time τ_{ren}, so that a jump which is unavailable at time t can become available at time t + τ_{ren} because of chains reorientation.

The dynamic percolation model is characterized by the parameters f, w and τ_{ren}. It has some interesting features [96,130-134]:

(i)   For observation times long compared to the renewal time, the motion is always diffusive

        i.e. the mean squared displacement is always proportional to time.

(ii) The diffusion coefficient is proportional to the average rate of renewal $\langle\lambda\rangle$. This corresponds well both to the wealth of experimental data indicating that the ionic motion is modulated by the segmental motions of the polymer host and to the expectation, that structural reorganization and conductivity arise from the same motion mechanism.

(iii) It is possible to show in great generality that

$$D_0(\omega + i\lambda) = D(\omega) \tag{2.27}$$

That is, the diffusion coefficient at frequency ω in the dynamic percolation problem may be found from the diffusion coefficient in the static percolation problem, analytically continued to frequency $\omega + i\lambda$.

(iv) The factor 'f' giving the number of available jumps, will be substantially different for cationic (strongly solvated) and anionic (weakly solvated) motions.

This model has the attractive feature of including the effects of segmental motion on ionic conduction, but not directly includes interionic interaction. Thus while it is the best microscopic model currently available for understanding the ionic conduction in polymer electrolytes, it is inadequate to fully expound inertial dynamics or interionic interactions.

2.3 Kinetics of Ion Transport in Composite Polymer Electrolytes

Effective Medium Theory Approach

For composite polymer electrolyte it has been recognized that changes in polymer microstructure occur at the interface between matrix electrolyte and the dispersed filler [135,136] and the enhancement in conductivity is connected with the existence of a highly conductive layer at the polymer filler interface. Therefore, in composite systems there are three components with different electrical properties, viz., (i) a highly conductive layer

covering the surface of a grain or particle additive, (ii) dispersed insulating grains or particles and (iii) a polymer matrix ionic conductor. We can consider a dispersed grain covered with the thin interface layer as a unit and call it a composite grain (Figure 2.2). According to the Maxwell-Garnett rule [137] the equivalent conductivity σ_c of the composite unit can be expressed as

$$\sigma_c = \sigma_1 \frac{2\sigma_1 + \sigma_2 + 2Y(\sigma_2 - \sigma_1)}{2\sigma_1 + \sigma_2 - Y(\sigma_2 - \sigma_1)} \qquad (2.28)$$

where σ_1 and σ_2 are the conductivity of interface layer and that of dispersed insulating grain respectively, Y is the volume fraction of dispersed grain in a composite unit and for spherical geometry can be calculated as

$$Y = 1 \Big/ \left(1 + \frac{t}{R}\right)^3 \qquad (2.29)$$

where t is the thickness of interface layer and R is the radius of dispersed grain.
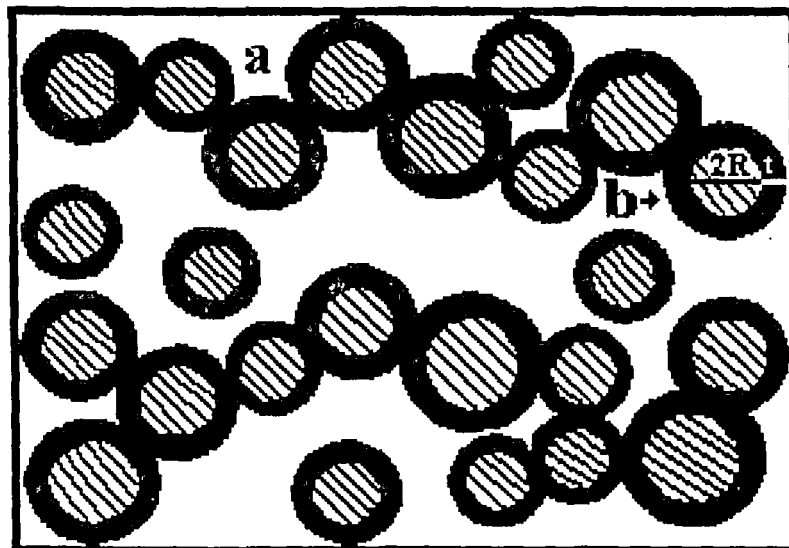
Figure 2.2: Schematic morphology of (a) quasi-two-phase composite electrolyte and (b) composite grain unit consisting of insulating grain and interface layer

According to the above considerations, the composite electrolyte can be treated as quasi two phase mixture consisting of an ionically conducting polymer matrix and composite units. The electrical properties of such a quasi two phase mixture can simply be described by Bruggeman equation [138] or the simple effective medium equation introduced by Landauer [139]. These simple approaches ignore the local field effects and are suitable only for the description of quasi two-phase mixture for volume fraction of composite units less than 0.1. In the quasi two-phase mixture as the volume fraction of composite units increases, the composite grains gradually join together to form agglomerated clusters and then the local field effects cannot be ignored. Nan [140,141] and Nakamura [142] have considered the following limiting situations to incorporate this fact:

(i) The matrix phase is the polymeric electrolyte and isolated composite units are scattered throughout.

(ii) The matrix phase consists of overlapping or touching composite units with a small amount of dispersed polymeric electrolyte in the interstices.

Because the local field effect is a geometrical effect and has no relation with the conductivity of the two phases, and since the matrix phase screens the effect of dispersed phase in the limiting composite unit [140], the equivalent conductivity bounds σ_3^a and σ_c^a of the two limiting cases mentioned above, can be calculated according to a simplified form of Nakamura's equations [141,142]

$$\sigma_3^a = \sigma_3 \left[(d-1) - (d-1)V_c \right] / (d-1+V_c) = 2\sigma_3 (1-V_c)/(2+V_c) \qquad (2.30a)$$

$$\sigma_c^a = \sigma_c (d-1)V_c / (d-V_c) = 2\sigma_c V_c / (3-V_c) \qquad (2.30b)$$

where $V_c = V_2/Y$, is the volume fraction of composite units, V_2 is the volume fraction of dispersed grains in the bulk electrolyte, σ_3 is the conductivity of the matrix polymeric

electrolyte and d is the dimensionality of the system (d = 3 for spherical grains). After introducing the improved conductivity parameters (equation (2.30)) in the self consistent EMT equation suggested by Kirpatrick [143], the conductivity σ_m of the composite electrolyte can be expressed as

$$\left(\frac{V_2}{Y}\right)(\sigma_c^a - \sigma_m)\Bigg/\left[\sigma_c^a + \left(\frac{1}{p_c}-1\right)\sigma_m\right] + \left(\frac{1-V_2}{Y}\right)(\sigma_3^a - \sigma_m)\Bigg/\left[\sigma_3^a + \left(\frac{1}{p_c}-1\right)\sigma_m\right] = 0 \quad (2.31)$$

$$\frac{V_2/Y(\sigma_c^a - \sigma_m)}{[\sigma_m + p_c(\sigma_c^a - \sigma_m)]} + \frac{(1-V_2/Y)(\sigma_3^a - \sigma_m)}{[\sigma_m + p_c(\sigma_3^a - \sigma_m)]} = 0 \quad (2.32)$$

where p_c is the continuous percolation threshold for the composite grains. Since the composite grains are allowed to overlap in the region of interface layer, p_c can be taken to be 0.28 for this random mixture on the basis of general percolation theory [141,144].

According to equation (2.32) one arrives at the highest enhancement in ionic conductivity when the composite units fill the total volume of the electrolyte, i.e., when $V_c=1$. This occurs for a characteristic value of $V_2 = V_2^*$ given by

$$V_2^* = \left(1 + \frac{t}{R}\right)^{-3} \quad (2.33)$$

For concentrations of filler exceeding V_2^*, the quasi two-phase system consists of a mixture of composite grains and dispersed bare insulating grains and no matrix electrolyte other than that present in the composite units. For such a situation, equation (2.32) can be rewritten in the following form

$$\frac{(1-V_2)(\sigma_c^b - \sigma_m)}{[\sigma_m + P_c(\sigma_c^b - \sigma_m)]} + \frac{(V_2 - V_2^*)(\sigma_2^b - \sigma_m)}{[\sigma_m + P_c(\sigma_2^b - \sigma_m)]} = 0 \quad (2.34)$$

where σ_c^b and σ_2^b (the modified conductivity parameters for the second limiting case) are calculated according to the method proposed by Nan [141] and Nakamura [142].

$$\sigma_c^b = 2\sigma_c (1 - V_2 + V_2^*)/[2(1 + V_2) - V_2^*] \qquad (2.35a)$$

$$\sigma_2^b = 2\sigma_2 (V_2 - V_2^*)/[3 - V_2 + V_2^*] \cdot \qquad (2.35b)$$

Equations (2.35a) and (2.35b) also consider local field effects. Here P_c is the percolation threshold of the dispersed bare insulating grains which do not overlap. Therefore P_c in equation (2.34) is different from the p_c in equation (2.32) and has been taken as the percolation threshold for a general random mixture, i.e., 0.15 [140,141]. Equations (2.32) and (2.34) are used to calculate the conductivity σ_m of composite polymer electrolytes.

This model is valid only at temperatures lower than the melting point of the crystalline PEO phase. Above the melting point of the crystalline PEO phase the conductivity of the matrix polymer ionic conductor is equal to the conductivity of its amorphous phase. Hence equations (2.30a) and (2.32) should be rewritten in the following form

$$\sigma_3^a = \sigma_{am}[(d-1) - (d-1)V_c]/(d-1+V_c) = 2\sigma_{am}(1-V_c)/(2+V_c) \qquad (2.36)$$

$$V_2/Y(\sigma_c^a - \sigma_m)/\sigma_m + p_c(\sigma_c^a - \sigma_m)] + (1 - V_2/Y)(\sigma_{am}^a - \sigma_m)/[\sigma_m + p_c(\sigma_{am}^a - \sigma_m)] = 0 \qquad (2.37)$$

Here σ_{am} is the conductivity of the polymer matrix equal to the conductivity of the amorphous polymer phase in this temperature (above the melting temperature of PEO, i.e., > 60 °C) range. It can be observed that in this temperature range two different approaches should be considered. The first is to consider the conductivity of the amorphous interface layer which is the same as for the amorphous phase of the matrix polymer ionic conductor. Generally the properties of the coating layer are different from those of the amorphous electrolyte phase, since the filler has an effect on the coating layer conductivity. The system is then treated as a mixture of two amorphous phases and its conductivity is calculated according to equations (2.34) and (2.37).

The applicability of the model presented above has been tested by Wieczorek and co-workers [135,136,145-148] for PEO based composite polymer electrolytes with dispersed inorganic and organic fillers. They found that for volume fraction of dispersed phase greater than V_2^*, the conductivity drops more rapidly than predicted by the model presented above. It has been shown that the t/R ratio decreases for concentrations of filler exceeding V_2^*, i.e., the concentration for which the maximum of conductivity is reached. Moreover, conductivity of an interface amorphous layer changes with the change of filler concentration. With the help of DSC data it was shown that T_g of the composite electrolyte varies with filler concentration. Since the structure of interface layer is highly amorphous, the temperature dependence of conductivity would follow the VTF relation

$$\sigma = AT^{-1/2} \exp(-E_a' / k(T - T_0))$$
(2.38)

where E_a' is a pseudo-activation energy for conduction, A is a pre-exponential factor and T_0 is a quasi equilibrium glass transition temperature usually 20-50 K lower than T_g. It was also assumed that the pseudo-activation energy E_a' and the pre-exponential factor A were independent of the concentration of fillers. Therefore, the interface layer conductivity is only dependent on T_0 and decreases with an increase in T_g. The T_g values taken from DSC experiments were used for calculation of interface layer conductivity (σ_1) for electrolytes with different concentrations of filler. To generalize the variation in T_g on the basis of the work of Bares [149] and Schneider and diMarzio [150] have proposed following empirical equation for the T_g of immiscible blends and mixed phase system

$$T_g = K_0 + K_1[f(V_2 / S_2)] + K_2[f(C_s, V_2)]$$
(2.39)

where V_2 and S_2 are respectively the volume fraction and surface area of the filler, C_s is the molar concentration of the dopant salt in the complex, and K_0, K_1, K_2 are adjustable parameters. It has been found that for a system with different concentrations of filler additive and a fixed concentration of dopant salt, the best fit to the experimental data can be obtained when T_g is approximated by the relation

$$T_g = K_0 + K_1 V_2 + K_2 V_2^2 \qquad (2.40)$$

In this equation, the effect of salt is included in K_0 which is identical to the T_g for pristine (without filler) polymer electrolyte. K_1 describes the influence of filler added on T_g of the composite system and K_2 is connected with polymer-filler-salt interaction.

On the other hand, estimation of the t/R parameter is based on the assumption that an increase in amorphous phase content for the composite electrolyte in comparison to the pristine system is due to the amorphous phase present in the surface layer. Therefore on the basis of equation (2.29), the volume fraction of this component and hence the t/R parameter can be approximated [136] as

$$1/(1 + t/R)^3 = V_2/(V_1 + V_2)$$

$$\text{or,} \quad R = \{(V_2 + V_1)/V_2\}^{1/3} - 1 \qquad (2.41)$$

where V_2 is the volume fraction of filler and V_1 is the volume fraction of surface layer.

The inclusion of variation of T_g and t/R parameters with filler concentration in the model for the calculation of the composite electrolyte conductivity has been found to fit well with the experimental results for a series of composite polymer electrolytes [146,148,151].

CHAPTER III

EXPERIMENTAL DETAILS

3.1 Parent Materials

Poly(vinylidene fluoride) PVDF ($M_W \approx 275000$) and Poly(vinylidene fluoride-co-hexafluoropropylene) P(VDF-HFP) ($M_W \approx 400000$) polymers were procured from Aldrich Chemicals Inc. (USA). Poly(methyl methacrylate) PMMA ($M_W \approx 15000$) polymer was obtained from Himedia (India). Three lithium salts, lithium perchlorate ($LiClO_4$), lithium trifluoromethane sulfonate ($LiCF_3SO_3$) and lithium hexafluoroarsenate ($LiAsF_6$) were obtained from Aldrich Chemicals Inc. Organic solvents, propylene carbonate (PC), diethyl carbonate (DEC) and dimethyl sulfoxide (DMSO) were procured from E-Merck (Germany). Fumed silica (SiO_2) having surface area ~ 380 m^2/g obtained from Aldrich Chemicals Inc. was heated upto 400 °C for 2 hours to remove the traces of water content. It is an amorphous, non-porous form of silicon dioxide and is electrochemically inert. Titania (TiO_2) powder having particle size ~ 1-10 μm was obtained from E-Merck and was used as-received. Common organic solvents acetone and tetrahydrofuran were also obtained from E-Merck.

PVDF   P(VDF-HFP)   PMMA
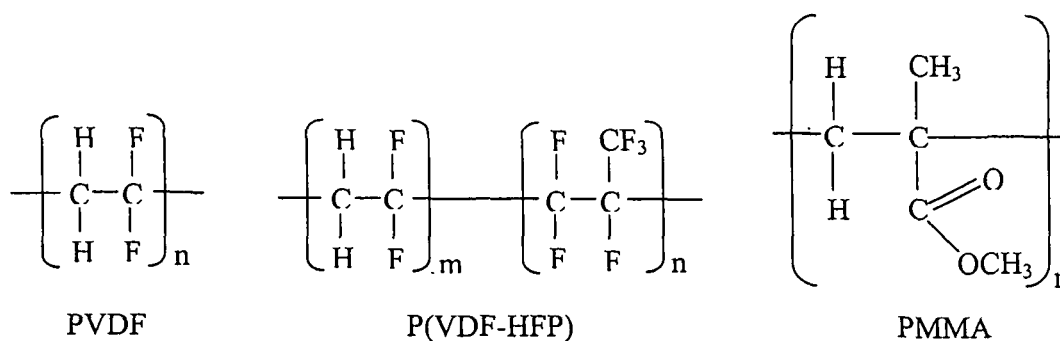
Figure 3.1: Chemical structure of different polymers used in the present work.

Figures 3.1 and 3.2 show the structure of polymers and solvents respectively used to fabricate polymer electrolytes. Tables 3.1, 3.2 and 3.3 show the basic physical properties of polymers, solvents and salts respectively.

Propylene carbonate   Diethyl carbonate
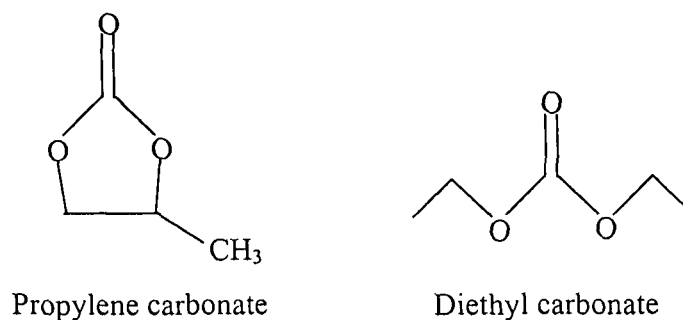
Figure 3.2: Chemical structure of solvents used in the present work.

Table 3.1: Some physical properties of polymers used to synthesize polymer electrolytes.

Polymer	Glass transition temperature T_g (°C)	Melting point mp, (°C)	Tensile strength N/mm²	Dielectric constant at 1 MHz	Density (gm/cm³)	Water absorption @ 24 hrs
PVDF	- 40 – (-30)	170	30-50	8.5	1.77	<0.03%
P(VDF-HFP)	-100 – (-90)	140	28-41	7.5	1.78	<0.04%
PMMA	105	160	2.9-3.3	2.9	1.19	0.3%

Table 3. 2: Some physical properties of organic solvents used to synthesize polymer gel electrolytes.

Solvents	Mol. weight	Melting point (°C)	Boiling point (°C)	Viscosity η at 25 °C (mPa. s)	Density ρ (g cm⁻³)	Dielectric constant ε
Propylene carbonate (PC)	102.09	- 48.8	242	2.53	1.2047	64.6
Diethyl carbonate (DEC)	118.13	- 43.0	126	0.748	0.9752	2.82

Table 3.3: Some physical properties of inorganic salts used to synthesize gel polymer electrolytes.

Salts	Mol. weight	Melting pt. (°C)	Lattice energy (kJ/mol)	Density ρ (gm cm^{-3})
LiClO$_4$	106.39	236	723	2.42
LiCF$_3$SO$_3$	156.01	~ 300	~ 916	0.64
LiAsF$_6$	195.85	~ 350 (decomposed)	~ 1074	2.68

3.2 Sample Preparation

Polymer electrolyte films were synthesized by solution casting technique consisting of the following steps:

(i) PVDF polymer as required was dissolved in dimethyl sulfoxide (DMSO).

(ii) P(VDF-HFP) and PMMA polymers were dissolved in acetone or tetrahydrofuran.

(iii) Salts LiClO$_4$, LiCF$_3$SO$_3$ and LiAsF$_6$ were dissolved in propylene carbonate (PC) and/or diethyl carbonate (DEC). PC has high dielectric constant (ε = 64.6) but has high viscosity (η = 2.53) also, whereas DEC has low dielectric constant (ε = 2.82) but has low viscosity (η = 0.748). PC+DEC (50% by volume each) solvent was used as a compromise for high dielectric constant and low viscosity to achieve high ionic conductivity.

(iv) Both polymer and salt solution were mixed together in a beaker and magnetically stirred during continuous heating for 12-14 hours at 50 °C.

(v) Ceramic filler was added to the above polymer-salt solution as required and continuously heated and stirred at 50 °C for 12 – 14 hours to make the solution homogeneous and viscous.

(vi) Above viscous solution was then cast on glass plates/patri dishes and allowed to dry at room temperature.
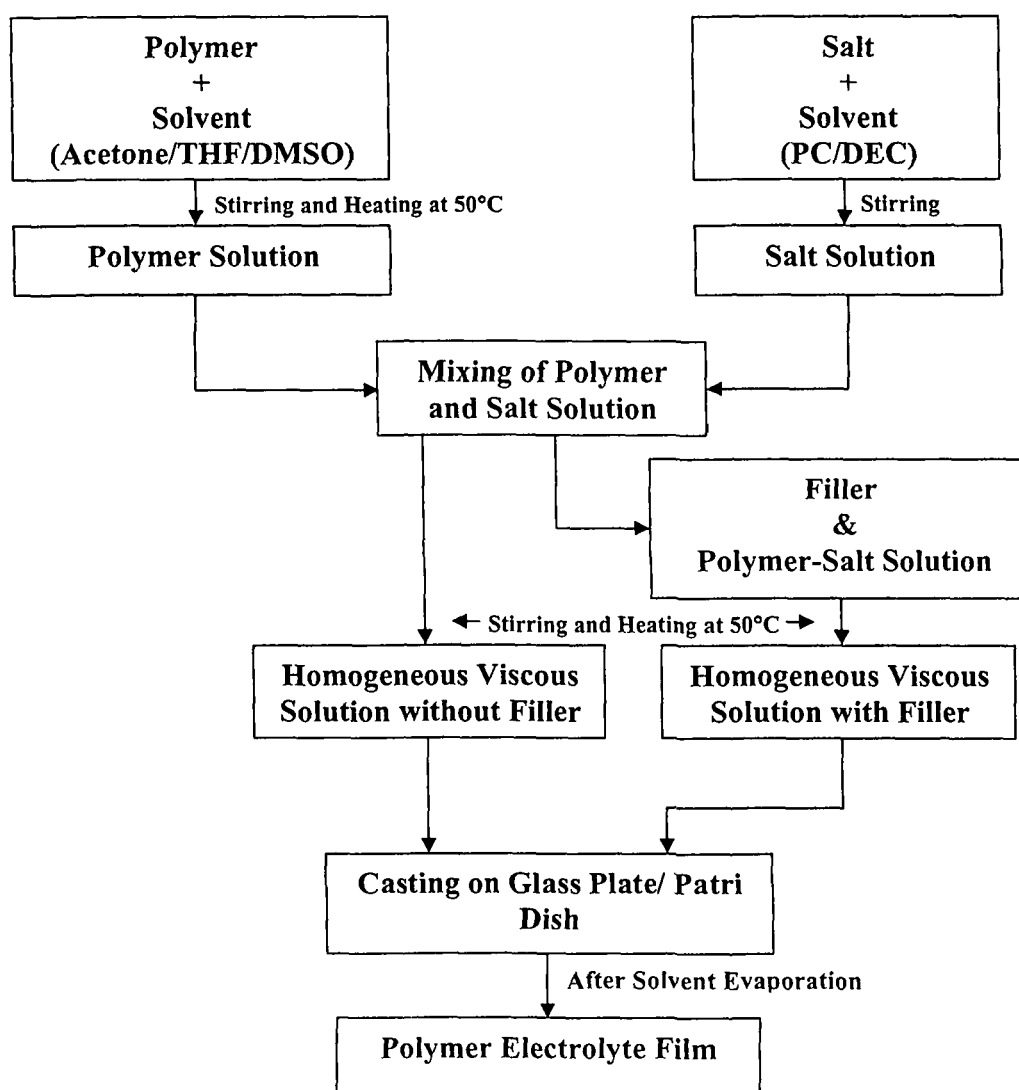
Figure 3.3: Block diagram of solution casting technique of sample preparation.

Figure 3.3 shows the block diagram of the solution casting technique. This procedure provided mechanically stable, free standing and flexible films of thickness in the range of 30 μm – 1mm.

3.3 Furnace and Temperature Controller

An indigenously built electrical resistive heating furnace comprising of an insulated heating element (Kanthal) uniformly wound on a alumina tube has been used. The resistance of the heating element was 30 Ω. High temperature cement was applied over the windings to fix them in place. This tube was kept in cylindrical stainless steel container with one end closed, and the space between the tube and wall of the container was filled with glass wool and plaster of paris to make it perfectly insulating to prevent heat loss. The top end was covered by fixing a circular asbestos followed by a wooden plate.

A PID type temperature controller (Nutronics, Model pp-3040) and a chromel-alumel thermocouple were used to control and measure the furnace temperature respectively. The temperature was controlled to within ± 1 °C.

3.4 Sample Holder

Figure 3.4 shows the schematic diagram of the sample holder made up of stainless steel/copper and a polymer (PVC) block. A stainless steel (SS)/Cu rod fixed with stainless steel/Cu base plate was passed through the centre hole of the PVC block and fixed with a nut. Four stainless steel/copper rods were fixed on the four corners of the PVC block such that it touches the base plate. Spring arrangement was attached with lower part of each of the four rods to apply uniform pressure due to spring action to ensure a firm contact between the electrodes and the sample. In this sample holder conductivity measurement on four samples

can be done simultaneously. These four rods and the base plate serve as blocking electrodes in measuring the ionic conductivity. The diameter of the bottom disc is ~ 1 cm. The sample is placed between the rod and base plate as shown in the figure 3.4.

Figure 3.4: Stainless steel sample holder for ionic conductivity measurement.

3.5 Conductivity Measurements

Figure 3.5 shows the set-up for conductivity measurements employed in this work. Hioki 3532-50 LCR HiTester has been employed for the complex impedance (modulus Z and phase angle θ) measurements. The instrument is interfaced with a computer to collect the data. It has a built-in frequency synthesizer and has a frequency range from 42 Hz to 5 MHz.

The impedance measurements were carried out at a temperature interval of 10 °C from room temperature to 100 °C. Sufficient time was allowed at each temperature for thermal

can be done simultaneously. These four rods and the base plate serve as blocking electrodes in measuring the ionic conductivity. The diameter of the bottom disc is ~ 1 cm. The sample is placed between the rod and base plate as shown in the figure 3.4.

Figure 3.4: Stainless steel sample holder for ionic conductivity measurement.

3.5 Conductivity Measurements

Figure 3.5 shows the set-up for conductivity measurements employed in this work. Hioki 3532-50 LCR HiTester has been employed for the complex impedance (modulus Z and phase angle θ) measurements. The instrument is interfaced with a computer to collect the data. It has a built-in frequency synthesizer and has a frequency range from 42 Hz to 5 MHz.

The impedance measurements were carried out at a temperature interval of 10 °C from room temperature to 100 °C. Sufficient time was allowed at each temperature for thermal

equilibration and reproducibility of the data. The ionic conductivity was subsequently obtained from

$$\sigma = \frac{L}{R_b A}$$

where L is the thickness and A is the cross-sectional area of the polymer electrolyte sample disc. R_b is the bulk resistance obtained from the complex impedance plot.

Figure 3.5: Conductivity measurement set-up.

3.6 Transport Number Measurements

Total ionic transference number of the gel polymer electrolytes was measured by Wagner's polarization technique [152,153] which is used to determine the ionic contribution to the total charge transport by measuring the residual electronic current passing through the electrolytes. The Wagner polarization cell Ag/polymer gel electrolyte/Ag was prepared to measure the transport number. A fixed small dc potential (300 mV) was applied across the blocking electrodes and the current passing through the cells was measured as a function of

time for five hours to allow the samples to become fully polarized. Initial total current (I_T) which is the sum of ionic (I_i) and electronic (I_e) currents ($I_T = I_i + I_e$), and final current after polarization which is only the electronic current I_e were measured. The transference numbers (t_{ion} and t_{ele}) have been calculated using the relations

$$t_{ion} = \frac{I_i}{I_{total}} = \frac{I_T - I_e}{I_T}$$

$$t_{ele} = \frac{I_e}{I_T}$$

3.7 Differential Scanning Calorimetry (DSC)

Differential Scanning Calorimeter (DSC) measures the amount of energy (heat) absorbed or released by a sample as it is heated, cooled, or held at a constant temperature. Typical applications of DSC include determination of melting point, glass transition temperature, curing and crystallization studies, identification of phase transformations and enthalpy of phase transitions. In DSC measurement, heat flow into a sample usually contained in a small aluminum capsule or pan is measured differentially, i.e. by comparing it to the flow into an empty reference pan. Both sample and the reference are heated uniformly at a constant rate. The difference in heat input is then plotted as a function of temperature to produce a trace. First order transitions which involve a latent heat produce peaks on a DSC trace. If part or all of a sample melts on heating, an endothermic peak is observed and if a sample recrystallizes on cooling an exothermic peak is produced. Second order transitions, which involve discontinuity in heat capacity at glass transition temperature T_g, show up as step. For a semi-crystalline polymer electrolyte containing several regions or phases, DSC can provide a range of useful information. An electrolyte contains amorphous, crystalline and high melting polymer-salt complex regions. Thermal behavior of these three regions is revealed by

48

DSC. Differential scanning calorimetry was carried out by Universal V2.5H TA instrument from room temperature to 400 °C at a constant heating/cooling rate of 10 °C/minute in nitrogen environment. Figure 3.6 shows the schematic diagram of the DSC set up used in the present work.
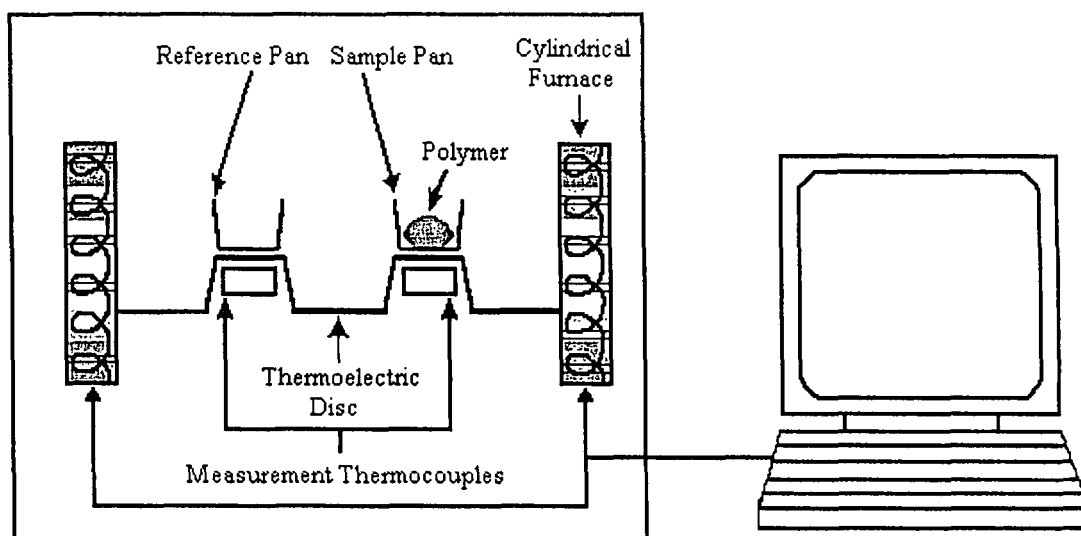
Figure 3.6: Schematic diagram of DSC setup.

3.8 Fourier Transform Infrared Spectroscopy (FTIR)

Fourier transform infrared (FTIR) spectroscopy is a powerful analytical tool for characterizing and identifying organic molecules, chemical bonds (functional groups) and the molecular structure of organic compounds. The wavelength of infra red radiation absorbed is characteristic of stretching/bending vibrational mode of a chemical bond. FTIR spectra of pure compounds are generally so unique that they are like a molecular fingerprint. FTIR spectra of polymer electrolyte samples were studied using a high performance Nicolet Impact 410 FTIR spectrophotometer with a resolution of 1 cm^{-1} in the mid IR region of 4000 – 400

49

cm^{-1}. In the present work FTIR was used to investigate polymer-salt-filler interactions in the polymer electrolyte systems.

3.9 X-ray Diffraction (XRD)

X-ray diffraction is one of the most important structural characterization tools used in materials science. X-ray diffraction patterns give information about different crystal parameters like crystallite size, d-spacing, diffraction planes, structure, phase and lattice constants. The intensities and the angles of diffracted X-ray beams are related to atomic arrangement of the crystal. XRD is mainly used to measure the degree of crystallinity of the polymer electrolyte samples which is an important parameter affecting the ionic conductivity. X-ray diffraction patterns for various polymer electrolyte samples have been recorded using the Philips X'pert Pro Diffractometer employing Cu K_α radiation. The generator was operated at 30 kV and 20 mA and scanning speed was fixed at 2 °/min in 2θ varying from 3° to 100°.

Degree of crystallinity

Generally a polymer is neither fully crystalline nor fully amorphous. The degree of crystallinity of a polymer can be measured by X-ray diffraction. A typical X-ray diffractogram consists of a plot of X-ray counts received by a detector versus the scattering angle of the detector as shown in figure 3.7.
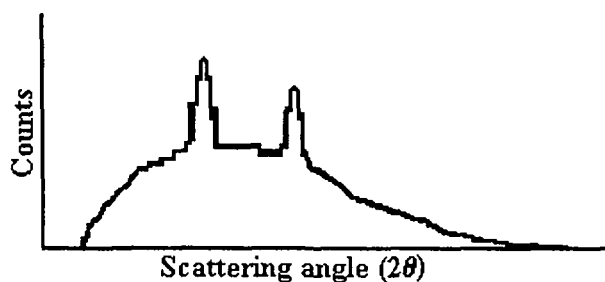
Figure 3.7: Typical X-ray diffractogram.

Depending upon its degree of crystallinity typical X-ray diffractogram of a polymer sample has sharp peaks superimposed on a broad amorphous hump as shown in figure 3.8. Total area under the diffractogram is the sum of the crystalline peaks and broad amorphous hump.
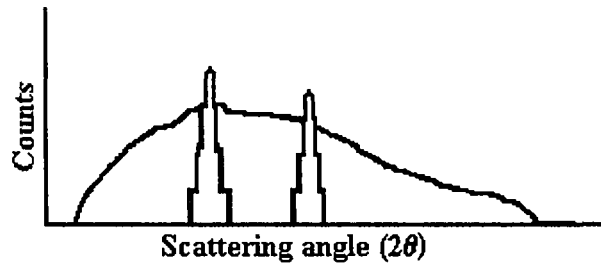
Figure 3.8: XRD pattern with crystalline peaks and amorphous hump.

For example, if a typical X-ray diffractogram has two crystalline peaks with areas A1 and A2 superimposed on a broad amorphous hump with an area of A3, then the degree (percentage) of crystallinity, K, of the polymer will be

$$K = \frac{A1 + A2}{A1 + A2 + A3} \times 100 = \frac{S}{S_0} \times 100$$

where S is the sum of areas of all the crystalline peaks and S_0 is the sum of areas of crystalline peaks and amorphous hump i.e. total area under the diffractogram. Area has been calculated by dividing the X-ray diffractogram into minute square $(0.5 \times 0.5 \ mm^2)$ grids and counting the number of grids.

The amount of crystallinity in a polymer depends on the following parameters:

❖ the secondary valence bonds which can be formed

❖ the structure of the polymer chain (degree of order)

❖ the physical treatment of the polymer

❖ the thermal history of the polymer

❖ the molecular weight of the polymer

3.10 Scanning Electron Microscopy (SEM)

The scanning electron microscope (SEM) is one of the most versatile instruments available for the examination and analysis of microstructural and morphological features of solid objects. The primary reason for the usefulness of SEM lies in its high depth of focus and high resolution that can be obtained when bulk objects are examined. The SEM study was carried out using JEOL JSM-35CF, scanning electron microscope with resolution 5 – 15 nm to examine the surface morphology, porosity and distribution of filler particles in the gel polymer electrolytes. The equipment has a range of magnification from 10X to 180,000X. Each specimen was gold coated using a sputtering unit (International Scientific Instruments PS-2 coating unit) before taking the micrographs. The micrographs were taken at 20 kV accelerating voltage and magnification was fixed according to need from 3000X to 10000X.

3.11 Swift Heavy Ion (SHI) Irradiation

Swift heavy ion irradiation of polymer electrolyte samples was carried out at Nuclear Science Centre, New Delhi. Irradiation experiments were performed in Material Science (MS) and General Purpose Scattering Chamber (GPSC) beam lines. For ion irradiation, the polymer electrolyte samples were cut in 1cm × 1cm area and fixed on sample holder (ladder) made up of copper (in MS) and Stainless Steel (in GPSC). Material Science ladder is rectangular and 24 samples can be loaded at a time with six samples each side. GPSC ladder is hexagonal and 36 samples can be loaded in a single run. The samples were put in the respective MS and GPSC vacuum chamber. Figures 3.9 and 3.10 show the MS and GPSC beam lines and chambers respectively. The samples during ion irradiation and ladder movement (up, down and rotation) were monitored and controlled from control room.

52

Parameters Related to Ion Irradiation:

Fluence (ϕ)

It is defined as the total number of irradiating ions incident per square centimeter (ions/ cm^2) of sample. It varies from sample to sample depending upon its size and material.

Fluences are calculated using the following formula

$$\text{Fluence}(\phi) = \frac{\text{Time (t)} \times \text{Beam Current} \times \text{pnA}}{\text{Ch arg e State}}$$

Beam currents for ion irradiation experiments are usually taken in the range of 2-5 nA.

$$1 \text{ pnA (particle nano} - \text{ampere)} = \frac{10^{-9} \text{Coul/sec}}{1.6 \times 10^{-19} \text{Coul}} = 6.25 \times 10^9 \text{particles/sec}$$

Count

During ion irradiation process, fluences are recorded by using a counter. Following relation relates the counts and the fluences

$$\text{Counts} = \frac{\phi \, q \, e}{S}$$

where ϕ is the fluence,

q is the charge state of ion beam,

e is the electronic charge (1.6×10^{-19} coulomb),

S is the scale of counter

Beam Energy

The energy of the acclerated ion beam depends on charge state (q) of the ion and the terminal potential V_T

$$E \text{ (MeV)} = (q + 1) V_T + V_{inj}$$

For the 15 UD Pelletron at Nuclear Science Centre, New Delhi, India the terminal potential V_T is in the range of 10 MV to 15 MV and Injector potential (V_{inj}) is in the range of 250 to 350 keV. The projected range of Li^{3+} and C^{5+} ion beams used in the present work was calculated by SRIM-98 code (SRIM-Stopping and Ranges of Ions in Matter) [154]. Table 3.4 gives the incident energy, corresponding electronic and nuclear energy losses and projected range obtain from SRIM-98 code for Li^{3+} and C^{5+} ion beams.

Table 3.4: Different parameters calculated by SRIM-98 code

Ion and Ion Energy	Electronic Energy Loss (S_e) (eV/Å)	Nuclear Energy Loss (S_n) (eV/Å)	Projected Range (μm)
Li^{3+}, 48 MeV	6.406×10^0	3.15×10^{-3}	453.77
C^{5+}, 70 MeV	2.879×10^1	1.439×10^{-2}	155.37

The thicknesses of the polymer electrolyte samples (10 - 30 μm) were kept less than the range calculated by SRIM programme so that all the incident ions cross the sample.
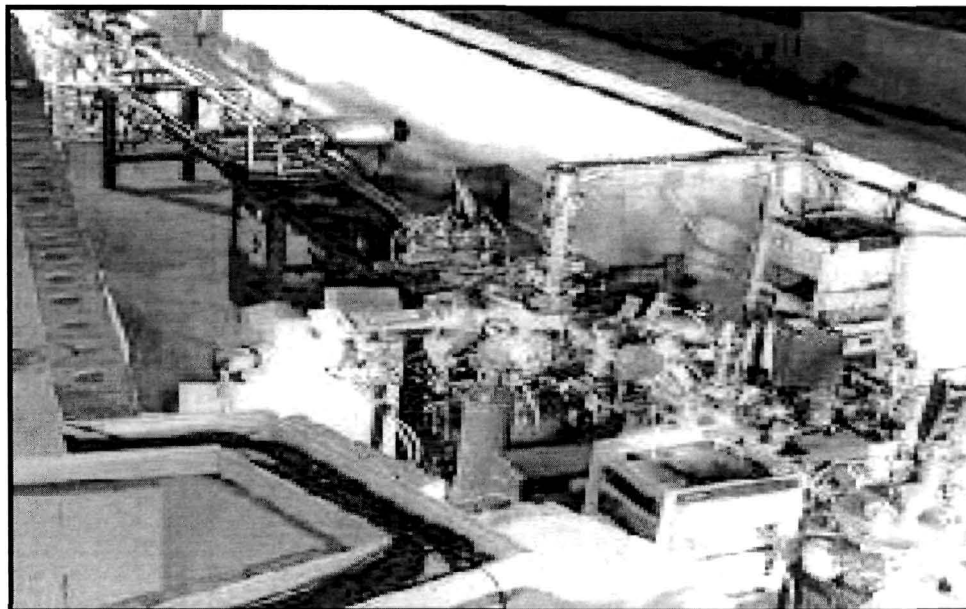
Figure 3.9: Material Science Beam Line and Chamber.
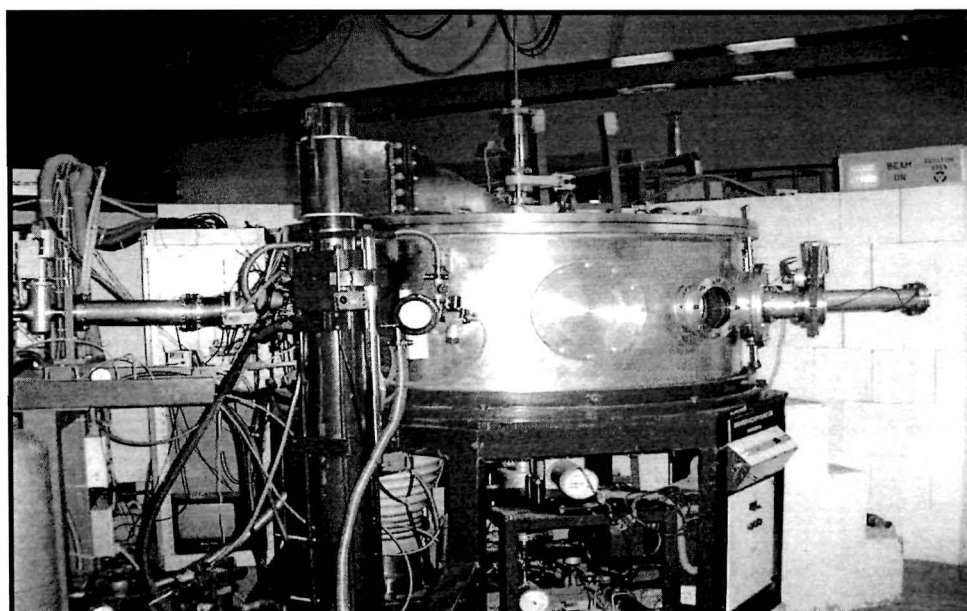
Figure 3.10: GPSC Beam Line and Chamber.

CHAPTER IV

[PVDF/P(VDF-HFP)]-(PC+DEC)-LiClO$_4$ GEL POLYMER ELECTROLYTE SYSTEMS

Polymer gel electrolytes have recently come into focus as useful electrolytes for rechargeable lithium batteries [69,155-158]. In these two phase hybrid electrolyte systems, the polymer matrix provides the system with mechanical strength, while the ionic conduction essentially occurs through the liquid electrolyte phase giving conductivities of the order of 10^{-3} S/cm, close to the values of pure liquid electrolytes. The challenge is to optimize all the components in order to achieve the best combination of constituents for a given application. The matrix should be almost inert with respect to ionic entities such that the ion transport is not disturbed. However, interactions between the components in the gel which are too weak might lead to phase separation.

All the gel polymer electrolyte samples were prepared by solution casting technique as described in Chapter III. For PVDF-(PC+DEC)-LiClO$_4$ system, appropriate amount of the polyvinylidene fluoride (PVDF) polymer was dissolved in dimethyl sulfoxide (DMSO) while stirring. The solvent, propylene carbonate (PC) and diethyl carbonate (DEC) were chosen because of their high dielectric constant, low viscosity, high boiling point and low melting point [88]. When the boiling point of a plasticizer is high, the evaporation of the liquid electrolyte i.e. syneresis will be small. High dielectric constant of propylene carbonate (PC, $\epsilon = 64.4$) enables to dissociate the salt into ions easily. Low viscosity of diethyl carbonate (DEC, $\eta = 0.748$) gives rise to high ionic mobility. The salt, lithium perchlorate (LiClO$_4$) was used due to low dissociation energy (723 kJ mol^{-1}) [159] so that it easily dissociates in the solvents (PC+DEC). Organic liquid electrolyte solutions comprising of LiClO$_4$ and

(PC+DEC) were mixed with PVDF solution while stirring at 50 °C. Samples were prepared by varying plasticizer – salt ratio. The resulting viscous solution was cast onto glass plates and patri dishes to get electrolyte films of different thicknesses (30 μm – 1mm).

When PVDF, a semicrystalline polymer, is copolymerized with hexafluropropylene (HFP), the degree of crystallinity of the resulting co-polymer is greatly reduced due to steric hindrance provided by bulky –CF_3 pendant group of HFP structural unit. This considerably enhances the plasticity of the copolymer as compared to PVDF. For P(VDF-HFP)-(PC+DEC)-$LiClO_4$ gel polymer electrolyte system, P(VDF-HFP) copolymer was dissolved in tetrahydrofuran (THF). $LiClO_4$ and (PC+DEC) were added as described for previous system to get polymer gel electrolyte film.

A comparative study has been carried out between PVDF polymer and P(VDF-HFP) copolymer based gel electrolytes with regard to their ionic conduction behavior. Ionic conductivities of PVDF-(PC+DEC)-$LiClO_4$ and P(VDF-HFP)-(PC+DEC)-$LiClO_4$ polymer gel electrolyte systems have been measured by complex impedance analysis described in Chapter II (section 2.1). Wagner's polarization method has been employed to measure transference number. XRD and FTIR studies have been conducted to investigate the crystallinity and ion-polymer interaction in the polymer gel electrolytes. Microstructural studies by SEM have been done to analyze the surface morphology of PVDF-(PC+DEC)-$LiClO_4$ and P(VDF-HFP)-(PC+DEC)-$LiClO_4$ systems. The results of various studies on PVDF-(PC+DEC)-$LiClO_4$ and P(VDF-HFP)-(PC+DEC)-$LiClO_4$ gel polymer electrolyte systems are presented in this Chapter.

4.1 Ionic Conductivity Measurements

The ionic conductivities of as-prepared gel polymer electrolytes were obtained from the complex impedance measurements as described in Chapter II. Figure 4.1 shows the complex impedance plot of PVDF-(PC+DEC)-LiClO₄ (25:70:5 wt%) gel polymer electrolyte at different temperatures. Z' and Z" represent the real and imaginary parts of the impedance data respectively at different temperatures. The ionic conductivity was then calculated from $\sigma = l/(R_b r^2 \pi)$, where l and r represent thickness and radius of the sample membrane discs respectively. R_b is the bulk resistance of the gel electrolyte obtained from complex impedance measurements. It is widely accepted that R_b could be obtained from the intercept on the real axis at the high frequency end of the Nyquist plot of complex impedance [159,160].
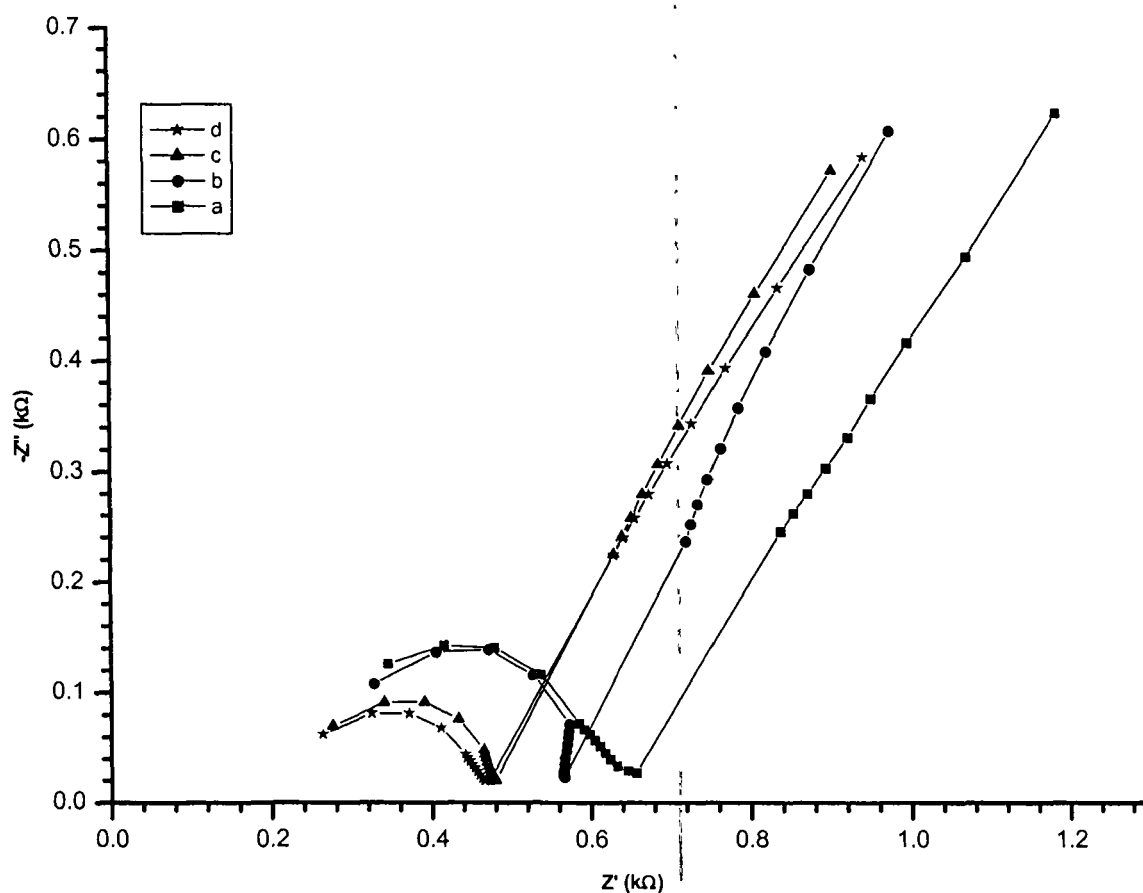
Figure 4.1: Temperature dependence of the complex impedance spectra of PVDF-(PC+DEC)-LiClO₄ (25:70:5 wt%) gel polymer electrolyte system. (a) 30°C, (b) 40°C, (c) 50°C, (d) 60°C.

Figure 4.2 shows the complex impedance spectra of P(VDF-HFP)-(PC+DEC)-LiClO₄ (25:60:15 wt%) gel polymer electrolyte system at different temperatures. According to the theoretical analysis given by Watanabe and Ogata [32] two semicircles should appear in impedance spectrum for a symmetric cell, i.e., one at higher frequencies corresponding to bulk electrolyte impedance and other at lower frequencies related to the interfacial impedance. Also it is reported [161-163] that high frequency semicircle does not appear in
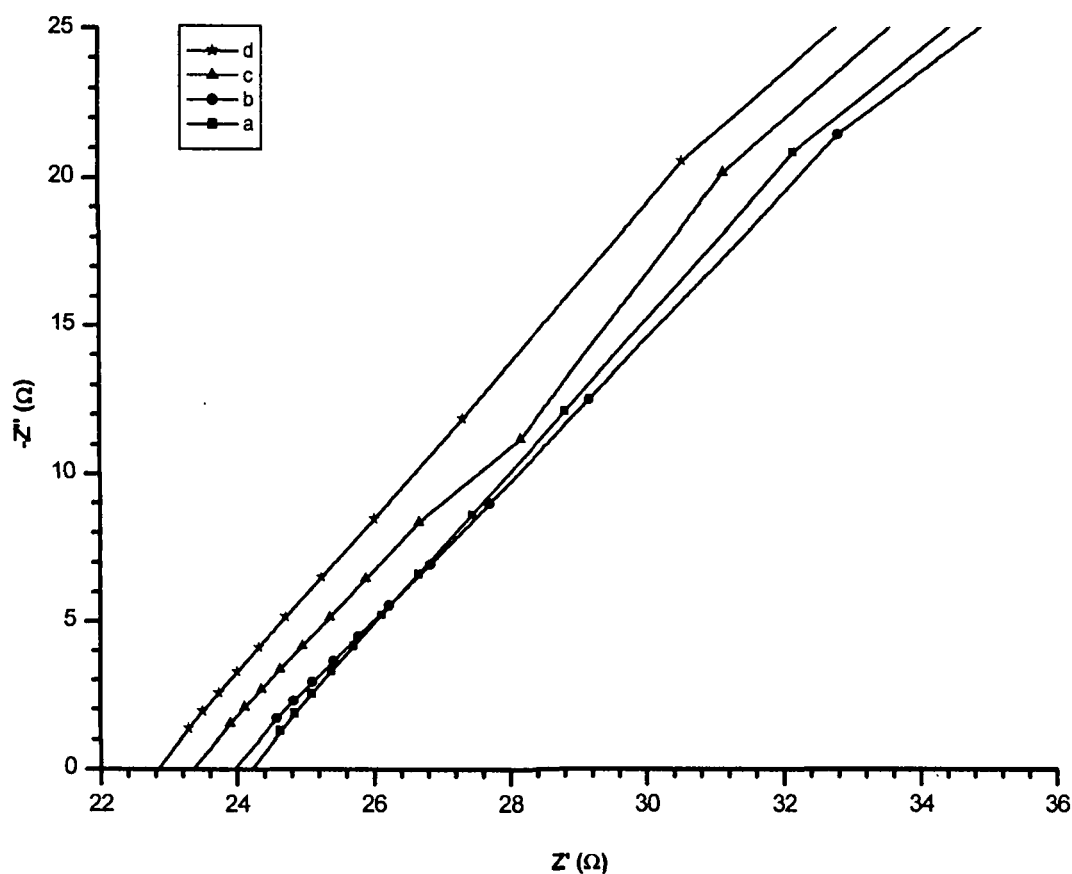
Figure 4.2: Temperature dependence of the complex impedance spectra of P(VDF-HFP)-(PC+DEC)-LiClO₄ (25:60:15 wt%) electrolyte system. (a) 30°C, (b) 40°C, (c) 50°C, (d) 60°C.

practical impedance plots for plasticized P(VDF-HFP) membranes as shown in figure 4.2. This phenomena is quite reasonable since the facile mobility in liquid and gel electrolyte systems, when compared with solid polymer electrolytes, indicates that ions possess small

dielectric relaxation times and hence the capacitive effect of the bulk electrolyte in the spectra are inconsequential [164]. In the lower frequency region inclined spike is observed instead of second semicircle since Cu electrodes which have been used in the present work, are perfectly blocking to lithium ions within the applied ac modulation range (0.01V). Causes responsible for ideality of the blocking electrodes commonly encountered in real measurements are still controversial, however surface roughness of the electrodes and the faradaic reaction occurring at the electrode/electrolyte interface seem to remain two preferential explanations [165]. High frequency region is independent of the electrode condition whereas the low frequency region behaves much like constant phase element (CPE) and is very sensitive to the roughness and electrode condition [164].

Figures 4.3 and 4.4 show the conductivity versus temperature inverse plots of PVDF and P(VDF-HFP) based gel polymer electrolytes respectively for different plasticizer-salt ratio with fixed amount of PVDF and P(VDF-HFP). It is evident from the figures that the ionic conductivity increases with the increase of salt concentration which leads to increase in carrier ion concentration in the systems. The same trend was observed for all the temperatures studied from 30 to 60 °C. The maximum on the conductivity-salt concentration curve may be explained in terms of formation of ion pairs. Up to the concentration level, corresponding to the conductivity plateau, more and more number of ions are made available for electrolytic conduction. At higher concentration in low dielectric media, essentially two types of ion pairs and solvated ion pairs are present [166].

These may be represented by the equilibria:

$$Li + S_n + ClO_4^- = (Li+)S_nClO_4^-$$

$$Li + S_n + ClO_4^- = (Li + ClO_4^-)S_{n-m} + S_m$$
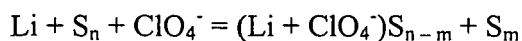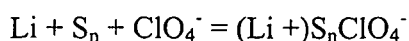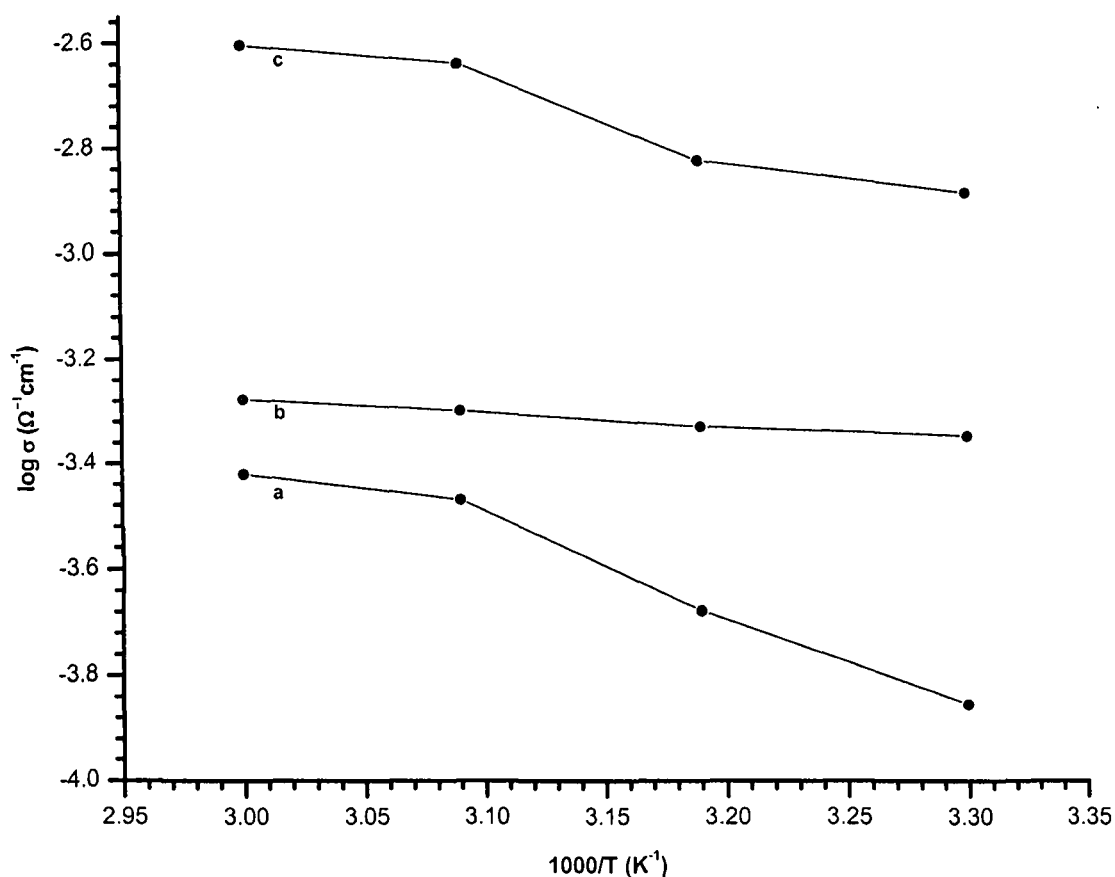
Figure 4.3: Temperature dependence of ionic conductivity of PVDF-(PC+DEC)-LiClO₄ gel polymer electrolyte system with composition (wt%), (a) 25:70:5, (b) 25:65:10 and (c) 25:60:15.

where S represents the solvating species. Re-dissociation of such ion pairs can occur due to long range coulombic forces giving rise to free ions, which contribute to conductance [167].

The high ionic conductivity in an electrolyte is obtained by increasing both ionic mobility and concentration of ionic charge carriers. The motion of ions in gel polymer electrolytes is liquid-like in which the movement of ions through the polymer matrix is assisted by the large amplitude segmental motion of the polymer backbone [168-170]. From the figures it is observed that ionic conduction in both PVDF and P(VDF-HFP) based gel polymer electrolyte systems obeys the VTF (Vogel-Tamman-Fulcher) relation [90-92], which describes the transport properties in a viscous matrix [171-174]. It supports the idea that the
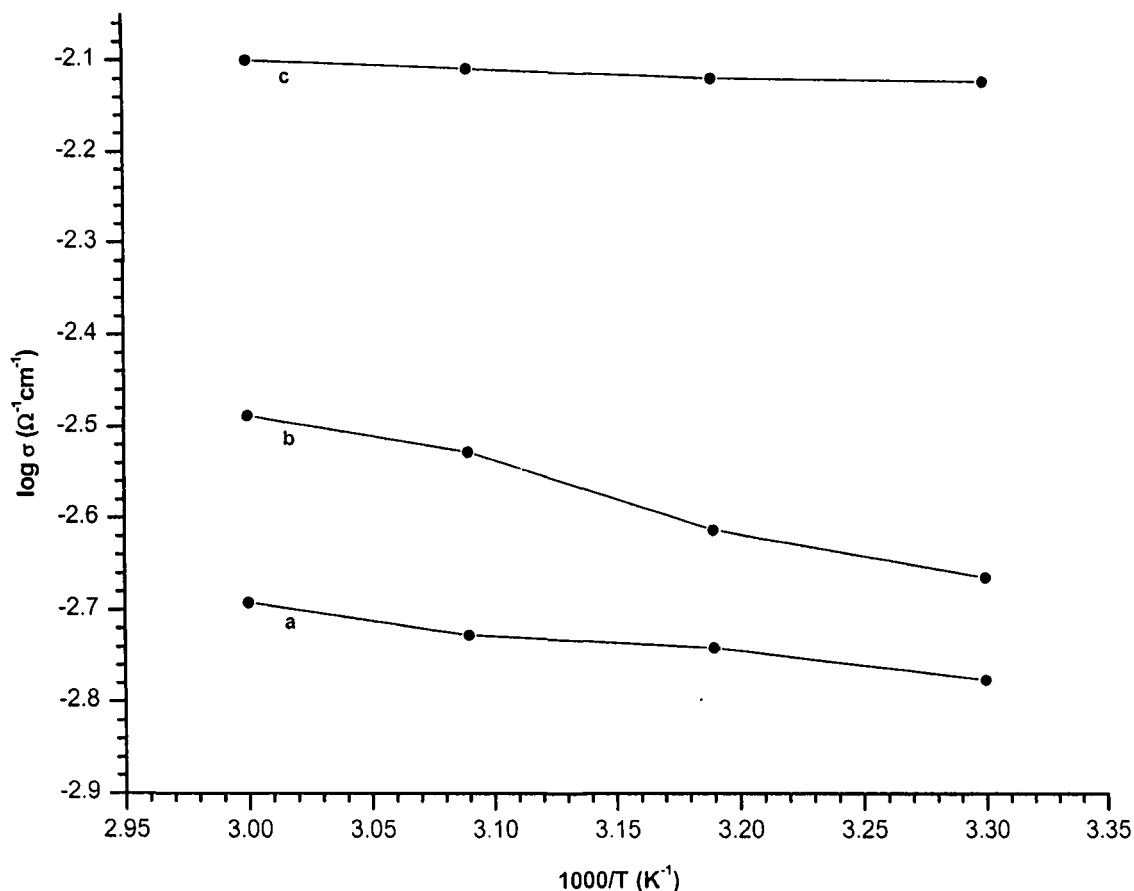
Figure 4.4: Temperature dependence of ionic conductivity of P(VDF-HFP)-(PC+DEC)-LiClO₄ gel polymer electrolyte system with composition (wt%), (a) 25:70:5, (b) 25:65:10 and (c) 25:60:15.

ions move through the plasticizer rich phase, which is conducting. If the conductivity versus temperature dependence curve is linear in larger temperature regime, then it is said to be Arrhenius. VTF (curved) behavior can be modeled as Arrhenius (linear) behavior by dividing the entire temperature range into smaller temperature regions. The interconnection between Arrhenius and VTF conductivity versus temperature behavior are widely reported and discussed in literature [93]. This behavior is rationalized by arguing that since VTF dependence is governed by the energy interval $k(T-T_0)$ and the Arrhenius dependence by energy kT (where k Boltzmann constant), for $T \gg T_0$ [94] i.e. when T_0 is quite smaller than T, the curvature of conductivity versus temperature plot becomes small and VTF equation

approaches Arrhenius equation. Free volume theory of Cohen and Turnbull [97] helps to understand the above behavior.

The conductivities for gel polymer electrolytes containing different weight ratios of PVDF, (PC+DEC) and $LiClO_4$ salt are presented in table 4.1. From the table it is observed that the highest conductivity ($\approx 1.3 \times 10^{-3}$ Scm^{-1}) composition at room temperature is 25 wt% PVDF, 60 wt% (PC+DEC) and 15 wt% $LiClO_4$.

Table 4.1: Conductivity of PVDF-(PC+DEC)-$LiClO_4$ gel polymer electrolyte at 303 K with varying composition (wt%).

PVDF	PC	DEC	LiClO₄	Conductivity (S cm⁻¹)
25	35	35	5	1.4×10^{-4}
25	32.5	32.5	10	4.5×10^{-4}
25	30	30	15	1.3×10^{-3}

The conductivity data of P(VDF-HFP) based gel polymer electrolytes containing different weight ratios of P(VDF-HFP), (PC+DEC) and $LiClO_4$ salt are presented in table 4.2. From the table it is seen that the highest conductivity ($\approx 7.5 \times 10^{-3}$ Scm^{-1}) composition at room temperature is 25 wt% P(VDF-HFP), 60 wt% (PC+DEC) and 15 wt% $LiClO_4$.

Table 4.2: Conductivity of P(VDF-HFP)-(PC+DEC)-$LiClO_4$ gel polymer electrolyte at 303 K with varying composition (wt%).

PVDF-HFP	PC	DEC	LiClO₄	Conductivity (S cm⁻¹)
25	35	35	5	1.7×10^{-3}
25	32.5	32.5	10	2.2×10^{-3}
25	30	30	15	7.5×10^{-3}

Higher conductivity in P(VDF-HFP) copolymer system could be attributed to the higher amorphicity due to steric hindrance provided by CF_3 pendant group in HFP monomer units which is randomly mixed with the VDF monomers in the polymer chain. Higher amorphicity

provides mobile Li^+ ion greater free volume giving rise to higher conductivity. On the other hand pure PVDF has higher degree of crystallinity because of single monomer throughout the polymer chain providing less free volume to the mobile ions, resulting in lower conductivity.

The mobility of ionic species is an important parameter to consider when designing new polymer electrolytes for batteries [175]. The concentration gradients formed, due to the non-unity transference number of lithium ions in polymer electrolytes, cause a decay of the current to lower steady state values. Thus, evaluation of polymer electrolytes requires consideration of transference numbers and ionic conductivities. Total ionic transference number of gel polymer electrolyte was measured by Wagner's polarization technique [152,153], which is used to determine the ionic contribution to the total charge transport by measuring the residual electronic current passing through the electrolyte. Ionic transference number of PVDF-(PC+DEC)-LiClO₄ and P(VDF-HFP)-(PC+DEC)-LiClO₄ gel polymer electrolyte (GPE) systems with varying compositions was measured with Ag/GPE/Ag as described in Chapter III (section 3.6). The ionic transference number was calculated using the relation

$$t_i = \frac{I_i}{I_{total}} = \frac{I_T - I_e}{I_T}$$

Tables 4.3 and 4.4 show the ionic transference number for the Ag/Electrolyte/Ag cell system using PVDF and P(VDF-HFP) based gel polymer electrolytes.

Table 4.3: Ionic transference numbers of PVDF-(PC+DEC)-LiClO₄ gel polymer electrolyte.

Gel Polymer Electrolyte System (GPE) PVDF-(PC+DEC)-LiClO₄ (wt%)	Transference Numbers
25:70:5	0. 89
25:65:10	0.89
25:60:15	0.90

Table 4.4: Ionic transference numbers of P(VDF-HFP)-(PC+DEC)-LiClO₄ gel polymer electrolyte.

Gel Polymer Electrolyte System (GPE) P(VDF-HFP)-(PC+DEC)-LiClO₄ (wt%)	Transference Numbers
25:70:5	0.94
25:65:10	0.95
25:60:15	0.98

High values of transport numbers from 0.89 – 0.90 in PVDF and from 0.94 – 0.98 in P(VDF-HFP) based gel polymer electrolytes suggest that the charge transport in these polymer electrolyte systems is predominantly ionic accompanied by mass transport, and electronic contribution to the total current is negligible.

4.2 X-ray Diffraction Study

The XRD patterns of PVDF, P(VDF-HFP), LiClO₄, P(VDF-HFP)-(PC+DEC)-LiClO₄ and PVDF-(PC+DEC)-LiClO₄ gel polymer electrolyte systems are shown in figure 4.5. PVDF is semicrystalline and shows its characteristic peaks at 2θ = 18.2°, 20°, 26.6° and 38° (Figure 4.5a). For P(VDF-HFP) samples in figure 4.5b three peaks appear at 2θ = 18.4°, 20° and 26.6°, which correspond well with the (100)+(020), (110) and (021) reflections of crystalline PVDF [176]. This is a confirmation of partial crystallization of the PVDF units in the copolymer to give an overall semi-crystalline morphology for P(VDF-HFP). Figures 4.5d and 4.5e show the X-ray diffractograms of P(VDF-HFP) and PVDF based gel polymer electrolyte systems respectively. The degree of crystallinity (K) of the gel polymer electrolyte is measured by the relation

$$K = \frac{S}{S_0} \times 100$$

where S is the sum of areas of all the crystalline peaks and S_0 is the sum of areas of crystalline peaks and amorphous hump i.e. total area under the diffractogram as described in Chapter III (section 3.9). Area has been calculated by dividing the X-ray diffractogram into minute square $(0.5 \times 0.5 \text{ mm}^2)$ grids and counting the number of grids.
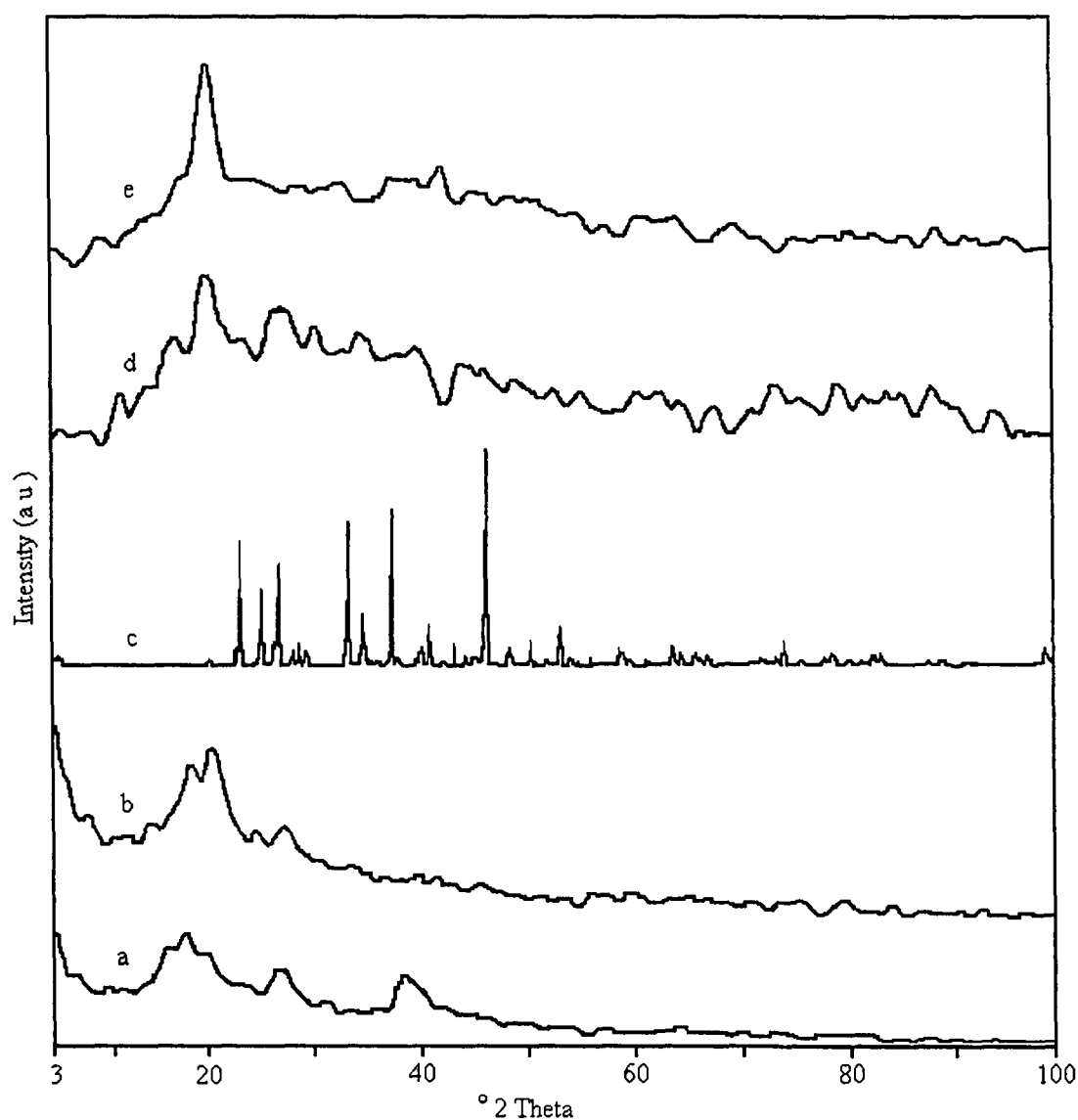
Figure 4.5: XRD patterns of (a) PVDF, (b) P(VDF-HFP), (c) LiClO₄, (d) P(VDF-HFP)-(PC+DEC)-LiClO₄ (25:60:15 wt%) and (e) PVDF-(PC + DEC)-LiClO₄ (25:60:15 wt%) gel polymer electrolytes.

The value of K found for pure PVDF is

$$K = \frac{50\,\text{sq unit}}{159\,\text{sq unit}} \times 100$$

$$K = 31.4\%$$

For pure P(VDF-HFP)

$$K = \frac{168\,\text{sq unit}}{560\,\text{sq unit}} \times 100$$

$$K = 30\%$$

For PVDF-(PC+DEC)-LiClO₄ gel polymer electrolyte

$$K = \frac{45\,\text{sq unit}}{220\,\text{sq unit}} \times 100$$

$$K = 20.45\%$$

and for P(VDF-HFP)-(PC+DEC)-LiClO₄ gel polymer electrolyte

$$K = \frac{30\,\text{sq unit}}{220\,\text{sq unit}} \times 100$$

$$K = 13.64\%$$

It is observed that crystallinity of gel polymer electrolyte is greatly reduced after the addition of PC+DEC and LiClO₄. Moreover peaks corresponding to LiClO₄ (Figure 4.5c) are not observed indicating that LiClO₄ is completely dissolved in (PC+DEC) solvents in the polymer matrix and does not remain as separate phase in the electrolytes. The intensity of the crystalline peaks is decreased and a noticeable broadening of the area under the peaks was observed. This is a clear indication of the reduction in the crystalline phase in the polymer complex at room temperature [177]. It is also observed that P(VDF-HFP) based electrolytes are more amorphous than PVDF based electrolytes as peaks are sharper and more in number

indicating larger crystallinity in PVDF based electrolyte. Higher amorphicity results in higher conductivity in P(VDF-HFP) based electrolytes as compared to PVDF based electrolytes.

4.3 Fourier Transform Infra-Red Spectroscopy

FTIR spectroscopy is important for the investigation of polymer structure as the IR spectra of these materials vary according to their compositions and are able to show the occurrence of complexation and interaction(s) between the various constituents [157,178].

Figure 4.6 shows the FTIR spectra of PVDF based electrolytes. Absorption peak at frequency 3023 cm^{-1} is assigned to C – H stretching vibrations of PVDF. Peak at frequency
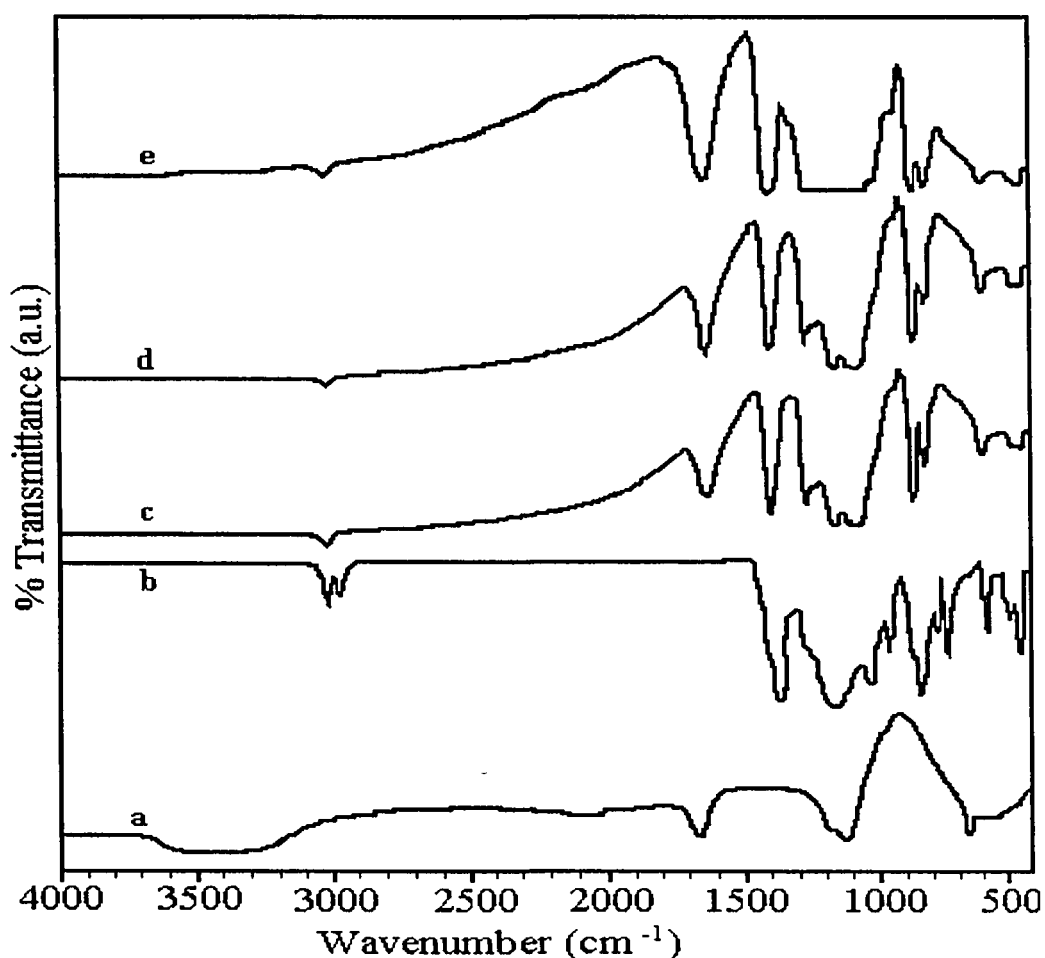
Figure 4.6: FTIR spectra of (a) LiClO₄, (b) PVDF (c) PVDF-(PC+DEC)-LiClO₄ (25:70:5 wt%), (d) PVDF-(PC+DEC)-LiClO₄ (25:65:10 wt%) and (e) PVDF-(PC+DEC)-LiClO₄ (25:60:15 wt%).

68

1640 cm^{-1} is assigned to C = O stretching vibration. Frequency 1415 cm^{-1} is assigned to C–F stretching vibration of PVDF. Frequency 1270 cm^{-1} is assigned to C–O stretching vibrations of plasticizer. Frequencies 1172 – 1066 cm^{-1} are assigned to –C–F– and –CF₂– stretching vibrations. Frequency 880 cm^{-1} is assigned to vinylidene group of PVDF. New peak observed in the polymer electrolyte system at frequency 837 cm^{-1} is assigned to C–Cl stretching vibrations. The vibrational peaks of PVDF (3021, 1400, 1183, 976, 876 cm^{-1}) are shifted to (3023, 1415, 1171, 950, 880 cm^{-1}) in the polymer electrolyte.

Figure 4.7 shows the FTIR spectra of P(VDF-HFP), LiClO₄ and P(VDF-HFP)-(PC+DEC)-LiClO₄ gel polymer electrolytes. The frequency 3000 cm^{-1} is assigned to C – H
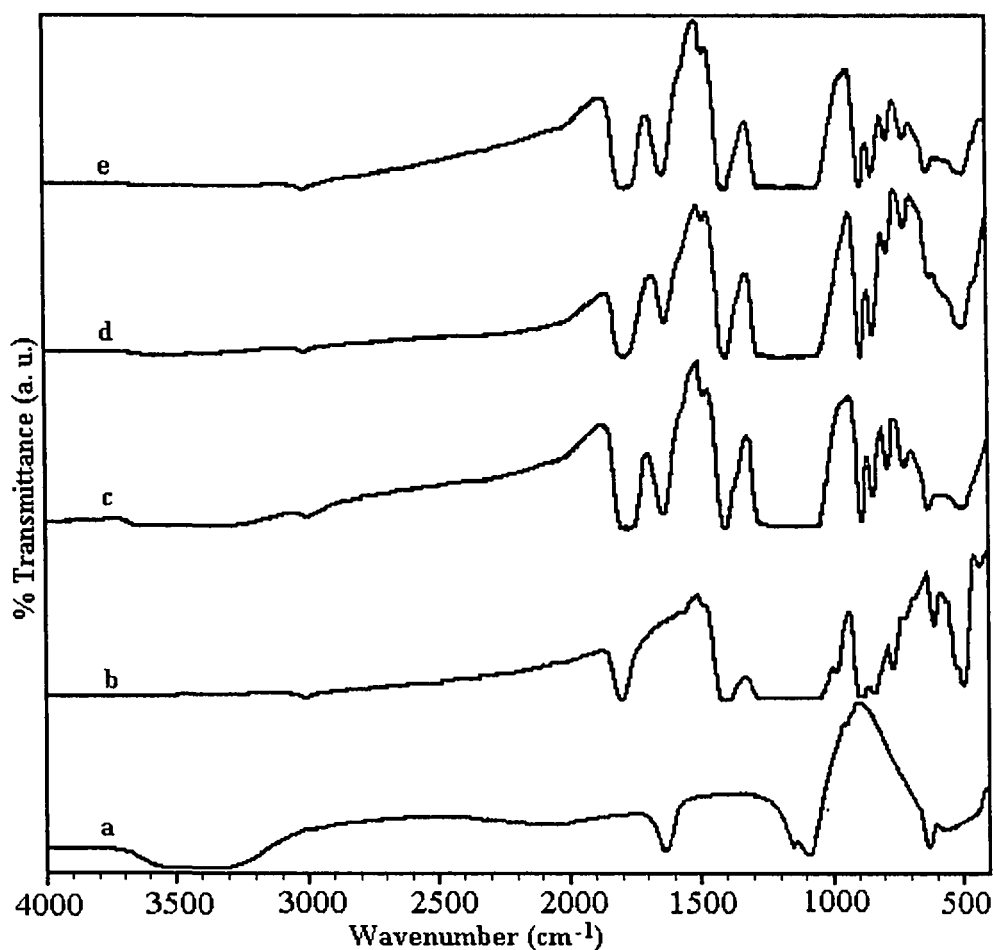
Figure 4.7: FTIR spectra of (a) LiClO₄, (b) P(VDF-HFP), (c) P(VDF-HFP)-(PC+DEC)-LiClO₄ (25:60:15 wt%), (d) P(VDF-HFP)-(PC+DEC)-LiClO₄ (25:65:10 wt%) and (e) P(VDF-HFP)-(PC+DEC)-LiClO₄ (25:70:5 wt%).

stretching vibrations of PVDF. The frequency 1791 cm^{-1} is assigned to $-CF=CF_2$, $-C-O-CO-O-C-$ group. Peak at frequency 1636 cm^{-1} is assigned to $C=O$ stretching vibration of plasticizer (PC+DEC). Frequencies 1483 cm^{-1} and 1400 cm^{-1} are assigned to $-CH_3$ asymmetric bending and C–F stretching vibrations of plasticizer, propylene carbonate and diethyl carbonate and P(VDF-HFP) respectively. Frequencies 1290-1060 cm^{-1} are assigned to $-C-F-$ and $-CF_2-$ stretching vibrations. Frequency 881 cm^{-1} is assigned to vinylidene group of polymer. The vibrational peaks of P(VDF-HFP) (3004, 1797, 1417, 882 and 839 cm^{-1}) are shifted to (3000, 1791, 1401, 881 and 837 cm^{-1}) in the polymer electrolyte. New absorption peaks at 781 cm^{-1} and 716 cm^{-1}, which correspond to C–Cl stretching [157,179], are observed in the electrolyte.

Appearance of new peaks at frequency 837 cm^{-1} in PVDF-(PC+DEC)-LiClO₄ and at 781 and 716 cm^{-1} in P(VDF-HFP)-(PC+DEC)-LiClO₄ which could be ascribed to C–Cl stretching vibration indicates that polymer carbon atoms interact with chlorine of ClO_4^- ions. Shifting and formation of new peaks suggest the polymer-salt interaction occur in both PVDF and P(VDF-HFP) based gel polymer electrolyte systems.

4.4 Scanning Electron Micrograph Study

The scanning electron micrographs of PVDF-(PC+DEC)-LiClO₄ (25:65:10 wt%) and P(VDF-HFP)-(PC+DEC)-LiClO₄ (25:60:15 wt%) gel polymer electrolyte systems are shown in figures 4.8 and 4.9. A macroscopic phase separation between the dense and porous layer is noticed. Ordered and almost spherical polymer particles of about 1.5 μm and void spaces are observed in this system (Figure 4.8). The void spaces are certainly the result of solvent removal [180] resulting in larger pore size. In case of P(VDF-HFP)-(PC+DEC)-LiClO₄ gel polymer electrolyte (Figure 4.9), although the macroscopic phase separation is absent,
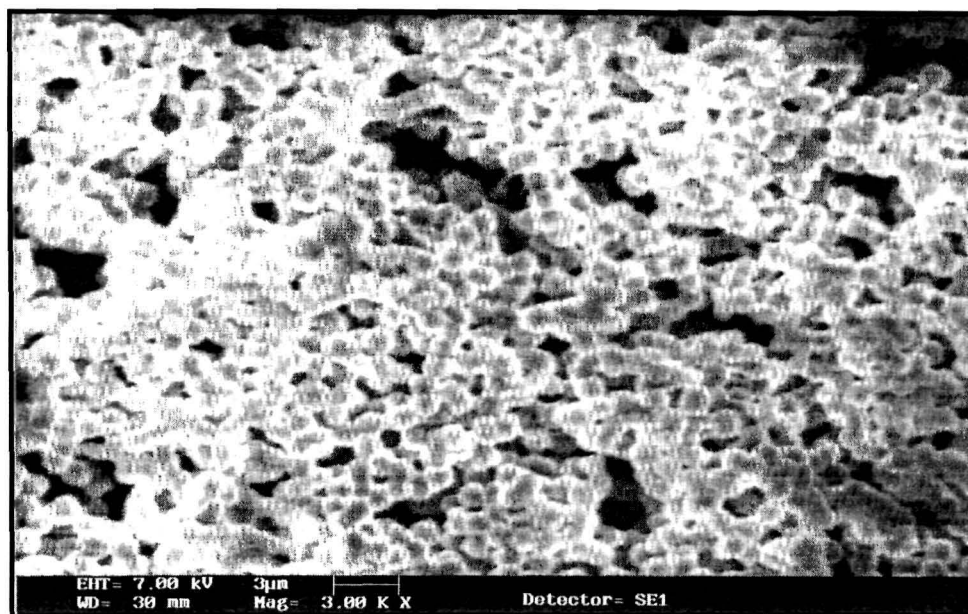
Figure 4.8: SEM image of PVDF-(PC+DEC)-LiClO$_4$ (25:65:10 wt%) gel polymer electrolyte, Magnification 3000X.
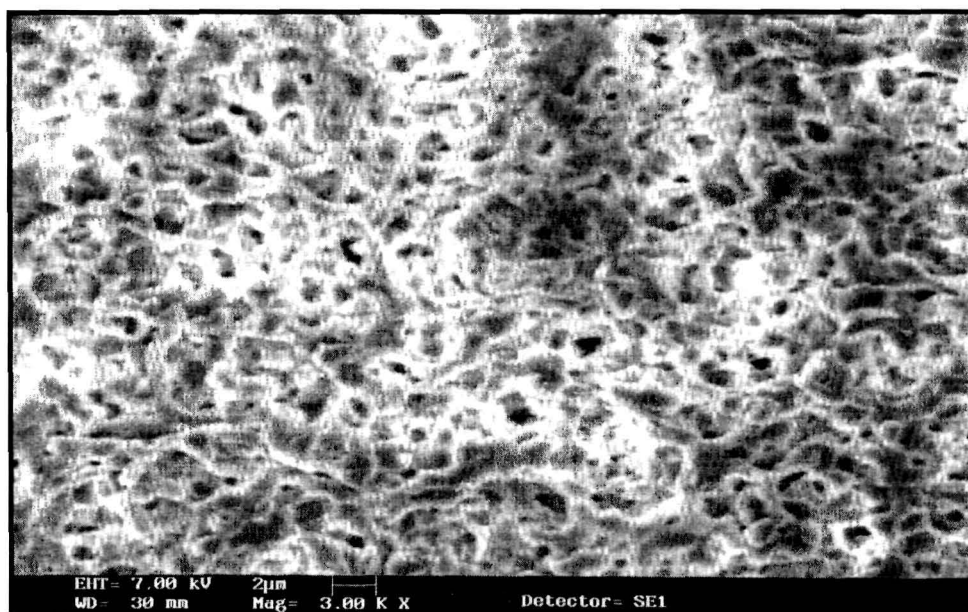
Figure 4.9: SEM image of P(VDF-HFP)-(PC+DEC)-LiClO$_4$ (25:60:15 wt%) gel polymer electrolyte, Magnification 3000X.

the film is still porous with microscopic phase separation. For this system, though the surface morphology is uniform but the ordered spherical grain structure is absent. The microstructure is disordered throughout the sample and the pore size is smaller. The result suggests that P(VDF-HFP) has higher solvent retention ability since the pores in microstructure occurs due to solvent removal [180,181]. SEM results are consistent with the view that higher conductivity and ionic transport number in P(VDF-HFP) based electrolytes arise from the increased amorphicity and solvent retention ability in these gel electrolytes.

4.5 Differential Scanning Calorimetry

To study the structural changes of the polymer electrolyte with the heat treatment, DSC thermograms were obtained on the gel polymer electrolyte. DSC plots for pure PVDF and PVDF based gel electrolyte systems are shown in figure 4.10. There is an endothermic peak around 170 °C (Figure 4.10a), which is attributed to the melting of PVDF. In the electrolyte systems (Figure 4.10 (b,c)) one endothermic peak is appearing around 126 °C, which is ascribed to the boiling point of diethyl carbonate (DEC) and another around 170 °C, which is attributed to the melting of PVDF [155].

DSC plots for pure P(VDF-HFP) and P(VDF-HFP) based gel electrolyte systems are shown in figure 4.11. The endothermic peak (Figure 4.11 (a)) around 140 °C is assigned to the melting of P(VDF-HFP). In case of P(VDF-HFP) based electrolytes (Figure 4.11 (b,c)) one broad peak is coming between 120 °C and 160 °C. The broadening of peak is due to overlapping of boiling point of DEC (126 °C) and melting point of P(VDF-HFP) (140 °C) [182]. From figures 4.10 and 4.11 it is observed that thermal instability in both these systems starts from around 80 °C, therefore these electrolyte systems can be used up to 80 °C.
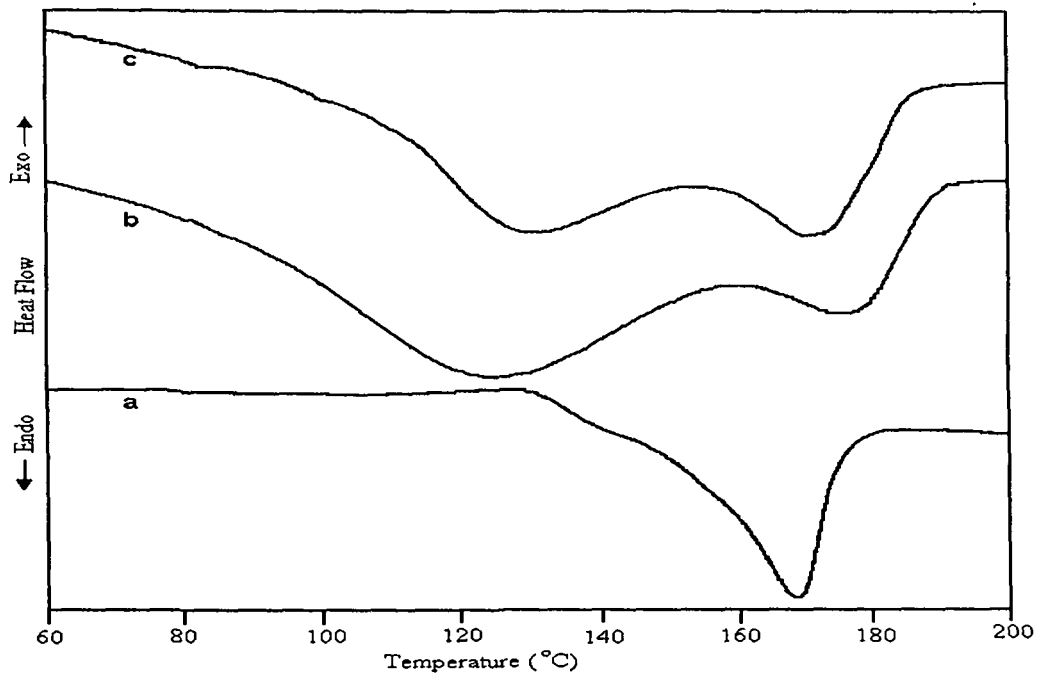
Figure 4.10: DSC curves of (a) PVDF, (b) PVDF-(PC+DEC)-LiClO₄ (25:70:5 wt%), (c) PVDF-(PC+DEC)-LiClO₄ (25:65:10 wt%) gel polymer electrolyte.
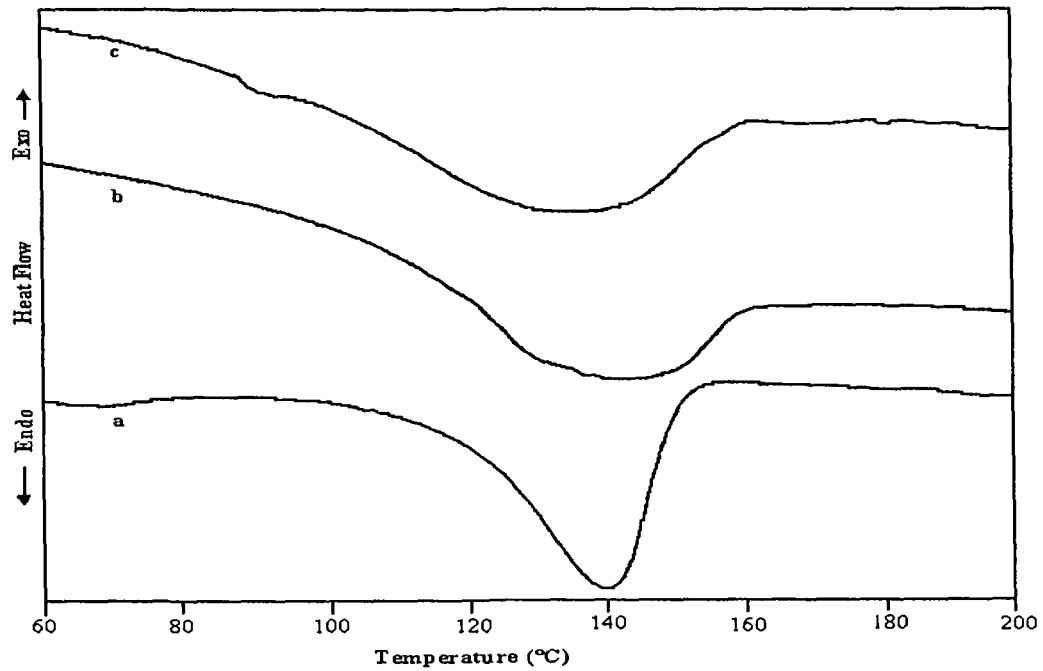
Figure 4.11: DSC curves of (a) P(VDF-HFP), (b) P(VDF-HFP)-(PC+DEC)-LiClO₄ (25:70:5 wt%) (c) P(VDF-HFP)-(PC+DEC)-LiClO₄ (25:65:10 wt%) gel polymer electrolyte.

4.6 Summary

Formation and redissociation of ion-pairs due to long range coulombic forces gives rise to free ions in the gel polymer electrolyte. Maximum ionic conductivity for PVDF-(PC+DEC)-LiClO$_4$ and P(VDF-HFP)-(PC+DEC)-LiClO$_4$ is found to be 1.3×10^{-3} S/cm and 7.5×10^{-3} S/cm at 303 K respectively. Higher ionic conductivity in P(VDF-HFP) based gel polymer electrolyte in comparison to PVDF based electrolyte could be attributed to higher amorphicity of the former electrolyte system due to steric hindrance provided by bulky pendant $-CF_3$ group in HFP monomer unit of the copolymer. Higher amorphicity provides higher flexibility to the polymer chains and mobile ions greater free volume giving rise to higher conductivity. This result is confirmed by XRD analysis which reveals that degree of crystallinity is reduced from 31.4% in PVDF to 20.45% in PVDF based gel polymer electrolyte system and 30% in P(VDF-HFP) to 13.64% in P(VDF-HFP) based gel polymer electrolyte system. Total ionic transport number was found to be higher for P(VDF-HFP) based electrolytes than that of PVDF based electrolytes. The motion of ions in the gel polymer electrolyte occurs in liquid like manner in which the movement of ions through the polymer matrix is assisted by the large amplitude segmental motion of the polymer backbone as indicated by FTIR analysis which suggests polymer-salt interaction for both PVDF and P(VDF-HFP) based gel polymer electrolytes.

SEM results are consistent with the view that higher conductivity and ionic transport number in P(VDF-HFP) based gel polymer electrolytes arise from the increased amorphicity and higher solvent retention ability than PVDF based gel polymer electrolytes. Good thermal stability of these polymer electrolyte systems up to 80 °C was confirmed by DSC measurements.

CHAPTER V

COMPOSITE GEL POLYMER ELECTROLYTE SYSTEMS

Composite polymer electrolytes (CPE) formed by polymer, salt and dispersed inorganic oxide sub-micron size particles have been the subject of great deal of research in the last decade because of their potential importance in the development of solid state batteries [50,183-188]. It is widely recognized that the ionic conductivity of polymer electrolytes can be considerably enhanced by the introduction of inorganic fillers, which inhibit polyether crystallinity and improves the mechanical properties of the electrolytes [189,190]. The ceramic component of composite polymer electrolytes can be classified into two categories, active and passive. The active components comprise of materials such as Li_3N and $LiAlO_2$. Due to the presence of lithium ions these materials participate in the conduction process. The passive components comprise of materials such as Al_2O_3, SiO_2, TiO_2, etc., which do not have lithium ions and participate passively in the ion transport process.

The conductivity enhancement has been ascribed to disorder caused by interactions between Lewis acid sites on the nanoparticle surface and the base species present in the system (polymer chain and anions groups). This leads to a weaker interaction between polymer and Li^+-ions [60,183,185,187]. Despite all research efforts to investigate the influence of filler particles on the Li^+ ion conductivity, few is reported about the interaction of the inorganic fillers with the polymer and ions. Conductivity enhancement in composite polymer electrolytes depends upon many factors such as the type of polymer-ceramic system, particle size, annealing parameters (or thermal history), filler concentration and temperature [47,191].

Work on composite polymer electrolytes started in 1982 when Weston and Steele [192] mixed polyethylene oxide PEO-LiClO₄ polymer complex with 10 vol% α-alumina powder with the purpose of improving the mechanical stability of the electrolyte. They also investigated the effect of filler on the ionic conductivity and transport number. Skaarup et al. [193] investigated mixed phase electrolytes consisting of Li_3N, $LiCF_3SO_3$ and PEO to take advantage of the desirable attributes of inorganic and polymer components of the mixed phase electrolyte and reported that at small volume fractions of polymers (0.05-0.10), the room temperature conductivity was larger by about a factor of 1000 than that of the polymer. The activation energy for conduction in the composite electrolyte was comparable to that of the inorganic phase, Li_3N. Plocharski and Wieczorek [194] investigated PEO-NaI polymer mixed with $Na_{3.2}Zr_2Si_{2.2}P_{0.8}O_{12}$ ceramic powder and reported at least one order of magnitude increase in the conductivity ascribed to the addition of ceramic powder. Plocharski et al. [195] further investigated the effect of Al_2O_3 and Nasicon powder on the properties of PEO–NaI electrolytes and found ionic conductivity exceeding 10^{-5} S cm^{-1} at room temperature. The enhanced conductivity was attributed to the higher volume fraction of the amorphous phase postulated to result from a higher nucleation rate during the solidification process. Skaarup et al. [196] investigated a mixed phase electrolyte containing lithium sulfide glasses in nonconducting polyethylene. Room temperature ionic conductivities of these electrolytes were about 1000 times higher than those of PEO-based polymer electrolytes. Capuano et al. [197] reported that incorporation of γ-Al_2O_3 or $LiAlO_2$ up to about 10 wt% in the PEO-based polymer electrolyte increases room temperature conductivity by 10 times. In addition, the composite electrolytes exhibited improved mechanical properties and enhanced interfacial stability. Subsequent work on these electrolytes by Croce et al. [198,199] suggested that the addition of finely dispersed ceramic powders such as γ-$LiAlO_2$ and zeolite effectively controls

the morphology and growth of the passivation layer on lithium electrode. Conductivity enhancement was also reported by Munichandraiah et al. [200] when zeolite up to 30% was introduced in the PEO-LiBF$_4$ polymer complex. The enhancement in conductivity was also accompanied by a decrease in heat of fusion and an increase in the glass transition temperature of PEO [55,56]. Kumar et al. [201] reported no increase in the room temperature conductivity when lithium borosulfate glass was incorporated in a PEO-LiBF$_4$ polymer complex; however, the charge-transfer resistance decreased by a factor of three due to the small addition of the lithium borosulphate glass. Przyluski et al. [202] investigated PEO-NaI-SiO$_2$ composite electrolytes. These electrolytes possessed about an order of magnitude higher conductivity than that of PEO-NaI electrolytes at ambient temperature. Enhancement of conductivity was attributed to decrease in crystallinity. Improved mechanical and thermal stabilities of these composite electrolytes were also reported. Kumar and Scanlon [203] investigated PEO-LiBF$_4$-Li$_3$N composite electrolytes containing 5 to 50% Li$_3$N. An order of magnitude increase in conductivity of the composite electrolytes at ambient temperature was reported. Furthermore, these materials exhibited improved lithium-electrolyte interfacial stability.

In this Chapter various studies on three composite systems P(VDF-HFP)-PMMA-PC-LiClO$_4$-TiO$_2$, P(VDF-HFP)-PMMA-(PC+DEC)-LiCF$_3$SO$_3$-fumed SiO$_2$ and P(VDF-HFP)-(PC+DEC)-LiAsF$_6$-fumed SiO$_2$ have been presented. In the first two systems P(VDF-HFP) is blended with PMMA. Polymer blends often exhibit properties that are superior compared to the properties of the individual component polymer [204-209]. Main advantage of the blend systems are simplicity of preparation and ease of control of physical properties by compositional change [210,211]. In miscible polymeric blends, there are often specific interactions between groups or polymer segments that lead to a decrease of the Gibbs energy

of mixing [212]. Composite polymer electrolytes of various compositions have been prepared by the solution casting technique as described in Chapter III (section 3.2). The ionic conductivity for all the samples at different temperatures was obtained from the complex impedance analysis. The resistance obtained from the high-frequency portion has been used to calculate the conductivity of various composites. Almost all composite polymer samples have been investigated by SEM for microstructural analysis and by XRD and DSC for crystallinity and thermal stability studies respectively. FTIR study has been carried out to investigate the polymer-ion-filler interaction.

The detailed results on P(VDF-HFP)-PMMA-PC-LiClO$_4$-TiO$_2$ system are presented first followed by those on P(VDF-HFP)-PMMA-(PC+DEC)-LiCF$_3$SO$_3$-fumed SiO$_2$ and P(VDF-HFP)-(PC+DEC)-LiAsF$_6$-fumed SiO$_2$ composite gel polymer electrolyte systems.

5.1 P(VDF-HFP)-PMMA-PC-LiClO$_4$-TiO$_2$ System

5.1.1 Ionic Conductivity Measurements

Ionic conductivity of the composite gel polymer electrolyte films was measured by complex impedance technique with electrolyte films sandwiched between symmetric stainless steel electrodes. Measurements were made over the frequency range of 42 Hz – 5 MHz and in the temperature range of 20 –100 °C. Figure 5.1 shows the complex impedance spectra of above mentioned electrolyte system at different temperatures. The figure shows the tilted spikes displaced from the origin which represent a resistor in series with a capacitor. The intercept on the real axis gives the value of bulk electrolyte resistance (R$_b$). The ionic conductivity of composite polymer electrolyte is calculated as described in Chapter IV (section 4.1).

Figure 5.2 shows the conductivity versus temperature inverse plots of composite gel polymer electrolyte. From the plots it is observed that conductivity increases with the increasing filler concentration. The enhancement of conductivity can be described from the following viewpoint. Dispersed phase submicron size filler particles prevent polymer chain reorganization, resulting in reduction in polymer crystallinity which gives rise to an increase in ionic conductivity. The reduction in crystallinity may also result from the Lewis acid-base interactions between the surface of submicron filler particles and the polymer chains. This allows mobile ions to move more freely either on the surface of the submicron particles or through a low density polymer phase at the interface, which results in enhanced ionic conductivity [50,213].
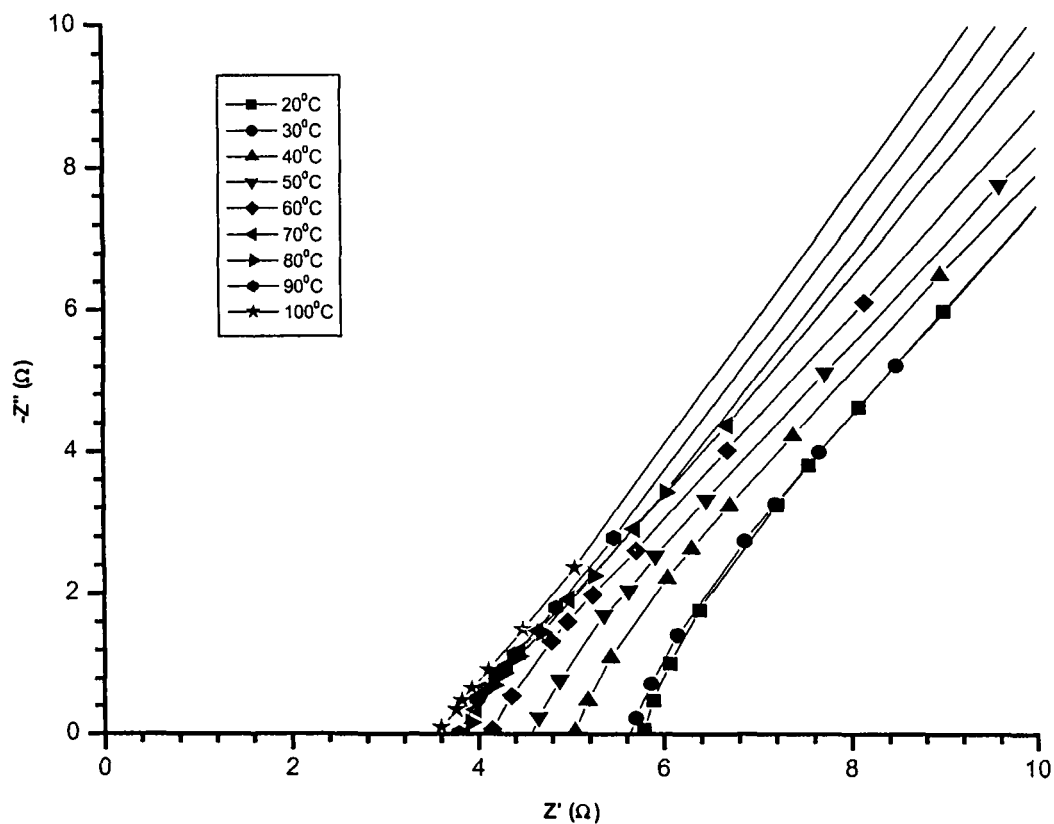
Figure 5.1: Complex impedance spectra of P(VDF-HFP)-PMMA-PC-LiClO$_4$-TiO$_2$ composite gel polymer electrolyte system at different temperatures.

Enhancement of conductivity can also be attributed to the generation of polymer-ceramic grain boundaries. The structure and chemistry of ceramic-polymer grain boundaries may have even more important role than the formation of an amorphous phase in the electrolyte. The grain boundaries are the sites of high defect concentration providing channels for faster ionic transport [63]. The selection of appropriate polymer and ceramic phase is an important consideration in the development of fast ion-conducting composite polymer electrolyte.
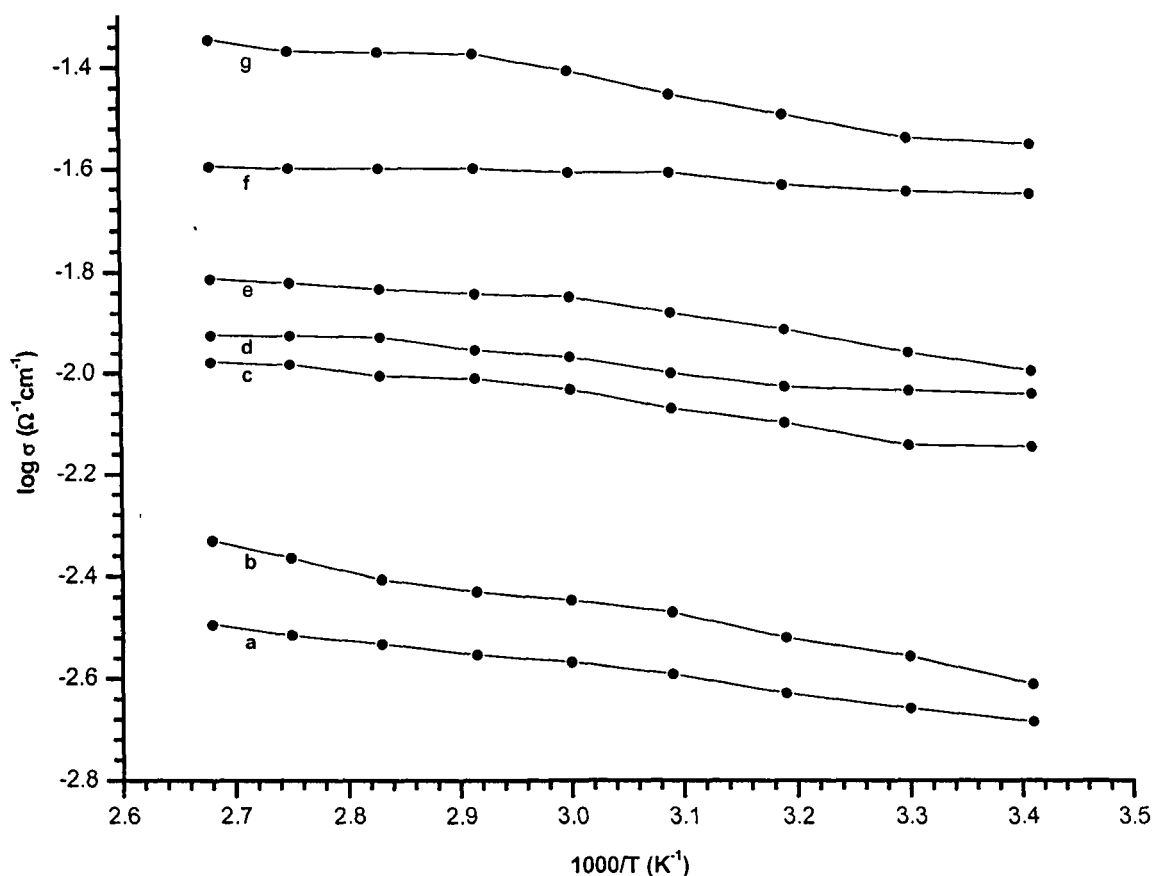
Figure 5.2: Temperature dependence of ionic conductivity of P(VDF-HFP)-PMMA-PC-LiClO₄-TiO₂ composite gel polymer electrolyte system with composition (wt%), (a) 20:10:50:20:0, (b) 20:10:50:10:10, (c) 20:10:50:12:8, (d) 20:10:50:14:6, (e) 20:10:45:20:5, (f) 20:10:40:20:10 and (g) 20:10:35:20:15.

The conductivity values for composite gel polymer electrolytes containing different weight ratios of P(VDF-HFP), PMMA, PC, LiClO$_4$ and TiO$_2$ are presented in table 5.1. Highest conductivity value of $\approx 2.8 \times 10^{-2}$ S/cm at 293 K which is comparable to the conductivity of liquid electrolyte, is measured for composition 20 wt% P(VDF-HFP), 10 wt% PMMA, 35 wt% PC, 20 wt% LiClO$_4$ and 15 wt% TiO$_2$. Conductivity at 373 K is found to be 4.5×10^{-2} S/cm for the same composition.

The variation in conductivity as a function of filler TiO$_2$ composition in polymer electrolyte system at various temperatures is given in figure 5.3. It is observed that conductivity increases with increase of filler concentrations as well as rise in temperature. Such high value of conductivities is attributed to higher amorphicity and increased defects concentration along the TiO$_2$ particles interface. However, the composite electrolyte films become brittle and fragile at higher concentrations of TiO$_2$.

Table 5.1: Composition (wt%) and conductivity of P(VDF-HFP)-PMMA-PC-LiClO$_4$-TiO$_2$ composite gel polymer electrolyte at 293 K.

P(VDF- HFP)	PMMA	PC	LiClO$_4$	TiO$_2$	Conductivity (S cm^{-1})
20	10	50	20	0	2.1×10^{-3}
20	10	50	10	10	2.5×10^{-3}
20	10	50	12	8	7.5×10^{-3}
20	10	50	14	6	9.1×10^{-3}
20	10	45	20	5	1×10^{-2}
20	10	40	20	10	2.2×10^{-2}
20	10	35	20	15	2.8×10^{-2}

The fact that motion of polymer chains contribute to the transport of lithium ions in the polymer electrolytes also has deleterious effects on the transport number. The chain motion also facilitates transport of anionic species and thus the measured conductivity

includes contribution from both the species. Although numerous transport number measurements have been reported, a reliable and universally acceptable measurement technique is still lacking as pointed out by Bruce et al. [214]. Generally in polymer electrolytes, cationic transport number is smaller than anionic transport number. It is because anionic species is more coupled to the polymeric structure than the cationic species. The vibrational frequencies and motion of large anionic species and polymer chains are expected to be more in phase than those of cationic species and polymer chains. As a result, when such
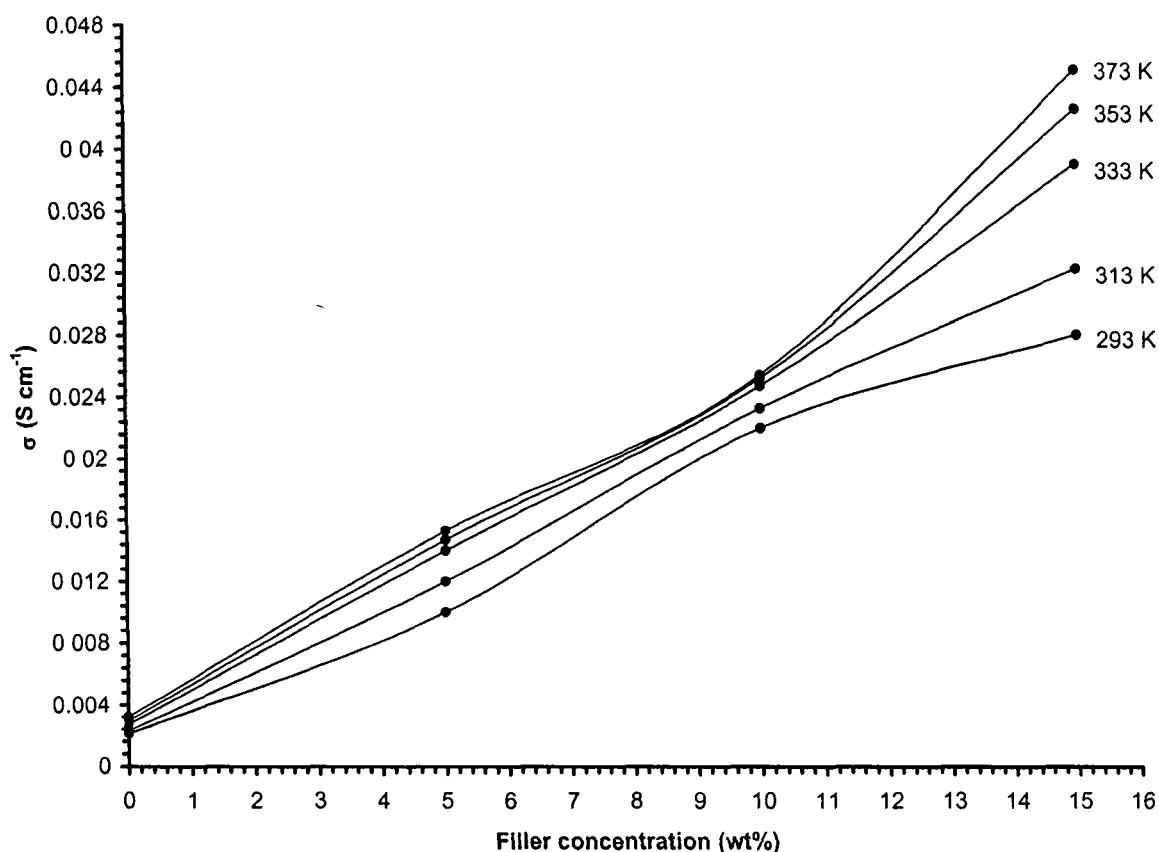
Figure 5.3: Conductivity versus filler concentration (wt%) of P(VDF-HFP)-PMMA-PC-LiClO₄-TiO₂ composite gel polymer electrolyte system at different temperatures

materials are used in a battery, extensive concentration gradients are set up during use and they affect its electrical performance. Total ionic transference number of composite gel polymer electrolyte was measured by Wagner's polarization technique [152,153], which is

82

used to determine the ionic contribution to the total charge transport by measuring the residual electronic current passing through the electrolytes as described in Chapter III (section 3.6). Wagner polarization cell Ag/electrolyte/Ag was prepared by coating silver (Ag) paste as blocking electrodes on to the faces of P(VDF-HFP)-PMMA based composite gel polymer electrolyte films. The ionic transference number was calculated using the relation

$$t_i = \frac{I_i}{I_{total}} = \frac{I_T - I_e}{I_T}$$

$$t_{ele} = \frac{I_e}{I_T}$$

Table 5.2 shows the ionic transference number for P(VDF-HFP)-PMMA-PC-LiClO$_4$-TiO$_2$ composite gel polymer electrolyte for different compositions. High value of transport number from 0.96 – 0.99 suggest that the charge transport in this polymer electrolyte systems is predominantly ionic accompanied by mass transport and electronic contribution to the total current is negligible.

Table 5.2: Ionic transference number of P(VDF-HFP)-PMMA-PC-LiClO$_4$-TiO$_2$ composite gel polymer electrolyte system.

P(VDF-HFP)-PMMA-PC-LiClO$_4$-TiO$_2$ Composite Gel Polymer Electrolyte (wt%)	Transference Numbers
20:10:50:10:10	0.96
20:10:50:12:8	0.96
20:10:50:14:6	0.97
20:10:45:20:5	0.97
20:10:40:20:10	0.98
20:10:35:20:15	0.99

5.1.2 X-ray Diffraction Study

Figure 5.4 shows the XRD patterns of P(VDF-HFP), PMMA, LiClO$_4$, TiO$_2$ and P(VDF-HFP)-PMMA-PC-LiClO$_4$-TiO$_2$ (20:10:35:20:15 wt%) composite gel polymer electrolyte respectively. Peaks at 2θ = 18.4°, 20° and 26.6° for P(VDF-HFP) polymer correspond well with the (100)+(020), (110) and (021) reflections of crystalline PVDF [176]. This confirms the partial crystallization of the PVDF units in the copolymer to give an overall semi-crystalline morphology for P(VDF-HFP). The degree of crystallinity (K) of polymer electrolyte is measured by the relation

$$K = \frac{S}{S_0} \times 100$$

where S is the sum of areas of all the crystalline peaks and S$_0$ is the sum of areas of crystalline peaks and amorphous hump i.e. total area under the diffractogram. Area has been calculated by dividing the X-ray diffractogram into minute square (0.5 × 0.5 mm^2) grids and counting the number of grids.

The degree of crystallinity (K) for pure P(VDF-HFP) is found to be

$$K = \frac{168 \text{ sq unit}}{560 \text{ sq unit}} \times 100$$

$$K = 30\%$$

For PMMA the value of K is

$$K = \frac{23 \text{ sq unit}}{90 \text{ sq unit}} \times 100$$

$$K = 25.5\%$$

and for P(VDF-HFP)-PMMA-PC-LiClO$_4$-TiO$_2$ (20:10:35:20:15 wt%) composite gel polymer electrolyte system degree of crystallinity (K) is found to be

$$K = \frac{3 \text{ sq unit}}{50 \text{ sq unit}} \times 100$$

$$K = 6\%$$

It is observed from figure 5.4e that crystallinity of composite gel polymer electrolytes is greatly reduced by the addition of PC, $LiClO_4$ and TiO_2. Peaks corresponding to $LiClO_4$ are not observed in the electrolyte since $LiClO_4$ (Figure 5.4c) is dissolved in the polymer matrix and does not remain a separate phase. Increased amorphicity in the electrolyte, which gives rise to higher ionic conductivity is attributed to the steric hindrance provided by the bulky pendant $-CH_3COO$ ester group of PMMA upon blending of P(VDF-HFP) with PMMA and addition of the plasticizer and filler TiO_2 [167,215].
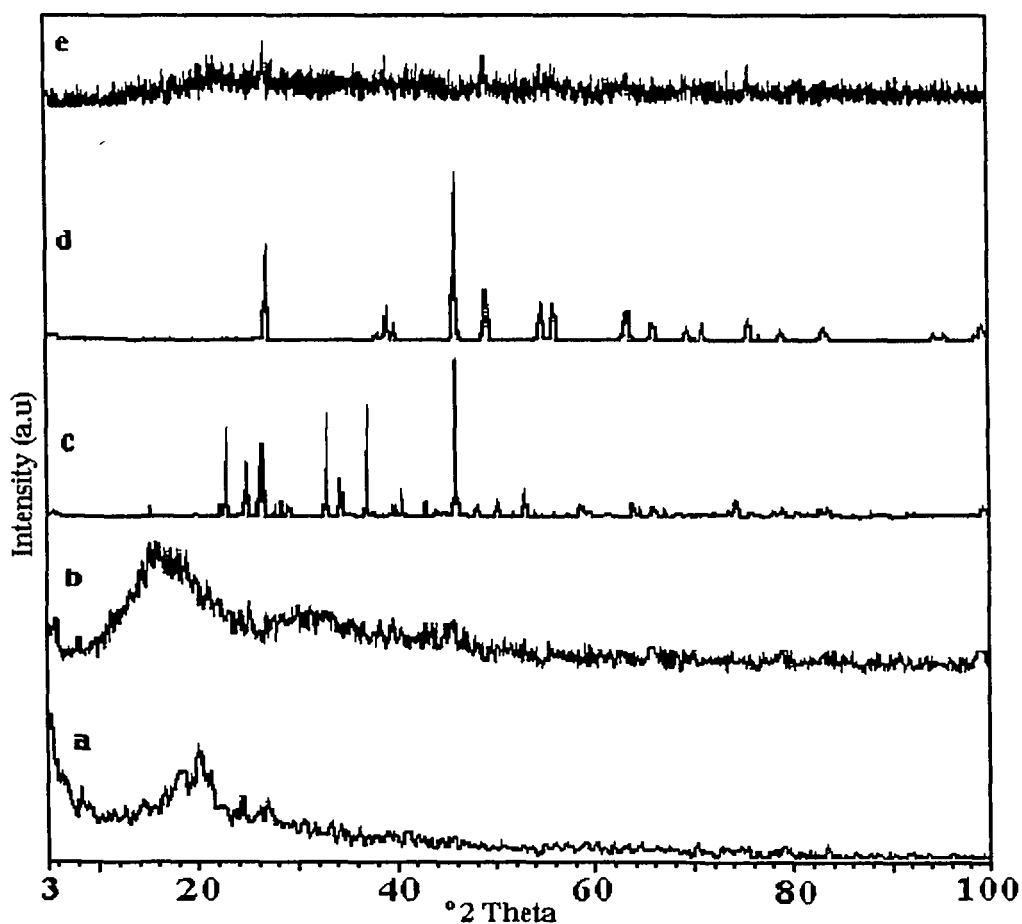
Figure 5.4: XRD patterns of (a) P(VDF-HFP), (b) PMMA (c) $LiClO_4$, (d) TiO_2 and (e) P(VDF-HFP)-PMMA-PC-$LiClO_4$-TiO_2 (20:10:35:20:15 wt%) composite gel polymer electrolyte.

5.1.3 Fourier Transform Infra-Red Spectroscopy

Infrared spectroscopy has been used to characterize the chain structure of polymers and has led the way in interpreting the reactions of multifunctional monomers including rearrangements and isomerizations [157,178]. FTIR spectra of P(VDF-HFP), PMMA, $LiClO_4$ and P(VDF-HFP)-PMMA-PC-$LiClO_4$-TiO_2 (20:10:35:20:15 wt%) composite gel polymer electrolyte are shown in figure 5.5. Absorption peak at frequency 2955 cm^{-1} is assigned to C–H stretching vibration. Peak at frequency 1786 cm^{-1} is assigned to $-CF=CF_2$, –C–O–CO–O–C– group. Frequency 1726 cm^{-1} is assigned to >C=O stretching vibration of PMMA. Frequency 1401 cm^{-1} is assigned to C–F stretching vibration of P(VDF-HFP). Frequencies 1290-1060 cm^{-1} are assigned to -C–F- and -CF_2- stretching vibrations. Frequency
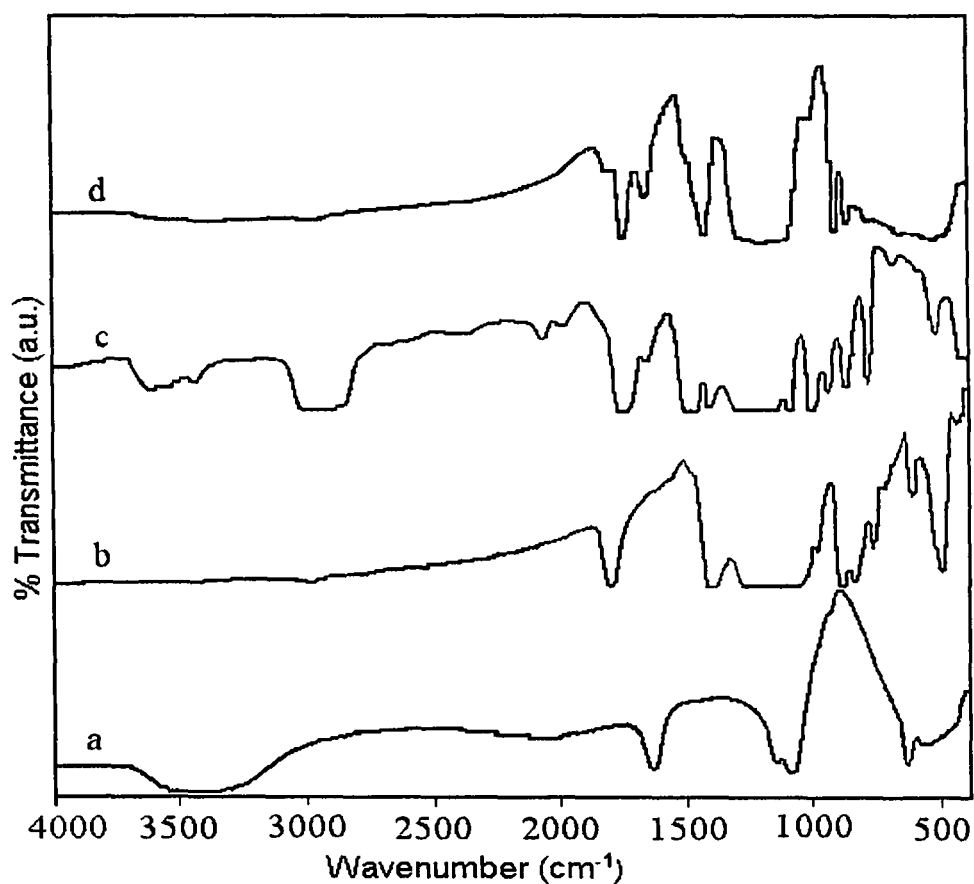
Figure 5.5: FTIR spectra of (a) $LiClO_4$, (b) P(VDF-HFP), (c) PMMA and (d) P(VDF-HFP)-PMMA-PC-$LiClO_4$-TiO_2 (20:10:35:20:15 wt%) composite gel polymer electrolyte system.

881 cm^{-1} is assigned to vinylidene group of polymer. The vibrational peaks of P(VDF-HFP)

(1797, 1417, 882 and 839 cm^{-1}) and PMMA (2946, 1740, 1637 and 482 cm^{-1}) are shifted to

(1786, 1401, 881 and 834 cm^{-1}) and (2955, 1726, 1638 and 485 cm^{-1}) in the polymer

complexes respectively. New absorption peak at frequency 747 cm^{-1} is observed in the

electrolyte which corresponds to C–Cl stretching [157,179]. This indicates that polymer

carbon atoms interact with chlorine atom of ClO$_4$ ions suggesting the polymer-ion interaction

in the composite gel polymer electrolytes.

5.1.4 Scanning Electron Micrograph Study

Scanning electron micrographs of P(VDF-HFP)-PMMA-PC-LiClO$_4$ (20:10:50:20

wt%) and P(VDF-HFP)-PMMA-PC-LiClO$_4$-TiO$_2$ (20:10:35:20:15 wt%) gel composite

polymer electrolytes are shown in figures 5.6a and 5.6b respectively. From figure 5.6a it is

observed that electrolyte film is a two phase system having polymer and the liquid electrolyte

phases. Here the film is interspersed with pores filled with liquid electrolyte, which form a

connected path through the polymer matrix [216]. With the addition of filler TiO$_2$ as shown in

figure 5.6b, the film surface becomes rough, but the submicron particles are well dispersed in

the entire surface region. The film roughness also supports the existence of micropores which

increase the liquid electrolyte uptake in the composite gel polymer electrolyte. The increased

porosity leads to the trapping of larger volumes of the liquid in the cavities accounting for the

increased ionic conductivity. The interaction between the surface group of TiO$_2$ and the

solvent/polymer molecules [217] is not negligible here and the highly porous surface

morphology of the polymer film is effectively produced as a result of the interaction of

dispersed filler particles with polymer component as well as the affinity with solvent

molecules [218]. In the present case of porous polymer electrolyte, however, the affinity
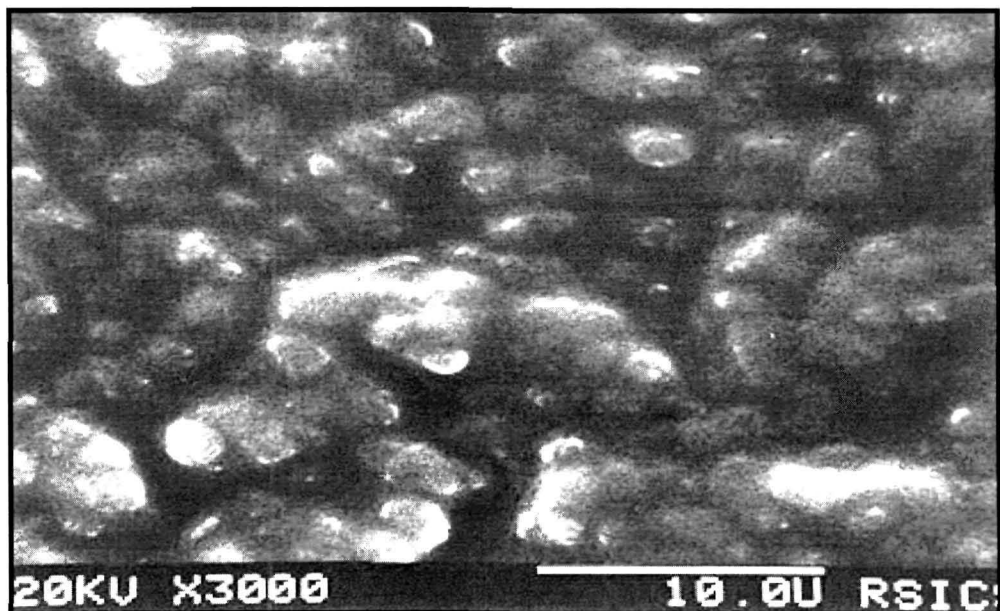
Figure 5.6a: SEM image of P(VDF-HFP)-PMMA-PC-LiClO$_4$ (20:10:50:20 wt%) gel polymer electrolyte.
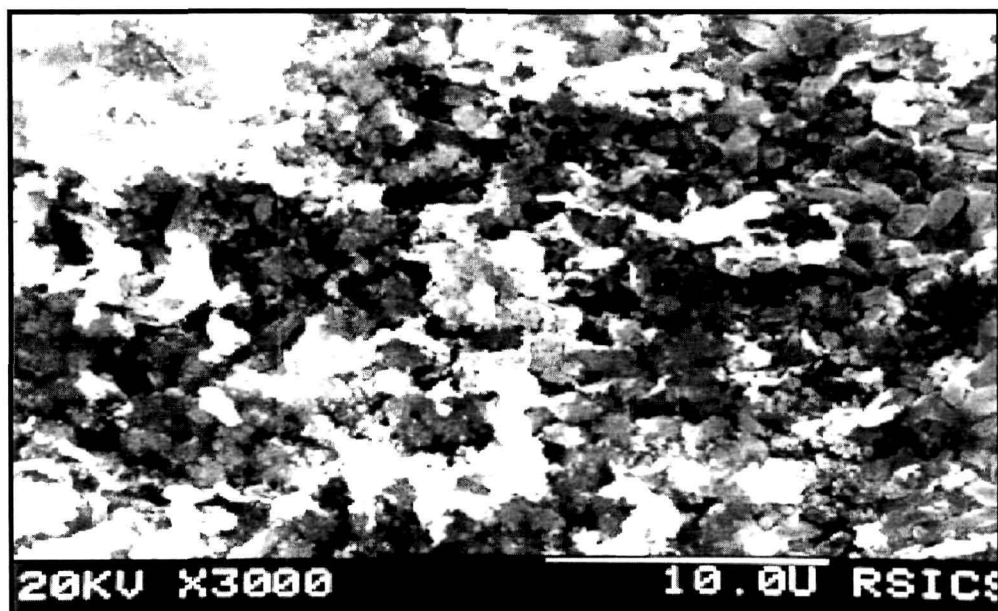
Figure 5.6b: SEM image of P(VDF-HFP)-PMMA-PC-LiClO$_4$-TiO$_2$ (20:10:35:20:15 wt%) composite gel polymer electrolyte.

of TiO_2 surface groups with solvent molecules is considered more important factor affecting the film morphology, rather than the interaction with polymer components. This is because the affinity is directly associated with the solvent evaporation during film casting to give final film morphology.

5.1.5 Differential Scanning Calorimetry

DSC plots for $P(VDF-HFP)-PMMA-PC-LiClO_4$ (20:10:50:20 wt%) and $P(VDF-HFP)-PMMA-PC-LiClO_4-TiO_2$ (20:10:35:20:15 wt%) gel polymer electrolyte systems are shown in figure 5.7. The endothermic peak in the curve shown in figure 5.7a at 91.2 °C is due to the melting of $LiClO_4 \cdot H_2O$ impurities. Peak around 145 °C is corresponding to melting temperature of $P(VDF-HFP)$ [182,219]. Peak observed at 250 °C is due to boiling point of plasticizer propylene carbonate. After addition of ceramic filler TiO_2 peaks are shifted to lower temperature side as shown in figure 5.7b. The melting peak of $P(VDF-HFP)$ is broadened and shifted to 142 °C and boiling point peak of PC is shifted to 247 °C. Reduced
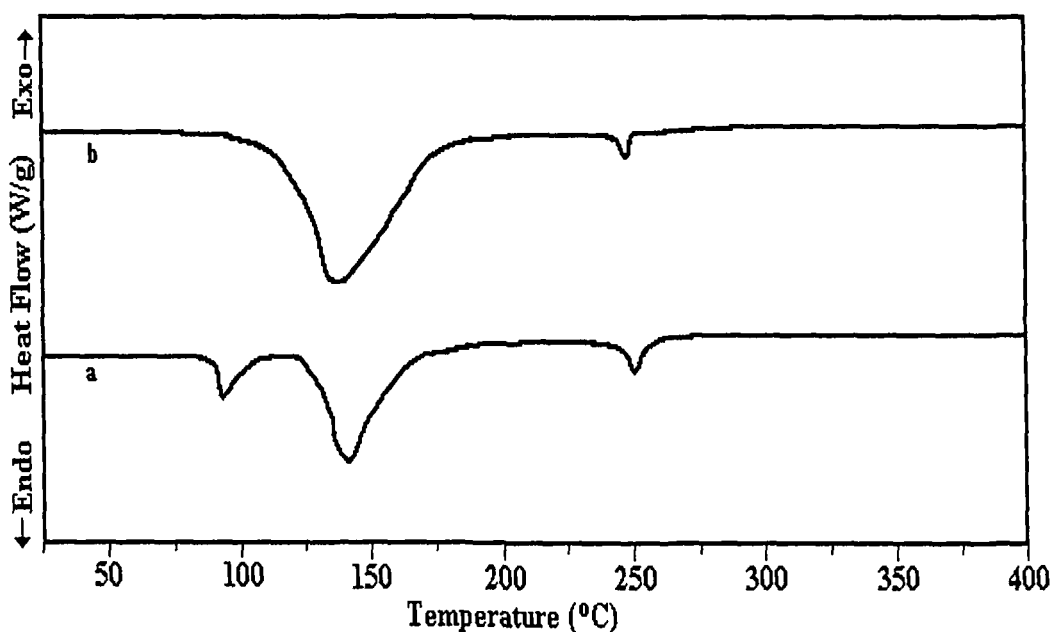
Figure 5.7: DSC curves of (a) $P(VDF-HFP)-PMMA-PC-LiClO_4$ (20:10:50:20 wt%) and (b) $P(VDF-HFP)-PMMA-PC-LiClO_4-TiO_2$ (20:10:35:20:15 wt%) gel polymer electrolyte.

89

melting temperature and broadening of melting endotherm with the addition of TiO_2 particles are consistent with the notion of the interaction of polymer with Li^+ ion, which reduces the crystallinity [53]. DSC curves show that $P(VDF-HFP)-PMMA-PC-LiClO_4$ gel polymer electrolyte system is stable upto 85 °C. In case of $P(VDF-HFP)-PMMA-PC-LiClO_4-TiO_2$ composite gel polymer electrolyte system, curve is almost linear upto 100 °C. Thus the thermal stability of the $P(VDF-HFP)-PMMA-PC-LiClO_4-TiO_2$ composite gel polymer electrolyte appears to increase after addition of filler as compared to that without filler.

5.2 P(VDF-HFP)-PMMA-(PC+DEC)-LiCF₃SO₃-fumed SiO₂ System

5.2.1 Ionic Conductivity Measurements

The ionic conductivity of $P(VDF-HFP)-PMMA-(PC+DEC)-LiCF_3SO_3$-fumed SiO_2 composite gel polymer electrolytes is calculated using the relation $\sigma = l/(R_b r^2 \pi)$, where l and r represent thickness and radius of the sample membrane discs respectively. R_b is the bulk resistance of the gel electrolyte obtained from complex impedance measurements. Figure 5.8 shows the complex impedance spectra of $P(VDF-HFP)-PMMA-(PC+DEC)-LiCF_3SO_3$-fumed SiO_2 (20:10:58:10:2 wt%) polymer electrolyte system at different temperatures. The impedance plots forming semi-circles represent the existence of a circuit element in which capacitor and resistor are combined in parallel.

Figure 5.9 shows the conductivity versus temperature inverse plot of $P(VDF-HFP)-PMMA-(PC+DEC)-LiCF_3SO_3$-fumed SiO_2 composite gel polymer electrolyte system. From the figure it is observed that the ionic conduction in the composite gel polymer electrolyte system obeys the VTF (Vogel-Tamman-Fulcher) relation [90-92], which describes the transport properties in a viscous matrix [171-174]. It supports the idea that the ions move through the plasticizer rich phase, which is conducting and involves the salt and plasticizer.
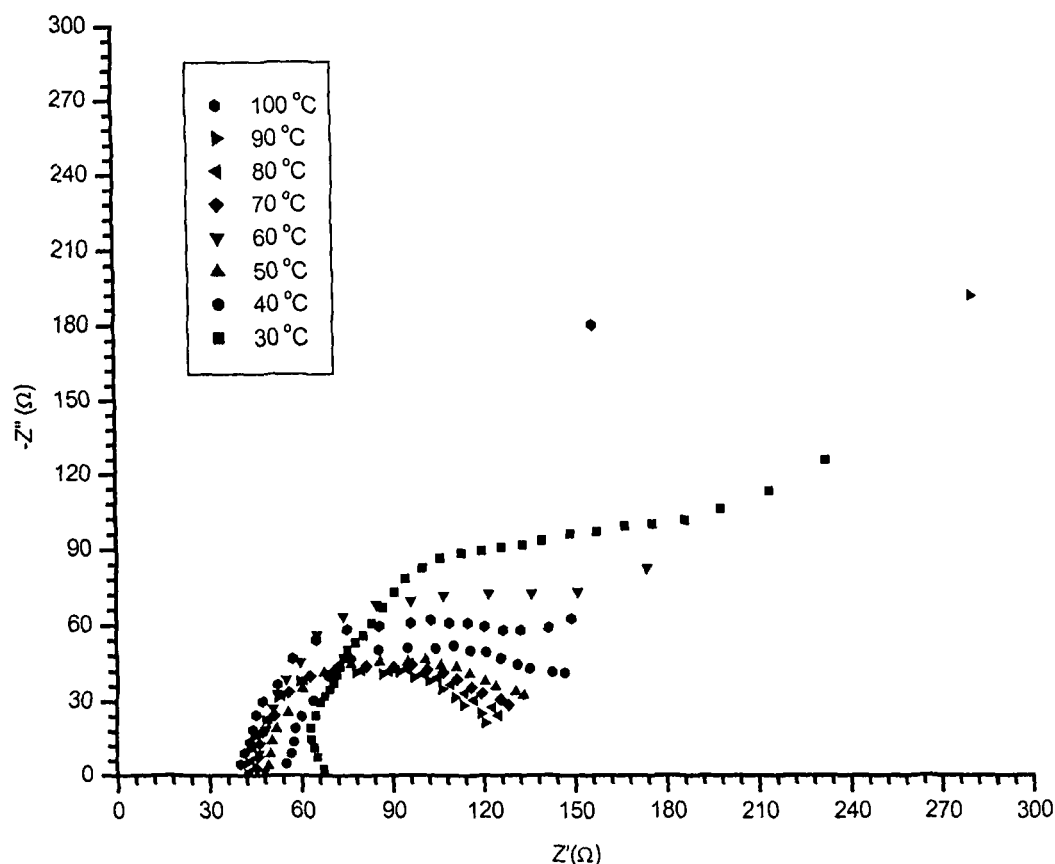
Figure 5.8: Impedance diagram of P(VDF-HFP)-PMMA-(PC+DEC)-LiCF₃SO₃-fumed SiO₂ (20:10:58:10:2 wt%) composite gel polymer electrolyte at difference temperatures.

If the conductivity versus temperature dependence curve is linear in larger temperature region then it is said to Arrhenius. VTF (curved) behavior can be modeled as Arrhenius (linear) behavior by dividing the entire temperature regime into smaller temperature regions. The interconnection between Arrhenius and VTF conductivity versus temperature behavior are widely reported and discussed in literature [93]. This behavior is rationalized by arguing that since VTF dependence is governed by the energy interval $k(T-T_0)$ and the Arrhenius dependence by energy kT (where k Boltzmann constant), for T » T_0 [94] i.e. when T_0 is quite smaller than T, the curvature of conductivity versus temperature plot becomes small and VTF equation approaches Arrhenius equation.

91

Figure 5.9: Temperature dependence of ionic conductivity of P(VDF-HFP)-PMMA-(PC+DEC)-LiCF$_3$SO$_3$-fumed SiO$_2$ composite gel polymer electrolytes at different compositions [wt%], (a) 20:10:60:10:0, (b) 20:10:58:10:2, (c) 20:10:57:10:3 and (d) 20:10:56:10:4.

Composition and conductivity data for composite gel polymer electrolytes containing different weight ratios of P(VDF-HFP), PMMA, LiCF$_3$SO$_3$, (PC+DEC) and fumed SiO$_2$ are presented in table 5.3. It is observed that ionic conductivity exhibits the highest value $\approx 1 \times 10^{-3}$ S/cm at 303 K for 4 wt% fumed SiO$_2$ and 56 wt% (PC+DEC). Conductivity at 373 K is found to be 2.1 $\times 10^{-3}$ S/cm for the same composition. The behavior of conductivity enhancement with temperature can be understood in terms of free-volume model [97,220]. As the temperature increases, the polymer chains flex and expand at increasing rate and produce free volume. The resulting conductivity, represented by the overall mobility of ions and the

Table 5.3: Composition (wt%) and conductivity of P(VDF-HFP)-PMMA-(PC+DEC)-LiCF$_3$SO$_3$-fumed SiO$_2$ composite gel polymer electrolyte at 303 K.

P(VDF-HFP)	PMMA	PC	DEC	LiCF$_3$SO$_3$	Fumed SiO$_2$	Conductivity (Scm^{-1})
20	10	30	30	10	0	4.5 × 10^{-4}
20	10	29	29	10	2	7.2 × 10^{-4}
20	10	28.5	28.5	10	3	9.1 × 10^{-4}
20	10	28	28	10	4	1 × 10^{-3}

polymer chains, is determined by the free volume around the polymer chains. This leads to an increase in ions and segmental mobilities that will assist the ion transport and virtually compensate for the retarding effect of the ion clouds. Enhancement of conductivity can also be attributed to the generation of polymer-ceramic grain boundaries. The structure and
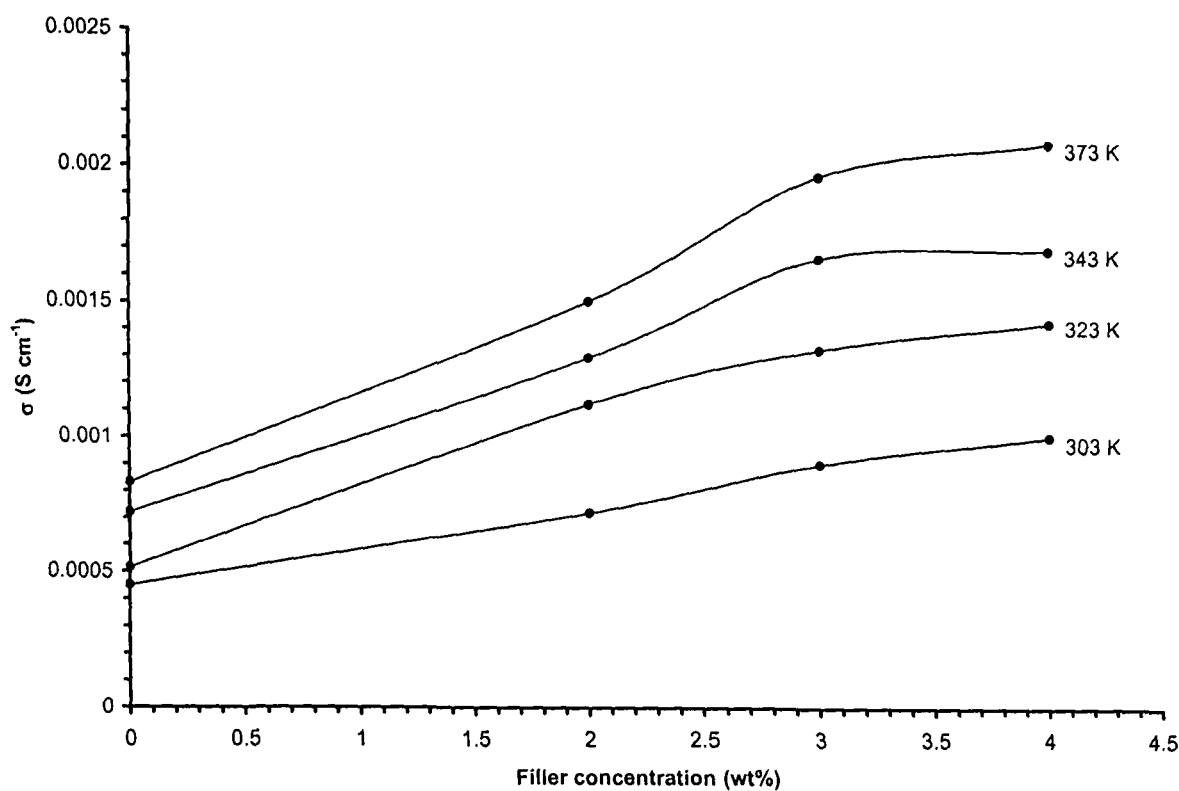
Figure 5.10: Conductivity versus filler concentration for P(VDF-HFP)-PMMA-(PC+DEC)-LiCF$_3$SO$_3$-fumed SiO$_2$ composite gel polymer electrolyte system at different temperatures.

chemistry of ceramic-polymer grain boundaries may have even more important role than the formation of an amorphous phase in the electrolyte. The grain boundaries are the sites of high defect concentration providing channels for faster ionic transport [63].

The variation in conductivity as a function of filler fumed SiO_2 composition in polymer electrolyte system at various temperatures is given in figure 5.10. It is observed that conductivity increases with increase of filler concentrations as well as rise in temperature. An increase in conductivity with the addition of upto 4 wt% silica is related to the enhancement in the capability of the polymer matrix for holding larger volume of the liquid electrolyte as silica assists in developing a highly porous granular microstructure. At still higher concentration of SiO_2 the electrolyte films become brittle and fragile.

Table 5.4: Ionic transference numbers of P(VDF-HFP)-PMMA-(PC+DEC)-$LiCF_3SO_3$-fumed SiO_2 composite gel polymer electrolyte.

P(VDF-HFP)-PMMA-(PC+DEC)-$LiCF_3SO_3$-SiO_2 composite gel Polymer Electrolyte (wt%)	Transference Numbers
20:10:60:10:0	0.9
20:10:58:10:2	0.92
20:10:57:10:3	0.93
20:10:56:10:4	0.94

Total ionic transference number of composite gel polymer electrolyte was measured by Wagner's polarization technique [152,153], which is used to determine the ionic contribution to the total charge transport by measuring the residual electronic current passing through the electrolytes. Silver (Ag) is used as blocking electrode. The Wagner polarization cell Ag/electrolyte/Ag was prepared by coating silver (Ag) paste as blocking electrodes on to

the faces of P(VDF-HFP) based gel composite polymer electrolyte films and calculated as described in Chapter III (section 3.6).

The resulting data are given in table 5.4, for all the compositions of the P(VDF-HFP)-PMMA-(PC+DEC)-LiCF$_3$SO$_3$-fumed SiO$_2$ composite gel polymer electrolyte system, the values of ionic transference numbers t$_{ion}$ are in the range 0.92 to 0.94. This suggests that the charge transport in these polymer electrolyte films is predominantly ionic and a negligible contribution comes from the electrons.

5.2.2 X-ray Diffraction Study

Figure 5.11 shows the XRD patterns of P(VDF-HFP), PMMA, LiCF$_3$SO$_3$, SiO$_2$ and P(VDF-HFP)-PMMA based composite polymer electrolytes respectively. For P(VDF-HFP) (Figure 5.11a) polymer three peaks are found at 2θ = 18.4°, 20° and 26.6°, which correspond well with the (100)+(020), (110) and (021) reflections of crystalline PVDF [176]. This is a confirmation of partial crystallization of the PVDF units in the copolymer to give an overall semi-crystalline morphology for P(VDF-HFP).

The degree of crystallinity (K) for pure P(VDF-HFP) is found to be

$$K = \frac{168\,\text{sq unit}}{560\,\text{sq unit}} \times 100$$

$$K = 30\%$$

For pure PMMA the value of K is

$$K = \frac{23\,\text{sq unit}}{90\,\text{sq unit}} \times 100$$

$$K = 25.5\%$$

and for P(VDF-HFP)-PMMA-(PC+DEC)-LiCF$_3$SO$_3$-fumed SiO$_2$ (20:10:10:56:4 wt%) composite gel polymer electrolyte system degree of crystallinity (K) is found to be
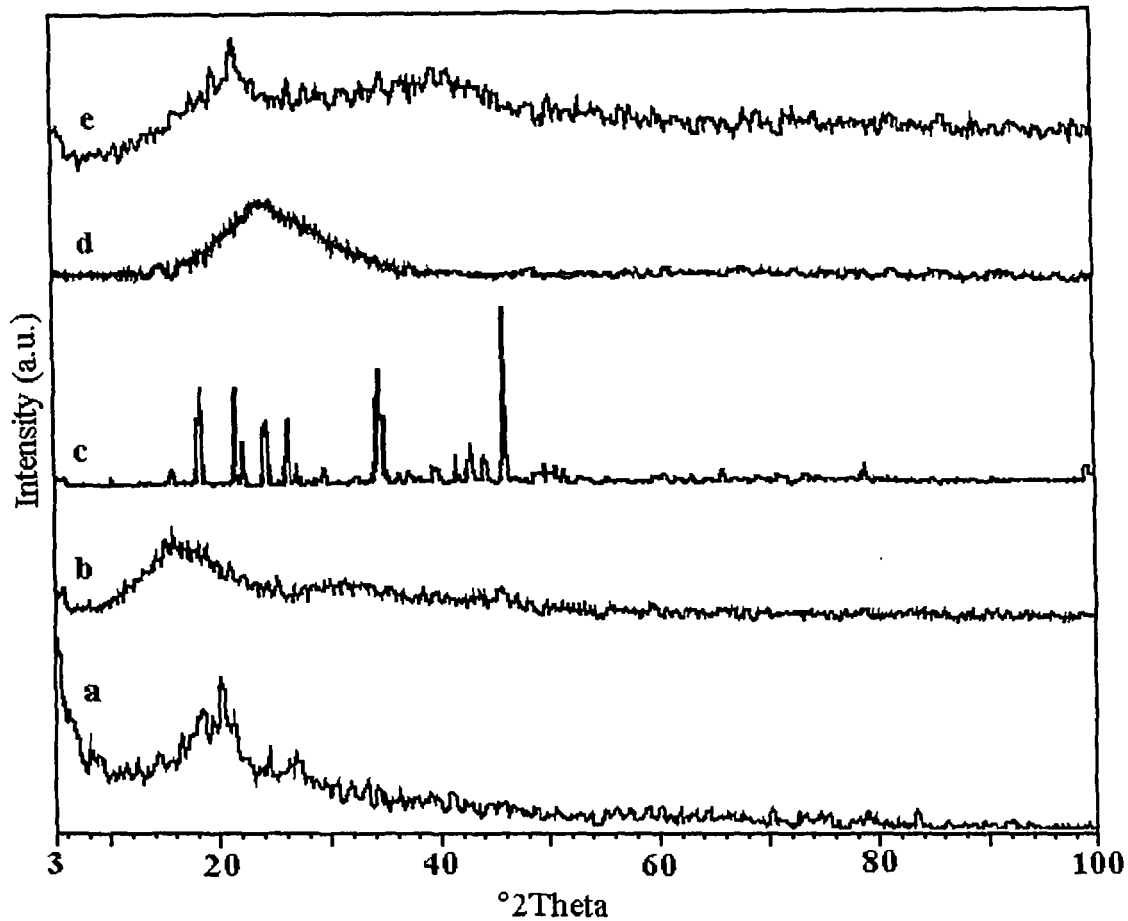
Figure 5.11: XRD patterns of (a) P(VDF-HFP), (b) PMMA (c) LiCF₃SO₃, (d) fumed SiO₂ and (e) P(VDF-HFP)-PMMA-(PC+DEC)-LiCF₃SO₃-fumed SiO₂ (20:10:10:56:4 wt%) composite gel polymer electrolyte.

$$K = \frac{68\,\text{sq unit}}{330\,\text{sq unit}} \times 100$$

$$K = 20.6\%$$

It is observed from figure 5.11e that crystallinity of composite gel polymer electrolyte is greatly reduced by the addition of PC, DEC, LiCF₃SO₃ and SiO₂. Peaks corresponding to LiCF₃SO₃ are not observed in the electrolyte leading to the conclusion that LiCF₃SO₃ (Figure 5.11c) is completely dissolved in the organic solvent trapped in the polymer matrix. Increased amorphicity in the electrolyte, which results in higher conductivity, is attributed to addition of filler fumed SiO₂ and solvent PC and DEC [167,215].

5.2.3 Fourier Transform Infra-Red Spectroscopy

FTIR spectra of P(VDF-HFP), PMMA and P(VDF-HFP)-PMMA-(PC+DEC)-LiCF$_3$SO$_3$-fumed SiO$_2$ composite gel polymer electrolytes are shown in figure 5.12. A band around 3746 cm^{-1} in pure fumed silica is attributed to O–H stretching of the hydroxyl groups which cover the surface of silica [221]. But when fumed silica is mixed with polymer electrolyte systems [Figure 5.12(d-f)] the maximum of this O–H stretching band shifts to around 3650 cm^{-1}. The band broadens, creating an asymmetric wing toward lower frequencies. This indicates that hydroxyl groups on silica surface are involved in bond interactions. Absorption peak at frequency 3004 cm^{-1} is assigned to CH$_3$ stretching vibration of PMMA. Peak at frequency 2959 cm^{-1} is assigned to C–H stretching vibration. Frequency 1783 cm^{-1} is assigned to –CF=CF$_2$, –C–O–CO–O–C– group. Peaks around frequencies 1726 and 1644 cm^{-1} are assigned to >C=O and C-O stretching vibration of PMMA. Frequency 1443 cm^{-1} is assigned to –CH$_3$ bending of PMMA. Peak at frequency 1400 cm^{-1} is assigned to C–F stretching vibration of P(VDF-HFP). Frequencies 1298-1039 cm^{-1} are assigned to -C–F- and -CF$_2$-stretching vibrations. Peak at frequency 883 cm^{-1} is assigned to vinylidene group of polymer. A band around 764 cm^{-1} in curves (c-f), is assigned to the δ_s(CF$_3$) stretching mode of the triflate ion. Frequencies of several triflate ion vibrational modes can be used as a measure of degree and nature of ionic association. Presence of free triflate ions, cation-anion pairs, and highly associated species can be ascertained from corresponding spectroscopically distinct bands; such bands can be observed in either SO$_3$ symmetric stretching spectral region [222,223] or CF$_3$ symmetric deformation region [224]. Although lithium cation interacts with SO$_3$ end of the triflate anion, δ(CF$_3$) mode is particularly sensitive to ionic association through redistribution of charge accompanying the formation of ionic pairs and aggregates [224,225]. The band around 764 cm^{-1} is indicative of highly associated triflate ion and has
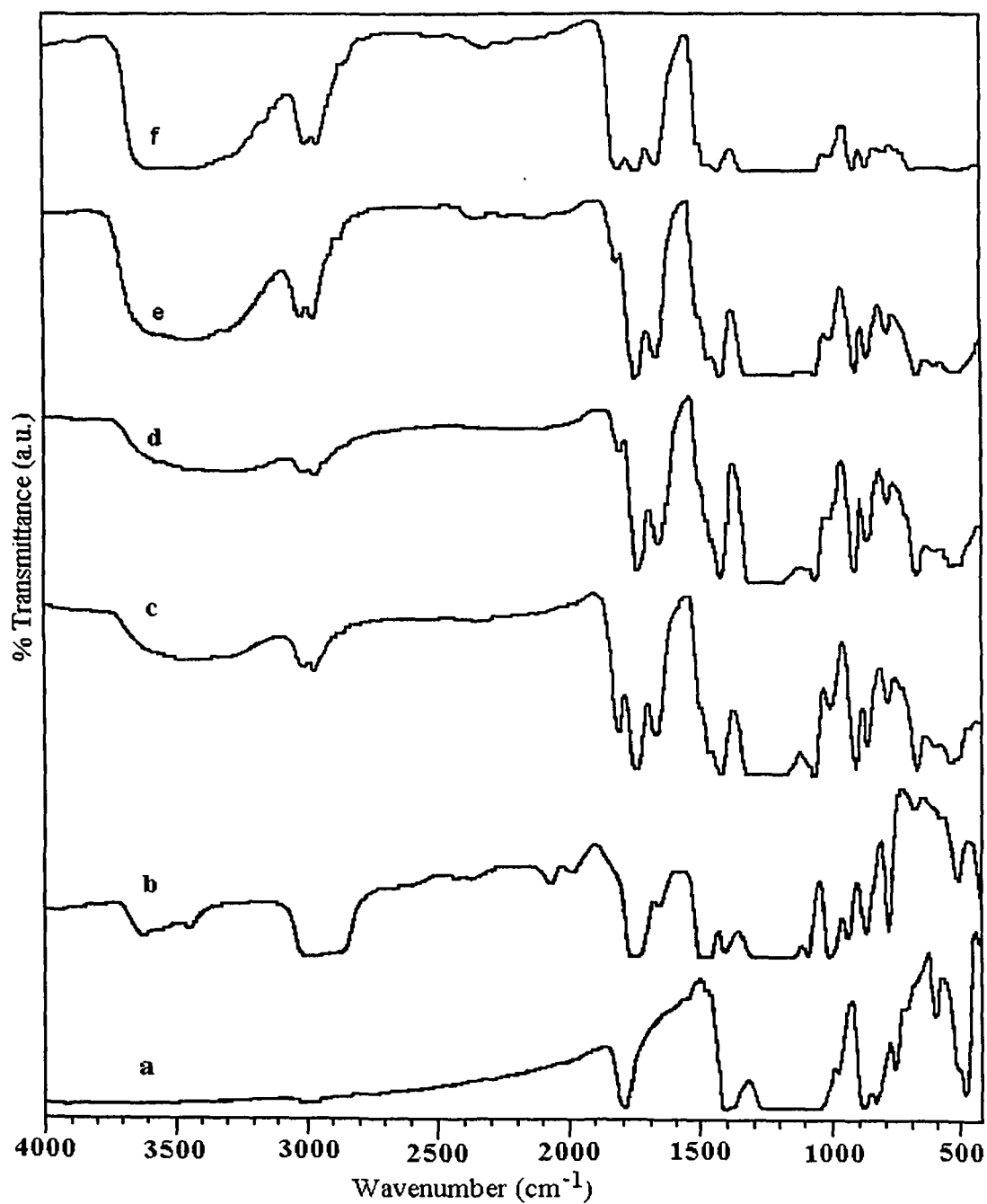
Figure 5.12: FTIR spectra of (a) P(VDF-HFP), (b) PMMA, (c) P(VDF-HFP)-PMMA-(PC+DEC)-LiCF₃SO₃-SiO₂ [20:10:60:10:0 wt%], (d) P(VDF-HFP)-PMMA-(PC+DEC)-LiCF₃SO₃-SiO₂ [20:10:58:10:2 wt%], (e) P(VDF-HFP)-PMMA-(PC+DEC)-LiCF₃SO₃-SiO₂ [20:10:57:10:3 wt%] and (f) P(VDF-HFP)-PMMA-(PC+DEC)-LiCF₃SO₃-SiO₂ [20:10:56:10:4 wt%] polymer electrolyte systems.

been assigned to a $[Li_2Tf]^+$ species [225,226]. The vibrational peaks of PVDF (1797, 1417, 882 and 839 cm^{-1}) and PMMA (2946, 1740, 1637, 1439, 755 and 654 cm^{-1}) are shifted to (1783, 1400, 883 and 837 cm^{-1}) and (2959, 1726, 1644, 1443, 757 and 645 cm^{-1}) respectively in P(VDF-HFP)-PMMA-(PC+DEC)-LiCF$_3$SO$_3$-fumed SiO$_2$ composite gel polymer electrolyte which indicates the interaction among the constituents of the polymer electrolyte.

5.2.4 Scanning Electron Micrograph Study

Scanning electron micrographs of P(VDF-HFP)-PMMA-(PC+DEC)-LiCF$_3$SO$_3$ (20:10:60:10 wt%) and P(VDF-HFP)-PMMA-(PC+DEC)-LiCF$_3$SO$_3$-fumed SiO$_2$ (20:10:57:10:3 wt%) composite gel polymer electrolytes are shown in figures 5.13a and 5.13b. From figure 5.13a it is observed that electrolyte film is a two phase system having polymer and the liquid electrolyte phases. Here the film is interspersed with pores filled with liquid electrolyte, which form a connected path through the polymer matrix [157]. The surface morphology of the composite gel electrolyte as shown in figure 5.13b shows uniformly dispersed SiO$_2$ particles alongwith polymer and pores filled with liquid electrolyte phases. The increased porosity leads to the entrapment of large volumes of liquid electrolyte in the micropores accounting for the increased ionic conductivity. These dispersed SiO$_2$ particles play an active role in the growth of microstructures resulting in completely different morphology with highly porous granular microstructure. SiO$_2$-liquid electrolyte interaction provides additional mechanism of ionic conductivity enhancement along the particle-liquid electrolyte interface [176].
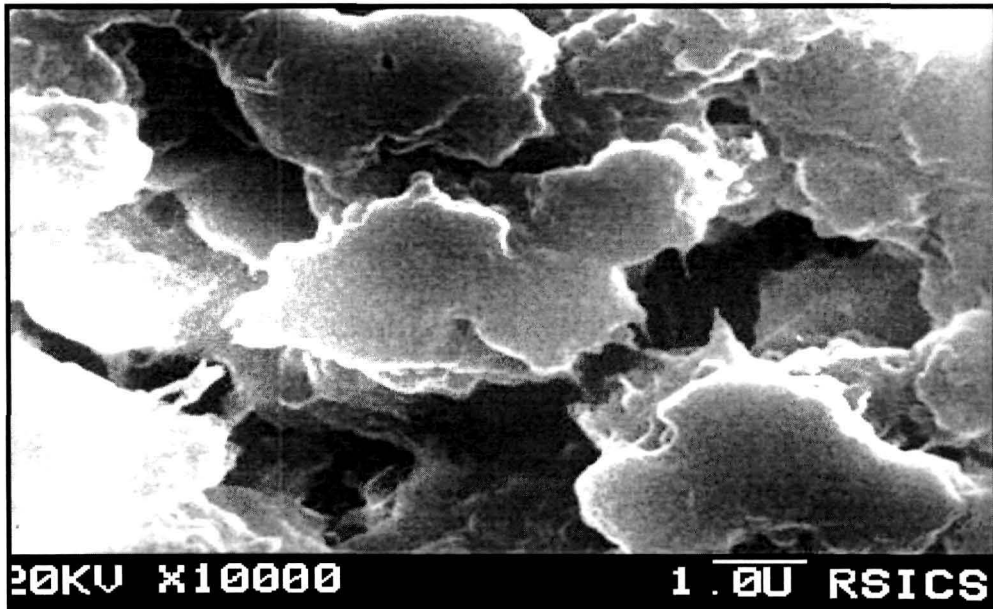
Figure 5.13a: SEM image of P(VDF-HFP)-PMMA-(PC+DEC)-LiCF$_3$SO$_3$ (20:10:60:10 wt%) gel polymer electrolyte.
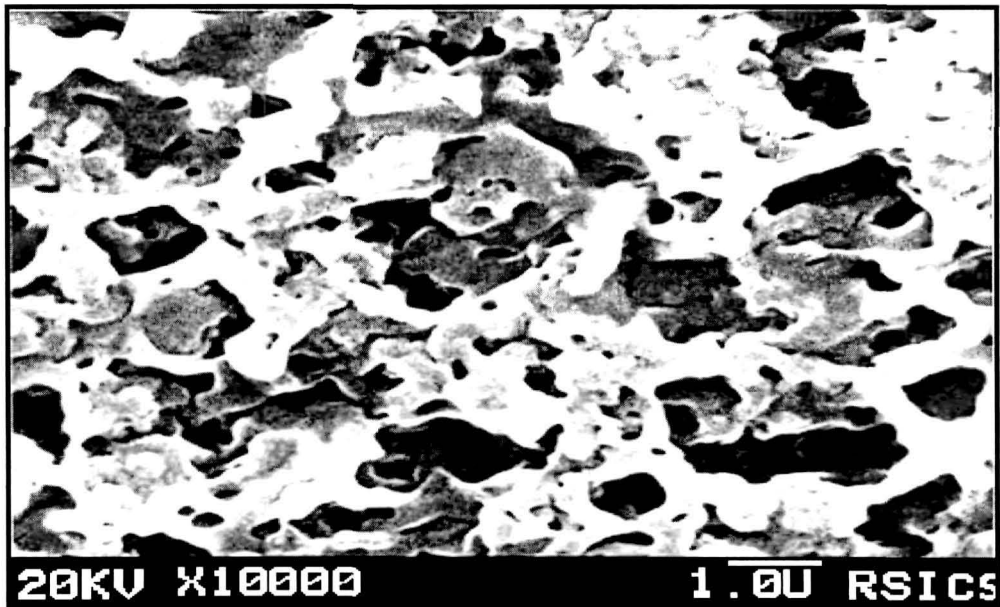
Figure 5.13b: SEM image of P(VDF-HFP)-PMMA-(PC+DEC)-LiCF$_3$SO$_3$-SiO$_2$ (20:10:57:10:3 wt%) gel composite polymer electrolyte.

5.2.5 Differential Scanning Calorimetry

DSC plots for P(VDF-HFP)-PMMA-(PC+DEC)-LiCF₃SO₃ (20:10:60:10 wt%) and

P(VDF-HFP)-PMMA-(PC+DEC)-LiCF₃SO₃-fumed SiO₂ (20:10:56:10:4 wt%) gel polymer

electrolyte systems are shown in figure 5.14. One endothermic broad peak is observed (Figure

5.14a) between 120 °C and 165 °C. The broadening of peak is due to overlapping of boiling

point of DEC (126 °C), melting point of P(VDF-HFP) (143 °C) and melting point of

PMMA (156 °C) [182]. After addition of fumed SiO₂ melting temperature of P(VDF-HFP)

and PMMA are reduced to 140 °C and 150 °C respectively (Figure 5.14b). Both the reduced

melting temperature and broadening of melting endotherm with the addition of fumed SiO₂

filler particles are consistent with the notion of the interaction of polymer with Li^+ ion, which

reduces the crystallinity [53]. DSC plots also show that for both systems up to 80 °C no

thermal event takes place. Thus both the electrolyte systems can be used up to 80 °C.
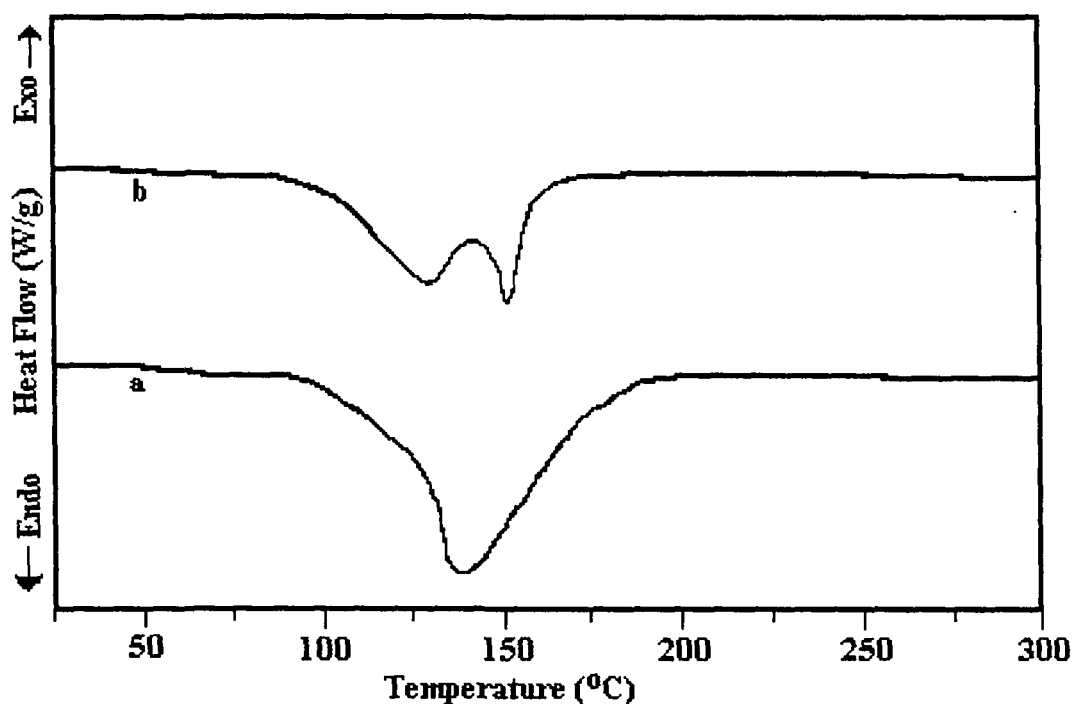
Figure 5.14: DSC curves of (a) P(VDF-HFP)-PMMA-(PC+DEC)-LiCF₃SO₃ (20:10:60:10
wt%) and (b) P(VDF-HFP)-PMMA-(PC+DEC)-LiCF₃SO₃-SiO₂ (20:10:56:10:4 wt%) gel
polymer electrolytes.

5.3 P(VDF-HFP)-(PC+DEC)-LiAsF₆-fumed SiO₂ System

5.3.1 Ionic Conductivity Measurements

Ionic conductivity of P(VDF-HFP)-(PC+DEC)-LiAsF₆-fumed SiO₂ composite gel polymer electrolytes is calculated as described in the previous section. Figure 5.15 shows the complex impedance spectra of P(VDF-HFP)-(PC+DEC)-LiAsF₆-fumed SiO₂ composite gel polymer electrolyte system. Formation of semi-circle in the impedance plot represents the existence of a component in which capacitor and resistor are combined in parallel.
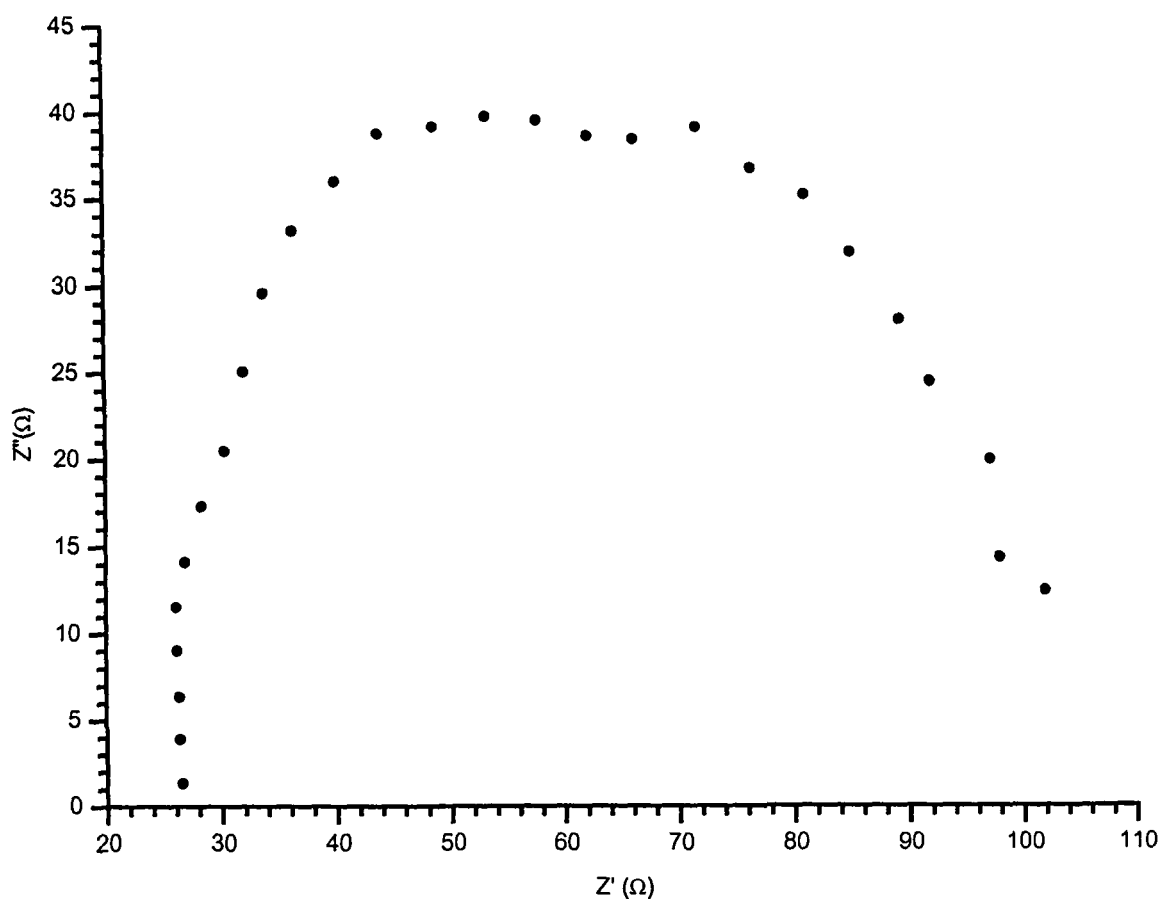
Figure 5.15: Impedance diagram of P(VDF-HFP)-(PC+DEC)-LiAsF₆-fumed SiO₂ composite gel polymer electrolyte. `

Figure 5.16 shows the conductivity versus temperature inverse plots of P(VDF-HFP)-(PC+DEC)-LiAsF$_6$-fumed SiO$_2$ composite gel polymer electrolyte system. From the figure it is observed that the ionic conduction in the composite gel polymer electrolyte system obeys the VTF (Vogel-Tamman-Fulcher) relation [90-92], which describes the transport properties in a viscous matrix [171-174].
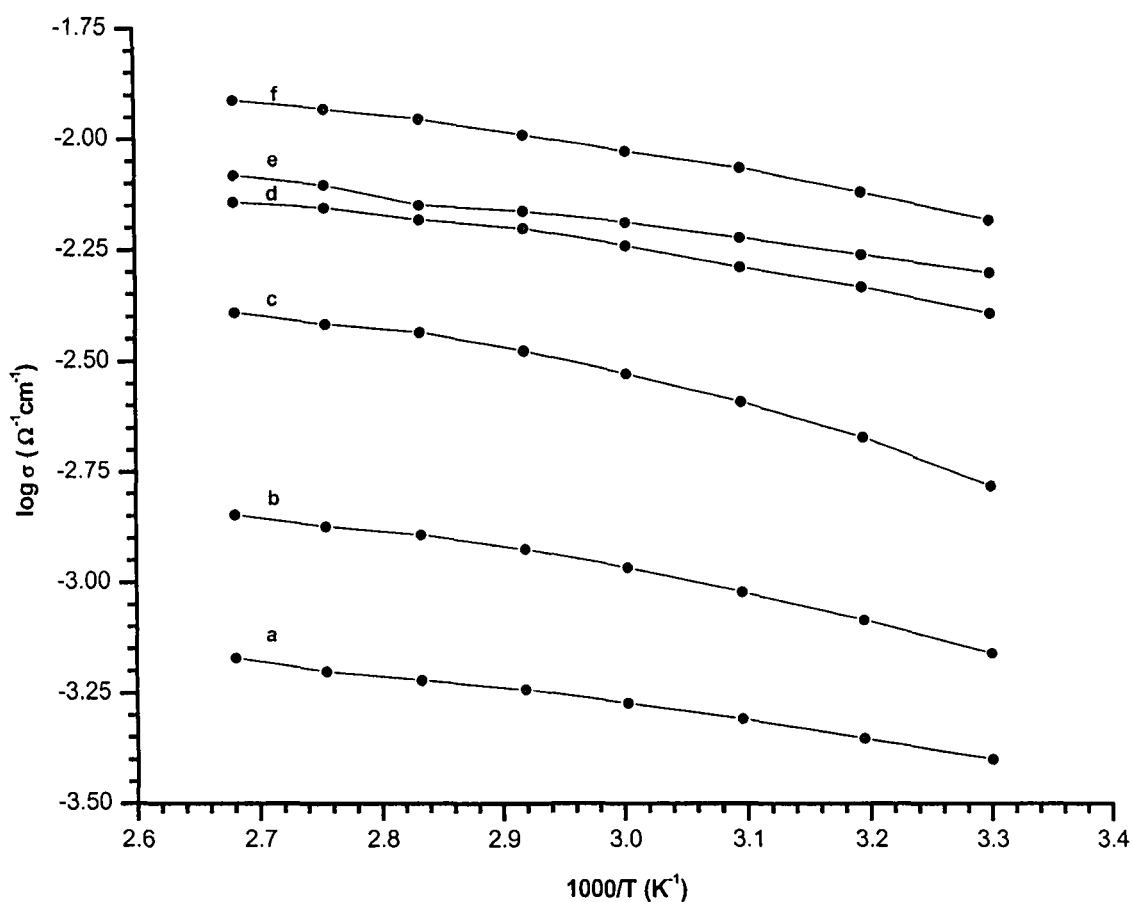
Figure 5.16: Temperature dependence of ionic conductivity of P(VDF-HFP)-(PC+DEC)-LiAsF$_6$-fumed SiO$_2$ composite gel polymer electrolytes at different concentrations (wt%), (a) 25:0:7:0, (b) 25:0:7:5, (c) 25:68:7:0, (d) 25:65:5:5, (e) 25:62:7:6 and (f) 25:59:9:7.

Composition and conductivity data for composite gel polymer electrolytes are presented in table 5.5. Highest conductivity ($\approx$ 6.6 $\times$ 10^{-3} S/cm) composition at 303 K is 25 wt% P(VDF-HFP), 9 wt% LiAsF$_6$, 59 wt% (PC+DEC) and 7 wt% fumed SiO$_2$.

Conductivity at 373 K is found to be 1.22×10^{-2} S/cm for the same composition. An increase in conductivity with the addition of up to 7 wt% silica could be attributed to the enhancement of the capability of holding the liquid electrolytes since silica supports the formation of porous microstructure [65]. The enhancement in ionic conductivity due to the addition of ceramic fillers can be explained by an improved effective-medium theory (EMT) [140,187]. From a microscopic perspective, the composite electrolyte can be treated as a quasi two-phase system, which consists of a polymeric ion-conducting matrix with dispersed composite units.

Table 5.5: Composition (wt%) and conductivity of P(VDF-HFP)-(PC+DEC)-LiAsF₆-fumed SiO₂ composite gel polymer electrolyte at 303 K.

P(VDF-HFP)	PC	DEC	LiAsF₆	Fumed SiO₂	Conductivity (Scm⁻¹)
25	0	0	7	0	3.9×10^{-4}
25	0	0	7	5	6.9×10^{-4}
25	34	34	7	0	1.6×10^{-3}
25	32.5	32.5	5	5	4.1×10^{-3}
25	31	31	7	6	5×10^{-3}
25	29.5	29.5	9	7	6.6×10^{-3}

The ionic conductivity could arise from the existence of a highly conducting layer at the electrolyte/filler interface [140,187]. This interface layer could be an amorphous polymer layer surrounding SiO₂ [187] and/or a space-charge layer [227,228].

The variation in conductivity as a function of filler fumed SiO₂ composition in polymer electrolyte system at various temperatures is given in figure 5.17. It is observed that conductivity increases with increase of filler concentrations as well as rise in temperature. Such high values of conductivity are attributed to higher amorphicity and increased defects concentration along the SiO₂ – polymer interface [63]. Composite gel polymer electrolyte films become mechanically unstable and fragile at higher concentration of SiO₂.
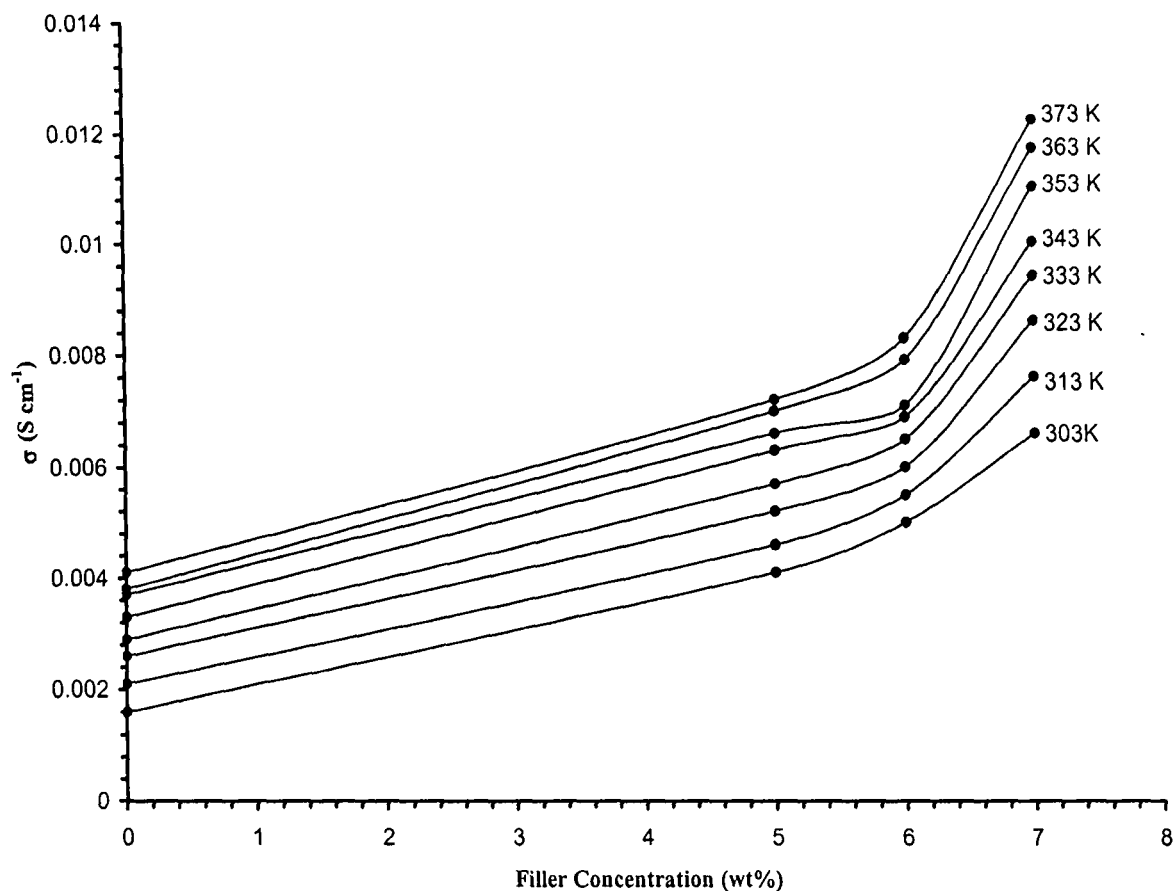
Figure 5.17: Conductivity versus filler concentration (wt%) for P(VDF-HFP)-(PC+DEC)-LiAsF$_6$-fumed SiO$_2$ composite gel polymer electrolyte system at different temperatures.

Table 5.6: Ionic transference numbers of P(VDF-HFP)-(PC+DEC)-LiAsF$_6$-fumed SiO$_2$ composite gel polymer electrolyte.

P(VDF-HFP)-LiAsF$_6$-(PC+DEC)-Fumed SiO$_2$ Composite Gel Polymer Electrolyte (wt%)	Transference Numbers
25 : 7 :68 : 0	0.91
25 : 5 : 65 : 5	0.92
25 : 7 : 62 : 6	0.93
25 : 9 : 59 : 7	0.95

Total ionic transference number of composite gel polymer electrolyte was measured by Wagner's polarization technique [152,153] as described in Chapter III (section 3.6). The

resulting data are given in table 5.6, for all the compositions of the P(VDF-HFP)-(PC+DEC)-LiAsF$_6$-fumed SiO$_2$ electrolyte system, the values of total ionic transference numbers are in the range 0.91 to 0.95 suggesting that the charge transport in these polymer electrolyte films is predominantly ionic and a negligible contribution comes from the electrons.

5.3.2 X-ray Diffraction Study

Figure 5.18 shows the XRD patterns of P(VDF-HFP), LiAsF$_6$, fumed SiO$_2$ and P(VDF-HFP)-LiAsF$_6$-(PC+DEC)-fumed SiO$_2$ composite gel polymer electrolyte system respectively. For P(VDF-HFP) polymer (Figure 5.18a) three peaks are found at 2θ = 18.4°,
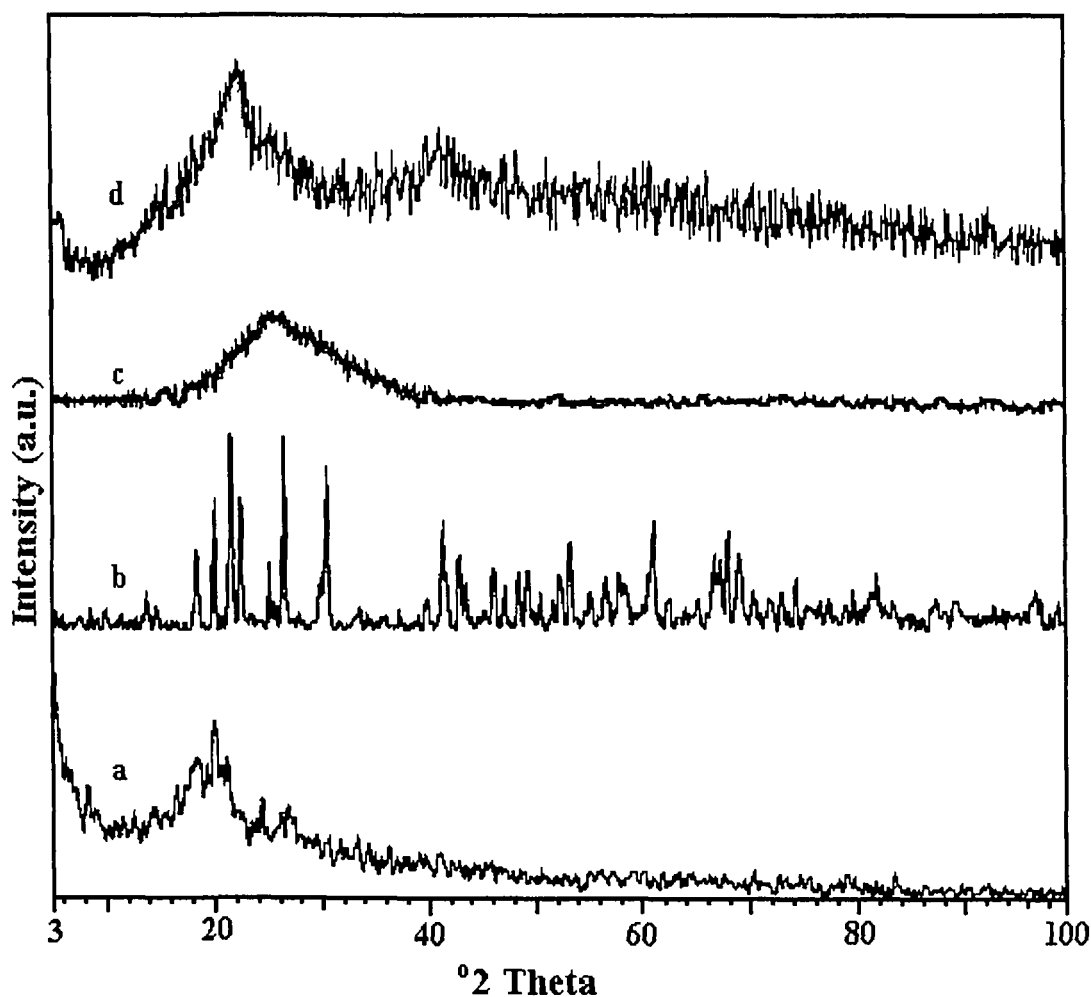
Figure 5.18: XRD patterns of (a) P(VDF-HFP), (b) LiAsF$_6$, (c) fumed SiO$_2$ and (d) P(VDF-HFP)-(PC+DEC)-LiAsF$_6$-fumed SiO$_2$ (25:62:7:6 wt%) composite gel polymer electrolyte

20° and 26.6°, which correspond well with the (100)+(020), (110) and (021) reflections of

crystalline PVDF [176]. This is a confirmation of partial crystallization of the PVDF units in

the copolymer to give an overall semi-crystalline morphology for P(VDF-HFP).

The percentage of degree of crystallinity (K) for pure P(VDF-HFP) is

$$K = \frac{168 \text{ sq unit}}{560 \text{ sq unit}} \times 100$$

$$K = 30\%$$

For P(VDF-HFP)-LiAsF$_6$-(PC+DEC)-SiO$_2$ composite gel polymer electrolyte, K is

$$K = \frac{57 \text{ sq unit}}{322 \text{ sq unit}} \times 100$$

$$K = 17.7\%$$

It is observed from figure 5.18d that crystallinity of composite gel polymer

electrolytes is greatly reduced by the addition of PC, DEC, LiAsF$_6$ and fumed SiO$_2$. Peaks

corresponding to LiAsF$_6$ are not observed in the electrolyte leading to the conclusion that

LiAsF$_6$ (Figure 5.18b) is completely dissolved in the polymer matrix and does not remain a

separate phase. Increased amorphicity in the electrolyte, which gives rise to higher

conductivity, is attributed to addition of fumed SiO$_2$ and plasticizer (PC+DEC) [167,215].

5.3.3 Fourier Transform Infra-Red Spectroscopy

Figure 5.19 shows the FTIR spectra of P(VDF-HFP), LiAsF$_6$, fumed SiO$_2$, P(VDF-

HFP)-LiAsF$_6$, P(VDF-HFP)-LiAsF$_6$-fumed SiO$_2$, P(VDF-HFP)-(PC+DEC)-LiAsF$_6$, P(VDF-

HFP)-(PC+DEC)-LiAsF$_6$-fumed SiO$_2$ composite gel polymer electrolyte systems with

different compositions. Figure 5.19(c) shows a band around 3742 cm^{-1} in pure fumed silica

that is attributed to the O–H stretching of the hydroxyl groups which cover the surface of the

silica [221]. Heating fumed silica to 400 °C removes most of the hydrogen bonded hydroxyl
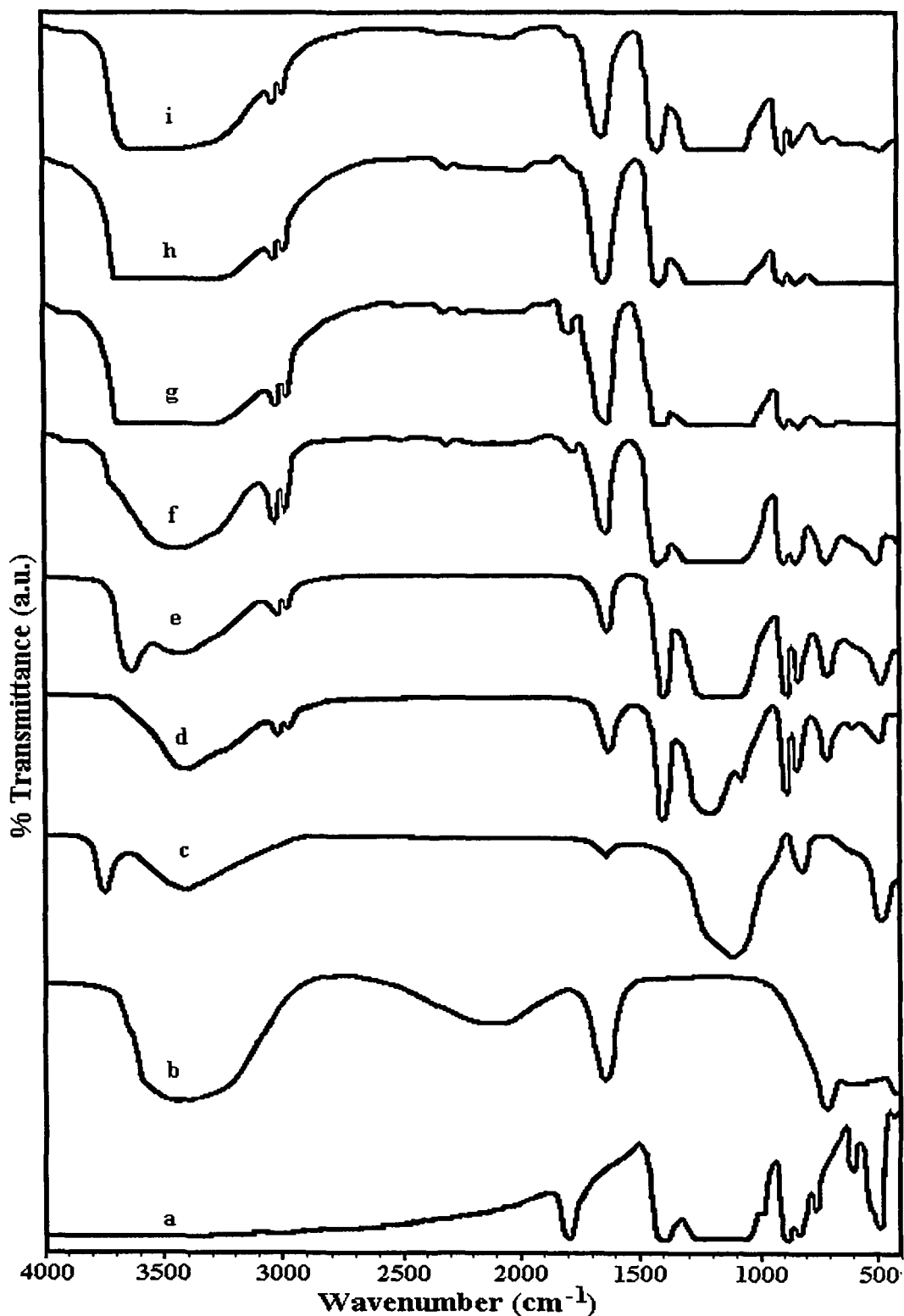
Figure 5.19: FTIR spectra of (a) P(VDF-HFP), (b) LiAsF₆, (c) fumed SiO₂, (d) P(VDF-HFP)-LiAsF₆ (70:30 wt%), (e) P(VDF-HFP)-LiAsF₆-SiO₂ (60:25:15 wt%), (f) P(VDF-HFP)-(PC+DEC)-LiAsF₆ (25:68:7 wt%), (g) P(VDF-HFP)-(PC+DEC)-LiAsF₆-SiO₂ (25:65:7:5 wt%), (h) P(VDF-HFP)-(PC+DEC)-LiAsF₆-SiO₂ (25:62:7:6 wt%), (i) P(VDF-HFP)-(PC+DEC)-LiAsF₆-SiO₂ (25:59:9:7 wt%) composite gel polymer electrolytes.

groups, leaving isolated, non-interacting hydroxyls as the primary groups covering the surface. Absorption peak around 3428 cm^{-1} is due to H bonded OH stretching vibration. Absorption peaks around 1097 cm^{-1} and 807 cm^{-1} are due to Si–OH stretching and Si–O–H bending vibrations respectively. Figure 5.19(e) shows that the O–H band shifts to lower wave numbers region when lithium hexafluoroarsenate is added to the P(VDF-HFP)/fumed silica composite. This indicates that the cation and/or the anion of the salt is interacting with silica's hydroxyl groups.

In figure 5.19(g – i), a broad band is observed around 3690 – 3230 cm^{-1}, indicating shifting of peaks corresponds to fumed SiO_2 in the complex systems. Absorption peaks at frequencies 3021 cm^{-1} and 2990 cm^{-1} are assigned to C–H stretching vibration of P(VDF-HFP). Frequency 1776 cm^{-1} is assigned to –CF=CF$_2$ group. The intensity of the peak is decreasing with the increase of filler concentration. It could be due to interaction of plasticizer with the filler. Frequency 1401 cm^{-1} is assigned to C–F stretching vibration of P(VDF-HFP). Frequencies 882-788 cm^{-1} are assigned to vinylidene group of polymer. Frequency 710 cm^{-1} is assigned to AsF$_6^-$ ion of the LiAsF$_6$ salt. The vibrational peaks of P(VDF-HFP) (1797, 1417, 882 and 839 cm^{-1}) are shifted to (1776, 1401, 885 and 837 cm^{-1}) in P(VDF-HFP)-LiAsF$_6$-(PC+DEC)-fumed SiO_2 composite gel polymer electrolytes clearly indicating polymer-ion interaction.

5.3.4 Scanning Electron Micrograph Study

Scanning electron micrographs of P(VDF-HFP)-(PC+DEC)-LiAsF$_6$ (25:68:7 wt%) and P(VDF-HFP)-(PC+DEC)-LiAsF$_6$-fumed SiO_2 (25:62:7:6 wt%) gel composite polymer electrolytes are shown in figures 5.20a and 5.20b respectively. From figure 5.20a it is observed that electrolyte film is a two phase system having polymer and the liquid electrolyte.
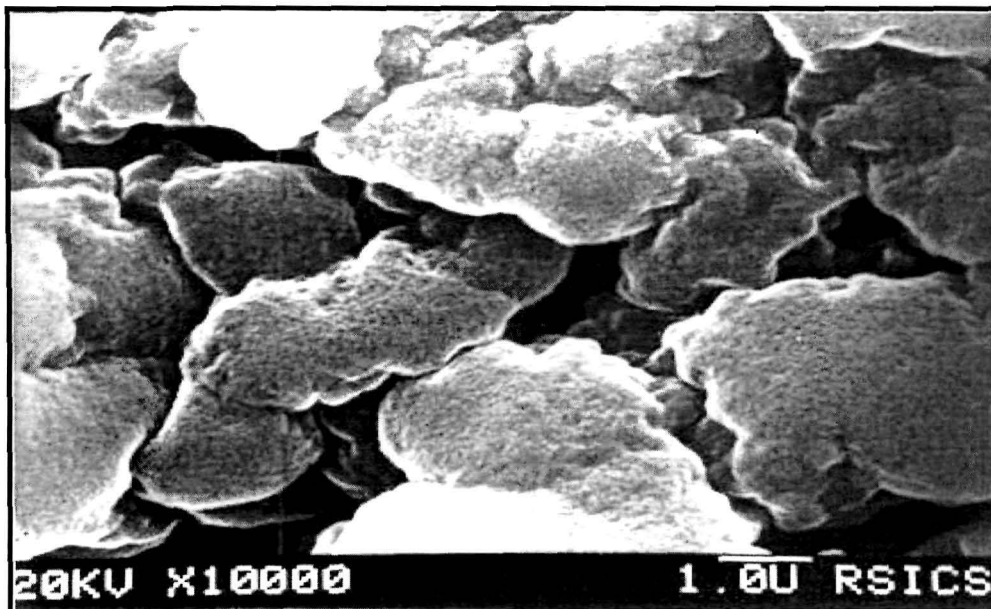
Figure 5.20a: SEM image of P(VDF-HFP)-(PC+DEC)-LiAsF$_6$ (25:68:7 wt%) gel polymer electrolyte.
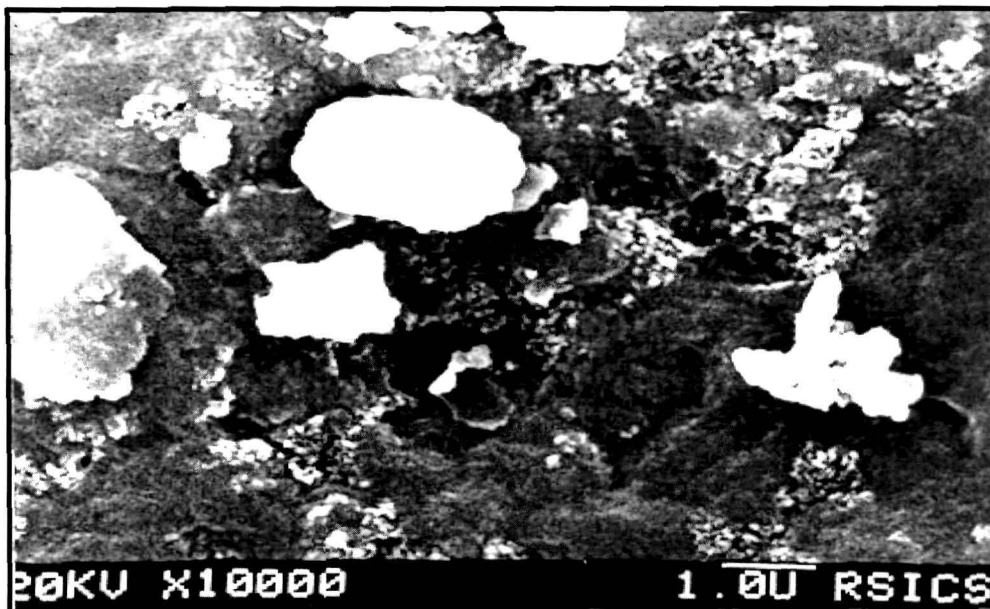
Figure 5.20b: SEM image of P(VDF-HFP)-(PC+DEC)-LiAsF$_6$-fumed SiO$_2$ (25:62:7:6 wt%) composite gel polymer electrolyte.

The film is interspersed with pores filled with liquid electrolyte, which form a connected path through the polymer matrix [216].

The surface morphology of the composite gel electrolyte as shown in figure 5.20b shows well dispersed SiO_2 particles alongwith polymer and pores filled with liquid electrolyte phases. The dispersed SiO_2 particles play active role in the growth of highly porous microstructures with completely different morphology. Besides polymer-ion interaction, SiO_2-liquid electrolyte interaction provides additional mechanism of ionic conductivity enhancement along the particle-liquid electrolyte interface giving higher conductivity in composite polymer gel electrolytes [16].

5.3.5 Differential Scanning Calorimetry

DSC plots for P(VDF-HFP)-(PC+DEC)-$LiAsF_6$ (25:68:7 wt%) and P(VDF-HFP)-(PC+DEC)-$LiAsF_6$-fumed SiO_2 (25:62:7:6 wt%) composite gel polymer electrolyte systems are shown in figure 5.21. One endothermic peak is observed (Figure 5.21a) at 107.5 °C, which is due to melting of $LiAsF_6.3H_2O$ and $LiAsF_6.H_2O$ impurities (probably, the sample took up some water while it was transferred to the container). The broad peak between temperatures 125 - 160 °C is due to overlapping of boiling point of DEC (126 °C) and melting point of P(VDF-HFP) (143 °C) [182,219]. The endothermic peak at 265 °C is due to the structural transformation of $LiAsF_6$ and the exothermic peak observed at 347 °C is due to dissociation of $LiAsF_6$ into LiF and AsF_4 [229,230].

After addition of fumed SiO_2 melting temperature of P(VDF-HFP) is reduced (Figure 5.21b). The broad peak corresponding to boiling point of DEC and melting point of P(VDF-HFP) is shifted to lower temperature 115 – 150 °C. DSC plots also show that in figure 5.21a,

up to 90 °C and in figure 5.21b, up to 100 °C, no thermal event occurs. Thus after addition of

filler thermal stability of the polymer electrolyte is enhanced.
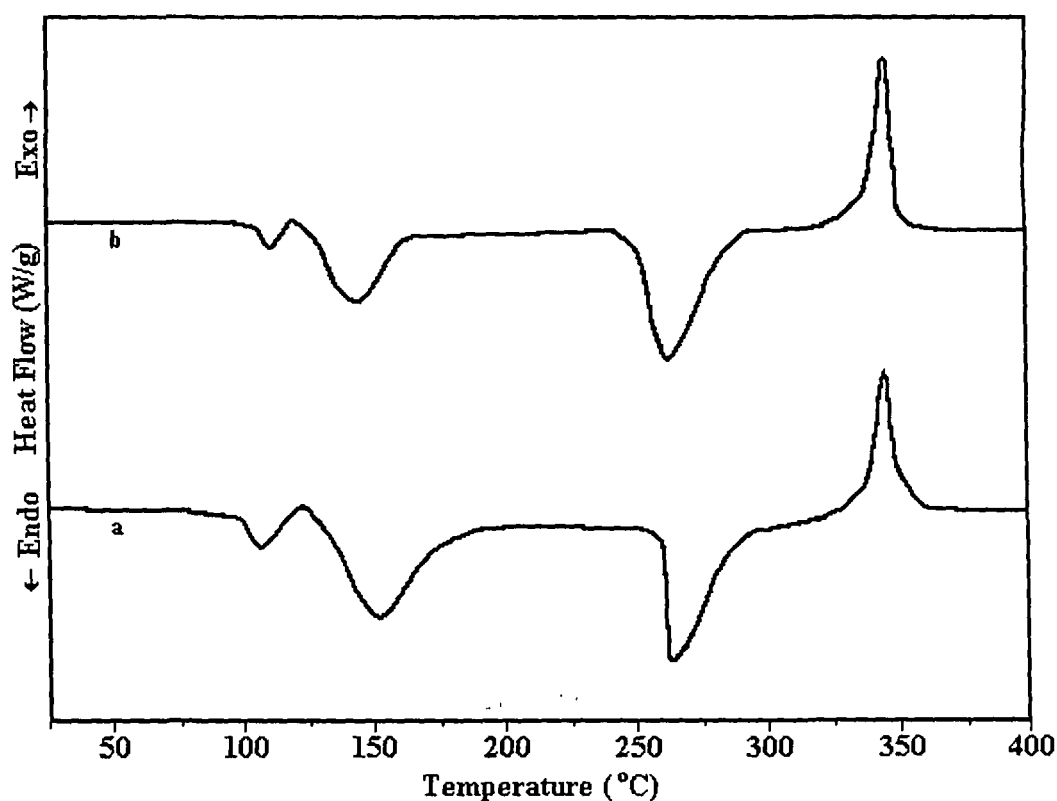
Figure 5.21: DSC curve of (a) P(VDF-HFP)-(PC+DEC)-LiAsF₆ (25:68:7 wt%) and (b) P(VDF-HFP)-(PC+DEC)-LiAsF₆-fumed SiO₂ (25:62:7:6 wt%) gel polymer electrolytes.

5.4 Summary

The compositional dependence of the conductivity of composite gel polymer

electrolytes suggest that matrix-particle interface plays a critical role in the conductivity

profiles of the composite electrolyte systems. Conductivity of the gel polymer electrolyte

systems increased after addition of fillers TiO_2 and fumed SiO_2. This is attributed to the fact

that dispersed phase submicron size filler particles prevent polymer chain reorganization,

resulting in reduction of polymer crystallinity which gives rise to an increase in ionic

conductivity. The reduction in crystallinity could also result from the Lewis acid-base interactions between submicron filler particles surface and polymer chains. This allows ions to move more freely either on the surface of the submicron filler particles or through a low density polymer phase at the interface, which results in enhanced ionic conductivity. Enhancement of conductivity can also be attributed to the generation of polymer-ceramic grain boundaries. The grain boundaries are the sites of high defect concentration providing channels for faster ionic transport along the grain boundaries. Maximum ionic conductivity for P(VDF-HFP)-PMMA-PC-LiClO$_4$-TiO$_2$, P(VDF-HFP)-PMMA-(PC+DEC)-LiCF$_3$SO$_3$-fumed SiO$_2$ and P(VDF-HFP)-(PC+DEC)-LiAsF$_6$-fumed SiO$_2$ composite gel polymer electrolyte is found to be 2.8×10^{-2} S/cm, 1×10^{-3} S/cm and 6.6×10^{-3} S/cm respectively.

XRD analysis reveals that degree of crystallinity is reduced from 30% in pure P(VDF-HFP) and 25.5% in pure PMMA to 6% in P(VDF-HFP)-PMMA-PC-LiClO$_4$-TiO$_2$ and 20.6% in P(VDF-HFP)-PMMA-(PC+DEC)-LiCF$_3$SO$_3$-fumed SiO$_2$ composite gel polymer electrolytes. The degree of crystallinity is reduced from 30% in pure P(VDF-HFP) to 17.7% in P(VDF-HFP)-(PC+DEC)-LiAsF$_6$-fumed SiO$_2$ composite gel polymer electrolyte. Increased amorphicity in the electrolyte, which gives rise to higher ionic conductivity is attributed to the steric hindrance provided by the bulky pendant –CH$_3$COO ester group of PMMA upon blending of P(VDF-HFP) with PMMA and addition of the plasticizer and filler. FTIR analyses suggest that hydroxyl groups on silica surface are involved in bond interactions with polymers and salts. SEM images show that with the addition of filler TiO$_2$ and fumed SiO$_2$, the film surfaces becomes rough but the submicron particles are well dispersed on the surface. The film roughness supports the existence of micropores. The increased porosity leads to trapping of large volumes of the liquid in the micropores accounting for the increased ionic conductivity.

CHAPTER VI

SWIFT HEAVY ION IRRADIATION EFFECTS IN GEL POLYMER ELECTROLYTES

High energy ion irradiation of polymers leads to remarkable changes in their physical and chemical properties [231-237]. Permanent modifications in the molecular weight distribution and solubility [237,238], electrical [239-244], optical [245-249] and mechanical properties [250-253] of polymers and other materials have been detected after ion irradiation. When an energetic ion traverses through a polymer, it loses its energy by interacting with target nuclei (nuclear stopping) and by interacting with target electrons (electronic stopping) processes. Nuclear stopping arises from collisions between the energetic ions and target nuclei which cause atomic displacement and chain scission. Electronic stopping is mainly determined by the charge state of the ion and its velocity as the orbital electrons of the moving ion are stripped off to a varying degree depending upon the ion velocity [113]. Energy transfer by nuclear stopping process becomes important when an ion slows down approximately to the Bohr velocity [orbital electron velocity = $(1/4\pi\epsilon_0)(e^2/\hbar) \approx 2.2 \times 10^6$ m/s]. Therefore for high energy ions, the maximum energy loss occurs near the end of the ion track. Nuclear collisions create recoil atoms due to momentum transfer from ion to target atom and these recoil atoms are thermalized by dissipating energy through phonons and collective excitations of target atoms (plasmons). For most ion energy ranges of interest, nuclear stopping by ions of low atomic number atoms of hydrogen and helium is negligible because the Rutherford scattering cross section and momentum transfer by the low mass atom is small [113]. Nuclear stopping however becomes important for ion species with a large number of nucleons. Polymers have a fairly large free volume, often larger than 20%, and the atomic

114

density in such a loose system is relatively small as compared to dense lattice structure such as metal. Therefore, in polymers, most nuclear displacements occur fairly independently. The probability to cause simultaneous displacement of two atoms from neighboring chains and create two radical pairs for cross linking is small in nuclear processes. Heavy ions with low energy (less than a few keV) have large nuclear energy transfer and thus cause bond breakage and chain scission and are not desirable for cross linking [254].

The electronic energy loss takes place in two ways: electronic excitations and ionizations of the target atoms. When the electronic transfer is high, a considerable volume around the ion projectile is influenced because of the coulombic field produced by glancing collisions and ionization by knock-on collisions [113]. This results in production of active chemical species i.e. cations, anions and radicals, and electrons along the polymer chains. Coulombic interactions among these active species cause violent bond stretching and segmental motion in the polymer chains. Electronic stopping causes more cross linking due to collective excitations (plasmons) of target atoms, which produce a large excited volume thereby resulting in coercive interactions among the ions and radical pairs produced within the volume.

Crystallinity is also affected by ion irradiation and most semi-crystalline polymers exhibit a decrease in crystallinity at high dose irradiation ($\approx$ 1 MGy $\approx$ 2 $\times$ 10^{12} ions/cm^2) [255]. Ordering of the molecular chains after low fluence ($\approx$ 200 kGy $\approx$ 4 $\times$ 10^{11} ions/cm^2) light ion irradiation has also been reported [256]. The recrystallization phenomena in polymers as a consequence of constructive phase transition, i.e., transition from amorphous to crystalline phase characterizing the growth of new crystallites or even formation of new lamellar stacks upon irradiation is a relatively new area of research offering many

potentialities [257,258]. Crystallinity plays a crucial role in almost all polymer properties such as mechanical, optical, electrical and even thermal properties.

In this Chapter studies on two gel polymer electrolyte systems P(VDF-HFP)-(PC+DEC)-LiClO$_4$ and P(VDF-HFP)-(PC+DEC)-LiCF$_3$SO$_3$ irradiated with Li^{3+} and C^{5+} swift heavy ion (SHI) have been presented. Polymer gel electrolyte samples have been prepared by solution casting technique as described in Chapter III (section 3.2) with film thicknesses < 30 μm. Ion irradiation of gel polymer electrolyte samples was performed at the 15 UD Pelletron accelerator available at the Nuclear Science Centre, New Delhi, India using General Purpose Scattering Chamber (GPSC) and Material Science (MS) beam line facilities. Gel polymer electrolyte samples were irradiated by 48 MeV Li^{3+} ion beam with five different fluences 5 × 10^{10}, 10^{11}, 5 × 10^{11}, 10^{12} and 5 × 10^{12} ions/cm^2, mounted in the GPSC high vacuum chamber. Irradiation was also done for the same gel polymer electrolyte systems by 70 MeV C^{5+} ion beam with eight different fluences 5 × 10^9, 10^{10}, 2 × 10^{10}, 6 × 10^{10}, 10^{11}, 3 × 10^{11}, 7 × 10^{11} and 10^{12} ions/cm^2 using ultra high vacuum chamber of MS beam line. Energies of 48 MeV for Li^{3+} and 70 MeV for C^{5+} ion beams have been chosen so that the samples undergo uniform irradiation effects as the projected ion range (453 μm for Li^{3+} ion and 155 μm for C^{5+} ion, according to stopping and ranges of ions in matter (SRIM) code [154]) was much larger than the polymer electrolyte film thickness (~30 μm). The ionic conductivity for all the irradiated samples with different fluences and temperatures was obtained from the complex impedance analysis. SEM and XRD analysis have been carried out for microstructural characterization and crystallinity study respectively. FTIR study has been conducted to investigate the molecular level polymer-ion interactions in irradiated gel polymer electrolytes. Detailed results of Li^{3+} and C^{5+} ion beam irradiated P(VDF-HFP)-(PC+DEC)-LiClO$_4$ gel polymer electrolyte system are presented first, followed by irradiated

P(VDF-HFP)-(PC+DEC)-LiCF$_3$SO$_3$ gel polymer electrolyte system irradiated with the same ion beams.

6.1 Li^{3+} and C^{5+} Ion Irradiated P(VDF-HFP)-(PC+DEC)-LiClO$_4$ System

6.1.1 Ionic Conductivity measurements

The ionic conductivity of pristine (unirradiated) and, Li^{3+} and C^{5+} ion irradiated P(VDF-HFP)-(PC+DEC)-LiClO$_4$ gel polymer electrolytes are calculated from the relation $\sigma = l /(R_b r^2 \pi)$, where l and r represent thickness and radius of the sample membrane discs respectively. R_b is the bulk resistance of the electrolyte obtained from complex impedance measurements. Figures 6.1 and 6.2 show the conductivity versus temperature inverse plots of pristine and, Li^{3+} and C^{5+} ion beam irradiated P(VDF-HFP)-(PC+DEC)-LiClO$_4$ gel polymer electrolytes respectively. From the figures it is observed that the ionic conduction in both the ion irradiated gel polymer electrolyte systems obey the VTF (Vogel-Tamman-Fulcher) relation [90-92], which describes the transport properties in a viscous matrix [171-174]. If the conductivity versus temperature dependence curve is linear in larger temperature region then it is said to Arrhenius. VTF (curved) behavior can be modeled as Arrhenius (linear) behavior by dividing the entire temperature regime into smaller temperature regions. The interconnection between Arrhenius and VTF behavior of σ(T) are widely reported and discussed in literature [93]. This behavior is rationalized by arguing that since VTF dependence is governed by the energy interval k(T-T$_0$) and the Arrhenius dependence by the energy kT (where k Boltzmann constant), for T » T$_0$ [94] i.e. when T$_0$ is quite smaller than T, the curvature of conductivity versus temperature plot becomes small and VTF equation approaches Arrhenius equation.

Figure 6.1: Temperature dependence of ionic conductivity of Li^{3+} ion irradiated P(VDF-HFP)-(PC+DEC)-LiClO$_4$ (20:70:10 wt%) gel polymer electrolyte (a) unirradiated, (b) 5×10^{10}, (c) 10^{11}, (d) 5×10^{11}, (e) 10^{12} and (f) 5×10^{12} ions/cm^2.

Table 6.1: Ionic conductivities of Li^{3+} ion irradiated P(VDF-HFP)-(PC+DEC)-LiClO$_4$ (20:70:10 wt%) gel polymer electrolyte with different fluences at 303K.

Fluence (ion/cm^2)	Conductivity σ (Scm^{-1})	σ/σ_0
Unirradiated	4.0×10^{-3}	1
5×10^{10}	9.2×10^{-3}	2.3
1×10^{11}	2.2×10^{-2}	5.05
5×10^{11}	1.2×10^{-3}	0.3
1×10^{12}	3.3×10^{-4}	0.08
5×10^{12}	1.25×10^{-4}	0.03
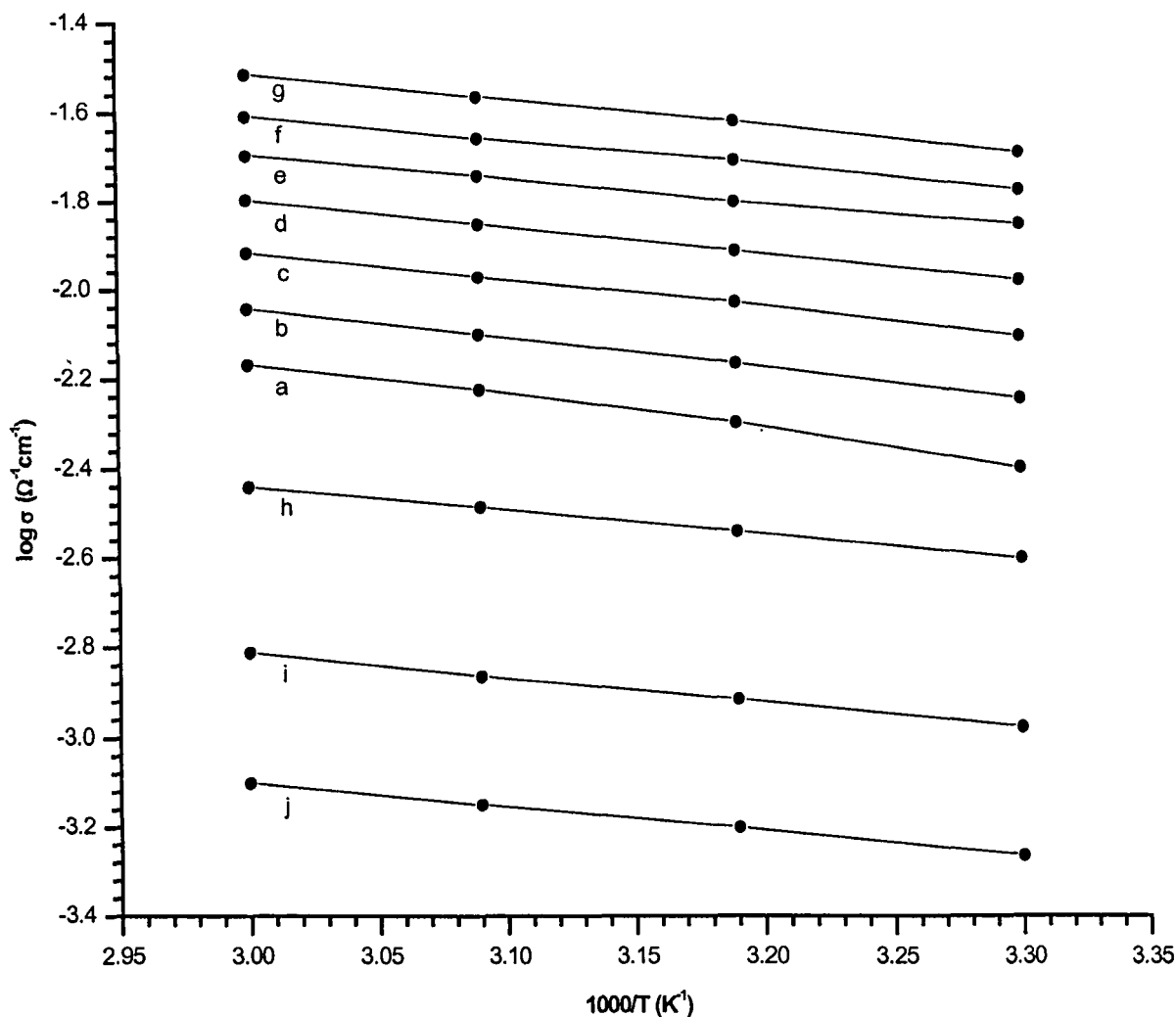
Figure 6.2: Temperature dependence of ionic conductivity of C^{5+} ion irradiated P(VDF-HFP)-(PC+DEC)-LiClO₄ (20:70:10 wt%) gel polymer electrolyte (a) unirradiated, (b) 5×10^9, (c) 7×10^9, (d) 10^{10}, (e) 2×10^{10}, (f) 6×10^{10}, (g) 10^{11}, (h) 3×10^{11}, (i) 7×10^{11} and (j) 10^{12} ions/cm².

Table 6.2: Ionic conductivities of C^{5+} ion irradiated P(VDF-HFP)-(PC+DEC)-LiClO₄ (20:70:10 wt%)gel polymer electrolyte with different fluences at 303K.

Fluence (ion/cm²)	Conductivity σ (Scm⁻¹)	σ/σₒ
Unirradiated	4.0×10^{-3}	1
5×10^9	5.7×10^{-3}	1.43
7×10^9	7.8×10^{-3}	1.95
1×10^{10}	1.0×10^{-2}	2.5
2×10^{10}	1.4×10^{-2}	3.5
6×10^{10}	1.6×10^{-2}	4
1×10^{11}	2.0×10^{-2}	5
3×10^{11}	2.5×10^{-3}	0.63
7×10^{11}	1.1×10^{-3}	0.28
1×10^{12}	5.5×10^{-4}	0.14
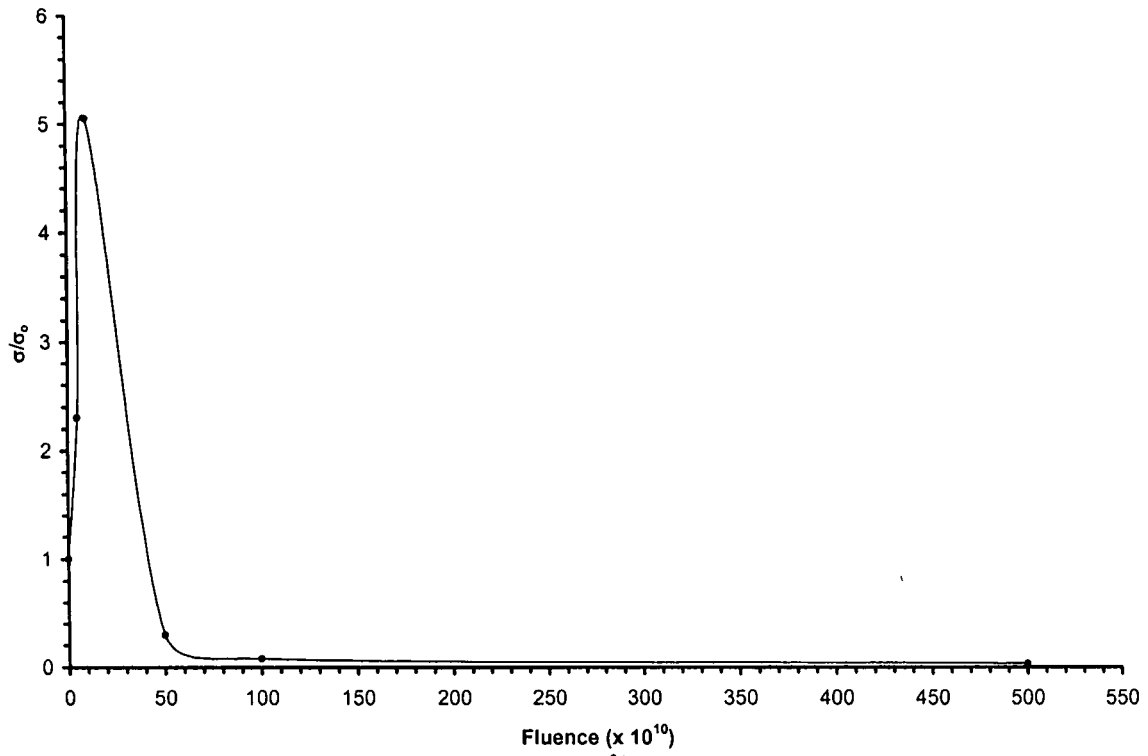
Figure 6.3: σ/σ_0 versus fluence curve of Li^{3+} ion irradiated P(VDF-HFP)-(PC+DEC)-$LiClO_4$ (20:70:10 wt%) gel polymer electrolyte.
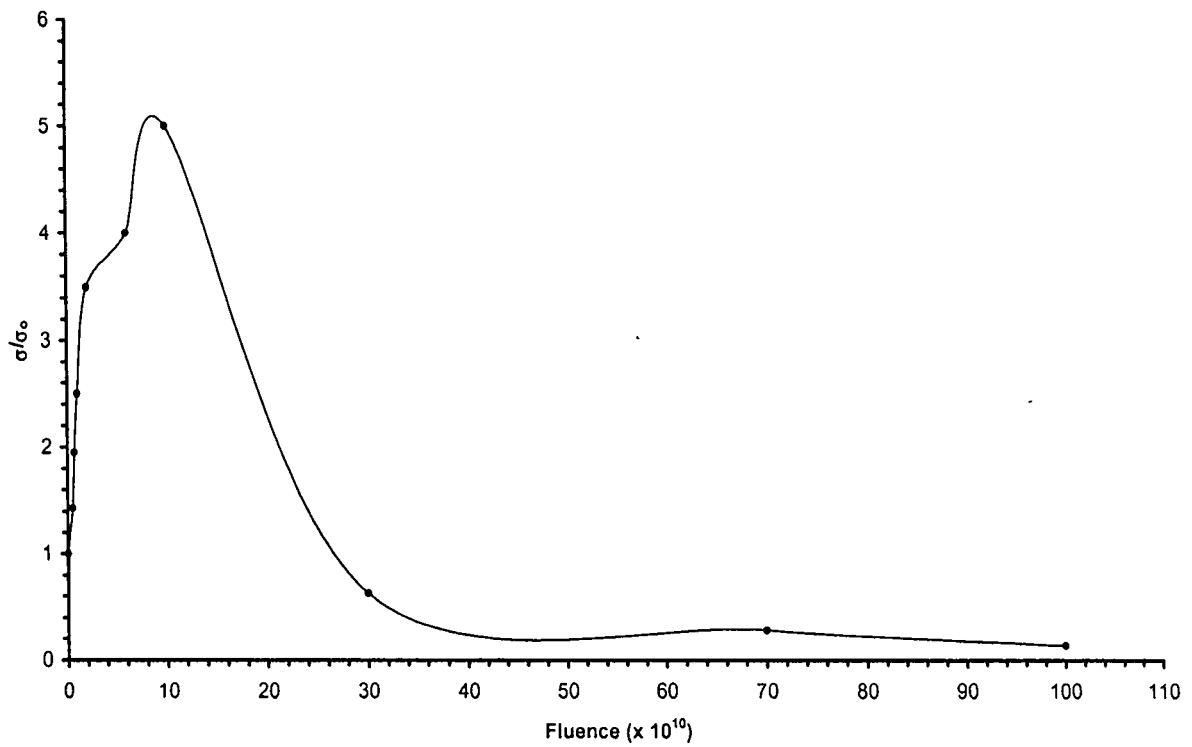
Figure 6.4: σ/σ_0 versus fluence curve of C^{5+} ion irradiated P(VDF-HFP)-(PC+DEC)-$LiClO_4$ (20:70:10 wt%) gel polymer electrolyte.

It is observed that irradiation with lower fluences ($\leq 10^{11}$ ions/cm^2) conductivity increases and with higher fluences ($>10^{11}$ ions/cm^2) it decreases (Figures 6.3 and 6.4). This could be attributed to the fact that at lower fluences bonds in the polymer chains are broken [259] and chain scission process dominates, which leads to faster ion transport through the polymer matrix assisted by large amplitude segmental motion of the polymer backbone. At higher fluences the activation energy for crosslinking process to occur is reached and the cross-linking process of polymer chain dominates due to collective excitation (plasmons), which produces a large excited volume resulting in coercive interaction among the ions and radical pairs produced in the adjacent chains within the volume [260,261]. These results are consistent with the fluence dependent effect of swift heavy ion irradiation on solubility of polymers [238].

The conductivity data for Li^{3+} and C^{5+} ion beam irradiated P(VDF-HFP)-(PC+DEC)-LiClO$_4$ gel polymer electrolytes with different fluences are presented in tables 6.1 and 6.2. From the table it is observed that the highest ionic conductivity value for Li^{3+} ion irradiated system is 2.2 $\times$ 10^{-2} S/cm at fluence of 1 $\times$ 10^{11} ions/cm^2 and 2 $\times$ 10^{-2} S/cm for C^{5+} ion irradiated system at the same fluence. Total ionic transference number for both Li^{3+} and C^{5+} ion irradiated P(VDF-HFP)-(PC+DEC)-LiClO$_4$ gel polymer electrolyte was measured by Wagner's polarization method [152,153] as described in Chapter III (section 3.6). The transference number for the system was measured to be 0.96 – 0.99 and 0.95 – 0.99 after Li^{3+} and C^{5+} ion irradiation respectively indicating that the conduction in the electrolyte system is predominantly ionic. Higher value of transference number suggests that conduction is predominantly ionic.

6.1.2 X-ray Diffraction Study

X-ray diffractograms of pristine and, Li^{3+} and C^{5+} ion irradiated P(VDF-HFP)-(PC+DEC)-$LiClO_4$ gel polymer electrolyte systems are shown in figures 6.5 and 6.6 respectively. X-ray diffraction from crystalline regions of P(VDF-HFP) gives sharp and well-defined peaks located at 2θ angular positions at 18°, 18.5° and 20°. From the Bragg's law, interplanar spacing of 0.492, 0.479 and 0.443 nm are obtained, corresponding respectively to the (100), (020) and (110) atomic planes of PVDF [255]. In pristine (unirradiated) gel polymer electrolyte [Figure 6.5c] only prominent peak at 20° is observed and other peaks are decreased in intensity which indicates the decrease in crystallinity. In figure 6.5d one broad hump is observed indicating almost amorphous structure of the ion irradiated electrolyte at low fluence. However after irradiation with a fluence of 1×10^{12} ions/cm^2 [Figure 6.5e] the peak intensities again increase which suggest the increase in the degree of crystallinity. From figure 6.6 it is observed that crystallinity decreases in C^{5+} ion irradiated P(VDF-HFP)-(PC+DEC)-$LiClO_4$ system also after low fluence ion irradiation ($\leq 10^{11}$ ions/cm^2) and increases at higher fluence ($> 10^{11}$ ions/cm^2) ion irradiation.

Generally for pure PVDF polymer crystallinity increases after low fluence ion irradiation and decreases after high fluence ion irradiation [255]. But in P(VDF-HFP) co-polymer, hexafluoropropylene (HFP) units help to reduce the crystallinity of the polymer. Also crystallinity reduces in the pristine gel polymer electrolyte due to polymer-salt-solvent interaction. After low fluence ion irradiation ($\leq 10^{11}$ ions/cm^2) crystallinity decreases due to breaking of bonds which amorphizes the sample. But at fluence 10^{12} ions/cm^2, reordering and crosslinking of bonds take place which form the new crystalline region in the polymer electrolyte. The degree of crystallinity (K) for the Li^{3+} and C^{5+} ion irradiated gel polymer electrolyte is calculated by the relation

$$K = \frac{S}{S_0} \times 100$$

where S is the sum of areas of all the crystalline peaks and S_0 is the sum of areas of crystalline peaks and amorphous hump i.e. total area under the diffractogram. Area has been calculated by dividing the X-ray diffractogram into minute square $(0.5 \times 0.5 \text{ mm}^2)$ grids and counting the number of grids.
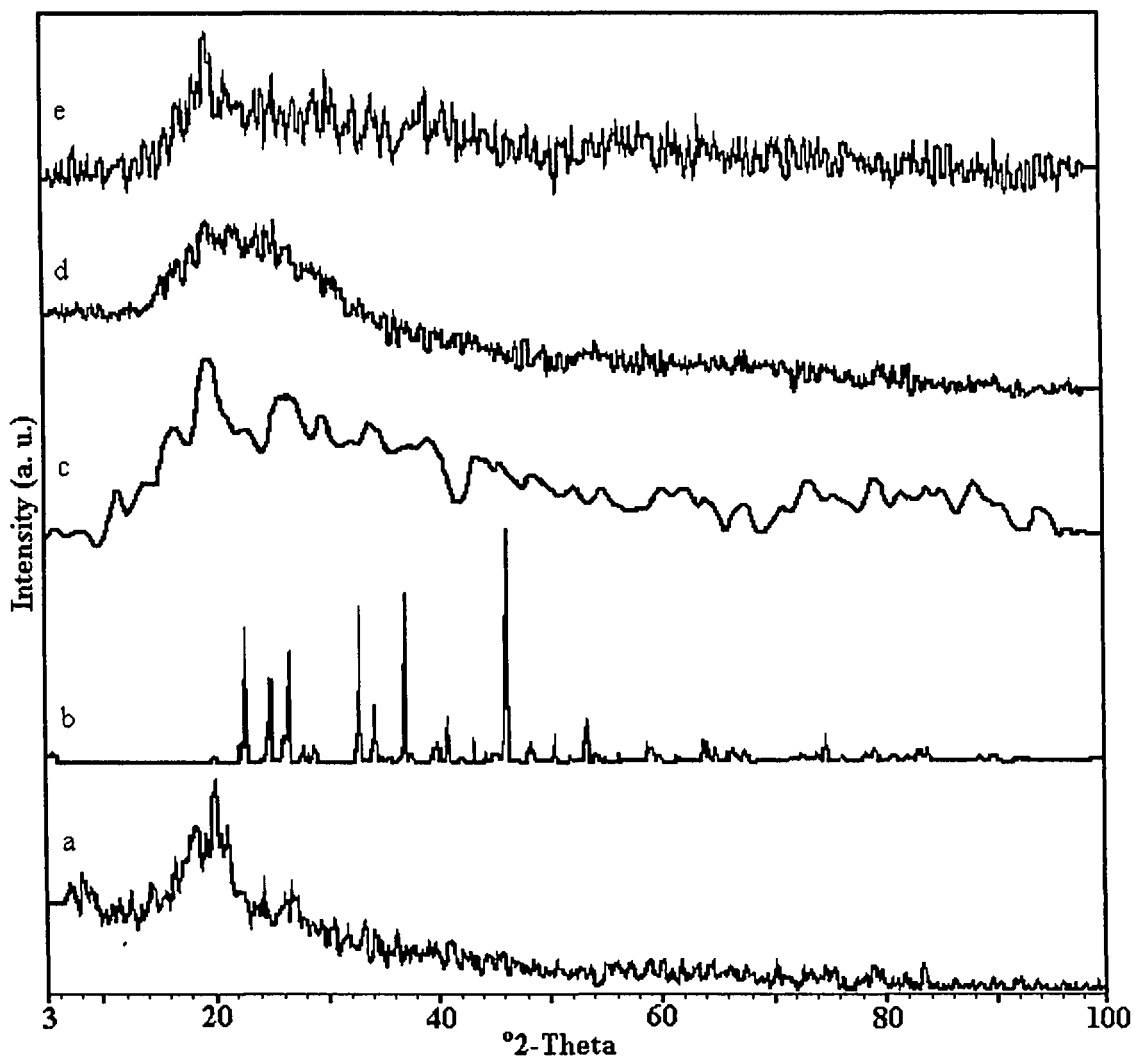
Figure 6.5: XRD patterns of (a) P(VDF-HFP), (b) LiClO₄, (c) unirradiated P(VDF-HFP)-(PC+DEC)-LiClO₄, (d) Li³⁺ ion irradiated P(VDF-HFP)-(PC+DEC)-LiClO₄ $(5 \times 10^{10}$ ions/cm²) and (e) Li³⁺ ion irradiated P(VDF-HFP)-(PC+DEC)-LiClO₄ $(5 \times 10^{12}$ ions/cm²) gel polymer electrolyte.

For pure P(VDF-HFP) (Figures 6.5a and 6.6a)

$$K = \frac{168 \text{ sq unit}}{560 \text{ sq unit}} \times 100; \quad K = 30\%$$

For unirradiated P(VDF-HFP)-(PC+DEC)-LiClO$_4$ (20:70:10 wt%) (Figure 6.5c and 6.6c) gel

polymer electrolyte

$$K = \frac{30 \text{ sq unit}}{220 \text{ sq unit}} \times 100; \quad K = 13.64\%$$
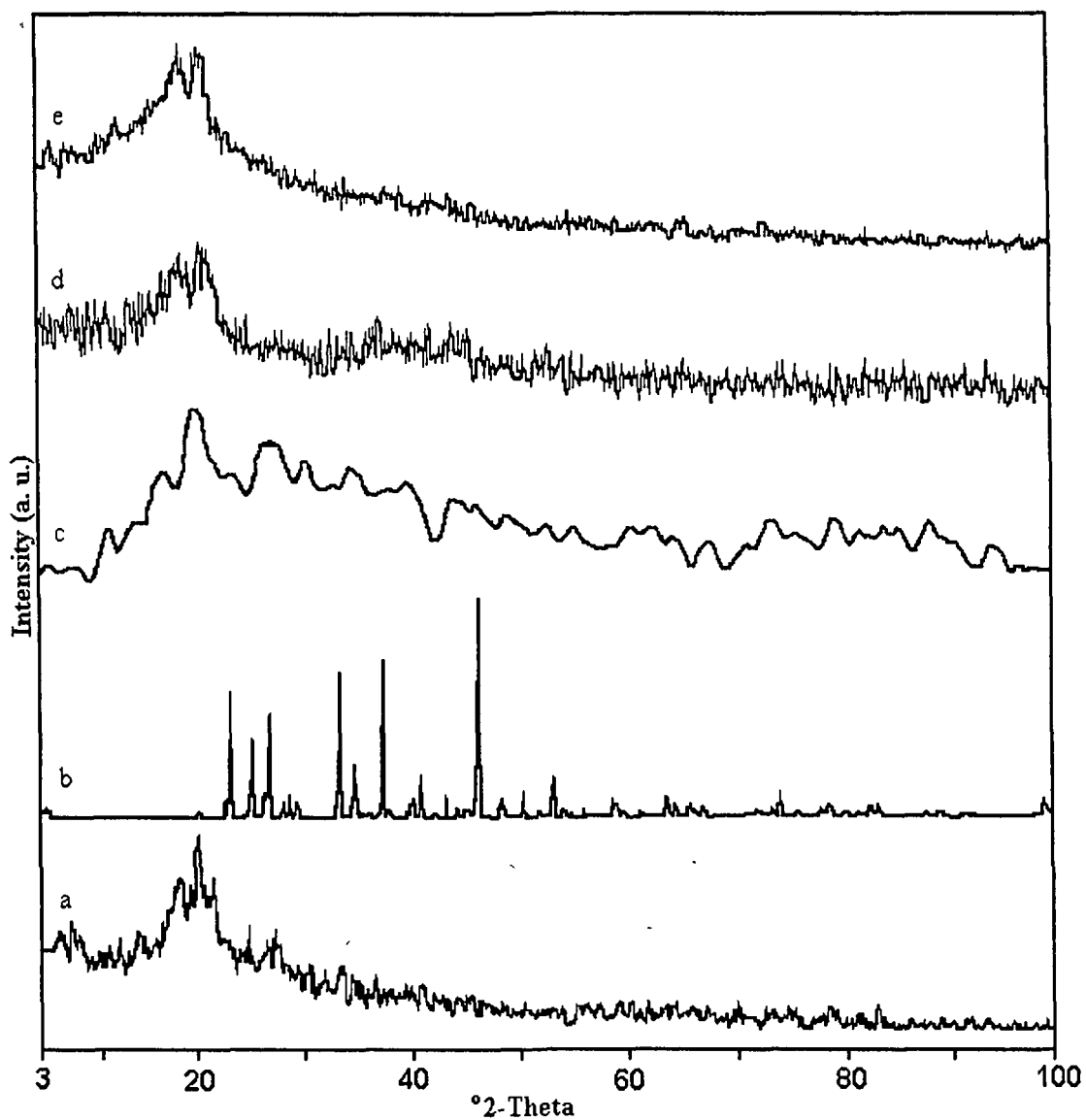
Figure 6.6: XRD patterns of (a) P(VDF-HFP), (b) LiClO$_4$, (c) unirradiated P(VDF-HFP)-(PC+DEC)-LiClO$_4$, (d) C^{5+} ion irradiated P(VDF-HFP)-(PC+DEC)-LiClO$_4$ (5 × 10^9 ions/cm^2) and (e) C^{5+} ion irradiated P(VDF-HFP)-(PC+DEC)-LiClO$_4$ (10^{12} ions/cm^2) gel polymer electrolyte.

For Li^{3+} ion irradiated P(VDF-HFP)-(PC+DEC)-LiClO$_4$ (20:70:10 wt%) (Figure 6.5d) gel polymer electrolyte with fluence of 5×10^{10} ions/cm^2

$$K = \frac{60 \text{ sq unit}}{572 \text{ sq unit}} \times 100; \quad K = 10.48\%$$

For Li^{3+} ion irradiated P(VDF-HFP)-(PC+DEC)-LiClO$_4$ (20:70:10 wt%) (Figure 6.5e) gel polymer electrolyte with fluence of 5×10^{12} ions/cm^2

$$K = \frac{36 \text{ sq unit}}{210 \text{ sq unit}} \times 100; \quad K = 17.1\%$$

For C^{5+} ion irradiated P(VDF-HFP)-(PC+DEC)-LiClO$_4$ (20:70:10 wt%) (Figure 6.6d) gel polymer electrolyte with fluence of 5×10^9 ions/cm^2

$$K = \frac{46 \text{ sq unit}}{400 \text{ sq unit}} \times 100; \quad K = 11.5\%$$

For C^{5+} ion irradiated P(VDF-HFP)-(PC+DEC)-LiClO$_4$ (20:70:10 wt%) (Figure 6.6e) gel polymer electrolyte with fluence of 10^{12} ions/cm^2

$$K = \frac{57 \text{ sq unit}}{304 \text{ sq unit}} \times 100; \quad K = 18.75\%$$

Ionic conductivity increases with ion irradiation at lower fluences and decreases at higher fluences as amorphicity increases in former case and decreases at higher fluence as ionic conduction essentially occurs through the amorphous phase in the polymer electrolytes [215].

6.1.3 Fourier Transform Infra-Red Spectroscopy

Figures 6.7 and 6.8 show the FTIR spectra of unirradiated and, Li^{3+} and C^{5+} ion irradiated P(VDF-HFP)-(PC+DEC)-LiClO$_4$ (20:70:10 wt%) gel polymer electrolyte systems respectively. The figures exhibit the crystalline CH$_2$ valance asymmetric and symmetric

stretching vibration bands, located at 3025 and 2985 cm^{-1} respectively. The absorbance intensities of the CH$_2$ crystalline bands can be observed rising remarkably with the ion fluence, denoting the advanced crystallization of the material. The sharp rise in the intensities of the crystalline bands upon irradiation suggests the newly created or even the thickening of the crystallites comprising a crystalline monomer. The partial recrystallization in
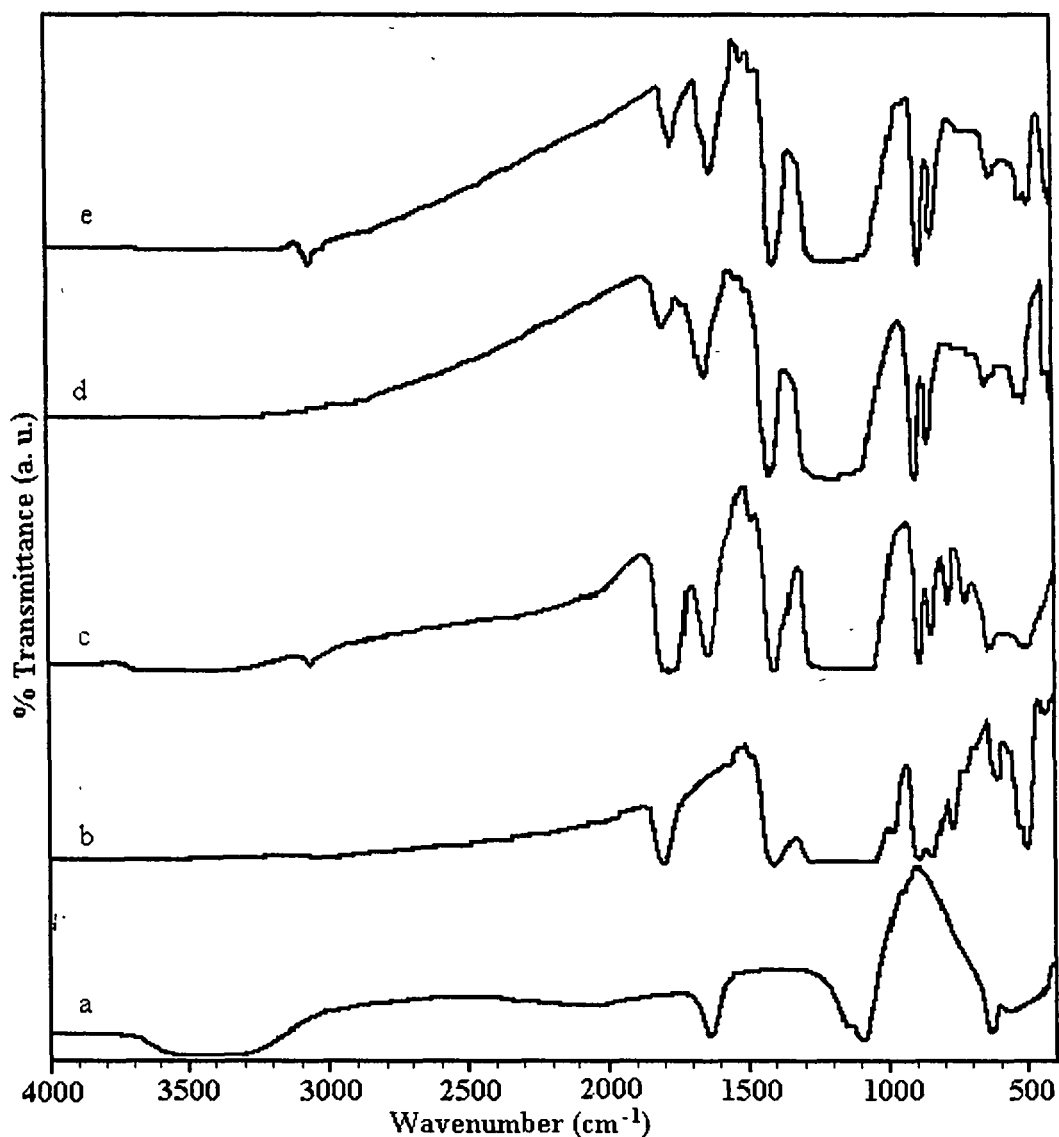
Figure 6.7: FTIR spectra of (a) LiClO$_4$, (b) P(VDF-HFP), (c) unirradiated P(VDF-HFP)-(PC+DEC)-LiClO$_4$, (d) Li^{3+} ion irradiated P(VDF-HFP)-(PC+DEC)-LiClO$_4$ [5×10^{10} ions/cm^2], and (e) Li^{3+} ion irradiated P(VDF-HFP)-(PC+DEC)-LiClO$_4$ [5×10^{12} ions/cm^2] gel polymer electrolytes.

P(VDF-HFP) based gel polymer electrolyte sample upon swift heavy ion impact is further evidenced by the simultaneous increase in the absorption intensities of the other notable crystalline bands such as at 614 and 881 cm^{-1}. These bands originate from the bending vibrations of the CH$_2$ group. Band around 796 cm^{-1}, which is present in the unirradiated gel polymer electrolyte is absent in the irradiated samples. The crystallization ability of polymer
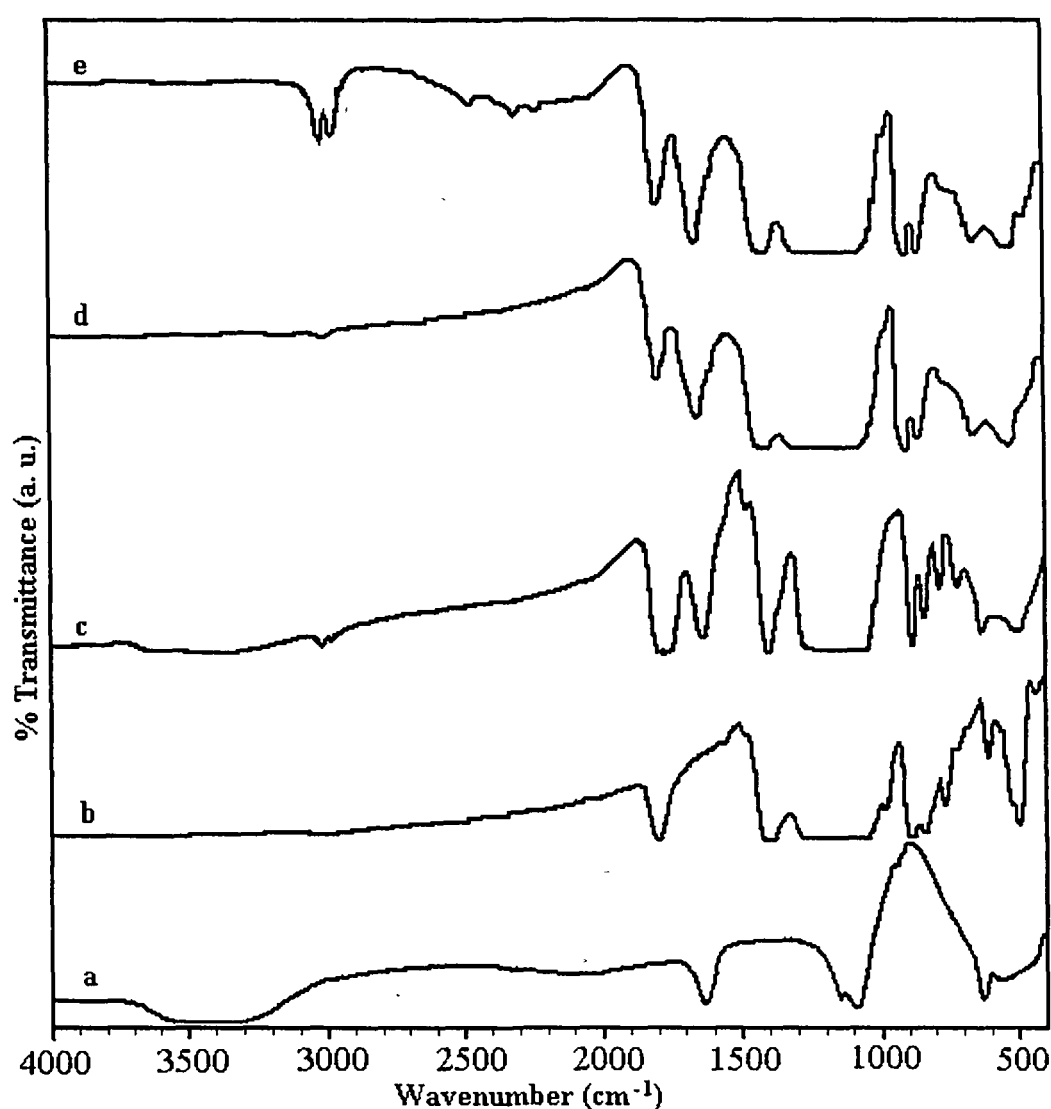
Figure 6.8: FTIR spectra of (a) LiClO₄, (b) P(VDF-HFP), (c) unirradiated P(VDF-HFP)-(PC+DEC)-LiClO₄, (d) C^{5+} ion irradiated P(VDF-HFP)-(PC+DEC)-LiClO₄ (5 × 10^9 ions/cm^2) and (e) C^{5+} ion irradiated P(VDF-HFP)-(PC+DEC)-LiClO₄ (10^{12} ions/cm^2) gel polymer electrolytes.

depends upon polarity also. The crystallizability of P(VDF-HFP) is attributable to the polar groups in the molecule (which leads to the formation of hydrogen bonds) increasing the inter chain forces of attraction [262]. The recrystallization in the present case for a polar polymer upon high LET (linear energy transfer i.e. the energy deposited per unit ion path length) irradiation seems to have occurred during secondary electron-phonon coupling, while transferring a huge amount of electronic energy into the lattice [262]. This in turn might have generated the molecular dipoles into a more ordered aligned one, facilitating a tighter packing and perfect bonding of the chain elements with each other. This is evident in the FTIR transmittance curve for the crystalline vibration band of a polar group corresponding to the CF_2 bending at 532 cm^{-1}. The specific decrease in the transmission intensity of the said band upon high ion fluence (10^{12} ions/cm^2) impact, possibly indicates the realignment of the molecular dipoles into a highly ordered state of chain cross-linked molecules in crystalline region of P(VDF-HFP), creating volume element as crystallites.

In the figures 6.7 and 6.8, peaks around frequency 1791 cm^{-1} is assigned to $-CF=CF_2$, $-C-O-CO-O-C-$ group. Frequency 1636 cm^{-1} is assigned to $>C=O$ stretching vibration of PC and DEC. Frequencies 1483 cm^{-1} and 1400 cm^{-1} are assigned to $-CH_3$ asymmetric bending and C-O stretching vibrations of plasticizer, propylene carbonate and diethyl carbonate. Frequencies 1290-1060 cm^{-1} are assigned to -C-F- and $-CF_2-$ stretching vibrations. Frequency 881 cm^{-1} is assigned to vinylidene group of polymer.

6.1.4 Scanning Electron Micrograph Study

The scanning electron micrographs of unirradiated and, Li^{3+} and C^{5+} ion irradiated P(VDF-HFP)-(PC+DEC)-$LiClO_4$ gel polymer electrolyte systems at fluence of 10^{11} ions/cm^2 are shown in figures 6.9 to 6.11. From the figures it is observed that ion irradiation changes
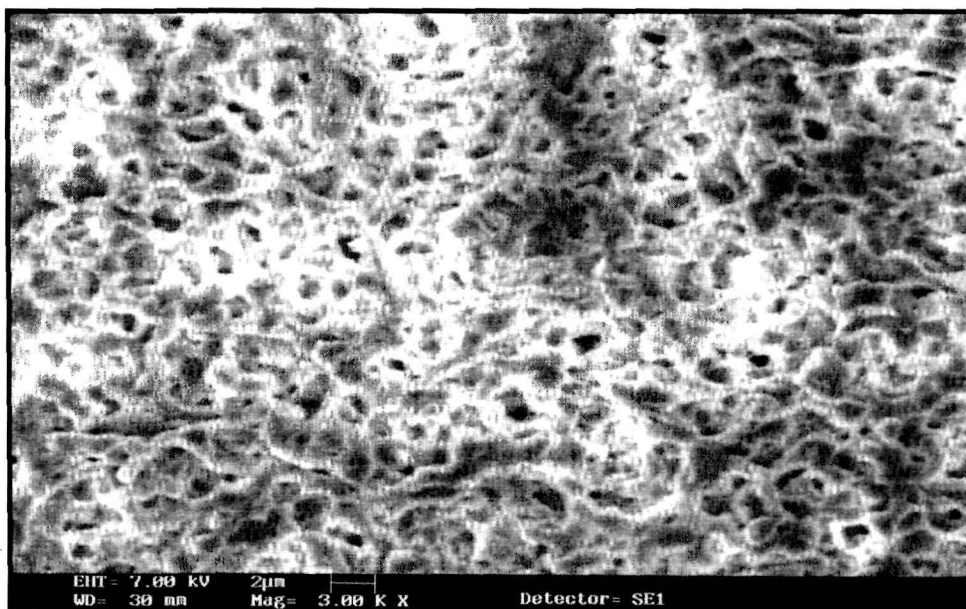
Figure 6.9: SEM image of unirradiated P(VDF-HFP)-(PC+DEC)-LiClO$_4$ gel polymer electrolyte.
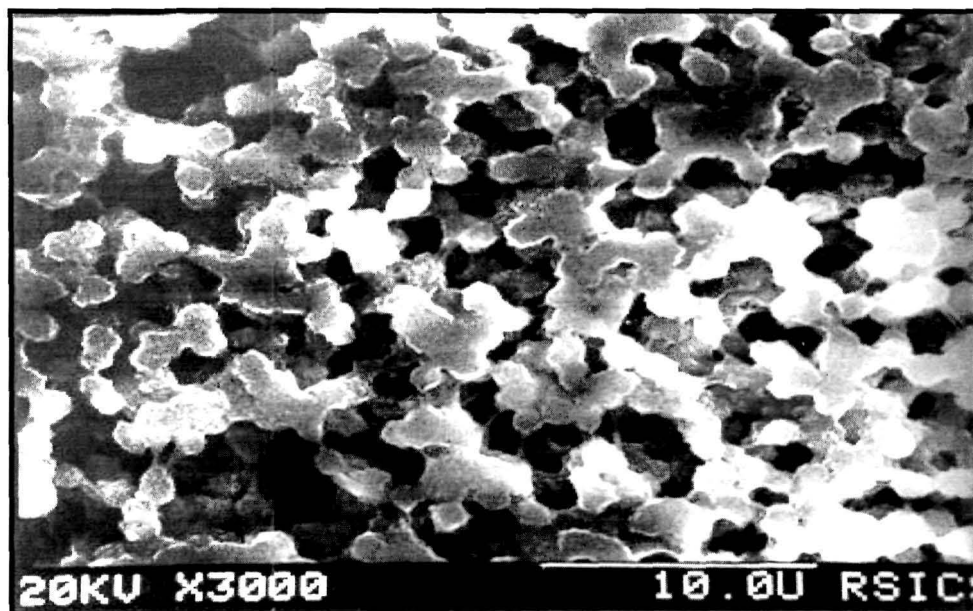
Figure 6.10: SEM image of Li^{3+} ion irradiated P(VDF-HFP)-(PC+DEC)-LiClO$_4$ gel polymer electrolyte.

129
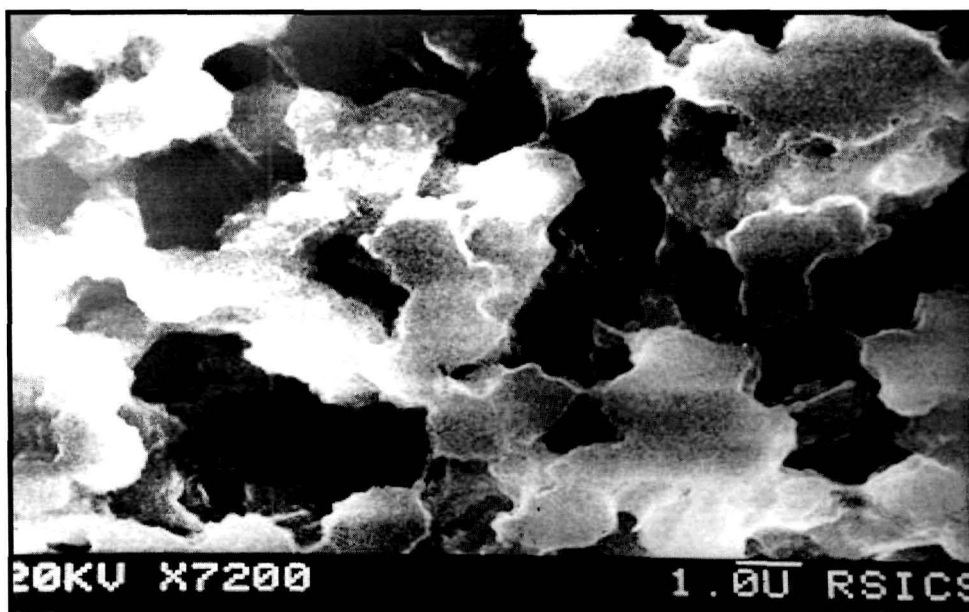
Figure 6.11: SEM image of C^{5+} ion irradiated P(VDF-HFP)-(PC+DEC)-LiClO$_4$ gel polymer electrolyte.

the morphology of the films completely. The microstructure changes from highly entangled and disordered with small pore size for unirradiated gel polymer electrolyte (Figure 6.9) to granular microstructure with larger pore size (Figure 6.10). Heavier C^{5+} ion irradiation produces larger grains and pore sizes (Figure 6.11). The increased porosity upon ion irradiation suggests that more liquid electrolyte could be trapped in the same volume of polymer giving rise to higher ionic conductivity.

6.2 Li^{3+} and C^{5+} Ion Irradiated P(VDF-HFP)-(PC+DEC)-LiCF$_3$SO$_3$ System

6.2.1 Ionic Conductivity Measurements

The ionic conductivity of unirradiated and, Li^{3+} and C^{5+} ion irradiated P(VDF-HFP)-(PC+DEC)-LiCF$_3$SO$_3$ (20:70:10 wt%) gel polymer electrolytes is calculated as discussed in section 6.1.1. Figures 6.12 and 6.13 show the conductivity versus temperature inverse plots of Li^{3+} and C^{5+} ion irradiated P(VDF-HFP)-(PC+DEC)-LiCF$_3$SO$_3$ (20:70:10 wt%) gel polymer

130

electrolyte systems respectively. From the figures it is observed that the ionic conduction in both the ion irradiated gel polymer electrolyte systems obey the VTF (Vogel-Tamman-Fulcher) relation [90-92], which describes the transport properties in a viscous matrix [171-174]. It supports the idea that the ions move through the plasticizer rich phase, which is the conducting medium and involves the salt and plasticizer.

From the figures it is observed that ionic conductivity increases upon Li^{3+} and C^{5+} ion irradiation upto a fluence of 10^{11} ions/cm^2 (Figure 6.14) and at higher fluence the conductivity decreases (Figure 6.15). This unusual result as explained in section 6.1.1 could be attributed to the fact that irradiation with a particular ion beam of given energy, a critical fluence provides activation energy required for cross linking to take place, which results in increased degree of crystallinity leading to decrease in ionic conductivity above the critical fluence. Conductivity data for Li^{3+} and C^{5+} ion irradiated gel polymer electrolytes with different fluences are presented in tables 6.3 and 6.4. It is found that room temperature ionic conductivity exhibits the highest value 2.6 × 10^{-3} S/cm for Li^{3+} irradiated and 1.8 × 10^{-3} S/cm for C^{5+} irradiated system at fluence of 10^{11} ions/cm^2. Conductivity at 343 K is found to be 3.1 × 10^{-3} S/cm and 2.3 × 10^{-3} S/cm for Li^{3+} and C^{5+} ion irradiated system at the same fluence respectively. The behavior of conductivity enhancement with temperature could be understood in terms of free-volume model [97,220]. As the temperature increases, the polymer chains flex at increasing rate and produce greater free volume. Ions and polymer segments can move faster into the free volume giving rise to higher conductivity as the temperature increases.
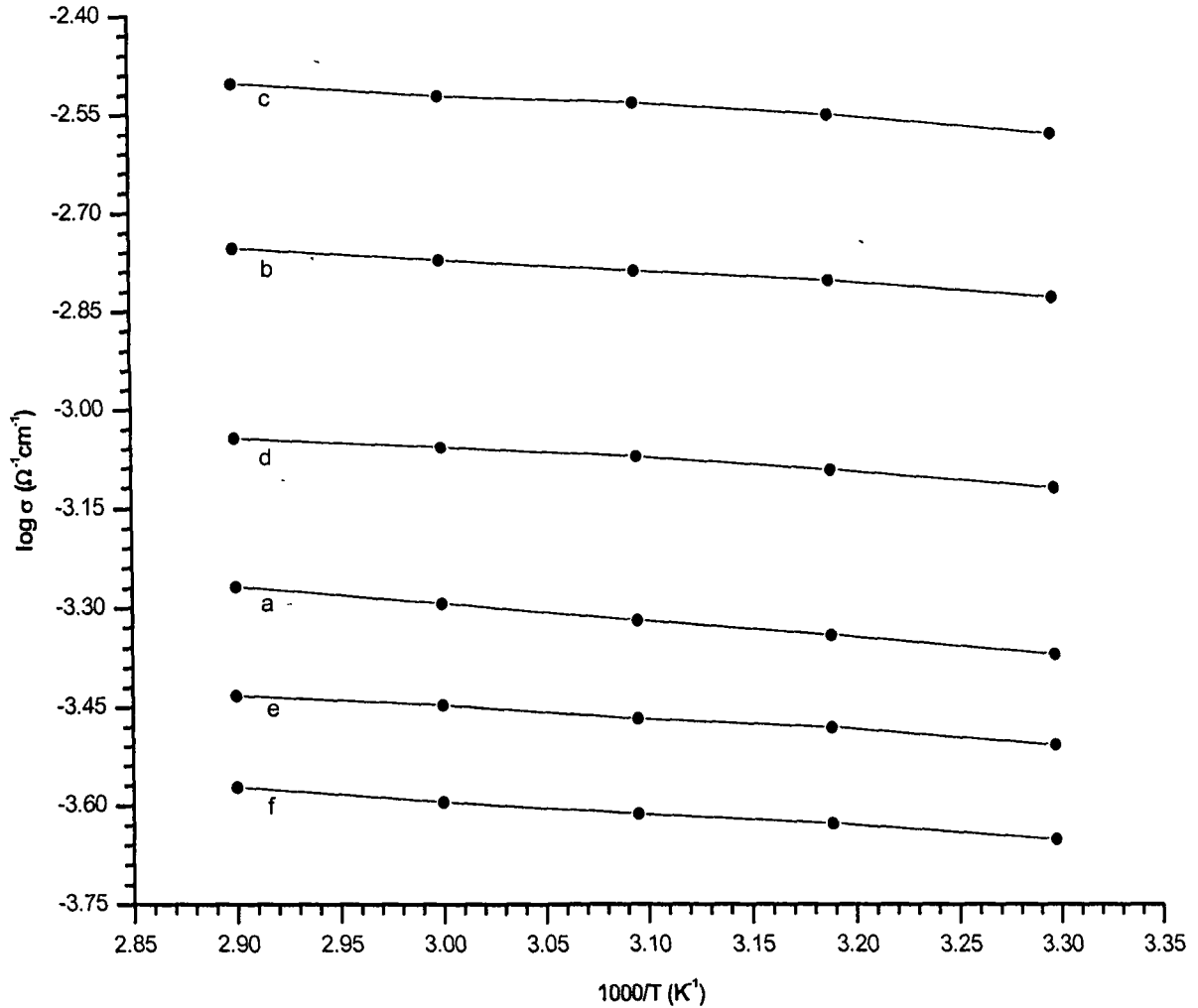
Figure 6.12: Temperature dependence of ionic conductivity of Li^{3+} ion irradiated P(VDF-HFP)-(PC+DEC)-LiCF$_3$SO$_3$ (20:70:10 wt%) gel polymer electrolyte (a) unirradiated, (b) 5×10^{10}, (c) 10^{11}, (d) 5×10^{11}, (e) 10^{12} and (f) 5×10^{12} ions/cm^2.

Table 6.3: Ionic conductivities of Li^{3+} ion irradiated P(VDF-HFP)-(PC+DEC)-LiCF$_3$SO$_3$ (20:70:10 wt%) gel polymer electrolyte with different fluences at 303 K.

Fluence (ion/cm^2)	Conductivity σ (Scm^{-1})	σ/σ_0
Unirradiated	4.2×10^{-4}	1
5×10^{10}	1.4×10^{-3}	3.33
1×10^{11}	2.6×10^{-3}	6.19
5×10^{11}	7.5×10^{-4}	1.78
1×10^{12}	3.1×10^{-4}	0.74
5×10^{12}	2.2×10^{-4}	0.52
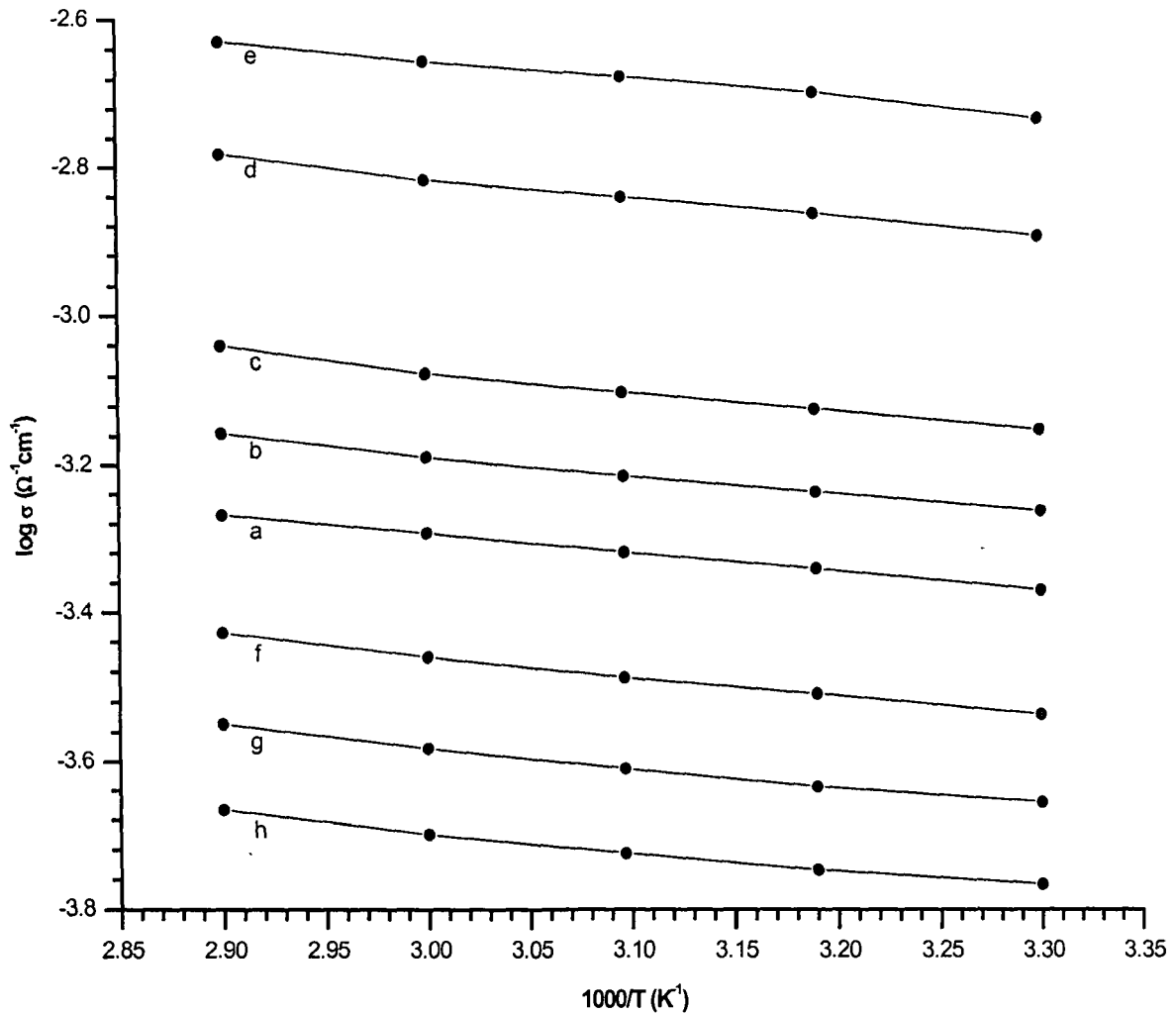
Figure 6.13: Temperature dependence of ionic conductivity of C^{5+} ion irradiated P(VDF-HFP)-(PC+DEC)-LiCF$_3$SO$_3$ (20:70:10 wt%) gel polymer electrolyte (a) unirradiated, (b) 10^{10}, (c) 2×10^{10}, (d) 6×10^{10}, (e) 10^{11}, (f) 3×10^{11}, (g) 7×10^{11} and (h) 10^{12} ions/cm^2.

Table 6.4: Ionic conductivities of C^{5+} ion irradiated P(VDF-HFP)-(PC+DEC)-LiCF$_3$SO$_3$ [20:70:10 wt%] gel polymer electrolyte with different fluences at 303 K.

Fluences (ions/cm^2)	Conductivity σ (S/cm)	σ/σ_0
Unirradiated	4.2×10^{-4}	1
10^{10}	5.4×10^{-4}	1.29
2×10^{10}	7×10^{-4}	1.67
6×10^{10}	1.2×10^{-3}	2.86
10^{11}	1.8×10^{-3}	4.29
3×10^{11}	2.9×10^{-4}	0.69
7×10^{11}	2.2×10^{-4}	0.52
10^{12}	1.7×10^{-4}	0.4
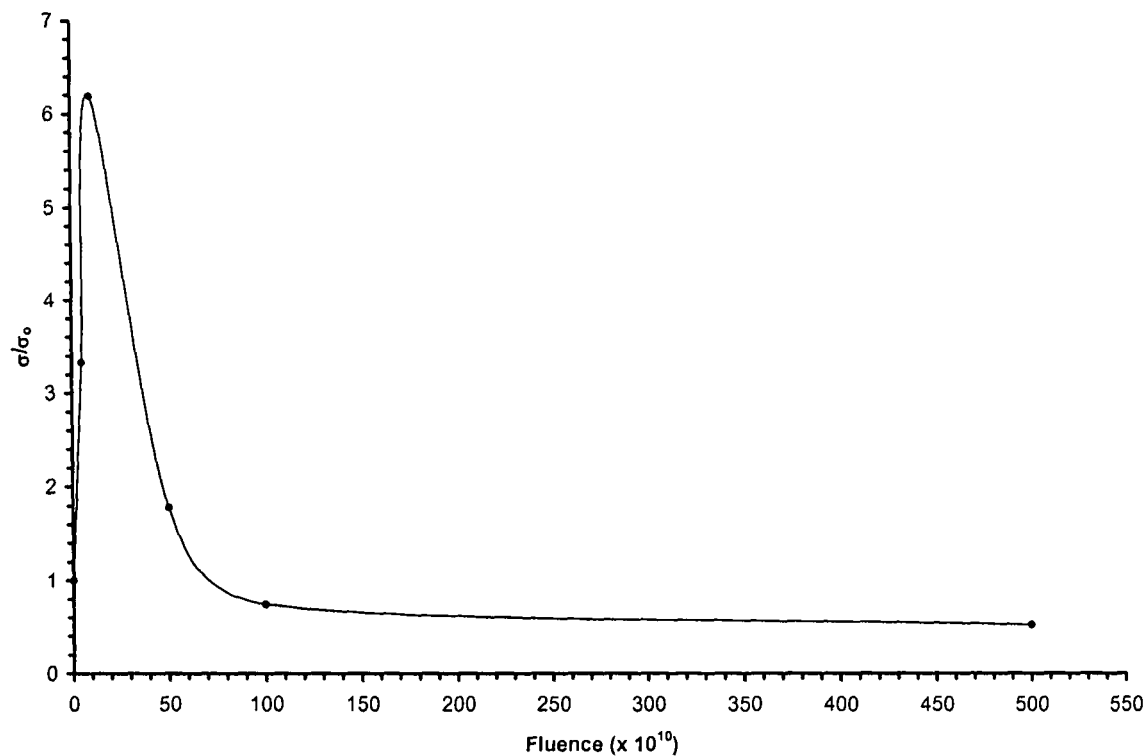
Figure 6.14: σ/σ_0 versus fluence curve of Li^{3+} ion irradiated P(VDF-HFP)-(PC+DEC)-$LiCF_3SO_3$ (20:70:10 wt%) gel polymer electrolyte.
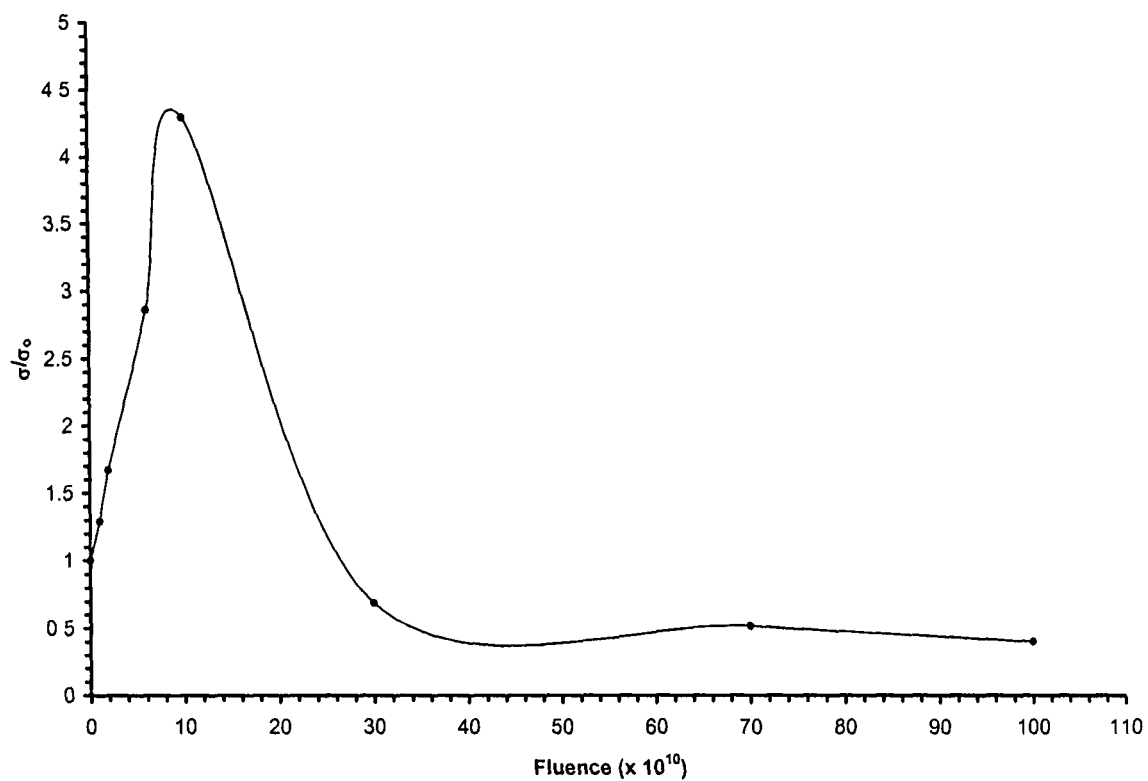
Figure 6.15: σ/σ_0 versus fluence curve of C^{5+} ion irradiated P(VDF-HFP)-(PC+DEC)-$LiCF_3SO_3$ (20:70:10 wt%) gel polymer electrolyte.

Total ionic transference number for both Li^{3+} and C^{5+} ion irradiated P(VDF-HFP)-(PC+DEC)-LiCF₃SO₃ gel polymer electrolyte systems was measured by Wagner's polarization method [152,153] as described in Chapter III (section 3.6) and found to be 0.95 – 0.97 and 0.93 – 0.96 respectively indicating that conduction is predominantly ionic.

6.2.2 X-Ray Diffraction Study

XRD patterns of unirradiated and, Li^{3+} and C^{5+} ion irradiated P(VDF-HFP)-(PC+DEC)-LiCF₃SO₃ (20:70:10 wt%) gel polymer electrolyte systems are shown in figures 6.16 and 6.17. For P(VDF-HFP) (Figure 6.16a and 6.17a) polymer three peaks are found at $2\theta = 18°$, $18.5°$ and $20°$, which correspond well with the (100), (020), (110) reflections of crystalline PVDF [176]. From the Bragg's law, interplanar spacing of 0.492, 0.479 and 0.443 nm was obtained, corresponding to the (100), (020) and (110) atomic planes of PVDF [255] respectively. In pristine gel polymer electrolyte [Figure 6.16c and 6.17c] only peak at 20° is observed distinctly and intensities of other peaks decrease which confirm the decrease in crystallinity which is due to addition of plasticizer, propylene carbonate and diethyl carbonate and salt.

The degree of crystallinity (K) for P(VDF-HFP) (Figures 6.16a and 6.17a) is

$$K = \frac{168\,sq\,unit}{560\,sq\,unit} \times 100 ; \quad K = 30\%$$

For unirradiated P(VDF-HFP)-(PC+DEC)-LiCF₃SO₃ (20:70:10 wt%) system (Figures 6.16c and 6.17c) degree of crystallinity (K) is

$$K = \frac{65\,sq\,unit}{298\,sq\,unit} \times 100 ; \quad K = 21.8\%$$

For Li^{3+} ion irradiated P(VDF-HFP)-(PC+DEC)-LiCF$_3$SO$_3$ (20:70:10 wt%) system with fluence of 5×10^{10} ions/cm^2 (Figure 6.16d)

$$K = \frac{22 \text{ sq unit}}{200 \text{ sq unit}} \times 100 \, ; \quad K = 11\%$$

For Li^{3+} ion irradiated P(VDF-HFP)-(PC+DEC)-LiCF$_3$SO$_3$ (20:70:10 wt%) system with fluence of 5×10^{12} ions/cm^2 (Figure 6.16e)

$$K = \frac{85 \text{ sq unit}}{320 \text{ sq unit}} \times 100 \, ; \quad K = 26.5\%$$
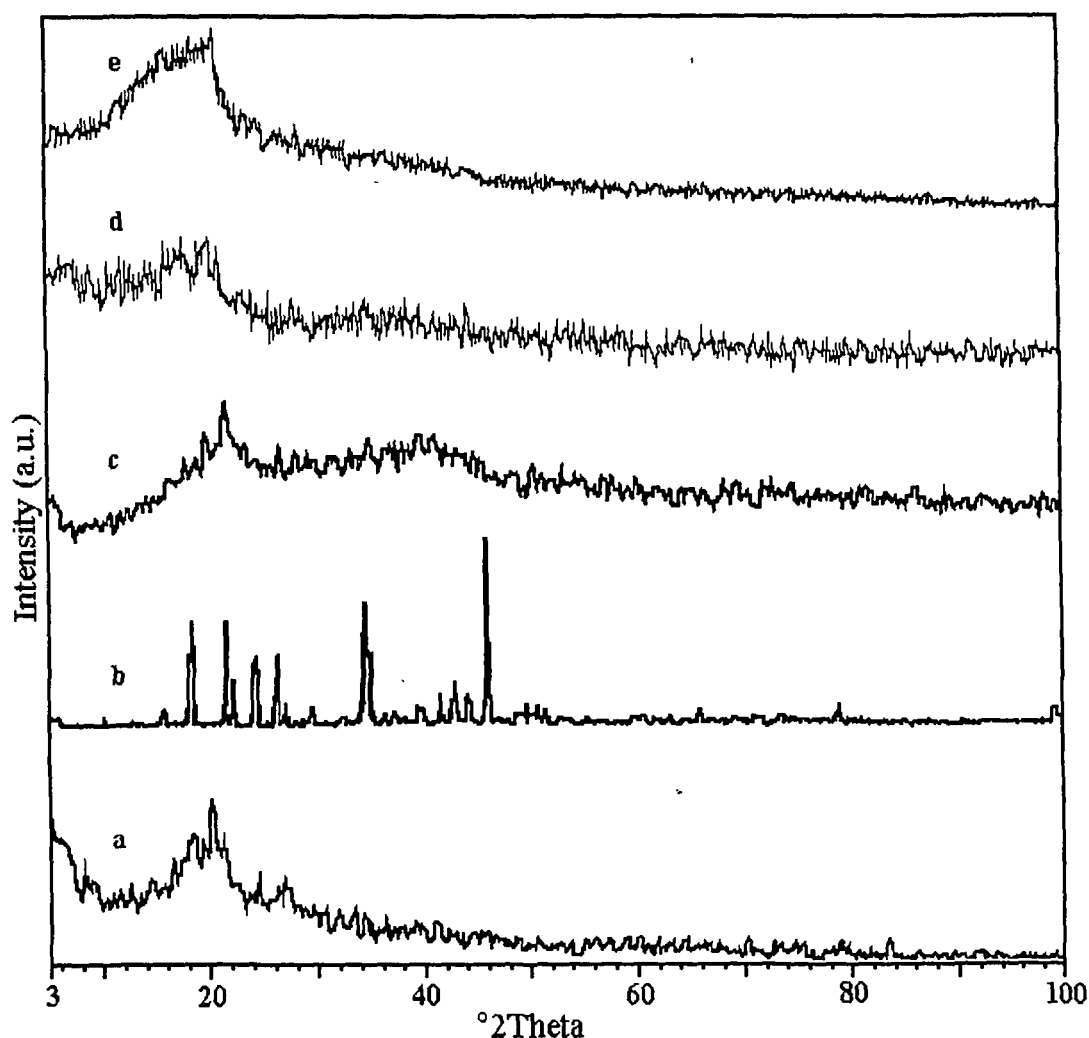
Figure 6.16: XRD patterns of (a) P(VDF-HFP), (b) LiCF$_3$SO$_3$, (c) unirradiated P(VDF-HFP)-(PC+DEC)-LiCF$_3$SO$_3$, (d) Li^{3+} ion irradiated P(VDF-HFP)-(PC+DEC)-LiCF$_3$SO$_3$ (5 × 10^{10} ions/cm^2) and (e) Li^{3+} ion irradiated P(VDF-HFP)-(PC+DEC)-LiCF$_3$SO$_3$ (5 × 10^{12} ions/cm^2) gel polymer electrolytes.

For C^{5+} ion irradiated P(VDF-HFP)-(PC+DEC)-LiCF$_3$SO$_3$ (20:70:10 wt%) system with fluence of 10^{10} ions/cm^2 (Figure 6.17d)

$$K = \frac{18 \text{ sq unit}}{186 \text{ sq unit}} \times 100; \quad K = 10.2\%$$

and for C^{5+} ion irradiated P(VDF-HFP)-(PC+DEC)-LiCF$_3$SO$_3$ (20:70:10 wt%) system with fluence of 10^{12} ions/cm^2 (Figure 6.17e)

$$K = \frac{124 \text{ sq unit}}{425 \text{ sq unit}} \times 100; \quad K = 29.2\%$$
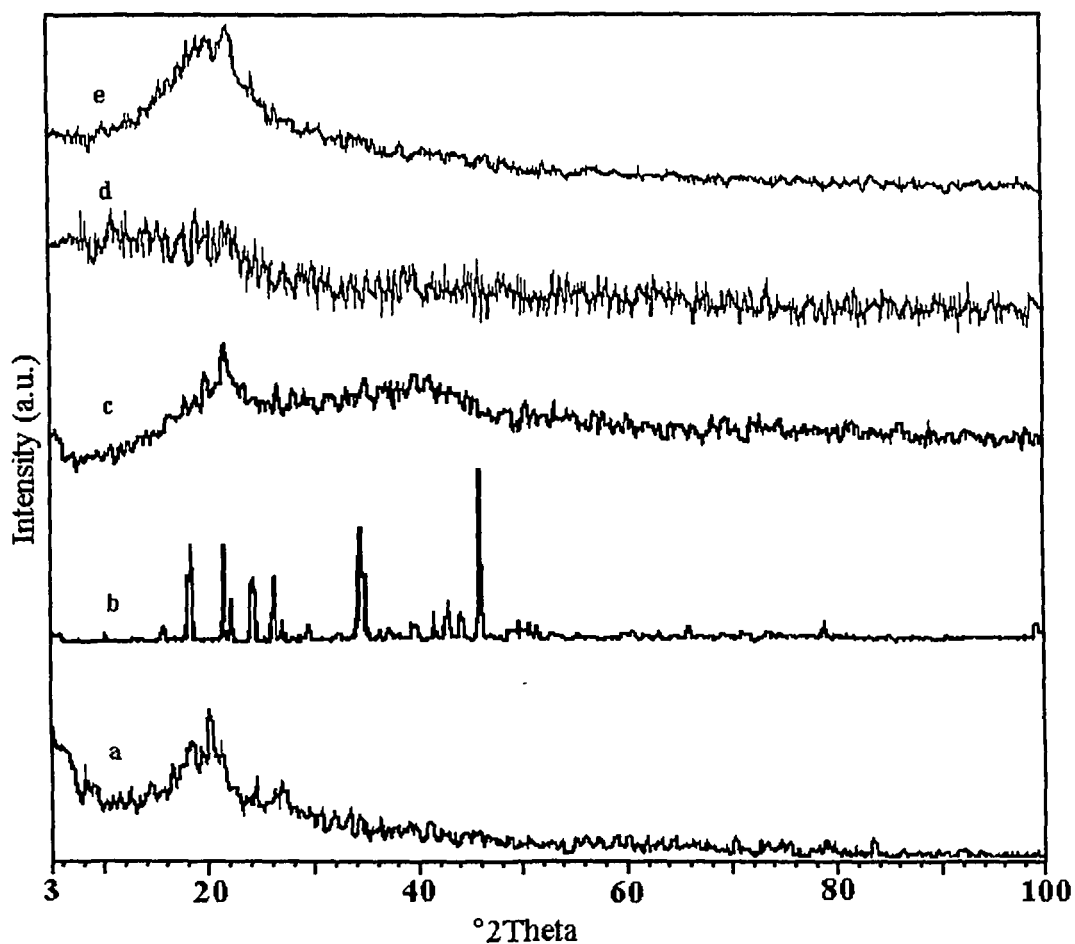
Figure 6.17: XRD patterns of (a) P(VDF-HFP), (b) LiCF$_3$SO$_3$, (c) unirradiated P(VDF-HFP)-(PC+DEC)-LiCF$_3$SO$_3$, (d) C^{5+} ion irradiated P(VDF-HFP)-(PC+DEC)-LiCF$_3$SO$_3$ (10^{10} ions/cm^2) and (e) C^{5+} ion irradiated P(VDF-HFP)-(PC+DEC)-LiCF$_3$SO$_3$ (10^{12} ions/cm^2) gel polymer electrolytes.

It is observed that after low fluence (10^{10} ions/cm^2) ion irradiation crystallinity decreases as compared to that of unirradiated gel polymer electrolyte and increases at higher fluence (10^{12} ions/cm^2) ion irradiation. This suggests that a threshold fluence is required for recrystallization to takes place. Peaks corresponding to LiCF$_3$SO$_3$ are not observed in the electrolyte indicating that LiCF$_3$SO$_3$ (Figures 6.16b and 6.17b) is completely dissolved in the organic solvent trapped in the polymer matrix. Ionic conductivity enhancement at lower fluences could be attributed to the fact that amorphicity increases due to chain scission at low fluences which in turn leads to higher ionic conductivity as discussed in section 6.1.1.

6.2.3 Fourier Transform Infra-Red Spectroscopy

Figures 6.18 and 6.19 show the FTIR spectra of unirradiated and, Li^{3+} and C^{5+} ion irradiated P(VDF-HFP)-(PC+DEC)-LiCF$_3$SO$_3$ (20:70:10 wt%) gel polymer electrolytes with varying fluences respectively. Upon low fluence ion irradiation ($\leq 10^{11}$ ions/cm^2) the CH$_2$ stretching asymmetric and symmetric vibration peaks of P(VDF-HFP) located at frequencies 3025 and 2985 cm^{-1} showed decrease in absorption intensities as compared to unirradiated gel polymer electrolyte system. However, after high fluence ion irradiation (10^{12} ions/cm^2), these vibrations showed a remarkable increase in their respective absorbance intensities. This hints at the possibility of the high LET beam-induced newly created crystallites as a result of remarkable molecular chain realignment [262]. These results suggest that at low fluence C–H bonds are breaking giving rise to decrease in intensity. At higher fluence, however, the reformation of bonds take place due to cross linking of polymer chains resulting in the increase in intensity of the peaks around 3025 and 2985 cm^{-1}.The partial recrystallization is further evidenced by the simultaneous increase in the FTIR absorption intensities of the other notable crystalline bands such as at 532 (CF$_2$ bending), 675 and 905 cm^{-1} (all due to CH$_2$

bending) at the similar ion fluence (10^{12} ions/cm^2). Being a polar polymer, the molecular

dipoles present in P(VDF-HFP) forming a hydrogen bond network get realigned upon

irradiation into a highly ordered state of chain molecules in the crystalline regions of P(VDF-

HFP), creating volume elements as crystallites [262].

In figures 6.18 and 6.19, the absorption peak at frequency 1783 cm^{-1} is assigned to

–CF=CF$_2$, –C–O–CO–O–C– group. Frequency 1644 cm^{-1} is assigned to C=O stretching

vibration of plasticizer (PC+DEC). Frequency 1400 cm^{-1} is assigned to -C–F- stretching

vibration of P(VDF-HFP). Frequencies in the band 1298-1039 cm^{-1} are assigned to -C–F- and
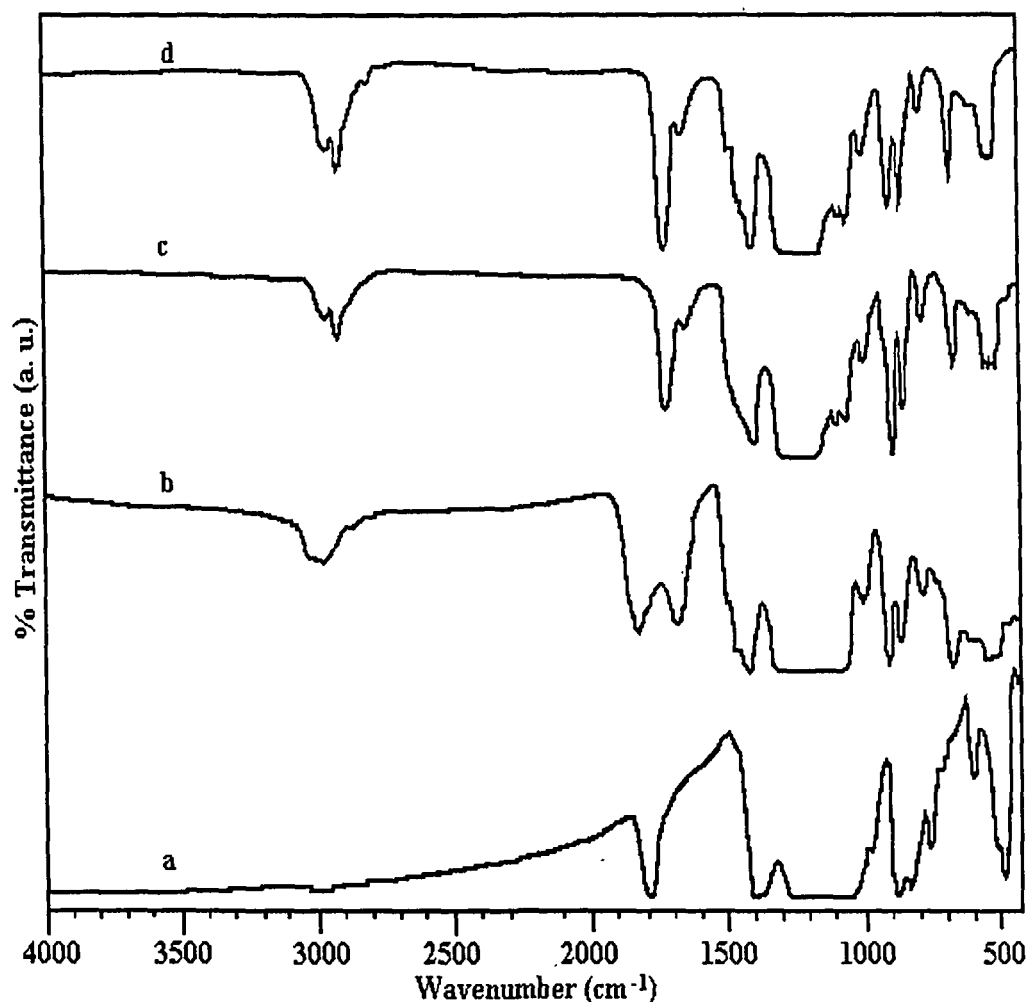
Figure 6.18: FTIR spectra of (a) P(VDF-HFP), (b) unirradiated P(VDF-HFP)-(PC+DEC)-LiCF$_3$SO$_3$, (c) Li^{3+} ion irradiated P(VDF-HFP)-(PC+DEC)-LiCF$_3$SO$_3$ [5×10^{10} ions/cm^2] and (d) Li^{3+} ion irradiated P(VDF-HFP)-(PC+DEC)-LiCF$_3$SO$_3$ [5×10^{12} ions/cm^2] system.

-CF$_2$- stretching vibrations. Frequency 883 cm^{-1} is assigned to vinylidene group of polymer.

Band at 764 cm^{-1} in curves (b-d) is assigned to the δ_s(CF$_3$) stretching mode of the triflate ion.

Frequencies of several triflate ion vibrational modes can be used as a measure of degree and

nature of ionic association. Presence of free triflate ions, cation-anion pairs, and highly

associated species can be ascertained from corresponding spectroscopically distinct bands;

such bands can be observed in either SO$_3$ symmetric stretching spectral region [222,223] or

CF$_3$ symmetric deformation region [224]. Although lithium cation interacts with SO$_3$ end of

the triflate anion, δ(CF$_3$) mode is particularly sensitive to ionic association through
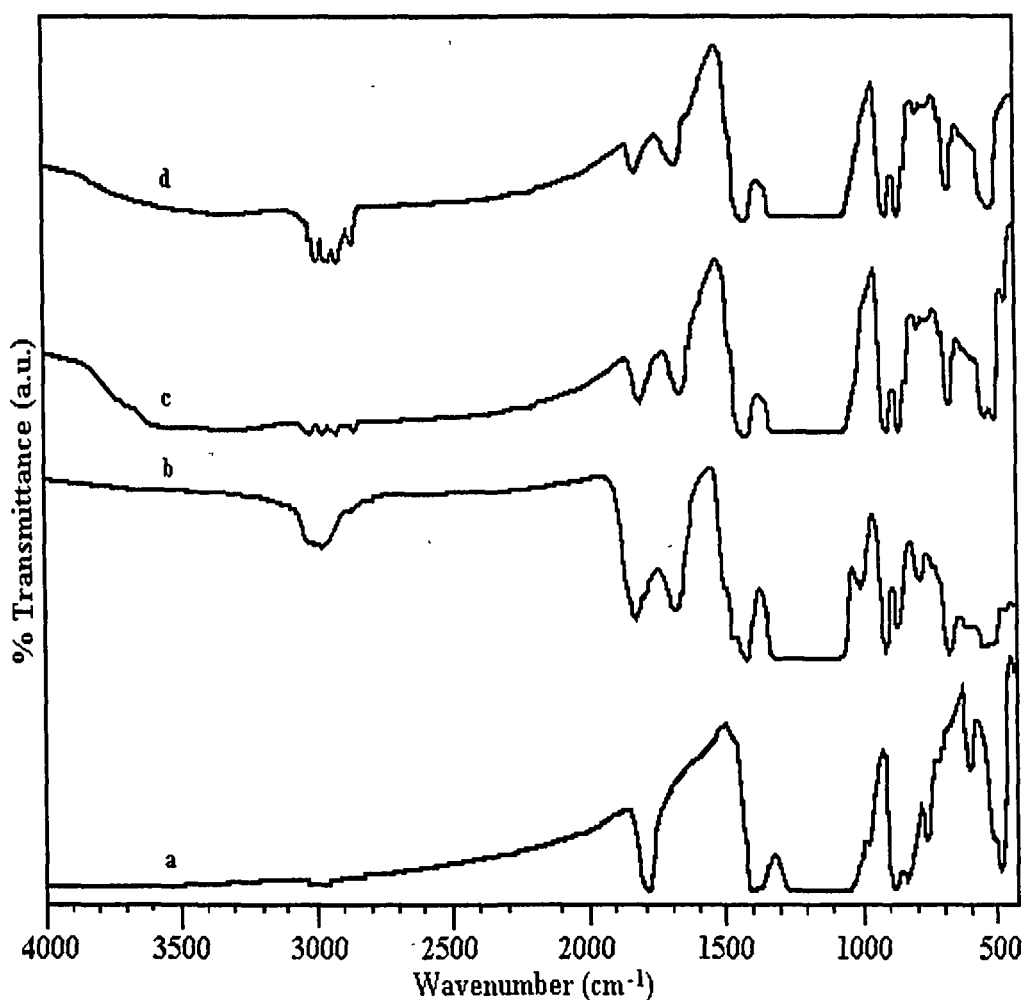
Figure 6.19: FTIR spectra of (a) P(VDF-HFP), (b) unirradiated P(VDF-HFP)-
(PC+DEC)-LiCF$_3$SO$_3$, (c) C^{5+} ion irradiated P(VDF-HFP)-(PC+DEC)-LiCF$_3$SO$_3$
(10^{10} ions/cm^2) and (d) C^{5+} ion irradiated P(VDF-HFP)-(PC+DEC)-LiCF$_3$SO$_3$
(10^{12} ions/cm^2) system

redistribution of charge accompanying the formation of ionic pairs and aggregates [224,225]. The band at 764 cm^{-1} is indicative of highly associated triflate ion and has been assigned to a [Li$_2$Tf]$^+$ species [225,226].

6.2.4 Scanning Electron Micrograph Study

Figures 6.20 to 6.22 show the scanning electron micrographs of unirradiated and, Li^{3+} and C^{5+} ion irradiated P(VDF-HFP)-(PC+DEC)-LiCF$_3$SO$_3$ gel polymer electrolyte systems with fluence 10^{11} ions/cm^2 respectively. From the figures it is observed that electrolyte film is a two phase system with the polymer phase interspersed with pores filled with liquid electrolyte, which form a connected path through the polymer matrix [157]. Upon ion irradiation of the polymer electrolyte porosity increases which indicates that more liquid electrolyte could be trapped in the same volume of polymer which gives rise to higher ionic conductivity in swift heavy ion irradiated polymer electrolytes.
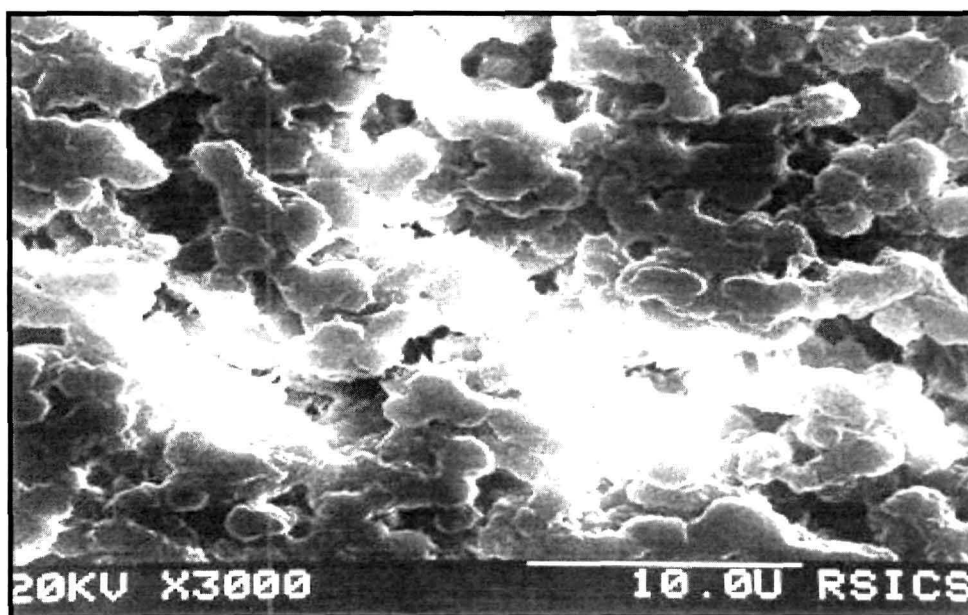
Figure 6.20: SEM image of unirradiated P(VDF-HFP)-(PC+DEC)-LiCF$_3$SO$_3$ gel polymer electrolyte.
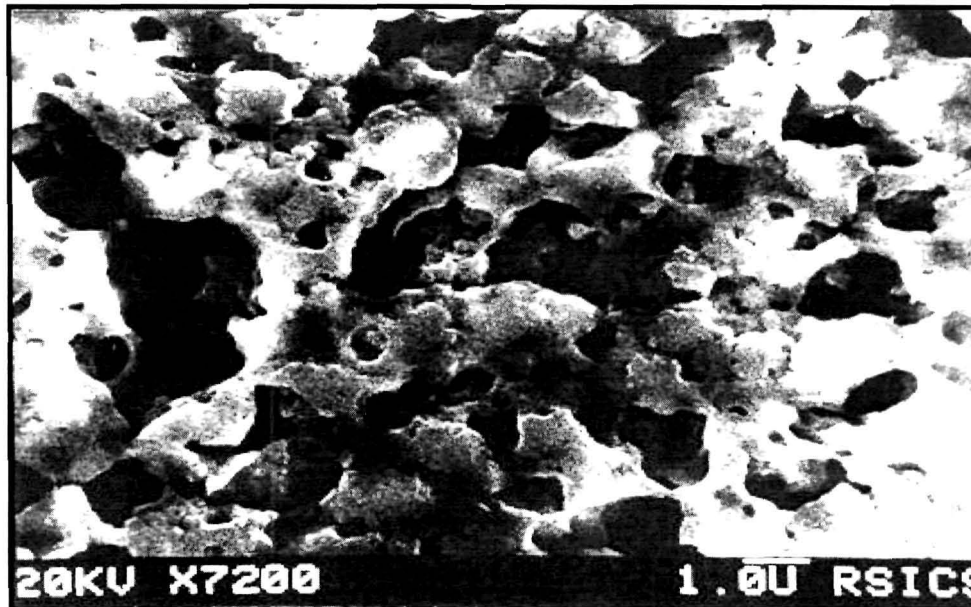
Figure 6.21: SEM image of Li^{3+} ion irradiated P(VDF-HFP)-(PC+DEC)-LiCF$_3$SO$_3$ gel polymer electrolytes
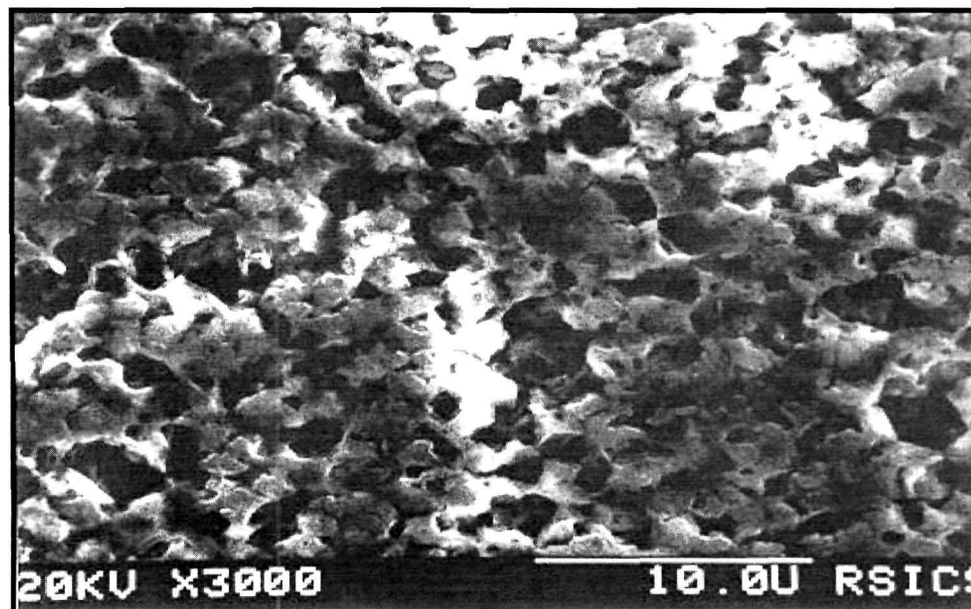
Figure 6.22: SEM image of C^{5+} ion irradiated P(VDF-HFP)-(PC+DEC)-LiCF$_3$SO$_3$ gel polymer electrolyte

6.3 Summary

High energy Li^{3+} and C^{5+} ions irradiation effects on ionic conduction in P(VDF-HFP)-(PC+DEC)-LiClO$_4$ and P(VDF-HFP)-(PC+DEC)-LiCF$_3$SO$_3$ gel polymer electrolytes have been studied extensively. Ion irradiation with both Li^{3+} and C^{5+} ion beams of gel polymer electrolytes below a threshold fluence ($\sim 10^{11}$ ions/cm^2) the conductivity increases and at higher fluences ($>10^{11}$ ions/cm^2) it decreases. This result could be explained in terms of fluence dependent chain scission and cross-linking processes in polymers. Below threshold fluence chain scission processes appear to dominate, which lead to faster ion transport through the polymer matrix assisted by large amplitude segmental motion of the polymer backbone. At higher fluences the critical energy required for cross-linking is reached and the cross linking processes of polymer chains take over due to collective excitation (plasmons) of polymer chains, which produces a large excited volume in the polymer electrolyte resulting in coercive interaction among the ions and radical pairs produced within the volume. Maximum ionic conductivity for Li^{3+} and C^{5+} ion irradiated P(VDF-HFP)-(PC+DEC)-LiClO$_4$ system is measured to be 2.2 × 10^{-2} S/cm and 2 × 10^{-2} S/cm respectively at fluence of 1 × 10^{11} ions/cm^2. For P(VDF-HFP)-(PC+DEC)-LiCF$_3$SO$_3$ system ionic conductivity exhibits the value 2.6 × 10^{-3} S/cm for Li^{3+} irradiated and 1.8 × 10^{-3} S/cm for C^{5+} irradiated system at fluence of 1 × 10^{11} ions/cm^2 at 303K.

XRD results confirmed that crystallinity decreases in Li^{3+} and C^{5+} ion irradiated P(VDF-HFP)-(PC+DEC)-LiClO$_4$ and P(VDF-HFP)-(PC+DEC)-LiCF$_3$SO$_3$ systems after low fluence ion irradiation ($\leq 10^{11}$ ions/cm^2) and increases at higher fluence ($> 10^{11}$ ions/cm^2) ion irradiation. Degree of crystallinity of Li^{3+} and C^{5+} ion irradiated P(VDF-HFP)-(PC+DEC)-LiClO$_4$ gel polymer electrolytes decreases to 10.48% and 11.5% respectively after low fluence (5 × 10^{10} and 5 ×10^9 ions/cm^2) ion irradiation and increases to 17.1% and 18.75%

respectively after high fluence (5×10^{12} and 10^{12} ions/cm^2) ion irradiation as compared to

13.64% of unirradiated P(VDF-HFP)-(PC+DEC)-LiClO$_4$ gel polymer electrolyte. In Li^{3+} and

C^{5+} ion irradiated P(VDF-HFP)-(PC+DEC)-LiCF$_3$SO$_3$ gel polymer electrolytes degree of

crystallinity decreases to 11% and 10.2% respectively at low fluence ion irradiation (5×10^{10}

and 10^{10} ions/cm^2) and increases to 26.5 % and 29.2% respectively at high fluence (5×10^{12}

and 10^{12} ions/cm^2) ion irradiation as compared to 21.8% of unirradiated P(VDF-HFP)-

(PC+DEC)-LiCF$_3$SO$_3$ gel polymer electrolyte.

The decrease in crystallinity after low fluence ($\leq 10^{11}$ ions/cm^2) ion irradiation could

be ascribed to chain scission and breaking of bonds which randomize the polymer chains. At

higher fluence of 10^{12} ions/cm^2 reordering and crosslinking of bonds take over the chain

scission processes forming the new crystalline region in the polymer electrolyte, which in turn

results in decrease in the ionic conductivity.

FTIR spectra for both Li^{3+} and C^{5+} ion irradiated P(VDF-HFP)-(PC+DEC)-LiClO$_4$

and P(VDF-HFP)-(PC+DEC)-LiCF$_3$SO$_3$ systems show a band around 3025 and 2985 cm^{-1}

due to CH$_2$ asymmetric and symmetric stretching vibrations. After irradiation with Li^{3+} and

C^{5+} ions for both the systems, the absorption intensity of this band decreases with irradiation

at low fluence of 10^{10} ions/cm^2. However, upon irradiation with a higher fluence of

10^{12} ions/cm^2, absorption intensity shows an increase. These results suggest that at low

fluence C–H bonds are breaking giving rise to decrease in intensity. At higher fluence,

however, the reformation of bonds takes place due to cross linking of polymer chains

resulting in the increase in intensity of the band around 3025 and 2985 cm^{-1}. These results are

consistent with conductivity and XRD results. SEM study shows that porosity increases upon

ion irradiation leading to trapping of more liquid electrolyte in the same volume of polymer

which could give rise to higher ionic conductivity.

CHAPTER VII

CONCLUSIONS AND FUTURE PROSPECTS

The present research puts forth the various aspects involved in developing high ion conducting gel polymer electrolytes. Following are the main conclusions of the present work:

1. (i) Maximum ionic conductivity for PVDF-(PC+DEC)-LiClO$_4$ and P(VDF-HFP)-(PC+DEC)-LiClO$_4$ is found to be 1.3 $\times$ 10^{-3} S/cm and 7.5 $\times$ 10^{-3} S/cm at 303 K respectively. Higher conductivity in P(VDF-HFP) based electrolyte in comparison to PVDF based electrolyte could be attributed to higher amorphicity of the former electrolyte system due to steric hindrance provided by bulky pendant –CF$_3$ group in HFP monomer unit of the copolymer. Higher amorphicity provides higher flexibility to the polymer chains and mobile Li$^+$ ion gets greater free volume giving rise to higher conductivity. XRD analysis reveals that degree of crystallinity is reduced from 31.4% in PVDF to 20.45% in PVDF based gel polymer electrolyte system and 30% in P(VDF-HFP) to 13.64% in P(VDF-HFP) based gel polymer electrolyte system. The XRD results confirm that P(VDF-HFP) based gel polymer electrolyte is more amorphous than PVDF based electrolyte.

(ii) Appearance of new peaks in the FTIR spectra at frequency 837 cm^{-1} in PVDF-(PC+DEC)-LiClO$_4$ and at 781 cm^{-1} and 716 cm^{-1} in P(VDF-HFP)-(PC+DEC)-LiClO$_4$ which could be ascribed to C–Cl stretching vibration. This indicates that polymer carbon atoms interact with chlorine of ClO$_4^-$ ions suggesting polymer-ion interaction.

(iii) The SEM micrographs of P(VDF-HFP) based system show higher porosity than PVDF based system indicating higher solvent retention ability of the former than the later, which in turn results in higher ionic conductivity in the former.

2. (i) Addition of filler particles to the gel polymer electrolytes show enhancement in ionic conductivity. Maximum ionic conductivity for P(VDF-HFP)-PMMA-PC-LiClO₄-TiO₂, P(VDF-HFP)-PMMA-(PC+DEC)-LiCF₃SO₃-fumed SiO₂ and P(VDF-HFP)-(PC+DEC)-LiAsF₆-fumed SiO₂ composite gel polymer electrolyte is found to be 2.8 × 10⁻² S/cm, 1 × 10⁻³ S/cm and 6.6 × 10⁻³ S/cm respectively. The enhancement in ionic conductivity upon addition of filler could be attributed to the fact that dispersed phase submicron size filler particles prevent polymer chain reorganization resulting in reduction of polymer crystallinity, which give rise to an increase in ionic conductivity. The reduction in crystallinity could result from the Lewis acid-base interactions between the surface of submicron filler particles and the polymer chains. This allows Li⁺ ions to move more freely either on the surface of filler particles or through a low density polymer phase at the interface, which results in enhanced ionic conductivity. Enhancement of conductivity could also be attributed to the generation of polymer-ceramic grain boundaries. The grain boundaries are the sites of high defect concentration which allow faster ionic transport. These grain boundaries serve as channels for the conducting ions. The selection of appropriate polymer and ceramic phases is an important consideration in the development of fast ion conducting composite polymer electrolyte.

The enhancement in ionic conductivity due to the addition of ceramic fillers has been explained by improved effective-medium theory. The composite electrolyte can be treated as a quasi two phase system consisting of polymeric ion-conducting matrix

and dispersed composite units. The ionic conductivity could arise from the existence of a highly conducting layer at the electrolyte/filler interface. At low ceramic filler concentrations, conductivity increases with filler content basically due to the increase in amount of the conductive layers. Conductivity enhancement can also be described in terms of free volume model. As the temperature increases, the polymer chains flex and expand at increasing rate and generate free volume. This leads to an increase in ion and segmental mobilities. The resulting conductivity, represented by the overall mobility of the ions and the polymer, is determined by the free volume around the polymer chains.

(ii) XRD analysis reveals that degree of crystallinity is reduced from 30% in pure P(VDF-HFP) and 25.5% in pure PMMA to 6% in P(VDF-HFP)-PMMA-PC-LiClO$_4$-TiO$_2$ and 20.6% in P(VDF-HFP)-PMMA-(PC+DEC)-LiCF$_3$SO$_3$-fumed SiO$_2$ composite gel polymer electrolytes. The degree of crystallinity is reduced from 30% in pure P(VDF-HFP) to 17.7% in P(VDF-HFP)-(PC+DEC)-LiAsF$_6$-fumed SiO$_2$ composite gel polymer electrolyte. Increased amorphicity in the electrolyte, which gives rise to higher ionic conductivity is attributed to the steric hindrance provided by the bulky pendant –CH$_3$COO ester group of PMMA upon blending of P(VDF-HFP) with PMMA and addition of the plasticizer and filler.

(iii) FTIR analysis of P(VDF-HFP)-PMMA-(PC+DEC)-LiCF$_3$SO$_3$-fumed SiO$_2$ system indicates that hydroxyl groups on silica surface are involved in bond interactions. Presence of free triflate ions, cation-anion pairs and highly associated species can be ascertained from corresponding spectroscopically distinct bands. Although lithium cation interacts with SO$_3$ end of the triflate anion, δ(CF$_3$) mode is particularly sensitive to ionic association through redistribution of charge accompanying the

147

formation of ionic pairs and aggregates. In P(VDF-HFP)-(PC+DEC)-LiAsF₆-fumed SiO_2 system, the shifting of O–H band to lower wave numbers region with the addition of lithium hexafluoroarsenate to P(VDF-HFP)/fumed SiO_2 composite indicates that the cation and/or the anion of the salt is interacting with silica's hydroxyl groups.

(iv) SEM images show that with the addition of filler TiO_2 and SiO_2, the film surfaces becomes rough but the submicron particles are well dispersed on the surface. The film roughness supports the existence of micropores. The increased porosity leads to trapping of large volumes of the liquid electrolyte in the micropores accounting for the increased ionic conductivity.

3. (i) Swift heavy ion Li^{3+} and C^{5+} irradiation effects on the ionic conduction in P(VDF-HFP)-(PC+DEC)-LiClO₄ and P(VDF-HFP)-(PC+DEC)-LiCF₃SO₃ gel polymer electrolytes have been studied extensively in the present work. For both types of gel polymer electrolytes, at lower fluences ($\leq 10^{11}$ ions/cm²) conductivity increases and at higher fluences ($> 10^{11}$ ions/cm²) it decreases. This result could be explained on the basis that at low fluence bond breaking and chain scission processes dominate giving rise to faster ion transport through the polymer matrix assisted by large amplitude segmental motion of the polymer backbone. At higher fluence the critical energy required for cross-linking is reached and the cross linking of polymer chains process dominate due to collective excitation (plasmons), which produces a large excited volume resulting in coercive interaction among the ions and radical pairs produced within the volume. Maximum ionic conductivity for Li^{3+} and C^{5+} ion irradiated P(VDF-HFP)-(PC+DEC)-LiClO₄ system is found to be 2.2×10^{-2} S/cm and 2×10^{-2} S/cm respectively at fluence of 10^{11} ions/cm² at 303 K. For P(VDF-HFP)-

(PC+DEC)-LiCF$_3$SO$_3$ system ionic conductivity exhibits the conductivity values of 2.6×10^{-3} S/cm for Li^{3+} irradiated and 1.8×10^{-3} S/cm for C^{5+} irradiated system at fluence of 10^{11} ions/cm^2 at 303 K.

(ii) XRD results reveal that crystallinity decreases in Li^{3+} and C^{5+} ion irradiated P(VDF-HFP)-(PC+DEC)-LiClO$_4$ and P(VDF-HFP)-(PC+DEC)-LiCF$_3$SO$_3$ systems after low fluence ion irradiation ($\leq 10^{11}$ ions/cm^2) and increases at higher fluence ($>10^{11}$ ions/cm^2) ion irradiation. Degree of crystallinity of Li^{3+} and C^{5+} ion irradiated P(VDF-HFP)-(PC+DEC)-LiClO$_4$ gel polymer electrolytes decreases to 10.48% and 11.5% respectively after low fluence (5×10^{10} and 5×10^9 ions/cm^2) ion irradiation and increases to 17.1% and 18.75% respectively after high fluence (5×10^{12} and 10^{12} ions/cm^2) ion irradiation as compared to 13.64% of unirradiated P(VDF-HFP)-(PC+DEC)-LiClO$_4$ gel polymer electrolyte. In Li^{3+} and C^{5+} ion irradiated P(VDF-HFP)-(PC+DEC)-LiCF$_3$SO$_3$ gel polymer electrolytes degree of crystallinity decreases to 11% and 10.2% respectively at low fluence ion irradiation (5×10^{10} and 10^{10} ions/cm^2) and increases to 26.5% and 29.2% respectively at high fluence (5×10^{12} and 10^{12} ions/cm^2) ion irradiation as compared to 21.8% of unirradiated P(VDF-HFP)-(PC+DEC)-LiCF$_3$SO$_3$ gel polymer electrolyte. This could be attributed to the fact that after low fluence ion irradiation crystallinity decreases due to chain scission and bond breaking which amorphizes the polymer. However, at a higher fluence of 10^{12} ions/cm^2, reordering and crosslinking of polymer chains take place forming the new crystalline region, which leads to decrease in the conductivity.

(iii) FTIR spectra for both Li^{3+} and C^{5+} ion irradiated P(VDF-HFP)-(PC+DEC)-LiClO$_4$ and P(VDF-HFP)-(PC+DEC)-LiCF$_3$SO$_3$ systems show a band around 3025 and 2985 cm^{-1} due to CH$_2$ asymmetric and symmetric stretching vibrations. After

irradiation with Li^{3+} and C^{5+} ions for both the systems, the absorption intensity of this band decreases with irradiation at low fluence of 10^{10} ions/cm². However, upon irradiation with a higher fluence of 10^{12} ions/cm², absorption intensity shows an increase. These results suggest that at low fluence C–H bonds break giving rise to decrease in intensity. At higher fluence, however, the reformation of bonds takes place due to cross linking of polymer chains resulting in the increase in intensity of the band around 3025 and 2985 cm^{-1}. These results are consistent with conductivity and XRD results.

(iv) SEM results exhibit that porosity of the gel polymer electrolytes is increased after irradiation. The increased porosity upon ion irradiation suggests that more liquid electrolyte is trapped in the same volume of polymer resulting in the higher ionic conductivity.

Future Prospects:

There is a vast scope of further development of high ion conducting gel polymer electrolyte materials and fabrication of electrochemical devices such as high energy density lithium batteries, supercapacitor, sensors etc. using them. Dispersion of insulating and semiconducting inorganic nanoparticles into polymer electrolytes and their investigations by Small Angle X-ray Spectroscopy will form good research problem to work upon. Movement of anions in polymer electrolytes deteriorates device performance, therefore cationic transport number needs to be enhanced. Intensive research on cationic monoconducting (single ion conducting) polymer electrolytes is going on, but researchers are far away from the goal. Research in this field has tremendous future prospects.

Swift heavy ion irradiation effects on polymer gel electrolyte is a new area of research, tremendous aspects are open to research in this field. Etching and filling of nano-ion tracks in polymer created by swift heavy ion irradiation with liquid electrolytes and making electrochemical devices using them constitute a fascinating research problem and work is going in that area. Research on ion beam induced modifications in solvent free polymer electrolytes, i.e., in PEO based electrolytes also has future prospects. Local Li^+ ion environment and ion transport in gel polymer electrolytes need to be probed by Li^+ solid state NMR technique.

References:

[1]   M. Faraday in: Experimental Investigations in Electricity, (Quaritch, London) (1839) No. 1340.

[2]   F. W. G. Kohlrausch, Ann. Phys. **17** (1882) 642.

[3]   C. Tubandt and S. Eggert, Z. Anorg. Chem. **110** (1920) 196.

[4]   J. Frenkel, Z. Physik **35** (1926) 652.

[5]   C. Wagner, Z. Phys. Chem. B **22** (1933) 181.

[6]   W. Schottky, Z. Phys. Chem. B **29** (1935) 335.

[7]   J. A. A. Ketelaar, Trans. Faraday Soc. **34** (1938) 874.

[8]   B. Reuter and K. Hardel, Nature Wissenchaften **48** (1961) 161.

[9]   J. N. Bradley and P. D. Greene, Trans. Faraday Soc. **62** (1966) 2069.

[10]   B. B. Owens and G. R. Argue, Science **157** (1967) 308.

[11]   Y. F. Y. Yao and J. T. Kummer, J. Inorg. Nucl. Chem. **29** (1967) 2453.

[12]   C. C. Liang, J. Electrochem. Soc. **120** (1973) 1289.

[13]   M. A. Ratner and A. Nitzan, Solid State Ionics **28/30** (1988) 3.

[14]   H. Tuller, D. P. Button and D. R. Uhlmann, J. Non-Cryst. Solids **40** (1980) 93.

[15]   J. N. Mundy and G. L. Jin, Solid State Ionics **21** (1986) 305.

[16]   J. Maier, Mat. Res. Bull. **20** (1985) 383.

[17]   T. Jow and J. B. Wagner Jr., J. Electrochem. Soc. **126** (1979) 1963.

[18]   K. Shahi and J. B. Wagner Jr., J. Electrochem. Soc. **128** (1981) 6.

[19]   D. E. Fenton, J. M. Parker and P. V. Wright, Polymer **14** (1973) 589.

[20]   M. B. Armand, J. M. Chabagno and M. Duclot in: Fast Ion Transport in Solids, (Edited by P. Vashisha, J. N. Mundy and G. K. Shenoy), North Holland, Amsterdam, (1979).

[21]   C. C. Lee and P. V. Wright, Polymer **23** (1982) 681.

[22]   D. R. Payne and P. V. Wright, Polymer **23** (1982) 690.

[23]   A. Killis, J. F. Le Nest and H. Cheradame, Makromol. Chem. Rapid Commun. **1** (1980) 595.

[24]   C. Berthier, W. Gorecki, M. Minier, M. B. Armand, J. M. Chabagno and P. Rigaud, Solid State Ionics **11** (1983) 91.

[25]   P. M. Blonsky, D. F. Shriver, P. Austin and H. R. Allcock, J. Am. Chem. Soc. **106** (1984) 6854.

[26]   D. J. Bannister, G. R. Davies, I. M. Ward and J. E. McIntyre, Polymer **25** (1984) 1600.

[27]   C. V. Nicholas, D. J. Wilson, C. Booth and J. R. M. Giles, Br. Polym. J. **20** (1988) 289.

[28]   M. A. Ratner and A. Nitzan, Faraday Discuss. Chem Soc. **88** (1989) 19.

[29]   C. A. Angell, Solid State Ionics **9/10** (1983) 3.

[30]   L. M. Torrel and C. A. Angell, Br. Polym. J. **20** (1988) 173.

[31]   H. Cheradame in: IUPAC Macromolecules, (Edited by H. Benoit and P. Rempp) Pergamon, New York, (1982) 351.

[32]   M. Watanabe and N. Ogata in: Polymer Electrolyte Reviews I, (Edited by J. R. MacCallum and C. A. Vincent), Elsevier, London, (1987).

[33]   A. Killis, J. F. Le Nest, A. Gandini, H. Cheradame and J. P. Cohen, Solid State Ionics **14** (1984) 231.

[34]   P. G. Hall, G. R. Davies, J. E. McIntyre, I. M. Ward, D. J. Bannister and K. M. F. Le Brock, Polym. Commun. **27** (1986) 98.

[35] J. Nishimoto, N. Furuya and M. Watanabe, Extended Abstracts of 62nd Meeting of Japanese Electrochemical Society, 3J12 (1995).

[36] A. Vallee, S. Besner and J. Prud'homme, Electrochim. Acta 37 (1992) 1579.

[37] N. Kobayashi, M. Uchiyama and E. Tsuchida, Solid State Ionics 17 (1986) 307.

[38] D. Benrabah, S. Sylla, F. Alloin, J-Y Sanchez and M. Armand, Electrochim. Acta 40 (1995) 2259.

[39] T. Fujinami, A. Tokimune, M. A. Mehta, G. C. Rawsky and D. F. Shriver, Chem. Mater. 9 (1997) 2236.

[40] C. A. Angell, C. Liu and E. Sanchez, Nature 362 (1993) 137.

[41] M. Watanabe, S. Yamada, K. Sanui and N. Ogata, J. Chem. Soc. Chem. Commun. 11 (1993) 929.

[42] H. Y. Sun, H. J. Sohn, O. Yamamoto, Y. Takeda and N. Imanishi, J. Electrochem. Soc. 146 (1999) 1672.

[43] G. Feuillade and Ph. Perche, J. Appl. Electrochem. 5 (1975) 63.

[44] E. Tsuchida, H. Ohro and K. Tsunemi, Electrochim. Acta 28 (1983) 591.

[45] T. Iijima, Y. Toyoguchi and N. Eda, Denki Kagaku 63 (1985) 619.

[46] T. Fukumasa, M. Morita, H. Tsutsumi, Y. Matsuda, T. Takahashi and H. Ashitaka, Extended Abstract of 31st Japanese Battery Symposium, 1A16 (1990) 35.

[47] B. Kumar, L. G. Scanlon and R. J. Spry, J. Power Sources 96 (2001) 337.

[48] P. S. Anantha and K. Hariharan, J. Phys. and Chem. of Solids 64 (2003) 1131.

[49] C. Capiglia, P. Mustarelli , E. Quartarone, C. Tomasi and A. Magistris, Solid State Ionics 118 (1999) 73.

[50] F. Croce, G. B. Apptecchi, L. Persi and B. Scrosati, Nature 394 (1998) 456.

[51] M. B. Armand, Adv. Mater. 2 (1990) 278.

[52]   Z. Gadjourova, Y. G. Andrew, D. P. Tunstall and P. G. Bruce, Nature **412** (2001) 520.

[53]   M. J. Reddy and P. P. Chu, Solid State Ionics, **149** (2002) 115.

[54]   C. A. Vincent, Progr. Solid State Chem. **17** (1987) 145.

[55]   A. J. Patrick, M. D. Glasse, R. J. Latham and R. G. Linford, Solid State Ionics **18/19** (1986) 1063.

[56]   J. J. Fontanella, M. C. Wintergill and J. P. Calame, J. Polym Sci. Polym. Phys. Ed. **23** (1985) 113.

[57]   I. Kelly, J. R. Owen and B. C. H. Steele, J. Power Sources **14** (1985) 13.

[58]   L. R. A. K. Bandara, M. A. K. L. Dissanayake and B. -E. Mellander, Electrochim. Acta **43 (10/11)** (1998) 1447.

[59]   S. Mitra and A. R. Kulkarni, Solid State Ionics **154/155** (2002) 37.

[60]   M. Forsyth, D. R. MacFarlane, A. Best, J. Adebahr, P. Jacobsson and A. J. Hill, Solid State Ionics **147** (2002) 203.

[61]   Z. Wang, W. Gao, L. Chen, Y. Mob and X. Huang, Solid State Ionics **154/155** (2002) 51.

[62]   W. Xu, L. M. Wang and C. A. Angell, Electrochim. Acta **48** (2003) 2037.

[63]   B. Kumar and L.G. Scanlon, J. Power Sources **52** (1994) 261.

[64]   P. P. Chu, M. J. Reddy and H. M. Kao, Solid State Ionics **156** (2003) 141.

[65]   W. J. Lee, H. R. Jung, M. S. Lee, J. H. Kim and K. S. Yang, Solid State Ionics **164** (2003) 65.

[66]   J. Zhou and P. S. Fedkiw, Electrochim. Acta **48** (2003) 2571.

[67]   B. Kumar, Journal of Electroceramics **5(2)** (2000) 127.

[68]   J. M. Tarascon, A. S. Gozdz, C. Schmutz, F. Shokoohi and P. C. Warren, Solid State Ionics **86** (1996) 49.

[69]   Y. Saito, C. Capigila, H. Yamamoto and P. Mustarelli, J. Electrochem Soc. **147(5)** (2000) 1645.

[70]   G. Girish Kumar and S. Sampath, Solid State Ionics **160** (2003) 289.

[71]   G. Żukowska, M. Rogowska, A. Wojda, E. Zygadlo-Monikowska, Z. Florjańczyk and W. Wieczorek, Solid State Ionics **136/137** (2000) 1205.

[72]   A. Magistris, P. Mustarelli, E. Quartarone, P. Piaggio and A. Bottino, Electrochim. Acta **46** (2001) 1635.

[73]   H. P. Chen and J. W. Fergus, J. Mater. Sci. Lett. **21** (2002) 285.

[74]   K. M. Abraham, H. S. Choe and D. M. Pasquariello, Electrochim. Acta **43(16/17)** (1998) 2399.

[75]   Y. W. Chen-Yang , H. C. Chen, F. J. Lin, C. C. Chen, Solid State Ionics **150** (2002) 327.

[76]   A. Zalewska, I. Pruszczyk, E. Sulek and W. Wieczorek, Solid State Ionics **157** (2003) 233.

[77]   O. Bohnke, G. Frand, M. Rezrazzi, C. Rousselot and C. Truche, Solid State Ionics **66** (1993) 97.

[78]   Y. K. Yarovoy, H. P. Wang and S. L. Wunder, Solid State Ionics **118** (1999) 301.

[79]   H. Ericson, C. Svanberg, A. Brodin, A. M. Grillone, S. Panero, B. Scrosati and P. Jacobsson, Electrochim. Acta **45** (2000) 1409.

[80]   M. Deepa, N. Sharma, S. A. Agnihotry, S. Singh, T. Lal and R. Chandra, Solid State Ionics **52/153** (2002) 253.

[81]   Y. Wang, J. Travas-Sejdic and R. Steiner, Solid State Ionics **148** (2002) 443.

[82]   A. M. Stephan and D. Teeters, Electrochim. Acta **48** (2003) 2143.

[83]   Y. Saito, A. M. Stephan and H. Kataoka, Solid State Ionics **160** (2003) 149.

[84] T. Michot, A. Nishimoto and M. Watanabe, Electrochim. Acta **45** (2000) 1347.

[85] S. S. Sekhon, Pradeep and S. A. Agnihotry in: Solid State Ionics: Science and Technology (Edited by B. V. R. Chowdari et. al.), World Scientific, Singapore, (1998) 217.

[86] R. G. Linford in: Applications of Electroactive Polymers, (Edited by B. Scrosati), Chapman and Hall, London, (1993) 1.

[87] S. Chandra, S. S. Sekhon and N. Arora, Ionics **6** (2000) 112.

[88] S. S. Sekhon, Bull. Mater. Sci., **26(3)** (2003) 321.

[89] J. Y. Song, C. L. Cheng, Y. Y. Wang and C. C. Wan, J. Electrochem. Soc. **149(9)** (2002) A1230.

[90] H. Vogel, Z. Phys. **22** (1922) 645.

[91] V. G. Tammann and H. G. Hesse, Anorg. Allg. Chem. **19** (1926) 245.

[92] G. S. Fulcher, J. Am. Ceram. Soc. **8** (1925) 339.

[93] J. R. MacCallum, C. A. Vincent, Polymer Electrolyte Review, 1 (1987) 185.

[94] Th. Joykumar Singh, T. Mimani, K. C. Patil and S. V. Bhat, Solid State Ionics **154/155** (2002) 21.

[95] M. L. Williams, R. F. Landel and J. D. Ferry, J. Am. Chem. Soc. **77** (1955) 3701.

[96] S. D. Druger, A. Nitzan and M. A. Ratner, J. Chem. Phys. **79(6)** (1983) 3133.

[97] M. H. Cohen and D. Turnbull, J. Chem. Phys. **31** (1959) 1164.

[98] M. Duclot, F. Alloin, O. Brylev, J-Y Sanchez and J. L. Souquet, Solid State Ionics **136/137** (2000) 1153.

[99] D. Bamford, G. Dlubek, A. Reiche, M. A. Alam, W. Meyer, P. Galvosas and F. Rittig, J. Chem. Phys. **115** (2001) 7260.

[100] G. Williams, in: Dielectric Spectroscopy of Polymeric Materials, Fundamentals and Applications, (Edited by J. P. Runt and J. J. Fitzgerald), American Chemical Society, Washington, DC, (1997).

[101] M. Mierzwa, G. Floudas, P. Stepanek and G. Wegner, Phys. Rev. B 62 (2000) 14012.

[102] P. B. Macedo and T. A. Litovitz, J. Chem. Phys 42 (1965) 245.

[103] S. N. Glasstone, K. Laidler and H. Eyring in: The Theory of Rate Processes, McGraw-Hill, New York, (1941).

[104] F. R. Blackburn, C. Y. Yang and M. D. Ediger, J. Phys. Chem. 100 (1996) 18249.

[105] D. M. Rück, Nucl. Instr. and Meth. B $166/167$ (2000) 602.

[106] T. Venkatesan, Nucl. Instr. and Meth. B $7/8$ (1985) 461.

[107] E. Balanzat, S. Bouffard, A. Le Moël and N. Betz, Nucl. Instr. and Meth. B 91 (1994) 140.

[108] V. N. Popok, V. B. Odzhaev, I. P. Kozlov, I. I. Azarko, I. A. Karpovich and D. V. Sviridov, Nucl. Instr. and Meth. B 129 (1997) 60.

[109] J. Davenas, I. Stevenson, N. Celette, S. Cambon, J. L. Gardette, A. Rivaton and L. Vignoud, Nucl. Instr. and Meth. B 191 (2002) 653.

[110] A. Laskarakis, C. Gravalidis and S. Logothetidis, Nucl. Instr. and Meth. B 216 (2004) 131.

[111] M. Guenther, G. Gerlach, G. Suchaneck, K. Sahre, K. –J. Eichhorn, V. Baturin and S. Duvanov., Nucl. Instr. and Meth. B 216 (2004) 143.

[112] V. Chailley, E. Balanzat and E. Dooryhee, Nucl. Instr. and Meth. B 105 (1995) 110.

[113] E. H. Lee, Nucl. Instr. and Meth. B 151 (1999) 29.

[114] M. Toulemonde, C. Trautmann, E. Balanzat, K. Hjort and A. Weidinger, Nucl. Instr. and Meth. B 216 (2004) 1.

[115] D. Raistrick, Solid State Ionics **18/19** (1986) 40.

[116] S. W. Martin and C. A. Angell, J. Non. Cryst. Solids **83** (1986) 185.

[117] D. P. Almond and A. R. West, Solid State Ionics **11** (1983) 57.

[118] I. M. Hodge, M. D. Ingram and A. R. West, J. Electroanal. Chem. **74** (1976) 125.

[119] R. J. Latham and R. G. Linford, "Ionic and Electronic Transport" in: Electrochemical Science and Technology of Polymers Vol. I, (Edited by R. G. Linford) Elsevier Applied Science, London, (1987) 1.

[120] W. I. Archer and R. D. Armstrong in: Electrochemistry Vol. VII, (Edited by H. R. Thirsk) The Chemical Society, London, (1980) 157.

[121] R. Dupon, D. H. Whitmore and D. F. Shriver, J. Electrochem. Soc. **128** (1981) 716.

[122] H. Cheradame in: IUPAC Macromolecules, (Edited by H. Benoit and P. Rempp) Pergamon, New York, (1982) 251.

[123] A. Killis, J. F. LeNest, A. Gandini and H. Cheradame, J. Polym. Sci., Polym. Phys. Ed. **19** (1981) 1073.

[124] S. Smedley, in: The Interpretation of Ionic Conductivity in Liquids, Plenum, New York, (1980).

[125] M. H. Cohen and G. S. Grest, Phys. Rev. B **21** (1980) 4113.

[126] J. H. Gibbs and E. A. DiMarzio, J. Chem. Phys. **28** (1958) 373.

[127] G. Adam and J. H. Gibbs, J. Chem. Phys. **43** (1965) 139.

[128] M. J. Goldstein, J. Phys. Chem. **77** (1973) 667.

[129] C. A. Angell and W. Sichina, Ann. N. Y. Acad. Sci. **279** (1976) 53.

[130] M. A. Ratner in: Polymer Electrolyte Reviews, (Edited by J. R. MacCallum, C. A. Vincent), Elsevier, London, (1987).

[131] S. D. Druger, A. Nitzan and M. A. Ratner, Solid State Ionics **9/10** (1983) 1115.

[132]   C. S. Harris, A. Nitzan, M. A. Ratner and D. F. Shriver, Solid State Ionics **18/19** (1986) 151.

[133]   S. D. Druger, M. A. Ratner and A. Nitzan, Phys. Rev. **331** (1985) 3939.

[134]   S. D. Druger, M. A. Ratner and A. Nitzan, Solid State Ionics **18/19** (1986) 106.

[135]   W. Wieczorek, K. Such, S. H. Chung and J. R. Stevens, J. Phys. Chem. **98** (1994) 9047.

[136]   W. Wieczorek, K. Such, Z. Florjanczyk and J. R. Stevens, J. Phys. Chem. **98** (1994) 6840.

[137]   J. C. Maxwell, in: A Treatise on Electricity and Magnetism, Vol. I, 2nd ed., Clarendon Press, Oxford, (1881) 435.

[138]   D. A. G. Bruggeman, Ann. Phys. (Leipzig) **24** (1935) 636.

[139]   R. Landuer, J. Appl. Phys. **23** (1952) 779.

[140]   C. W. Nan and D. M. Smith, Mater. Sci. Eng. **B10** (1991) 99.

[141]   C. W. Nan, Prog. Mater. Sci. **37** (1993) 1.

[142]   M. Nakamura, Phys. Rev. B **29** (1984) 3691.

[143]   S. Kirpatrick, Rev. Mod. Phys. **45** (1973) 574.

[144]   T. DeSimone, R. M. Stratt and S. Demoulini, Phys. Rev. Lett. **56** (1986) 1140.

[145]   Z. Florjanczyk, W. Krawiec, D. Greszta, W. Wieczorek and M. Siekierski, Bull. Electrochem. **8** (1992) 524.

[146]   J. Przyluski, M. Siekierski and W. Wieczorek, Electrochim. Acta **40** (1995) 2101.

[147]   J. Przyluski, W. Wieczorek and Z. Florjanczyk, in: Solid State Ionics: Materials and Applications, (Edited by B. V. R. Chowdari, S. Chandra, S. Singh and P. C. Srivastava), World Scientific Publ. Co., Singapore, (1992) 209.

[148]   W. Wieczorek and M. Siekierski, J. Appl. Phys. **76** (1994) 2220.

[149] J. Bares, Macromolecules **8** (1975) 244.

[150] H. A. Schneider and E. A. DiMarzio, Polymer **33** (1992) 3453.

[151] M. C. Wintersgill, J. J. Fontanella, J. P. Calme, M. K. Smith, T. B. Jones, S. G. Greenbaum, K. G. Adamic. A. N. Shetty and C. G. Andeen, Solid State Ionics **18/19** (1986) 326.

[152] J. B. Wagner and C. J. Wagner, Chem. Review **26** (1957) 1597.

[153] S. Chandra, in: Superionic Solids- Principle and Application, Amsterdam: NHPC, (1981).

[154] J. F. Ziegler, J. P. Biersack and U. Littmark, in: Stopping and Ranges of Ions in Matter, Pergamon, New York, (1985).

[155] P. Periasamy, K. Tatsumi, M. Shikano, T. Fujieda, Y. Saito, T. Sakai, M. Mizuhata, A. Kajinami and S. Deki, J. Power Sources **88** (2000) 269.

[156] H. Huang and S. L. Wunder, J. Elecrochem. Soc. **148(3)** (2001) A279.

[157] C. S. Kim and S. M. Oh, Electrochim. Acta **45** (2000) 2101.

[158] Y. Saito, H. Kataoka, T. Sakai and S. Deki, Electrochim. Acta **46** (2001) 1747.

[159] M. Watanabe, K. Sanui, N. Ogata, T. Kobayashi and Z. Ohtaki, J. Appl. Phys. **57(1)** (1985) 123.

[160] K. M. Abraham, Z. Jiang and B. Carroll, Chem. Mater. **9(9)** (1997) 1978.

[161] J. Y. Song, Y. Y. Wang and C. C. Wan, J. Electrochem. Soc. **145** (1998) 1207.

[162] K. M. Abraham, M. Alamgir and D. K. Hoffman, J. Electrochem. Soc. **142** (1995) 683.

[163] G. B. Appetecchi, F. Croce, A. De Paolis and B. Scrosati, J. Electroanal. Chem. **463** (1999) 248.

[164] J. Y. Song, Y. Y. Wang and C. C. Wan, J. Electrochem. Soc. **147(9)** (2000) 3219.

[165] P. G. Bruce, in: Polymer Electrolyte Review- I, (Edited by J. R. MacCallum and C. A. Vincent), Elsevier, New York, (1987) 42.

[166] M. Morita, F. Tachihara and Y. Matsuda, Electrochim. Acta 32 (1987) 299.

[167] A. M. Stephan, Y. Saito, N. Muniyandi, N. G. Renganathan, S. Kalyanasundaram and R. N. Elizabeth, Solid State Ionics 148 (2002) 467.

[168] H. Cheradame and P. Niddam-Mercier, Faraday Discuss. Chem. Soc. 88 (1989) 77.

[169] M. A. Ratner and D. F. Shriver, Mater. Res. Soc. Bull. 14(9) (1989) 39.

[170] K. M. Abraham, in: Applications of Electroactive Polymers, (Edited by B. Scrosati), Chapman & Hall, London, (1993) 75.

[171] S. Rajendran, T. Uma and T. Mahalingam, European Polymer Journal 36 (2000) 2617.

[172] Z. Wen, T. Itoh, M. Ikeda, N. Hirata, M. Kubo and O. Yamamoto, Journal of Power Sources 90 (2000) 20.

[173] H. Wang, H. Huang, S. L. Wunder, J. Electrochem. Soc., 147(8) (2000) 2853.

[174] K. Hayamizu, Y. Aihara, W. S. Price, J. Chemical Physics, 113(11) (2000) 4785.

[175] A. Ferry, M. M. Doeff and L. C. DeJonghe, Electrochim. Acta 43 (1998) 1387.

[176] S. Abbrent, J. Plestil, D. Hlavata, J. Lindgren, J. Tegenfeldt and A. Wendsjo, Polymer 42 (2001) 1407.

[177] C. J. Leo, G. V. Subba Rao and B. V. R. Chowdari, Solid State ionics 148 (2002) 159.

[178] D. L. Pavia, G. M. Lampman and G. S. Kriz, in: Introduction to Spectroscopy, Harcourt college publ., USA, (2001).

[179] R. M. Silverstein, G. C. Bassler and T. C. Morrill, in: Spectroscopic Identification of Organic Compounds (Fifth Ed.), John Wiley & Sons. Inc, USA, (1991).

[180] C. S. Kim and S. M. Oh, Electrochim Acta 46 (2001) 1323.

[181] A. M. Stephan and Y. Saito, Solid State Ionics 148 (2002) 475.

[182] Y. Liu, J. Y. Lee and L. Hong, Solid State Ionics, 150 (2002) 317.

[183] E. Quartarone, P. Mustarelli and A. Magistris, Solid State Ionics 110 (1998) 1.

[184] A. S. Best, A. Ferry, D. R. MacFarlane and M. Forsyth, Solid State Ionics 126 (1999) 269.

[185] M. Marcinek, A. Bac, P. Lipka, A. Zalewska, G. Zukowska, R. Borkowska and W. Wieczorek, J. Phys. Chem. B 104 (2000) 11088.

[186] J. Fan, S. R. Raghavan, X. Y. Yu, S. A. Khan, P. S. Fedkiw, J. Hou and G. L. Baker, Solid State Ionics 111 (1998) 117.

[187] W. Wieczorek, D. Raducha, A. Zalewska and J. R. Stevens, J. Phys. Chem. B 102 (1998) 8725.

[188] S. A. Khan, G. L. Baker and S. Colson, Chem. Mater. 6 (1994) 2359.

[189] H. J. Walls, J. Zhou, J. A. Yerian, P. S. Fedkiw, S. A. Khan, M. K. Stowe and G. L. Baker, J. Power Sources, 89 (2000) 156.

[190] S. R. Raghavan, M. W. Riley, P. S. Fedkiw and S. A. Khan, Chem. Mater., 10 (1998) 244.

[191] B. Kumar, L. Scanlon, R. Marsh, R. Manson, R. Higgins and R. Baldwin, Electrochim. Acta 46 (2001) 1515.

[192] J. E. Weston and B. C. H. Steele, Solid State Ionics 7 (1982) 75.

[193] S. Skaarup, K. West and B. Zachau-Christiansen, Solid State ionics 28/30 (1988) 975.

[194] J. Plocharski and W. Wieczorek, Solid State Ionics 28/30 (1988) 979.

[195] J. Plocharski, W. Wieczorek, J. Przyluski and K. Such, Appl. Phys. A49 (1989) 55.

[196] S. Skaarup, K. West, P. M. Julian and D. M. Thomas, Solid State Ionics 40/41 (1990) 1021.

[197] F. Capuano, F. Croce and B. Scrosati, J. Electrochem. Soc. 138 (1991) 1918.

[198] F. Croce, F. Gerace and B. Scrosati, Proc. 35th Int. Power Sources Symposium, Cherry Hill, NJ, USA, (1992) 267.

[199] F. Croce and B. Scrosati, J. Power Sources **43/44** (1993) 9. .

[200] N. Munichandraiah, L. G. Scanlon, R. A. Marsh, B. Kumar and A. K. Sircar, Proc. Meet. The Electrochemical Society, Honolulu, HI, USA, (1993).

[201] B. Kumar, J. D. Schaffer, N. Munichandraiah and L. G. Scanlon, J. Power Sources **47** (1994) 63.

[202] J. Przyluski, K. Such, H. Wycislik, W. Wieczorek and Z. Florianczyk, Synth, Met. **35** (1990) 241.

[203] B. Kumar and L. G. Scanlon, Proc. 36th Int. Power Sources Symposium, Cherry Hill, NJ, USA, (1994) 236.

[204] H. J. Rhoo, H. T. Kim, J. K. Park and T. S. Hwang, Electrochim. Acta **42** (1997) 1571.

[205] B. Oh and Y. R. Kim, Solid State Ionics **124 (1-2)** (1999) 83.

[206] K. Pielichowski, Eur. Polym. J. **35** (1999) 27.

[207] A. M. Stephan, T. P. Kumar, N. G. Renganathan, S. Pitchumani, R. Thirunakaran and N. Muniyandi, J. Power Sources **89** (2000) 80.

[208] M. Tang and W. R. Liau, Eur. Polym. J. **36** (2000) 2597.

[209] K. Pielichowski and I. Hamerton, Eur. Polym. J. **36** (2000) 171.

[210] J. L. Acosta and E. Morales, Solid State Ionics **85** (1996) 85.

[211] A. M. Rocco, R. P. Pereira and M. I. Felisberti, Polymer **42** (2001) 5199.

[212] S. M. S. Neiro, D. C. Dragunski, A. F. Rubira and E. C. Muniz, Eur. Polym. J. **36** (2000) 583.

[213] M. M. E. Jacob, E. Hackett and E. P. Giannelis, J. Mater. Chem. **13** (2003) 1.

[214] P. G. Bruce, J. Evans and C. A. Vincent, Solid State Ionics **28-30** (1988) 918.

[215] S. Panero, D. Satolli, A. D'Epifano and B. Scrosati, J. Electrochem Soc. **149(4)** (2002) A414.

[216] R. A. Zoppi and M. C. Goncalves, Solid State Ionics **147** (2002) 157.

[217] F. Croce, L. Persi, B. Scrosati, F. Serraino-Fiory, E. Plichta and M. A. Hendrickson, Electrochim. Acta **46** (2001) 2457.

[218] K. M. Kim, J. M. Ko, N. G. Park, K. S. Ryu, S. H. Chang, Solid State Ionics **161** (2003) 121.

[219] D. Saikia and A. Kumar, Electrochim. Acta **49**(16) (2004) 2581.

[220] S. Rajendran and T. Uma, J Power Sources **88** (2000) 282.

[221] B. Morrow and A. McFarlan, J Phys. Chem. **96** (1992) 1395.

[222] S. Sehantz, J. Sandahl, L. Borgesson, L. M. Torrell and J. R. Stevens, Solid State Ionics **28/30** (1988) 1047.

[223] S. Sehantz, L. M. Torrell and J. R. Stevens, J Chem.Phys **94** (1991) 6862.

[224] J. P. Manning and R. Frech, Polymer **33** (1992) 3487.

[225] W. Huang, R. Frech, R. Wheeler, J Phys. Chem. **98** (1994) 100.

[226] S. R. Starkey and R.Frech, Electrochim. Acta **42(3)** (1997) 471.

[227] J. Maier, Prog. Solid State Chem. **23** (1995) 171.

[228] N. Sata, K. Eberman, K. Eberl and J. Maier, Nature **408** (2000) 946.

[229] E. W. Lawless, C. J. W. Wiegand, Yu. Mizumoto, and C. Weis, Inorg. Chem., **10** (1971) 1084.

[230] E. G. Ippolitov, M. A. Maifat and B. M. Zhigarnovskii, V All-Union Symp. on the Chemistry of Inorganic Fluorides, Dnepropetrovsk, (1978) 132.

[231] L. Calcagno and G. Foti, Nucl. Instr. and Meth. B **19/20** (1987) 895.

[232]   A. Charlesby, in: Atomic Radiation and Polymers, Pergamon, London, (1960).

[233]   T. Venkatesan, L. Calcagno, B. S. Elman and G. Foti, in: Ion Beam Modifications of Insulators, (Edited by P. Mazzoldi and G. Arnold), Elsevier, Amsterdam, (1978) 301.

[234]   G. R. Davies, Inst. Phys. Conf. Ser. No. **58** (1980) 50.

[235]   S. Osaki and T. Kotaka, Ferroelectrics **32** (1981) 177.

[236]   A. M. Guzman, J. D. Carlson, J. E. Bares and P. P. Pronko, Nucl. Instr. and Meth. B **7/8** (1985) 468.

[237]   G. M. Mladenov and B. Emmoth, Appl. Phys. Lett. **38** (1981) 1000.

[238]   T. M. Hall, A. Wagner and L. F. Thompson, J. Appl. Phys. **53** (1982) 3997.

[239]   S. H. Lin, K. L. Sheng, T. W. Rong, J. R. Bao, W. M. Wang, H. H. Wan, Z. Y. Zhou, X. F. Zhu and F. J. Yang, Nucl. Instr. and Meth. B **59/60** (1991) 1257.

[240]   S. Schiestel, W. Ensinger and G. K. Wolf, Nucl. Instr. and Meth. B **91** (1994) 473.

[241]   N. Koshida and Y. Suzuki, J. Appl. Phys. **61** (1987) 5488.

[242]   C. Z. Wang and K. M. Ho, Phys. Rev. Lett. **71** (1993) 1184.

[243]   Y. Q. Yang, R. E. Giedd, M. G. Moss and J. Kaufmann, Nucl. Instr. and Meth. B **127/128** (1997) 710.

[244]   D. Saikia, A. M. P. Hussain, A. Kumar, F. Singh, D. K.Avasthi and N. C. Mishra, NSC Annual Report, (2002-2003) 214.

[245]   D. Fink, M. Müller, L. T. Chadderton, P. H. Cannington, R. G. Elliman and D. C. McDonald, Nucl. Instr. and Meth. B **32** (1988) 125.

[246]   J. Davenas, G. Boiteux, X. L. Xu and E. Adem, Nucl. Instr. and Meth. B **32** (1988) 136.

[247]   J. Davenas, G. Boiteux and M. Fallavierm, Nucl. Instr. and Meth. B **38** (1989) 796.

[248]   R. A. Lessard and G. Manivannan, Nucl. Instr. and Meth. B **105** (1995) 229.

[249] T. Mohanty, N. C. Mishra, F. Singh, U. Tiwari and D. Kanjilal, Nucl. Instr. and Meth. B **212** (2003) 179.

[250] E. H. Lee, Y. Lee, W. C. Oliver and L. K. Mansur, J. Mater. Res. **8** (1993) 377.

[251] R. Öchsner, A. Kluge, S. Z. Malonn, L. Gong and H. Ryssel, Nucl. Instr. and Meth. B **80/81(2)** (1993) 1050.

[252] J. C. Pivin, Thin Solid Films **263** (1995) 185.

[253] M. V. Swain, A. J. Perry, J. R. Treglio and E. D. Demaree, J. Mater. Res. **12** (1997) 1917.

[254] J. D. Hunn and C. P. Christensen, Solid State Technol. **37** (1994) 57.

[255] R. Percolla, L. Calcagno, G. Foti and G. Ciavola, Appl. Phys. Lett. **65(23)** (1994) 2966.

[256] F. Hosoi, Y. Aoki, M. Hagiwara, H. Omichi and M. M. Salleh, Rad. Eff. Def. Solids **126** (1993) 351.

[257] A. Biswas, S. Lotha, D. Fink, J. P. Singh, D. K. Avasthi, B. K. Yadav, S. K. Bose, D. T. Khating and A. M. Avasthi, Nucl. Instr. and Meth. B **159** (1999) 40.

[258] M. Mateev and S. Karageorgiev, Rad. Eff. Def. Solids **152** (2000) 109

[259] M. Gaafar, Nucl. Instr. and Meth. B **174** (2001) 507.

[260] E. H. Lee, G. R. Rao, M. B. Lewis and L. K. Mansur, J. Mater. Res. **9** (1994) 1043.

[261] M. B. Lewis, E. H. Lee and G. R. Rao, J. Nucl. Mater. **211** (1994) 46.

[262] A. Biswas, R. Gupta, N. Kumar, D. K. Avasthi, J. P. Singh, S. Lotha, D. Fink, S. N. Paul and S. K. Bose, Appl. Phys. Lett. **78(26)** (2001) 4136.

List of Publications

A. *In Journals*

(i) D. Saikia & A. Kumar, "Ionic Conduction in P(VDF-HFP)/PVDF-(PC+DEC)-LiClO$_4$ Polymer Gel Electrolyte", *Electrochimica Acta* **49 (2004) 2581- 2589.**

(ii) D. Saikia & A. Kumar, "Fast Ion Transport in P(VDF-HFP)-PMMA-PC-LiClO$_4$-TiO$_2$ Composite Gel Polymer Electrolytes", *Indian J. of Pure & Appl. Phys* **41(2003) 961-966.**

(iii) D. Saikia & A. Kumar, "Ionic Transport in P(VDF-HFP)-PMMA-LiCF$_3$SO$_3$-(PC+DEC)-SiO$_2$ Composite Gel Polymer Electrolyte", *European Polymer Journal* **(In Press)**.

(iv) D. Saikia & A. Kumar, "Ionic Conduction Studies in P(VDF-HFP)-LiAsF$_6$-(PC+DEC)-fumed SiO$_2$ Composite Gel Polymer Electrolyte System", *Physica Status Solidi (a)* **(In Press)**.

(v) D. Saikia, A. Kumar, F. Singh, N. C. Mishra & D. K. Avasthi, "Study of Lithium Ion Irradiation Effects in P(VDF-HFP)-(PC+DEC)-LiClO$_4$ Gel Polymer Electrolytes", *Nucl. Instr. and Meth. B* **(Communicated)**.

(vi) D. Saikia, A. Kumar, F. Singh, N. C. Mishra & D. K. Avasthi, "Ionic Conduction in C^{5+} Ion Irradiated P(VDF-HFP) Based Gel Polymer Electrolytes", **Journal of Applied Physics (Communicated)**.

(vii) D. Saikia, A. Kumar, F. Singh, N. C. Mishra & D. K. Avasthi, "Study of Li^{3+} Ion Irradiation Effects on Ionic Conduction in P(VDF-HFP)-(PC+DEC)-LiCF$_3$SO$_3$ Gel Polymer Electrolytes", *Electrochimica Acta* **(Communicated)**.

(viii) A. Kumar, D. Saikia, F. Singh & D. K. Avasthi, "Study of C^{5+} Ion Irradiation Effects on Ionic Conduction in P(VDF-HFP)-(PC+DEC)-LiCF$_3$SO$_3$ Gel Polymer Electrolytes", *Solid State Ionics* **(Communicated)**.

B. *Paper/Poster Presented in Conferences*

(i) D. Saikia & A. Kumar, "FTIR and Transport Number Studies on PVC-PS-NH$_4$SCN-DBP based Gel Polymer Blend Electrolyte", Proceedings of the 5th National Conference on Solid State Ionics, Nagpur University 15-17 February, 2002, pp. 89-91.

(ii) A. Kumar & D. Saikia, "Investigation of Ionic Conduction in PVDF/P(VDF-HFP)-LiClO$_4$-(PC+DEC) Polymer Gel Electrolytes", Proceedings of the Seventh International Symposium on Advances in Electrochemical Science & Technology, Chennai, India, 27-29 November, 2002, pp. D52-D55.

(iii) D. Saikia & A. Kumar, "Characterization of P(VDF-HFP)-PMMA-PC-LiClO$_4$-TiO$_2$ Blend Polymer Electrolytes", 14th AGM & Theme Symposium on Novel Polymeric Materials, BARC, Mumbai, 11-13 February, 2003.

(iv) A. Kumar & D. Saikia, "Ion transport in P(VDF-HFP)-LiAsF$_6$-(PC+DEC)-fumed SiO$_2$ Composite Gel Polymer Electrolytes", International Conference on Ionic Devices, Anna University, Chennai, 28-30 November, 2003.

(v) D. Saikia, A. Kumar, A. M. P. Hussain, F. Singh & D. K. Avasthi, "Study of Swift heavy Ion Irradiation Effects in Polymer electrolytes", National Conference on Materials and Their Applications, Kurukshetra University, Kurukshetra, 11-13 March, 2004.

(vi) A. Kumar, D. Saikia & A. M. P. Hussain, "Advanced Electroactive Polymers: Polymer Electrolytes and Conducting Polymers", XXVII Annual Meeting of EMSI and Conference on Electron Microscopy and Allied Fields, National Physical Laboratory, New Delhi, 1-3 April, 2004.

(vii) D. Saikia, A. M. P. Hussain, A. Kumar, F. Singh and D. K. Avasthi, "Ionic Conduction in C$^+$ Ion Irradiated P(VDF-HFP)-(PC+DEC)-LiClO$_4$ Polymer

Electrolyte System", 6th National Conference on Solid State Ionics, Jadavpur University, October 5-7, 2004.

(viii) A. Kumar, D. Saikia, F. Singh and D. K. Avasthi, "Ionic Conduction in C^{5+} Ion Irradiated P(VDF-HFP)-(PC+DEC)-LiCF$_3$SO$_3$ Gel Polymer Electrolyte System", International Conference on Electroactive Polymers: Material and Devices, Dalhousie, Himachal Pradesh, India, November 1-5, 2004.

C. *In Reports*

(i) D. Saikia, A. M. P. Hussain, A. Kumar, F. Singh, D. K. Avasthi & N. C. Mishra, "Investigation of Swift Heavy Ion Irradiation Effects on Ionic Conduction in P(VDF-HFP)-LiClO$_4$ Polymer Electrolytes", NSC Annual Report, 2002-2003.

(ii) D. Saikia, A. Kumar, A. M. P. Hussain, F. Singh, D. K. Avasthi & N. C. Mishra, "Lithium Ion Irradiation Effects in P(VDF-HFP) based Polymer Electrolytes", NSC Annual Report, 2003-2004.